Design and Analysis of Sliding Mode Control Algorithms for Power Networks

Michele Cucuzzella

ecsee

The research reported in this thesis is part of the research program of the Ph.D. School in Electronics, Computer Science and Electrical Engineering (ECSEE) of the University of Pavia. The author has successfully completed the educational program of the Ph.D. School ECSEE.

A catalogue record is available from the University of Pavia Library.

Typeset by the author with the LaTeX documentation system.
Cover design: Alessandro Battaglia. Background based on image under creative common license.
Pictures by Michele Cucuzzella.

Design and Analysis of Sliding Mode Control Algorithms for Power Networks

THESIS

to obtain the degree of doctor from University of Pavia,
by virtue of authority of the rector, Prof. Fabio Rugge,
and of a Committee selected by the Ph.D. School ECSEE
for the defense on Month 00th, 2018 at 00:00 o'clock

by

Michele Cucuzzella

born in Ragusa, Italy

This thesis has been approved by the supervisor Prof. Antonella Ferrara. It will be defended in front of the Committee:

Prof. . . . .
Prof. . . . .
Prof. . . . .
Prof. . . . .
Prof. . . . .

Lo scienziato non è l'uomo che fornisce le vere risposte;
è quello che pone le vere domande.

[Claude Lévi-Strauss, *Le cru et le cuit*, 1964]

Acknowledgement

It is not easy to thank in a few lines all the people who have contributed to the development of this work: some with constant support, other with hints and tips or just encouraging words. In particular, I wish to express my sincere gratitude to my supervisor, Prof. Antonella Ferrara, for her constant helpfulness, smart ideas, valuable advices and enthusiastic support, which have fuelled my passion for research. I would like to thank also my friends and colleagues Gian Paolo and Sebastian for their significant contribution during these years. I also thank the senior laboratory technician, Gianluca, for supporting me every day in these three years. Finally, I would like to thank all my best friends, my girlfriend Martina and my family for their constant moral support over the years.

Pavia, Month 00th, 2018 *Michele Cucuzzella*

List of Co-Authors

Antonella Ferrara
University of Pavia
Via Ferrata 5
Pavia - Italy, 27100
antonella.ferrara@unipv.it

Lalo Magni
University of Pavia
Via Ferrata 5
Pavia - Italy, 27100
lalo.magni@unipv.it

Arjan van der Schaft
University of Groningen
Nijenborgh 9
Groningen - the Netherlands, 9747 AG
a.j.van.der.schaft@rug.nl

Claudio De Persis
University of Groningen
Nijenborgh 4
Groningen - the Netherlands, 9747 AG
c.de.persis@rug.nl

Alberto Cavallo
University of Campania "L. Vanvitelli"
via Roma 29
Aversa - Italy, 81031
alberto.cavallo@unicampania.it

Gian Paolo Incremona
Politecnico di Milano
Piazza Leonardo da Vinci 32
Milan - Italy, 20133
gp.incremona@gmail.com

Sebastian Trip
University of Groningen
Nijenborgh 4
Groningen - the Netherlands, 9747 AG
s.trip@rug.nl

Gianmario Rinaldi
University of Pavia
Via Ferrata 5
Pavia - Italy, 27100
gianmario.rinaldi01@universitadipavia.it

Riccardo Lazzari
RSE S.p.A.
Via Rubattino Raffaele 54
Milan - Italy, 20134
Riccardo.Lazzari@rse-web.it

Carlo Sandroni
RSE S.p.A.
Via Rubattino Raffaele 54
Milan - Italy, 20134
Carlo.Sandroni@rse-web.it

Mauro Guastalli
University of Pavia
Via Ferrata 5
Pavia - Italy, 27100
mauro.guastalli01@universitadipavia.it

Simone Rosti
University of Pavia
Via Ferrata 5
Pavia - Italy, 27100
simoneenrico.rosti01@universitadipavia.it

Acronyms

The list of abbreviations is hereafter reported.

AC	Alternate Current
AGC	Automatic Generation Control
ASSOSM	Adaptive Suboptimal Second Order Sliding Mode
DC	Direct Current
DGu	Distributed Generation unit
D-SSOSM	Distributed Suboptimal Second Order Sliding Mode
ET	Event-Triggered
GCOM	Grid-Connected Operation Mode
HOSM	Higher Order Sliding Mode
HVDC	High Voltage Direct Current
IGBTs	Insulated Gate Bipolar Transistors
IOM	Islanded Operation Mode
LFC	Load Frequency Control
MIMO	Multi-Input Multi-Output
MPC	Model Predictive Control
NCSs	Networked Control Systems
OLFC	Optimal Load Frequency Control
PCC	Point Common Coupling
PI	Proportional-Integral
PLL	Phase Locked Loop
PWM	Pulse Width Modulation
QSL	Quasi Stationary Line

RES	Renewable Energy Sources
RMS	Root Mean Square
RSE	Ricerca sul Sistema Energetico
SISO	Single-Input Single-Output
SM	Sliding Mode
SMC	Sliding Mode Control
SOSM	Second Order Sliding Mode
SSOSM	Suboptimal Second Order Sliding Mode
VSC	Variable Structure Control
Vsc	Voltage source converter
3SM	Third Order Sliding Mode

Notation

The symbols are chosen according to the following conventions. Scalar values or signals are denoted by italics letters such as x. Generally, vectors are indicated by boldface lower-case letters such as $\boldsymbol{x}$, and matrices by boldface upper-case letters such as $\boldsymbol{A}$. Accordingly, the elements $x_1, \ldots, x_n$ of a vector $\boldsymbol{x}$ or $a_{11}, a_{12}, \ldots, a_{nm}$ (or equivalently $A_{11}, A_{12}, \ldots, A_{nm}$) of a matrix $\boldsymbol{A} \in \mathbb{R}^{n \times m}$ are represented by italics letters. Some signals (e.g. direct current signals and powers) are denoted by upper-case letters such as $\boldsymbol{V} = [V_1, \ldots, V_n]^T$ and $\boldsymbol{P} = [P_1, \ldots, P_n]^T$, while diagonal matrices are indicated as $\boldsymbol{R} = \mathrm{diag}(r_1, \ldots, r_n)$. The r-th time derivative of a signals $x(t)$, with $r > 2$, is denoted by $x^{(r)}(t)$. Sets are symbolized by calligraphic letters such as $\mathcal{W}$, while $\mathcal{W}^{\mathrm{sup}} := \sup_{\boldsymbol{w} \in \mathcal{W}}\{\|\boldsymbol{w}\|\}$. Given the set $\mathcal{W}$, $\partial\mathcal{W}$ will denote the boundary of $\mathcal{W}$. The inequality $\boldsymbol{A} \succ 0$ states that the matrix $\boldsymbol{A}$ is positive definite. For any symmetric matrix $\boldsymbol{A}$, $\lambda_{\max}(\boldsymbol{A})$ and $\lambda_{\min}(\boldsymbol{A})$ denote the largest and the smallest eigenvalue of matrix $\boldsymbol{A}$, respectively. Given $\boldsymbol{x} \in \mathbb{R}^n$, $\boldsymbol{y} \in \mathbb{R}^n$, let $\boldsymbol{x} \cdot \boldsymbol{y}$ denote the vector dot product, let $\boldsymbol{x} \times \boldsymbol{y}$ denote the cross product, while let $\boldsymbol{x} \circ \boldsymbol{y} \in \mathbb{R}^n$, with $(\boldsymbol{x} \circ \boldsymbol{y})_i = x_i\, y_i, i = 1, \ldots, n$, denote the Hadamard product (also known as Schur product). The symbol $\mathbb{1}_n \in \mathbb{R}^n$ denotes the vector consisting of all ones, while $\mathbb{I}_n \in \mathbb{R}^{n \times n}$ indicates the identity matrix. Finally, $\|\cdot\|$ is used to denote the Euclidean norm, $\|\cdot\|_\infty$ to denote the infinity norm, and $|\cdot|$ to denote the absolute value.

Contents

1

Introduction

Nowadays, due to economical, technological and environmental reasons, the most relevant challenge in power grids deals with the transition of the traditional power generation and transmission systems towards the large scale introduction of smaller distributed generation units [GBZ+10]. The massive penetration of the distributed generation avoids indeed the remanufacturing of the traditional electrical systems and reduces the network losses, by generating energy close to the end-users [PDH+05]. Moreover, due to the ever-increasing energy demand and the public concern about global warming and climate change, much effort has been focused on the diffusion of environmentally friendly renewable energy sources, posing significant challenges to the planning and operation of the existing power networks [PKK11]. Traditionally, electricity is mostly produced in large power plants, transported over long distances via high voltage transmission networks and then distributed to end-users through medium and low voltage distribution networks. The latter have been conceived as networks with only unidirectional power flows to satisfy the end-user electrical demand, by controlling the supply. However, due to the increased share of volatile and unpredictable sources, like wind and solar energy, the uncertainty of the generation side needs to be managed as well. For this reason, the physical nature of the grid poses unique and difficult challenges. It is indeed well known that when several distributed generation units are interconnected to each other, issues such as voltage and frequency deviations arise together with protections problems [WW08]. In this context, in order to integrate different types of renewable energy sources and, in addition, electrify remote areas, the so-called microgrids have been proposed as a new concept of electric power networks [LSH10, Las02]. However, regulating the frequency to its nominal value even in traditional power systems is still challenging because current implementations are not adequate to deal with an increasing share of renewable energy sources [ADGS16]. Furthermore, the collective behaviour of the network implies coordination among the individual agents. This requires the development of novel decentralized and distributed control schemes that exploit the widely distributed sensors and actuators. To ensure high reliability of the electrical system even in presence of model uncertainties, nonlinearity, unpredictable demand dynamics and unbalanced loads, it becomes necessary to adopt advanced robust control techniques [ABK+93]. This work particulary contributes to the establishment of system theoretical properties of the physical power network (both microgrids and traditional power plants). This enables the design of decentralized and distributed controllers that improve the stability of the network, while increasing the economic efficiency of its operation.

1.1 Challenges

In this thesis, the following challenges are addressed:

- the design of robust control strategies of sliding mode type for nonlinear uncertain systems characterized by unknown uncertainty bounds or quantized uncertainty, while guaranteeing chattering alleviation;
- the design of event-triggered sliding mode control strategies for networked control systems capable of preventing the possible congestion of the network, taking into account delayed transmissions and guaranteeing the avoidance of the notorious Zeno behaviour;
- the design of robust sliding modes for the load frequency control in traditional power systems aimed at minimizing the generation costs or scheduling the power flows, while dealing with the increasing diffusion of renewable energy sources;
- the design of robust sliding mode control strategies for islanded AC and DC microgrids including buck and boost power converters, in order to encourage the diffusion of renewable energy sources.

1.2 Contributions

In this thesis we present methods and results that lead to the following main contributions.

Contribution 1.1 (Adaptive Suboptimal Second Order Sliding Mode Control). The proposed algorithm allows to relax the common assumption on the knowledge of the bounds of the uncertainty. Four adaptive strategies are designed and analysed. In the first two strategies, the control amplitude is continuously adjusted, so as to arrive at dominating the effect of the uncertainty on the controlled system. When a suitable control amplitude is attained, the origin of the state space of the auxiliary system becomes attractive. In the other two strategies, a suitable blend between two components, one mainly working during the reaching phase, the other being the predominant one in a vicinity of the sliding manifold, is generated, so as to reduce the control amplitude in steady state.

Contribution 1.2 (Second Order Sliding Mode Control with Quantized Uncertainty). The proposed algorithm extends the result published in the literature for second order systems with optimal reaching. The novelty of the proposed approach is the design of a nonsmooth switching line, based on the quantization of the uncertainties affecting the system. The quantized uncertainty levels allow one to define nested box sets in the auxiliary state space and select suitable control amplitudes for each set, in order to guarantee the convergence of the system state to the sliding manifold in a finite time. The proposed algorithm is theoretically analyzed, proving the existence of an upperbound of the reaching time to the origin.

Contribution 1.3 (Practical Sliding Modes in Networked Control Systems). The proposed approaches are based on novel sliding mode control strategies of event-triggered type for a class of nonlinear uncertain systems. By virtue of its event-triggered nature, the proposed control strategies are appropriate for networked control systems (feedback systems including communication networks). The objective of the proposed control schemes is indeed to reduce the number of data transmissions over the communication network, in order to avoid problems typically due to the network congestion such as jitter and packet loss. In particular, an event-triggered sliding mode and an event-triggered second order sliding mode control schemes are designed for a class of nonlinear uncertain networked control systems, guaranteeing satisfactory performance of the controlled system even in presence of delayed transmissions, and avoiding the notorious Zeno behaviour.

Contribution 1.4 (Sliding Mode Control for Power Systems). We study a nonlinear power network partitioned into control areas, where each area is modelled by an equivalent generator including voltage and second order turbine-governor dynamics. The proposal is a passivity based design of distributed sliding modes for optimal load frequency control in power networks, where besides frequency regulation also minimization of generation costs is robustly achieved (economic dispatch). We propose also an energy function based design of decentralized sliding modes for automatic generation control, where frequency regulation is achieved, and power flows are controlled towards their desired values. A significant contribution is given by the design of a novel sliding mode observer-based scheme to estimate and reconstruct the unmeasured state in power networks including hydroelectric and thermal power plants.

Contribution 1.5 (Sliding Mode Control for Microgrids). We study the model of both AC and DC microgrids partitioned into distributed generation units and local loads. In particular we propose robust decentralized control strategies of sliding mode type to regulate the voltage of each node of an AC microgrid. A novel robust distributed control algorithm for the voltage regulation in buck-based DC microgrids is proposed, exploiting a communication network to achieve current sharing using a consensus-like algorithm. Finally, a robust decentralized control scheme for voltage regulation in boost-based DC microgrids is proposed and satisfactorily validated through experimental tests on a real DC microgrid test facility.

1.3 Outline of the Thesis

This thesis consists of three main parts. Part I, focuses on the design of new sliding mode control strategies for a class of nonlinear uncertain systems characterized by unknown uncertainty bounds, quantized uncertainty and the presence of a communication network in the control loop, respectively. Part II and Part III rely on the design of robust sliding mode control schemes for traditional power systems and emerging microgrids, respectively. This thesis is the collection of several research works. The chapters are based on lecture notes, journal or conference articles, which are either published or currently under review.

Part I

Chapter 2

This chapter is based on the lecture notes prepared by Antonella Ferrara for the Ph.D. School on *Sliding Mode Control* held at the Politecnico di Milano in January 2014. Michele Cucuzzella attended that school as a master student. Moreover, some paragraphs of this chapter are part of the book *Optimization Based Advanced Sliding Mode Control*, authored by Antonella Ferrara, Gian Paolo Incremona and Michele Cucuzzella, that will appear in 2018. In this chapter the basic concepts of Sliding Mode Control are outlined.

Chapter 3

This chapter addresses Contributions 1.1 and 1.2. It is mainly based on the following publications:

[ICF16] G. P. Incremona, M. Cucuzzella, and A. Ferrara. Adaptive suboptimal second order sliding mode control for microgrids. *International Journal of Control*, 89(9):1849–1867, Jan. 2016.

[ICF17] G. P. Incremona, M. Cucuzzella, and A. Ferrara. Second order sliding mode control for nonlinear affine systems with quantized uncertainty. *Automatica*, 86:46–52, Dec. 2017.

In this chapter the basic concepts of higher order sliding mode control are recalled, and new control algorithms of adaptive and switched nature are presented and theoretically analyzed, respectively.

Chapter 4

This chapter addresses Contribution 1.3. It is mainly based on the following publications:

[CF18] M. Cucuzzella, and A. Ferrara. Practical second order sliding modes in single-loop networked control of nonlinear systems", *Automatica*, 89:235–240, Mar. 2018.

[FC18] A. Ferrara and M. Cucuzzella. Event-triggered sliding mode control strategies for a class of nonlinear uncertain systems. *New perspectives and applications of modern control theory*, eds: J. B. Clempner, W. Yu, Springer International Publishing, Chapter 16:397–425, 2018.

[CF16] M. Cucuzzella, and A. Ferrara. Event-triggered second order sliding mode control of nonlinear uncertain systems. *Proc. European Control Conference*, pages 295–300, Aalborg, Denmark, June 2016.

[CIF16] M. Cucuzzella, G. P. Incremona, A. Ferrara. Event-triggered sliding mode control algorithms for uncertain systems: experimental assessment. *Proc. American Control Conference*, 6549–6554, Boston, MA, USA, July 2016.

In this chapter, the concept of event-triggered control is recalled and combined with sliding mode controllers, taking into account delayed transmissions and guaranteeing the avoidance of the notorious Zeno behaviour.

Part II

Chapter 5

This chapter addresses Contribution 1.4. It is mainly based on the following publications:

[TCDPvdSF] S. Trip, M. Cucuzzella, C. De Persis, A. van der Schaft, and A. Ferrara. Passivity based design of sliding modes for optimal load frequency control. *Transactions on Control Systems Technology.* SECOND REVIEW RUN.

[RCF17] G. Rinaldi, M. Cucuzzella, and A. Ferrara. Third order sliding mode observer-based approach for distributed optimal load frequency control. *IEEE Control Systems Letters* , 1(2):215–220, June 2017.

[CTDPF17] M. Cucuzzella, S. Trip, C. De Persis and A. Ferrara. Distributed second order sliding modes for optimal load frequency control. *Proc. American Control Conference*, pages 3451–3456, Seattle, WA, USA, May 2017.

In this chapter a passivity based design of distributed sliding modes is proposed for optimal load frequency control in power networks, where besides frequency regulation also minimization of generation costs is achieved (economic dispatch). The stability of the power network is theoretically analyzed.

Chapter 6

This chapter addresses Contribution 1.4. It is mainly based on the paper:

[TCFDP17] S. Trip, M. Cucuzzella, A. Ferrara and C. De Persis. An energy function based design of second order sliding modes for automatic generation control. *Proc. 20th IFAC World Congress*, pages 12118–12123, Toulouse, France, July 2017

In this chapter an energy function based design of decentralized sliding modes is proposed for automatic generation control in power networks, where frequency regulation is achieved, and power flows are controlled towards their desired values. The stability of the power network is theoretically analyzed.

Chapter 7

This chapter addresses Contribution 1.4. It is mainly based on the paper:

[RCF] G. Rinaldi, M. Cucuzzella, and A. Ferrara. Sliding mode observers for a network of thermal and hydroelectric power plants. *Automatica.* SECOND REVIEW RUN.

In this chapter the design of a novel sliding mode observer-based scheme to estimate and reconstruct the unmeasured state variables in power networks including hydroelectric and thermal power plants is presented and theoretically analyzed.

Part III

Chapter 8

This chapter addresses Contribution 1.5. It is mainly based on the following publications:

[CIF15a] M. Cucuzzella, G. P. Incremona, and A. Ferrara. Design of robust higher order sliding mode control for microgrids. *IEEE Journal on Emerging and Selected Topics in Circuits and Systems*, 5(3):393–401, Sept. 2015.

[CIF17a] M. Cucuzzella, G. P. Incremona, and A. Ferrara. Decentralized sliding mode control of islanded ac microgrids with arbitrary topology. *IEEE Transactions on Industrial Electronics*, 64(8):6706–6713, Apr. 2017.

[CIF15b] M. Cucuzzella, G. P. Incremona, and A. Ferrara. Master-slave second order sliding mode control for microgrids. *Proc. American Control Conference*, pages 5188–5193, Chicago, IL, USA, July 2015.

[CIF15c] M. Cucuzzella, G. P. Incremona, and A. Ferrara. Third order sliding mode voltage control in microgrid. *Proc. European Control Conference*, pages 2384–2389, Linz, Austria, July 2015.

In this chapter, a robust decentralized sliding mode control scheme for voltage regulation in islanded AC microgrids is proposed and theoretically analyzed, proving the finite time convergence to the desired voltages, and the asymptotic stability of the whole microgrid system.

Chapter 9

This chapter addresses Contribution 1.5. It is mainly based on the following publications:

[CTDPFvdS] M. Cucuzzella, S. Trip, C. De Persis, X. Cheng, A. Ferrara, and A. van der Schaft. A robust consensus algorithm for current sharing and voltage regulation in dc microgrids. *Transactions on Control Systems Technology.* SECOND REVIEW RUN.

[CRCF17] M. Cucuzzella, S. Rosti, A. Cavallo and A. Ferrara. Decentralized sliding mode voltage control in dc microgrids. *Proc. American Control Conference*, pages 3445–3450, Seattle, WA, USA, May 2017.

[TCDPCF] S. Trip, M. Cucuzzella, C. De Persis, X. Cheng and A. Ferrara. Sliding modes for voltage regulation and current sharing in dc microgrids. *Proc. American Control Conference*, Milwaukee, WI, USA, June 2018. SUBMITTED.

In this chapter, a novel distributed control algorithm is proposed for current sharing and voltage regulation in buck-based DC microgrids. The proposed control scheme is formally analyzed, proving the achievement of proportional current sharing, while guaranteeing that the weighted average voltage of the microgrid is identical to the weighted average of the voltage references.

Chapter 10

This chapter addresses Contribution 1.5. It is mainly based on the following publications:

[CLTRSF] M. Cucuzzella, R. Lazzari, S. Trip, S. Rosti, C. Sandroni, and A. Ferrara. Sliding mode voltage control of boost-based DC microgrids. *Control Engineering Practice*. PROVISIONALLY ACCEPTED.

[CLTSF] M. Cucuzzella, R. Lazzari, S. Trip, C. Sandroni, and A. Ferrara. A decentralized second order sliding mode voltage control for DC microgrids application: experimental assessment. *Proc. European Control Conference*, Limassol, Cyprus, June 2018. SUBMITTED.

In this chapter, a robust decentralized control scheme for voltage regulation in boost-based DC microgrids is proposed and theoretically analyzed, proving the local asymptotic stability of the whole microgrid system. Satisfactory experimental tests on a real DC microgrid test facility validate the theoretical results.

Chapter 11

In this chapter, some conclusions and directions for future research are given.

1.4 List of Publications

The publications list of Michele Cucuzzella is hereafter reported.

Journal Papers

[CIF15a] M. Cucuzzella, G. P. Incremona, and A. Ferrara. Design of robust higher order sliding mode control for microgrids. *IEEE Journal on Emerging and Selected Topics in Circuits and Systems*, 5(3):393–401, Sept. 2015.

[ICF16] G. P. Incremona, M. Cucuzzella, and A. Ferrara. Adaptive suboptimal second order sliding mode control for microgrids. *International Journal of Control*, 89(9):1849–1867, Jan. 2016.

[CIF17a] M. Cucuzzella, G. P. Incremona, and A. Ferrara. Decentralized sliding mode control of islanded ac microgrids with arbitrary topology. *IEEE Transactions on Industrial Electronics*, 64(8):6706–6713, Apr. 2017.

[RCF17] G. Rinaldi, M. Cucuzzella, and A. Ferrara. Third order sliding mode observer-based approach for distributed optimal load frequency control. *IEEE Control Systems Letters* , 1(2):215–220, June 2017.

[ICF17] G. P. Incremona, M. Cucuzzella, and A. Ferrara. Second order sliding mode control for nonlinear affine systems with quantized uncertainty. *Automatica*, 86:46–52, Dec. 2017.

[CF18] M. Cucuzzella, and A. Ferrara. Practical second order sliding modes in single-loop networked control of nonlinear systems", *Automatica*, 89:235–240, Mar. 2018.

[CLTRSF] M. Cucuzzella, R. Lazzari, S. Trip, S. Rosti, C. Sandroni, and A. Ferrara. Sliding mode voltage control of boost-based DC microgrids. *Control Engineering Practice*. PROVISIONALLY ACCEPTED.

[CTDPFvdS] M. Cucuzzella, S. Trip, C. De Persis, X. Cheng, A. Ferrara, and A. van der Schaft. A robust consensus algorithm for current sharing and voltage regulation in dc microgrids. *Transactions on Control Systems Technology*. SECOND REVIEW RUN.

[TCDPvdSF] S. Trip, M. Cucuzzella, C. De Persis, A. van der Schaft, and A. Ferrara. Passivity based design of sliding modes for optimal load frequency control. *Transactions on Control Systems Technology*. SECOND REVIEW RUN.

[RCF] G. Rinaldi, M. Cucuzzella, and A. Ferrara. Sliding mode observers for a network of thermal and hydroelectric power plants. *Automatica*. SECOND REVIEW RUN.

Books

[FIC18] A. Ferrara, G. P. Incremona and M. Cucuzzella. *Optimization Based Advanced Sliding Mode Control*. SIAM. EXPECTED TO APPEAR 2018.

Book Chapters

[FC18] A. Ferrara and M. Cucuzzella. Event-triggered sliding mode control strategies for a class of nonlinear uncertain systems. *New perspectives and applications of modern control theory*, eds: J. B. Clempner, W. Yu, Springer International Publishing, Chapter 16:397–425, 2018.

International Conference Papers

[CIF15b] M. Cucuzzella, G. P. Incremona, and A. Ferrara. Master-slave second order sliding mode control for microgrids. *Proc. American Control Conference*, pages 5188–5193, Chicago, IL, USA, July 2015.

[CIF15c] M. Cucuzzella, G. P. Incremona, and A. Ferrara. Third order sliding mode voltage control in microgrid. *Proc. European Control Conference*, pages 2384–2389, Linz, Austria, July 2015.

[CF16] M. Cucuzzella, and A. Ferrara. Event-triggered second order sliding mode control of nonlinear uncertain systems. *Proc. European Control Conference*, pages 295–300, Aalborg, Denmark, June 2016.

[CIF16] M. Cucuzzella, G. P. Incremona, A. Ferrara. Event-triggered sliding mode control algorithms for uncertain systems: experimental assessment. *Proc. American Control Conference*, 6549–6554, Boston, MA, USA, July 2016.

[CIGF16] M. Cucuzzella, G. P. Incremona, M. Guastalli and A. Ferrara. Sliding mode control for maximum power point tracking of photovoltaic inverters in microgrids. *55th IEEE Conference on Decision and Control*, pages 7294–7299, Las Vegas, NV, USA, Dec. 2016.

[CTDPF17] M. Cucuzzella, S. Trip, C. De Persis and A. Ferrara. Distributed second order sliding modes for optimal load frequency control. *Proc. American Control Conference*, pages 3451–3456, Seattle, WA, USA, May 2017.

[CRCF17] M. Cucuzzella, S. Rosti, A. Cavallo and A. Ferrara. Decentralized sliding mode voltage control in dc microgrids. *Proc. American Control Conference*, pages 3445–3450, Seattle, WA, USA, May 2017.

[TCFDP17] S. Trip, M. Cucuzzella, A. Ferrara and C. De Persis. An energy function based design of second order sliding modes for automatic generation control. *Proc. 20th IFAC World Congress*, pages 12118–12123, Toulouse, France, July 2017

[ICMF17] G. P. Incremona, M. Cucuzzella, L. Magni and A. Ferrrara. MPC with sliding mode control for the energy management system of microgrids. *Proc. 20th IFAC World Congress*, pages 7658–7663, Toulouse, France, July 2017.

[ICFM17] G. P. Incremona, M. Cucuzzella, A. Ferrara and L. Magni. Model predictive control and sliding mode control for current sharing in microgrids. *56th IEEE Conference on Decision and Control* pages –, Melbourne, Australia, Dec. 2017.

[TCDPCF] S. Trip, M. Cucuzzella, C. De Persis, X. Cheng and A. Ferrara. Sliding modes for voltage regulation and current sharing in dc microgrids. *Proc. American Control Conference*, Milwaukee, WI, USA, June 2018. SUBMITTED.

[CLTSF] M. Cucuzzella, R. Lazzari, S. Trip, C. Sandroni, and A. Ferrara. A decentralized second order sliding mode voltage control for DC microgrids application: experimental assessment. *Proc. European Control Conference*, Limassol, Cyprus, June 2018. SUBMITTED.

PART 1

Part I

VARIABLE STRUCTURE AND SLIDING MODE CONTROL

2

Sliding Mode Control

Abstract. In this chapter the basic concepts of Sliding Mode Control are outlined. The major properties of this control approach are discussed and some examples are also reported. The robustness properties against the uncertainties and nonlinearities affecting the controlled system are analyzed, and the concept of approximability is discussed. This chapter is based on the lecture notes prepared by Antonella Ferrara for the Ph.D. School on *Sliding Mode Control* held at the Politecnico di Milano in January 2014. Michele Cucuzzella attended that school as a master student. Moreover, some paragraphs of this chapter are part of the book *Optimization Based Advanced Sliding Mode Control*, authored by Antonella Ferrara, Gian Paolo Incremona and Michele Cucuzzella, that will appear in 2018.

2.1 Sliding Motion and Sliding Mode

Sliding Mode Control (SMC) is a nonlinear control method, belonging to the framework of Variable Structure Control (VSC), that adjusts the dynamics of systems by the application of a switching control [SL91, Utk92, Kha96, ES98]. SMC methodology allows the models to be imprecise, where imprecisions come from structured (or parametric) and/or unstructured (e.g. unmodeled dynamics) uncertainties. The basic concept is the design of a controller ensuring finite-time arrival of the state space trajectory to a suitable surface in both its sides. This implies the generation of the so-called “sliding motion” on that surface. The latter is named *switching surface* and the sliding motion can occur on one or more than one surfaces defined in the state space of the controlled system. When the sliding motion is contemporarily enforced on all the defined surfaces, the controlled system is said to be in “sliding mode”.

Given some initial conditions $\boldsymbol{x}_0 = \boldsymbol{x}(t_0)$, the goal of SMC is to steer the state trajectories of the controlled system to the so-called *sliding subspace* or *sliding manifold*, i.e., the intersection of the switching surfaces, in order to enforce a sliding mode (see Fig. 2.1 for an illustrative example). If this is the case, the states belong to the sliding subspace, and the controlled *equivalent system* features an order reduction. Moreover, the dynamic performance can be arbitrarily specified by suitably selecting the sliding manifold, and it is invariant with respect to a significant class of parameter uncertainties and disturbances.

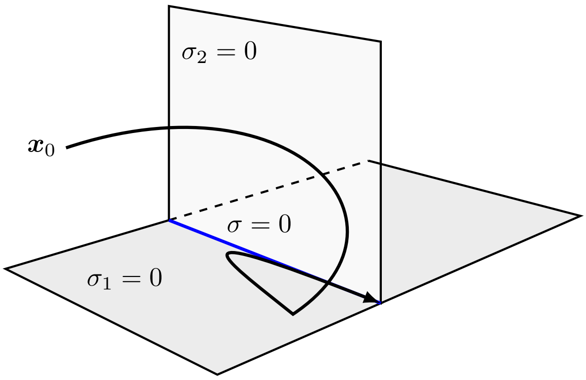

Fig. 2.1. Schematic view of "sliding motion" and "sliding mode" concepts: given the initial conditions $\boldsymbol{x}_0$, the state trajectory is steered to the sliding manifold $\boldsymbol{\sigma} = \mathbf{0}$ given by the intersection of the switching surfaces $\sigma_1 = 0$, $\sigma_2 = 0$.

2.1.1 Design of a Sliding Mode Control

The design of SMC consists of two phases:

- the design of the sliding manifold;
- the design of the control law.

The sliding manifold is usually designed so as to obtain the desired dynamics of the controlled system while this is in sliding mode. Specifically, the equivalent system has to be asymptotically stable so that the state trajectories of the controlled system converge to the origin of the state space. The corresponding control law is chosen in order to enforce a sliding mode.

For the readers' convenience, a simple example is hereafter reported. Consider the double integrator

$$\begin{bmatrix} \dot{x}_1 \\ \dot{x}_2 \end{bmatrix} = \begin{bmatrix} 0 & 1 \\ 0 & 0 \end{bmatrix} \begin{bmatrix} x_1 \\ x_2 \end{bmatrix} + \begin{bmatrix} 0 \\ 1 \end{bmatrix} u, \tag{2.1}$$

where $\boldsymbol{x} \in \mathbb{R}^2$ is the state vector, $u \in \mathbb{R}$ is the input variable such that $|u| \leq 1$. For the sake of simplicity, the dependence of all the variables on time t is omitted, when obvious. The sliding manifold is selected as a linear combination of the state as

$$\sigma = c_1 x_1 + x_2 = 0, \tag{2.2}$$

with c_1 positive constant, while the control law on $\sigma = 0$ is discontinuous and chosen as

$$u = \begin{cases} -1 & \text{if } \sigma > 0 \\ 1 & \text{if } \sigma < 0 \; . \end{cases} \tag{2.3}$$

The goal is to steer the state trajectories to the sliding manifold $\sigma = 0$. If the sliding mode is enforced, i.e., $\dot{x}_1 + c_1 x_1 = 0$, the system dynamics becomes

$$x_1(t) = x_1(t_r)\mathrm{e}^{-c_1(t-t_r)}, \tag{2.4}$$

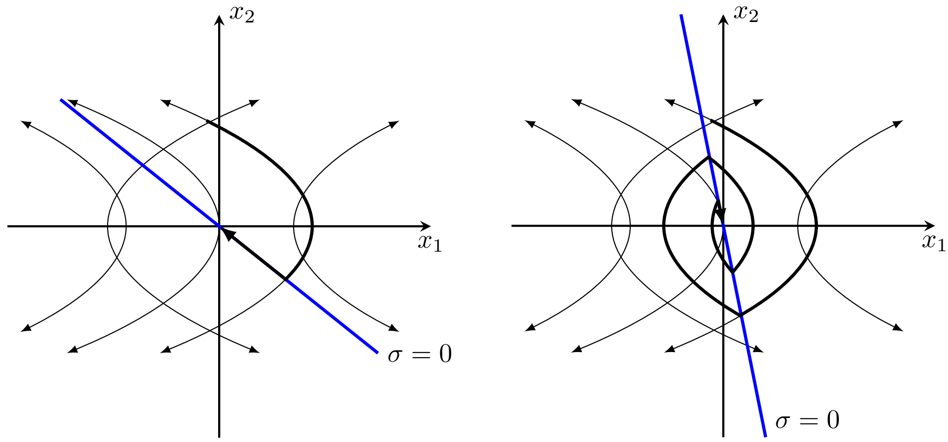

(a) c_1 small (b) c_1 large

Fig. 2.2. Schematic view of the state trajectory in case of a double integrator. **(a)** c_1 is selected small. **(b)** c_1 is selected large.

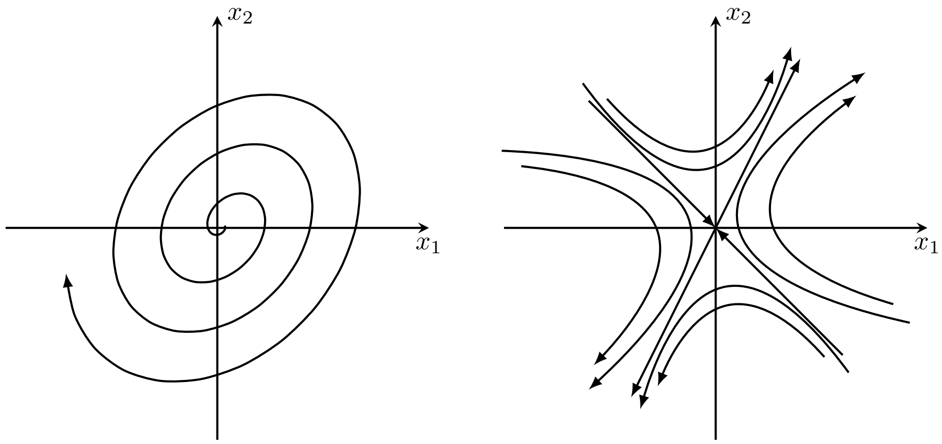

(a) $\kappa(x_1) = -3$ (b) $\kappa(x_1) = 2$

Fig. 2.3. Schematic view of the state trajectory in case of unstable system. **(a)** The control law is $u = 2x_1$. **(b)** The control law is $u = -3x_1$.

where t_r is the so-called *reaching time* instant, that is the time after which the sliding manifold $\sigma = 0$ is attained. System (2.4) is a reduced order system with desired dynamics. The state trajectory depends indeed on the amplitude of the constant value c_1. Particularly, one has that if c_1 is small the trajectory follows a parabola arc, and then, it slides on the line $\sigma = 0$ towards the origin (see Fig. 2.2 a). If c_1 is large, the state trajectory follows a sequence of decreasing parabola arcs, and then converges to the origin of the state space (see Fig. 2.2 b).

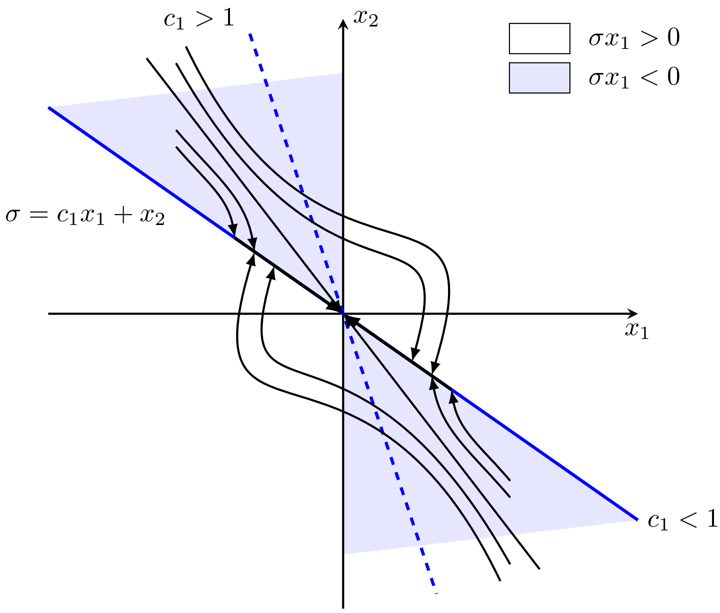

Fig. 2.4. State trajectory of the closed-loop system, and sliding manifold when $c_1 < 1$ (solid blue line) and $c_1 > 1$ (dashed blue line).

The previous example shows that the state trajectory depends on the parameter c_1. Now, it is worth investigating what happens if the system is unstable. Consider system

$$\begin{bmatrix} \dot{x}_1 \\ \dot{x}_2 \end{bmatrix} = \begin{bmatrix} 0 & 1 \\ 1 & 2 \end{bmatrix} \begin{bmatrix} x_1 \\ x_2 \end{bmatrix} + \begin{bmatrix} 0 \\ 1 \end{bmatrix} u, \tag{2.5}$$

where, in this case, the control input u depends on the state feedback x_1 as follows

$$u = \kappa(x_1)x_1, \ \kappa(x_1) = \begin{cases} -3 & \text{if } \sigma x_1 > 0 \\ 2 & \text{if } \sigma x_1 < 0, \end{cases} \tag{2.6}$$

where σ is selected as in (2.2). It can be proved that the controlled system has an unstable focus if $\kappa(x_1) = -3$, and a saddle point if $\kappa(x_1) = 2$, as illustrated in Fig. 2.3. Moreover, the combination of these two control actions ensures the convergence towards the origin, which becomes an asymptotically stable equilibrium point of the state space. Particularly, as shown in Fig. 2.4, a sliding mode is enforced only if $c_1 < 1$.

2.2 Preliminaries on Sliding Mode

In case of SMC, the considered class of systems is that of nonlinear systems with respect to the state, and linear with respect to the control variable, i.e.,

$$\dot{\boldsymbol{x}}(t) = \boldsymbol{f}(\boldsymbol{x}, t) + \boldsymbol{B}(\boldsymbol{x}, t)\boldsymbol{u}(t), \tag{2.7}$$

where $\boldsymbol{x} \in \mathbb{R}^n$, $\boldsymbol{u} \in \mathbb{R}^m$, while $\boldsymbol{f} : \mathbb{R}^n \times \mathbb{R} \to \mathbb{R}^n$ and $\boldsymbol{B} : \mathbb{R}^n \times \mathbb{R} \to \mathbb{R}^{n \times m}$ are smooth bounded vector fields.

2.2.1 The Class of Systems

The design and the analysis of a SMC are simpler if the nonlinear considered system is expressed according to one of the canonical forms, hereafter recalled for the readers' convenience.

2.2.1.1 Reduced Form

In the canonical reduced form, the state vector $\boldsymbol{x}$ is split into $\boldsymbol{x}_1 \in \mathbb{R}^{n-m}$ and $\boldsymbol{x}_2 \in \mathbb{R}^m$. Then, if the matrix $\boldsymbol{B}(\boldsymbol{x}, t)$ is such that

$$\boldsymbol{B}(\boldsymbol{x}, t) = \begin{bmatrix} \mathbf{0}_{(n-m)\times m} \\ \boldsymbol{B}^*(\boldsymbol{x}, t) \end{bmatrix}, \tag{2.8}$$

where $\mathbf{0}_{(n-m)\times m} \in \mathbb{R}^{(n-m)\times m}$ is a matrix with null entries and $\boldsymbol{B}^* : \mathbb{R}^n \times \mathbb{R} \to \mathbb{R}^{m\times m}$ is an invertible matrix, system (2.7) can be expressed as

$$\begin{aligned} \dot{\boldsymbol{x}}_1(t) &= \boldsymbol{A}_1(\boldsymbol{x}, t) \\ \dot{\boldsymbol{x}}_2(t) &= \boldsymbol{A}_2(\boldsymbol{x}, t) + \boldsymbol{B}^*(\boldsymbol{x}, t)\boldsymbol{u}(t), \end{aligned} \tag{2.9}$$

where $\boldsymbol{A}_1 : \mathbb{R}^n \times \mathbb{R} \to \mathbb{R}^{n-m}$ and $\boldsymbol{A}_2 : \mathbb{R}^n \times \mathbb{R} \to \mathbb{R}^m$.

2.2.1.2 Controllability Form

System (2.7) is split into m subsystems each of which is expressed in the canonical controllability form. Consider the state vector expressed as

$$\boldsymbol{x} = \begin{bmatrix} \boldsymbol{x}_1 \\ \vdots \\ \boldsymbol{x}_m \end{bmatrix}, \tag{2.10}$$

where $\boldsymbol{x}_i \in \mathbb{R}^{n_i}$, $i = 1, \ldots, m$ and $\sum_{i=1}^m n_i = n$. Assume that each subsystem is as follows:

$$\dot{\boldsymbol{x}}_i = \boldsymbol{A}_i\boldsymbol{x}_i + \boldsymbol{f}_i(\boldsymbol{x}) + \boldsymbol{b}_i(\boldsymbol{x})\boldsymbol{u}, \tag{2.11}$$

where $\boldsymbol{A}_i \in \mathbb{R}^{n_i\times n_i}$ is

$$\boldsymbol{A}_i = \begin{bmatrix} \mathbf{0}_{n_i-1} & \mathbb{I}_{n_i-1} \\ 0 & \mathbf{0}_{n_i-1}^T \end{bmatrix}, \tag{2.12}$$

with $\mathbb{I}_{n_i-1} \in \mathbb{R}^{(n_i-1)\times(n_i-1)}$ being the identity matrix, while $\boldsymbol{f}_i(\boldsymbol{x}) = [0, \ldots, 0, f_{i0}(\boldsymbol{x})]^T \in \mathbb{R}^{n_i}$, with $f_{i0}(\boldsymbol{x}) \in \mathbb{R}$, and $\boldsymbol{b}_i(\boldsymbol{x}) \in \mathbb{R}^{n_i\times m}$ is

$$\boldsymbol{b}_i(\boldsymbol{x}) = \begin{bmatrix} \mathbf{0}_{(n_i-1)\times m} \\ \boldsymbol{b}_{i0}(\boldsymbol{x}) \end{bmatrix}, \tag{2.13}$$

where $\boldsymbol{b}_{i0}(\boldsymbol{x}) \in \mathbb{R}^{1\times m}$. The whole system results in being equal to

$$\dot{\boldsymbol{x}} = \boldsymbol{A}\boldsymbol{x} + \boldsymbol{f}(\boldsymbol{x}) + \boldsymbol{b}(\boldsymbol{x})\boldsymbol{u}, \tag{2.14}$$

where $\boldsymbol{A} = \mathrm{diag}\{\boldsymbol{A}_1, \ldots, \boldsymbol{A}_m\}$, $\boldsymbol{f}(\boldsymbol{x}) = \left[\boldsymbol{f}_1^T(\boldsymbol{x}), \cdots, \boldsymbol{f}_m^T(\boldsymbol{x})\right]^T$ and $\boldsymbol{b}(\boldsymbol{x}) = \left[\boldsymbol{b}_1^T(\boldsymbol{x}), \cdots, \boldsymbol{b}_m^T(\boldsymbol{x})\right]^T$.

2.2.1.3 Decoupled Input-Output Form

Consider a Single-Input Single-Output (SISO) system with output $y = c(\boldsymbol{x})$. Let r denote the *relative degree* of the system, i.e., the minimum order r of the time derivative $y^{(r)}$ of the output in which the control u explicitly appears. In case of Multi-Input Multi-Output (MIMO) system, by considering the generic output y_i, $i = 1, \ldots, m$, the relative degree r_i is the minimum order r_i of the time derivative $y_i^{(r_i)}$ in which one of the components of the control $\boldsymbol{u}$ explicitly appears. The system total relative degree is $r = r_1 + \cdots + r_m$.

At this point, two different cases can be considered: $r = n$ and $r < n$, n being the system order. In the first case, the system

$$\begin{aligned} \dot{\boldsymbol{x}} &= \boldsymbol{A}(\boldsymbol{x}) + \boldsymbol{B}(\boldsymbol{x})\boldsymbol{u} \\ \boldsymbol{y} &= \boldsymbol{c}(\boldsymbol{x}) \end{aligned} \tag{2.15}$$

can be represented by m differential decoupled equations of the following type

$$\begin{aligned} y_i^{(r_i)} = {} & f_i(y_1, \ldots, y_1^{(r_1-1)}, \ldots, y_m, \ldots, y_m^{(r_m-1)}) \\ & + g_i(y_1, \ldots, y_1^{(r_1-1)}, \ldots, y_m, \ldots, y_m^{(r_m-1)})u_i \,. \end{aligned} \tag{2.16}$$

If instead the relative degree is such that $r < n$ the so-called *normal form* is considered.

2.2.1.4 Normal Form

Consider $r < n$ and let $z_{i,j}$, $i = 1, \ldots, m$ and $j = 1, \ldots, r_i - 1$, denote the m outputs $y_i = c_i(\boldsymbol{x}, \boldsymbol{u})$ and their time derivatives up to order $j = r_i - 1$. The latter are r *external* variables. Let η_k, $k = 1, \ldots, n - r$ be the *internal* variables, the dynamics of which describe the *internal* behaviour of the system when input and initial conditions have been chosen in such a way as to keep the output identically zero. These dynamics, which are rather important in many of our developments, are called the *zero dynamics* of the system. The resulting system can be written in the following form

$$\begin{aligned} \dot{z}_{i,j} &= z_{i,j+1} \\ &\;\vdots \\ \dot{z}_{i,r_i} &= \alpha_i(\boldsymbol{z}, \boldsymbol{\eta}) + \sum_{k=1}^{m} \beta_{i,k}(\boldsymbol{z}, \boldsymbol{\eta}) u_k \\ \dot{\boldsymbol{\eta}} &= \boldsymbol{\gamma}(\boldsymbol{z}, \boldsymbol{\eta}), \end{aligned} \tag{2.17}$$

where α_i, $\beta_{i,k} : \mathbb{R}^{m\times(r_i-1)} \times \mathbb{R}^{n-r} \to \mathbb{R}$, and $\boldsymbol{\gamma} : \mathbb{R}^{m\times(r_i-1)} \times \mathbb{R}^{n-r} \to \mathbb{R}^{n-r}$.

2.2.2 The Control Signal

Also for the control signal it is possible to select different forms, hereafter reported.

2.2.2.1 Relè Form

In this case the control law is of the following type

$$u_i(t) = \begin{cases} u_i^+(\boldsymbol{x}, t) & \text{if } \sigma_i(\boldsymbol{x}) > 0 \\ u_i^-(\boldsymbol{x}, t) & \text{if } \sigma_i(\boldsymbol{x}) < 0, \end{cases} \tag{2.18}$$

with $i = 1, \ldots, m$ and $\sigma_i(\boldsymbol{x}) = 0$ being the i-th switching surface associated with the sliding subspace belonging to $\mathbb{R}^{n-m}$, and $\boldsymbol{\sigma}(\boldsymbol{x}) = [\sigma_1(\boldsymbol{x}), \ldots, \sigma_m(\boldsymbol{x})]^T$ being the sliding variable vector. During the design phase the values u_i^+, u_i^- and the vector $\boldsymbol{\sigma}$ have to be selected.

2.2.2.2 Augmented Control

By considering the so-called *equivalent control* $u_{eq,i}$ (see Subsection 2.2.6.2), obtained by posing the first time derivatives of the sliding variables $\dot{\sigma}_i$ equal to zero, one has the following control law

$$u_i(t) = u_{eq,i}(t) + u_{N,i}(t), \tag{2.19}$$

with $u_{N,i}$ of relè type.

2.2.2.3 State Feedback Control with Switching Gain

The state feedback control has the form

$$\boldsymbol{u}(t) = \boldsymbol{\Psi}_i(\boldsymbol{x})\boldsymbol{x}(t), \tag{2.20}$$

with $\boldsymbol{\Psi} \in \mathbb{R}^{m\times n}$ and entries

$$\psi_{i,j} = \begin{cases} \alpha_{i,j} & \text{if } \sigma_i(\boldsymbol{x})x_j > 0 \\ \beta_{i,j} & \text{if } \sigma_i(\boldsymbol{x})x_j < 0, \end{cases} \tag{2.21}$$

with $i = 1, \ldots, m$ and $j = 1, \ldots, n$.

2.2.2.4 Unit Vector Control

In case of unit vector control, the control law is expressed as

$$u_i = \alpha_i \frac{\sigma_i(\boldsymbol{x})}{\|\boldsymbol{\sigma}(\boldsymbol{x})\|}, \tag{2.22}$$

where $\alpha_i \in \mathbb{R}$ and $\boldsymbol{\sigma}$ have to be selected.

2.2.2.5 Simplex Control

A way to extend the variable structure control strategy to the multi-input case is that based on a set of $m+1$ control vectors forming a simplex in $\mathbb{R}^m$, and on the corresponding switching of the controlled system among the control vectors (see Fig. 2.5). Specifically, the system state space is partitioned into $m+1$ non-overlapping (in the sense that the interiors are pairwise disjoint) regions, and within each region a particular control vector (among those of the simplex) is associated in such a way that the system trajectory is forced to slide on a pre-specified manifold [BFUZ97].

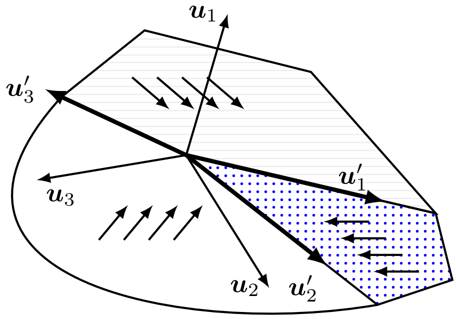

Fig. 2.5. Simplex in $\mathbb{R}^2$.

2.2.3 The Sliding Manifold

Although the sliding manifold $\boldsymbol{\sigma}(\boldsymbol{x}) = \mathbf{0}$ could be chosen as a nonlinear function of the state $\boldsymbol{x}$, it is common way to define the sliding manifold as linear combination of the states. In case of MIMO systems, it can be defined as

$$\boldsymbol{\sigma}(\boldsymbol{x}(t)) = \boldsymbol{C}\boldsymbol{x}(t) = \mathbf{0}, \tag{2.23}$$

where $\boldsymbol{\sigma} \in \mathbb{R}^m$ and the matrix $\boldsymbol{C} \in \mathbb{R}^{m \times n}$. In the following, the choice of the sliding manifold in case of systems in canonical form will be considered.

2.2.3.1 Reduced Form

In case of reduced form, as previously discussed, the state vector is split into two parts $\boldsymbol{x}_1$ and $\boldsymbol{x}_2$. Then, one has that

$$\boldsymbol{\sigma}(\boldsymbol{x}) = \boldsymbol{\sigma}(\boldsymbol{x}_1, \boldsymbol{x}_2) = \begin{bmatrix}\boldsymbol{C}_1 \ \boldsymbol{C}_2\end{bmatrix} \begin{bmatrix}\boldsymbol{x}_1 \\ \boldsymbol{x}_2\end{bmatrix} = \mathbf{0}, \tag{2.24}$$

where $\boldsymbol{C}_2$ is non singular. When the control system is in sliding mode, it exhibits the following dynamics

$$\begin{aligned} \boldsymbol{x}_2 &= -\boldsymbol{C}_2^{-1}\boldsymbol{C}_1\boldsymbol{x}_1 \\ \dot{\boldsymbol{x}}_1 &= \boldsymbol{A}_1(t, \boldsymbol{x}) = \boldsymbol{A}_1(t, \boldsymbol{x}_1, -\boldsymbol{C}_2^{-1}\boldsymbol{C}_1\boldsymbol{x}_1). \end{aligned} \tag{2.25}$$

Moreover, note that if $\boldsymbol{A}_1$ is linear, i.e.,

$$\dot{\boldsymbol{x}}_1 = \boldsymbol{A}_1(t, \boldsymbol{x}) = \boldsymbol{A}_{1,1}\boldsymbol{x}_1 + \boldsymbol{A}_{1,2}\boldsymbol{x}_2, \tag{2.26}$$

the equivalent (reduced order) dynamics results in being

$$\dot{\boldsymbol{x}}_1 = [\boldsymbol{A}_{1,1} - \boldsymbol{A}_{1,2}\boldsymbol{C}_2^{-1}\boldsymbol{C}_1]\boldsymbol{x}_1 = [\boldsymbol{A}_{1,1} + \boldsymbol{A}_{1,2}\boldsymbol{F}]\boldsymbol{x}_1, \tag{2.27}$$

where $\boldsymbol{F} = -\boldsymbol{C}_2^{-1}\boldsymbol{C}_1$. Assuming that the couple $(\boldsymbol{A}_{1,1}, \boldsymbol{A}_{2,2})$ is controllable, the desired dynamics of the system can be imposed by suitably choosing $\boldsymbol{F}$ (for instance, by poles assignment, optimal control, etc.).

2.2.3.2 Controllability Form

In case of controllability form, the system is partitioned into m subsystems, and the sliding variables can be chosen as

$$\sigma_i = \boldsymbol{c}_i^T \boldsymbol{x}_i, \tag{2.28}$$

where σ_i, $i = 1, \ldots, m$, is the i-th component of $\boldsymbol{\sigma} \in \mathbb{R}^m$. The problem to solve is that of finding $\boldsymbol{c}_i$ for each subsystem in order to make the controlled system asymptotically stable. The equivalent dynamics of the n_i-th component of vector $\boldsymbol{x}_i$ can be determined by posing $\sigma_i = 0$. Each equivalent subsystem is of order $n_i - 1$, while the associated polynomial has the elements of $\boldsymbol{c}_i$ as coefficients.

2.2.3.3 Decoupled Input-Output Form

Analogously to the previous case, the sliding manifold is chosen as

$$\sigma_i(\boldsymbol{x}_i) = (p + \lambda)^{n_i - 1} \boldsymbol{x}_i, \quad p := \frac{d}{dt}(\cdot), \tag{2.29}$$

where $\lambda > 0$, [SL91].

2.2.3.4 Normal Form

In the case of normal form, the so-called zero-dynamics, obtained by posing equal to zero the output and its derivatives, has to be asymptotically stable. Specifically, by choosing $\boldsymbol{y} = \boldsymbol{c}\boldsymbol{x}$, the zero-dynamics is written as

$$\begin{aligned} \boldsymbol{z} &= \boldsymbol{0} \\ \dot{\boldsymbol{\eta}} &= \boldsymbol{\gamma}(\boldsymbol{0}, \boldsymbol{\eta}) \ . \end{aligned} \tag{2.30}$$

Then, the sliding variable is chosen as

$$\sigma_i = \boldsymbol{c}_i^T \boldsymbol{z}_i, \tag{2.31}$$

with $i = 1, \ldots, m$, and $\boldsymbol{c}_i$ selected as for the case in the controllability form, that is, in order to assign the desired dynamics to the equivalent system of reduced order.

2.2.4 Existence Conditions

After having defined the sliding manifold it is necessary to ensure the existence of a siding mode. A sliding mode exists in a vicinity of the sliding manifold $\boldsymbol{\sigma} = \boldsymbol{0}$, if the tangent vector to the controlled system trajectory is always towards the sliding manifold. Specifically, the sliding mode is ideal if the trajectory of the controlled system is such that $\boldsymbol{\sigma}(t) = \boldsymbol{0}$, for any $t \geq t_r$. Note that, in practice, because of delays, hysteresis, sampling time, the system trajectory does not exactly reach the sliding manifold but switches around it (*chattering*, see Fig. 2.6).

The existence problem can be viewed as a stability problem. In particular, it is required that, given the initial conditions, the system trajectories reach and remain on the sliding

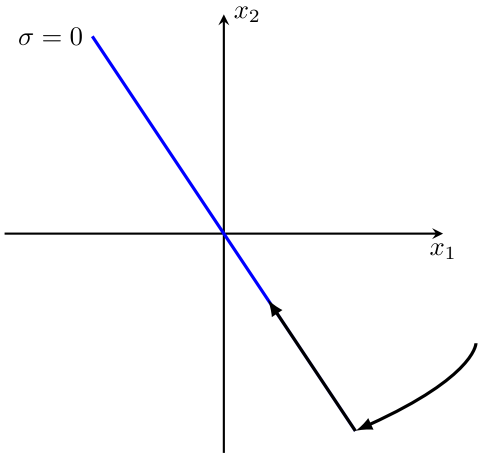

(a) ideal sliding mode

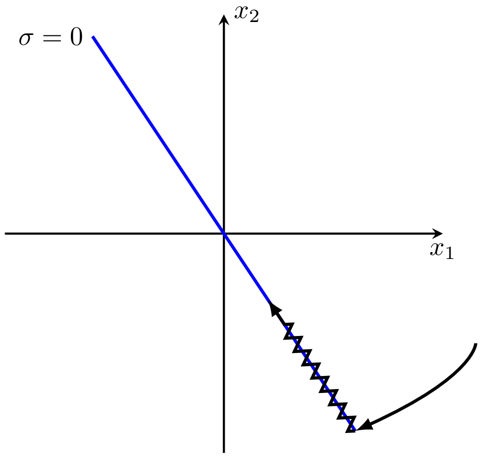

(b) sliding mode with chattering

Fig. 2.6. Schematic view of the state trajectory in case of sliding mode. **(a)** Ideal sliding mode. **(b)** Sliding mode with chattering.

manifold. The attractive domain can coincide with the whole state space, thus enforcing a *globally reachable sliding mode.*

According to the *Lyapunov's second method*, it is possible to prove the existence of a sliding mode by considering a positive definite *Lyapunov function*, $V(t, \boldsymbol{x})$, with negative first time derivative within the attractive region. In case of SISO system the Lyapunov function can be written as

$$V(t, \boldsymbol{x}) = \frac{1}{2}\sigma^2(\boldsymbol{x}) \ . \tag{2.32}$$

The first time derivative of (2.32) is computed as

$$\dot{V}(t, \boldsymbol{x}) = \sigma\dot{\sigma} < 0 \ . \tag{2.33}$$

Equation (2.33) represents the so-called *reachability condition*, which will be better discussed in the following.

2.2.5 Reachability Condition

An alternative way to express the reachability condition can be the following

$$\sigma\dot{\sigma} \leq -\gamma^2|\sigma| \tag{2.34}$$

that is

$$\dot{V}(t, \boldsymbol{x}) \leq -\gamma^2\sqrt{2V(t, \boldsymbol{x})} \ . \tag{2.35}$$

In this case it is possible to find an upperbound of the reaching time t_r by integrating (2.34) from t_0 to t_r, i.e.,

$$t_r \leq \frac{|\sigma(t_0)|}{\gamma^2} + t_0 \ . \tag{2.36}$$

The reachability condition, in case of MIMO systems, can be also expressed as

$$\dot{\boldsymbol{\sigma}} = -\boldsymbol{Q}\,\mathrm{sign}(\boldsymbol{\sigma}) - \boldsymbol{K}\boldsymbol{\phi}(\boldsymbol{\sigma}), \tag{2.37}$$

with $\boldsymbol{Q}$ and $\boldsymbol{K}$ being positive definite diagonal matrices, the discontinuous function $\mathrm{sign}(\boldsymbol{\sigma}) = [\mathrm{sign}(\sigma_1), \ldots, \mathrm{sign}(\sigma_m)]^T$, and $\boldsymbol{\phi}(\boldsymbol{\sigma}) = [\phi_1(\sigma_1), \ldots, \phi_m(\sigma_m)]^T$. Moreover, the scalar functions ϕ_i, $i = 1, \ldots, m$, satisfy the following condition

$$\sigma_i \phi_i(\sigma_i) > 0, \quad \sigma_i \neq 0, \tag{2.38}$$

with $i = 1, \ldots, m$. The matrix $\boldsymbol{Q}$ and function $\boldsymbol{\phi}$ can be chosen in three different ways on the basis of the rate that one would like to obtain during the reaching phase. More specifically, one has that in case of constant rate, $\boldsymbol{\sigma}$ is such that

$$\dot{\boldsymbol{\sigma}} = -\boldsymbol{Q}\,\mathrm{sign}(\boldsymbol{\sigma}) \tag{2.39}$$

or in case of constant rate and proportional component,

$$\dot{\boldsymbol{\sigma}} = -\boldsymbol{Q}\,\mathrm{sign}(\boldsymbol{\sigma}) - \boldsymbol{K}\boldsymbol{\sigma} \tag{2.40}$$

while, in case of decreasing rate, one has

$$\dot{\sigma}_i = -k_i |\sigma_i|^{\alpha}\,\mathrm{sign}(\sigma_i), \tag{2.41}$$

with $0 < \alpha < 1$, $i = 1, \ldots, m$.

Finally, other two ways to express the reachability condition are

$$\begin{cases} \dot{\sigma}_i > 0 & \text{if } \sigma_i < 0 \\ \dot{\sigma}_i < 0 & \text{if } \sigma_i > 0 \end{cases} \tag{2.42}$$

or, equivalently

$$\sigma_i \dot{\sigma}_i < 0, \tag{2.43}$$

with $i = 1, \ldots, m$. Otherwise, one can write

$$\lim_{\sigma_i \to 0^+} \dot{\sigma}_i < 0, \qquad \lim_{\sigma_i \to 0^-} \dot{\sigma}_i > 0\,. \tag{2.44}$$

2.2.6 Solutions to Variable Structure Systems

SMC generates a controlled system which is described by a differential equation with nonlinear discontinuous second hand side. The classical results on the solution of differential equations do not hold in case of SMC. However, the evolution of the system on $\sigma = 0$ is unique. In the following two different approaches will be analyzed: the *Filippov's method* and the *equivalent control approach* [Fil88, Utk92, ES98].

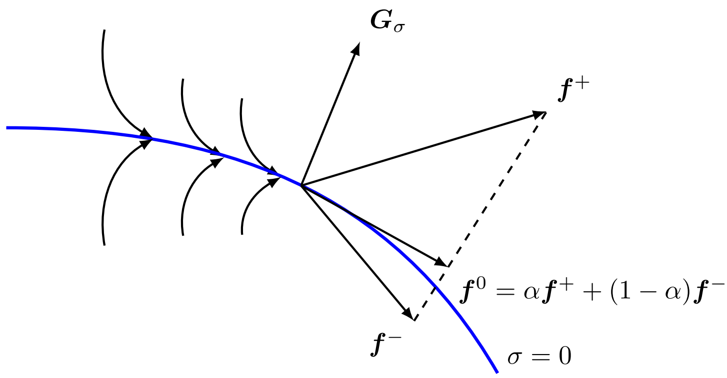

Fig. 2.7. Schematic view of Filippov's solution.

2.2.6.1 Filippov's Method

Given the following SISO system of order n, i.e.,

$$\dot{\boldsymbol{x}}(t) = \boldsymbol{f}(\boldsymbol{x}, u, t), \tag{2.45}$$

with u chosen as in (2.18), it is possible to show that the controlled system on the sliding manifold $\sigma(\boldsymbol{x}) = 0$ coincides with the solution of the following equation

$$\dot{\boldsymbol{x}}(t) = \alpha \boldsymbol{f}^+ + (1-\alpha)\boldsymbol{f}^- = \boldsymbol{f}^0, \tag{2.46}$$

with $0 \leq \alpha \leq 1$, $\boldsymbol{f}^+ = \boldsymbol{f}(\boldsymbol{x}, u^+, t)$, $\boldsymbol{f}^- = \boldsymbol{f}(\boldsymbol{x}, u^-, t)$, and $\boldsymbol{f}^0$ being the resulting vector field in sliding mode (see Fig. 2.7). In sliding mode, $\sigma(\boldsymbol{x}) = \dot{\sigma}(\boldsymbol{x}) = 0$, and by solving with respect to α the following equation

$$\boldsymbol{G}_\sigma \cdot \boldsymbol{f}^0 = 0, \tag{2.47}$$

where $\boldsymbol{G}_\sigma$ is the gradient of σ, one has that

$$\alpha = \frac{\boldsymbol{G}_\sigma \cdot \boldsymbol{f}^-}{\boldsymbol{G}_\sigma \cdot (\boldsymbol{f}^- - \boldsymbol{f}^+)} \,. \tag{2.48}$$

The latter holds only if $\boldsymbol{G}_\sigma \cdot (\boldsymbol{f}^- - \boldsymbol{f}^+) > 0$, and $\boldsymbol{G}_\sigma \cdot \boldsymbol{f}^+ \leq 0$ and $\boldsymbol{G}_\sigma \cdot \boldsymbol{f}^- \geq 0$. The idea of the Filippov's method is that the solution of a differential equation with nonlinear discontinuous second hand side exists and is uniquely defined on $\sigma(\boldsymbol{x}) = 0$ [Fil88]. It is equivalent to the solution of a differential equation with continuous function $\dot{\boldsymbol{x}} = \boldsymbol{f}^0$, with $\boldsymbol{f}^0$ depending on α which is obtained by posing $\dot{\sigma}(\boldsymbol{x}) = 0$. This method represents a possible way to determine the evolution of the controlled system in sliding mode. An alternative approach is the so-called equivalent control approach.

2.2.6.2 Equivalent Control Method

Given system (2.7) with $\boldsymbol{u}$ chosen as in (2.18), suppose that a sliding mode is enforced from the time instant $t_r \geq t_0$ on the sliding manifold $\boldsymbol{\sigma}(\boldsymbol{x}) = \boldsymbol{0}$. Then, consider the following equality

$$\dot{\boldsymbol{\sigma}}(\boldsymbol{x}) = \left[\frac{\partial \boldsymbol{\sigma}}{\partial \boldsymbol{x}}\right] \dot{\boldsymbol{x}} = \left[\frac{\partial \boldsymbol{\sigma}}{\partial \boldsymbol{x}}\right] [\boldsymbol{f}(\boldsymbol{x}, t) + \boldsymbol{B}(\boldsymbol{x}, t)\boldsymbol{u}] = \mathbf{0}, \tag{2.49}$$

where the rows of matrix $[\partial\boldsymbol{\sigma}/\partial\boldsymbol{x}] \in \mathbb{R}^{m\times n}$ are the gradients of the functions $\sigma_i(\boldsymbol{x})$. Assume now that a solution to (2.49) with respect to $\boldsymbol{u}$ exists. This solution is the equivalent control $\boldsymbol{u}_{eq}$ [Utk92]. Substituting $\boldsymbol{u}_{eq}$ into the original system, one has

$$\dot{\boldsymbol{x}} = \boldsymbol{f}(\boldsymbol{x}, t) + \boldsymbol{B}(\boldsymbol{x}, t)\boldsymbol{u}_{eq}, \tag{2.50}$$

which is a differential equation with continuous second hand side describing the evolution of the system starting from $\boldsymbol{x}(t_r)$ and $\boldsymbol{\sigma}(t_r) = \mathbf{0}$.

2.2.7 Computation of the Equivalent Control

Consider as hypothesis that the matrix $[\partial\boldsymbol{\sigma}/\partial\boldsymbol{x}]\boldsymbol{B}(\boldsymbol{x}, t)$ is not singular for any t and $\boldsymbol{x}$, such that

$$\boldsymbol{u}_{eq} = -\left(\left[\frac{\partial \boldsymbol{\sigma}}{\partial \boldsymbol{x}}\right] \boldsymbol{B}(\boldsymbol{x}, t)\right)^{-1} \left[\frac{\partial \boldsymbol{\sigma}}{\partial \boldsymbol{x}}\right] \boldsymbol{f}(\boldsymbol{x}, t) \,. \tag{2.51}$$

Assuming to start at t_0 with $\boldsymbol{\sigma}(t_0) = \mathbf{0}$, the dynamics of the controlled system can be expressed as

$$\dot{\boldsymbol{x}} = \left(\mathbb{I}_n - \boldsymbol{B}(\boldsymbol{x}, t)\left(\left[\frac{\partial \boldsymbol{\sigma}}{\partial \boldsymbol{x}}\right] \boldsymbol{B}(\boldsymbol{x}, t)\right)^{-1} \left[\frac{\partial \boldsymbol{\sigma}}{\partial \boldsymbol{x}}\right]\right) \boldsymbol{f}(\boldsymbol{x}, t). \tag{2.52}$$

Consider now the particular case with $\boldsymbol{\sigma}(\boldsymbol{x}) = \boldsymbol{C}\boldsymbol{x}$, such that $[\partial\boldsymbol{\sigma}/\partial\boldsymbol{x}] = \boldsymbol{C}$. Then one has

$$\dot{\boldsymbol{x}} = \left(\mathbb{I}_n - \boldsymbol{B}(\boldsymbol{x}, t)\left(\boldsymbol{C}\boldsymbol{B}(\boldsymbol{x}, t)\right)^{-1} \boldsymbol{C}\right) \boldsymbol{f}(\boldsymbol{x}, t). \tag{2.53}$$

2.2.8 Order Reduction

Consider, for the sake of simplicity, the particular case with $\boldsymbol{\sigma}(\boldsymbol{x}) = \boldsymbol{C}\boldsymbol{x}$. In sliding mode the dynamics of the controlled system is described by n differential equations in (2.53) and m algebraic equations $\boldsymbol{\sigma}(\boldsymbol{x}) = \boldsymbol{C}\boldsymbol{x} = \mathbf{0}$. If $\mathrm{rank}(\boldsymbol{C}) = m$, that is $[\partial\boldsymbol{\sigma}/\partial\boldsymbol{x}]\boldsymbol{B}(\boldsymbol{x}, t)$ is not singular for any t and $\boldsymbol{x}$, it is possible to obtain m state variables depending on the other $n - m$ ones. The resulting system of order $n - m$ represents the continuous system of reduced order which is equivalent to the system controlled with a discontinuous law, given the initial condition $\boldsymbol{\sigma}(\boldsymbol{x}) = \mathbf{0}$.

2.3 Sliding Mode Control Design

In this section the robustness properties and the design of a sliding mode control will be discussed. Specifically, the following uncertain system will be considered

$$\dot{\boldsymbol{x}}(t) = \boldsymbol{f}\left(\boldsymbol{x}(t), t\right) + \Delta\boldsymbol{f}\left(\boldsymbol{x}(t), t, \boldsymbol{r}(t)\right) + \left(\boldsymbol{B}\left(\boldsymbol{x}(t), t\right) + \Delta\boldsymbol{B}\left(\boldsymbol{x}(t), t, \boldsymbol{r}(t)\right)\right)\boldsymbol{u}(t), \tag{2.54}$$

where $\boldsymbol{r}$ is the vector function of all the unknown parameters belonging to a compact set, $\Delta\boldsymbol{f}$ and $\Delta\boldsymbol{B}$ belong to the image space of $\boldsymbol{B}(\boldsymbol{x}(t), t)$ for any $\boldsymbol{x}$ and t, that is the so-called *matching condition* holds. If the matching condition holds, it is possible to rewrite (2.54) as

$$\dot{\boldsymbol{x}}(t) = \boldsymbol{f}(\boldsymbol{x}(t), t) + \boldsymbol{B}(\boldsymbol{x}(t), t)\boldsymbol{u}(t) + \boldsymbol{B}(\boldsymbol{x}(t), t)\boldsymbol{w}_m(\boldsymbol{x}(t), t, \boldsymbol{r}(t), \boldsymbol{u}(t)), \tag{2.55}$$

where $\boldsymbol{w}_m$ is the matched uncertainty. Note that the nominal system does not need to be stable, but the equivalent system (i.e., when $\boldsymbol{\sigma}(\boldsymbol{x}) = \boldsymbol{0}$) must be asymptotically stable. In this case, an alternative form to that in (2.18) is the augmented control (2.19). Generally, the control approaches can be of two types: free control structure according to which $u_i(t)$ is chosen to satisfy the reachability condition, and preassigned control structure, where the control parameter u_i^+, u_i^-, $\alpha_{i,j}$ and $\beta_{i,j}$ are set to fulfill the reachability condition. The control law will depend on the type of reachability condition which is used, as will be clarified in the following.

2.3.1 Lyapunov Function Method

Assume that there exists a scalar nonnegative function such that

$$\|\boldsymbol{w}_m(\boldsymbol{x}(t), t, \boldsymbol{r}(t), \boldsymbol{u}(t))\| \leq \rho(\boldsymbol{x}(t), t)\ . \tag{2.56}$$

Now, making reference to (2.19), it is possible to compute the equivalent control with $\boldsymbol{w}_m = \boldsymbol{0}$ as

$$\boldsymbol{u}_{eq} = -\left(\left[\frac{\partial \boldsymbol{\sigma}}{\partial \boldsymbol{x}}\right]\boldsymbol{B}(\boldsymbol{x}, t)\right)^{-1}\left(\left[\frac{\partial \boldsymbol{\sigma}}{\partial \boldsymbol{x}}\right]\boldsymbol{f}(\boldsymbol{x}, t) + \frac{\partial \boldsymbol{\sigma}}{\partial t}\right), \tag{2.57}$$

while the discontinuous control $\boldsymbol{u}_N$ is computed starting from the Lyapunov function [DZM88]

$$V(\boldsymbol{x}, t) = \frac{1}{2}\boldsymbol{\sigma}^T(\boldsymbol{x}, t)\boldsymbol{\sigma}(\boldsymbol{x}, t)\ . \tag{2.58}$$

In order to enforce a sliding mode it is necessary to have

$$\dot{V} = \boldsymbol{\sigma}^T\dot{\boldsymbol{\sigma}} = \boldsymbol{\sigma}^T\frac{\partial \boldsymbol{\sigma}}{\partial t} + \boldsymbol{\sigma}^T\left[\frac{\partial \boldsymbol{\sigma}}{\partial \boldsymbol{x}}\right](\boldsymbol{f} + \boldsymbol{B}\boldsymbol{u} + \boldsymbol{B}\boldsymbol{w}_m) < 0\ . \tag{2.59}$$

Substituting (2.57) in (2.59) one obtains

$$\dot{V} = \boldsymbol{\sigma}^T\left[\frac{\partial \boldsymbol{\sigma}}{\partial \boldsymbol{x}}\right]\boldsymbol{B}\left(\boldsymbol{u}_N + \boldsymbol{w}_m\right)\ . \tag{2.60}$$

From (2.56) and (2.60), the discontinuous control can be expressed as

$$\boldsymbol{u}_N = -\frac{\boldsymbol{B}^T\nabla_{\boldsymbol{x}}V(\boldsymbol{x}, t)}{\|\boldsymbol{B}^T\nabla_{\boldsymbol{x}}V(\boldsymbol{x}, t)\|}\hat{\rho}(\boldsymbol{x}, t), \tag{2.61}$$

where $\nabla_{\boldsymbol{x}}V$ is the gradient of V and $\hat{\rho} = \alpha + \rho$, with $\alpha > 0$.

2.3.2 Finite Time Reachability Condition Method

Consider now the example reported in [SL91]. Given the system

$$\ddot{x}(t) + a(t)\dot{x}^2\cos(3x) = u, \tag{2.62}$$

with $1 \leq a \leq 2$ and $f = -a(t)\dot{x}^2 \cos(3x)$. Moreover, consider the model $\hat{f} = -1.5\dot{x}^2 \cos(3x)$ and $F = 0.5\dot{x}^2|\cos(3x)|$ such that $|\hat{f} - f| \leq F$. The sliding manifold is chosen as

$$\sigma(x) = \dot{\tilde{x}} + c_1\tilde{x} = 0, \tag{2.63}$$

where $\tilde{x} = x - x_d$ is the error signal. The *nominal equivalent control* is computed by posing $\dot{\sigma}$ relying on the nominal model as

$$\hat{u}_{eq} = -\hat{f} + \ddot{x}_d - c_1\dot{\tilde{x}}. \tag{2.64}$$

In order to satisfy the reachability condition (2.34) the discontinuous control is chosen as

$$\hat{u}_N = -K\,\mathrm{sign}(\sigma), \tag{2.65}$$

with $K \geq F + \gamma^2$. One has

$$\begin{aligned}
\sigma\dot{\sigma} &= \sigma\left(f + u - \ddot{x}_d + c_1\dot{\tilde{x}}\right) \\
&= \sigma\left(f + \hat{u}_{eq} + u_N - \ddot{x}_d + c_1\dot{\tilde{x}}\right) \\
&= \sigma\left(f - \hat{f} + \ddot{x}_d - c_1\dot{\tilde{x}} + u_N - \ddot{x}_d + c_1\dot{\tilde{x}}\right) \\
&= \sigma\left(f - \hat{f}\right) - K\sigma\,\mathrm{sign}(\sigma) \\
&= \sigma\left(f - \hat{f}\right) - K|\sigma| \leq -\gamma^2|\sigma|.
\end{aligned} \tag{2.66}$$

If the system is of the type

$$\ddot{x}(t) = f(t) + bu, \tag{2.67}$$

with $0 < b_{\min} \leq b \leq b_{\max}$, b being time-varying or depending on the state, one can choose the estimate $\hat{b}$, for instance as

$$\hat{b} = \sqrt{b_{\min}b_{\max}}\,. \tag{2.68}$$

Considering (2.63) as sliding manifold, the equivalent control (2.64) becomes

$$\hat{u}_{eq} = -\hat{b}^{-1}(\hat{f} + \ddot{x}_d - c_1\dot{\tilde{x}}), \tag{2.69}$$

such that, in order to satisfy the reachability condition (2.34), the discontinuous component of the control law is

$$\hat{u}_N = -\hat{b}^{-1}K\,\mathrm{sign}(\sigma), \tag{2.70}$$

with $K \geq \beta(F + \gamma^2) + (\beta - 1)|\hat{u}_{eq}|$, β being equal to $\sqrt{b_{\max}/b_{\min}}$.

2.4 Linearization of Nonlinear Systems

Consider a SISO system of the following type

$$\begin{aligned}
\dot{x}_i(t) &= x_{i+1}(t) \qquad i = 1, \ldots, n-1 \\
\dot{x}_n(t) &= f(\boldsymbol{x}, t) + B(\boldsymbol{x}, t)(u(t) + d(\boldsymbol{x}, t))
\end{aligned} \tag{2.71}$$

where the unknown functions f, B and d are such that

$$\begin{aligned} |f(\boldsymbol{x},t)| &< F \\ 0 < B_{\min} < B(\boldsymbol{x},t) &< B_{\max} \\ |d(t)| &< \delta, \end{aligned} \tag{2.72}$$

with F, $B_{\min}$, $B_{\max}$ and δ being positive constants. Consider the following reference model

$$\begin{aligned} \dot{y}_i(t) &= y_{i+1}(t) \qquad i = 1, \ldots, n-1 \\ \dot{y}_n(t) &= -\sum_{i=1}^{n-1} a_i y_i(t) + b\hat{u}(t), \end{aligned} \tag{2.73}$$

and the tracking error $e_j = x_j - y_j$, with $j = 1, \ldots, n$. Hence, the error dynamics results in being

$$\begin{aligned} \dot{e}_i(t) &= e_{i+1}(t) \qquad i = 1, \ldots, n-1 \\ \dot{e}_n(t) &= f(\boldsymbol{x},t) + B(\boldsymbol{x},t)(u(t) + d(t)) + \sum_{i=1}^{n-1} a_i y_i(t) - b\hat{u}(t) \ . \end{aligned} \tag{2.74}$$

By choosing the sliding variable as a linear combination of the error components, i.e.,

$$\sigma(\boldsymbol{e}) = e_n + \sum_{i=1}^{n-1} c_i e_i, \tag{2.75}$$

one has that its first time derivative is

$$\begin{aligned} \dot{\sigma}(\boldsymbol{e}) &= \dot{e}_n + \sum_{i=1}^{n-1} c_i \dot{e}_i \\ &= f + B(u+d) + \sum_{i=1}^{n-1} a_i y_i - b\hat{u} + \sum_{i=1}^{n-1} c_i \dot{e}_i \ . \end{aligned} \tag{2.76}$$

Consider now the control law $u = -K\,\mathrm{sign}(\sigma)$ in order to satisfy

$$\sigma\dot{\sigma} = \sigma\left(f + B(u+d) + \sum_{i=1}^{n-1} a_i y_i - b\hat{u} + \sum_{i=1}^{n-1} c_i \dot{e}_i\right) \tag{2.77}$$

$$= \sigma\left(f + B(-K\,\mathrm{sign}(\sigma) + d) + \sum_{i=1}^{n-1} a_i y_i - b\hat{u} + \sum_{i=1}^{n-1} c_i \dot{e}_i\right) \tag{2.78}$$

$$\leq -\gamma^2|\sigma|, \tag{2.79}$$

with $K > \left|B^{-1}\left(f + B(-K\,\mathrm{sign}(\sigma) + d) + \sum_{i=1}^{n-1} a_i y_i - b\hat{u} + \sum_{i=1}^{n-1} c_i \dot{e}_i + \gamma^2\right)\right|$. If the reachability condition (2.34) is satisfied, in a finite time, the controlled system is equivalent to the following linear system of order $n-1$ with assignable poles c_i, i.e.,

$$\begin{aligned} \dot{e}_i(t) &= e_{i+1}(t) \qquad i = 1, \ldots, n-2 \\ \dot{e}_{n-1}(t) &= e_n = -\sum_{j=1}^{n-1} c_j \dot{e}_j. \end{aligned} \tag{2.80}$$

2.5 Approximability Property

In this section the concept of *approximability*, reported in [Utk92, BPZ07], will be recalled. Consider the nonlinear MIMO system

$$\dot{\boldsymbol{x}}(t) = \boldsymbol{f}(\boldsymbol{x}, t) + \boldsymbol{B}(\boldsymbol{x}, t)\boldsymbol{u}(t), \tag{2.81}$$

where $\boldsymbol{u} \in \mathbb{R}^m$. Suppose that a sliding mode is enforced on the manifold $\boldsymbol{\sigma}(\boldsymbol{x}) = \boldsymbol{0}$. Then, the equivalent dynamics of the controlled system is expressed by (2.52).

Consider now a more accurate model of system (2.81):

$$\dot{\boldsymbol{x}}(t) = \boldsymbol{f}(\boldsymbol{x}, t) + \boldsymbol{B}(\boldsymbol{x}, t)\tilde{\boldsymbol{u}}(t), \tag{2.82}$$

where the new control input $\tilde{\boldsymbol{u}}$ gathers some imperfections such as hysteresis and delays. However, the "cost" of such regularization is that the evolution of the state $\boldsymbol{x}$ does not occur on the manifold $\boldsymbol{\sigma}(\boldsymbol{x}) = \boldsymbol{0}$, but in some neighbourhood of this manifold, i.e.,

$$\left\{\boldsymbol{x} \in \mathbb{R}^n \,:\, \|\boldsymbol{\sigma}(\boldsymbol{x})\| \leq \Delta\right\}, \tag{2.83}$$

with $\Delta > 0$. For the sake of clarity, let $\boldsymbol{x}^\star$ denote the solution to (2.52), and $\boldsymbol{x}$ denote the solution to (2.82). The following theorem in [Utk92] is hereafter recalled.

Theorem 2.1 (Approximability). *If*

1. *there exists a solution $\boldsymbol{x}(t)$ to system (2.82) in the interval $[0, T]$, and $\boldsymbol{x}(t)$ belongs to the neighbourhood of the sliding manifold $\boldsymbol{\sigma} = \boldsymbol{0}$;*
2. *there exists a Lipschitz constant L for the equivalent dynamics*

$$\dot{\boldsymbol{x}}^\star(t) = \boldsymbol{f}(\boldsymbol{x}^\star, t) - \boldsymbol{B}(\boldsymbol{x}^\star, t)\left(\boldsymbol{G}(\boldsymbol{x}^\star)\boldsymbol{B}(\boldsymbol{x}^\star, t)\right)^{-1}\boldsymbol{G}(\boldsymbol{x}^\star)\boldsymbol{f}(\boldsymbol{x}^\star, t), \tag{2.84}$$

   where $\boldsymbol{G} = \partial\boldsymbol{\sigma}/\partial\boldsymbol{x}$;
3. *there exist bounded partial derivatives of $\boldsymbol{B}(\boldsymbol{x}, t)\left(\boldsymbol{G}(\boldsymbol{x})\boldsymbol{B}(\boldsymbol{x}, t)\right)^{-1}$;*
4. *there exist two positive constants M and N such that*

$$\|\boldsymbol{f}(\boldsymbol{x}, t) + \boldsymbol{B}(\boldsymbol{x}, t)\tilde{\boldsymbol{u}}(\boldsymbol{x}, t)\| \leq M + N\|\boldsymbol{x}\|; \tag{2.85}$$

then, for any pair of solutions $\boldsymbol{x}$ and $\boldsymbol{x}^\star$ with initial condition $\|\boldsymbol{x}(0) - \boldsymbol{x}^\star(0)\| \leq P\Delta$, with $P > 0$, there exists a positive constant H such that $\|\boldsymbol{x}(t) - \boldsymbol{x}^\star(t)\| \leq H\Delta$, $\forall\, t \in [0, T]$.

Proof. In order to prove the theorem it is necessary to compute the norm of the difference between the solutions to the differential equations describing the actual and the ideal evolution of the state. The actual evolution within the neighbourhood of the sliding manifold (2.83) implies that the first time derivative of the sliding variable is $\dot{\boldsymbol{\sigma}} \neq \boldsymbol{0}$, i.e.,

$$\dot{\boldsymbol{\sigma}} = \boldsymbol{G}(\boldsymbol{x})\left(\boldsymbol{f}(\boldsymbol{x}, t) + \boldsymbol{B}(\boldsymbol{x}, t)\tilde{\boldsymbol{u}}\right), \tag{2.86}$$

with

$$\tilde{\boldsymbol{u}} = -\left(\boldsymbol{G}(\boldsymbol{x})\boldsymbol{B}(\boldsymbol{x}, t)\right)^{-1}\boldsymbol{G}(\boldsymbol{x})\boldsymbol{f}(\boldsymbol{x}, t) + \left(\boldsymbol{G}(\boldsymbol{x})\boldsymbol{B}(\boldsymbol{x}, t)\right)^{-1}\dot{\boldsymbol{\sigma}}\,. \tag{2.87}$$

The actual evolution of the system is

$$\dot{\boldsymbol{x}} = \boldsymbol{f}(\boldsymbol{x},t) - \boldsymbol{B}(\boldsymbol{x},t)\left(\boldsymbol{G}(\boldsymbol{x})\boldsymbol{B}(\boldsymbol{x},t)\right)^{-1}\boldsymbol{G}(\boldsymbol{x})\boldsymbol{f}(\boldsymbol{x},t) + \boldsymbol{B}(\boldsymbol{x},t)\left(\boldsymbol{G}(\boldsymbol{x})\boldsymbol{B}(\boldsymbol{x},t)\right)^{-1}\dot{\boldsymbol{\sigma}}, \quad (2.88)$$

while the ideal state evolution is

$$\dot{\boldsymbol{x}}^\star = \boldsymbol{f}(\boldsymbol{x}^\star,t) - \boldsymbol{B}(\boldsymbol{x}^\star,t)\left(\boldsymbol{G}(\boldsymbol{x}^\star)\boldsymbol{B}(\boldsymbol{x}^\star,t)\right)^{-1}\boldsymbol{G}(\boldsymbol{x}^\star)\boldsymbol{f}(\boldsymbol{x}^\star,t)\,. \quad (2.89)$$

The corresponding integral equations are

$$\begin{aligned}\boldsymbol{x}(t) = \boldsymbol{x}(0) &+ \int_0^t \Big(\boldsymbol{f}(\boldsymbol{x},\zeta) - \boldsymbol{B}(\boldsymbol{x},\zeta)\left(\boldsymbol{G}(\boldsymbol{x})\boldsymbol{B}(\boldsymbol{x},\zeta)\right)^{-1}\boldsymbol{G}(\boldsymbol{x})\boldsymbol{f}(\boldsymbol{x},\zeta)\Big)\,d\zeta \\ &+ \int_0^t \boldsymbol{B}(\boldsymbol{x},\zeta)\left(\boldsymbol{G}(\boldsymbol{x})\boldsymbol{B}(\boldsymbol{x},\zeta)\right)^{-1}\dot{\boldsymbol{\sigma}}d\zeta\end{aligned} \quad (2.90)$$

and

$$\boldsymbol{x}^\star(t) = \boldsymbol{x}^\star(0) + \int_0^t \Big(\boldsymbol{f}(\boldsymbol{x}^\star,\zeta) - \boldsymbol{B}(\boldsymbol{x}^\star,\zeta)\left(\boldsymbol{G}(\boldsymbol{x}^\star)\boldsymbol{B}(\boldsymbol{x}^\star,\zeta)\right)^{-1}\boldsymbol{G}(\boldsymbol{x}^\star)\boldsymbol{f}(\boldsymbol{x}^\star,\zeta)\Big)\,d\zeta\,. \quad (2.91)$$

Integrating by parts the last term in (2.91), one has

$$\begin{aligned}||\boldsymbol{x}(t)-\boldsymbol{x}^\star(t)|| \le P\Delta &+ \int_0^t L\,||\boldsymbol{x}(\zeta)-\boldsymbol{x}^\star(\zeta)||\,d\zeta + \left.\left|\left|\boldsymbol{B}(\boldsymbol{x},\zeta)\left(\boldsymbol{G}(\boldsymbol{x})\boldsymbol{B}(\boldsymbol{x}^\star,\zeta)\right)^{-1}\boldsymbol{\sigma}\right|\right|\right|_0^t \\ &+ \int_0^t \left|\left|\frac{d}{d\zeta}\boldsymbol{B}(\boldsymbol{x},\zeta)\left(\boldsymbol{G}(\boldsymbol{x})\boldsymbol{B}(\boldsymbol{x},\zeta)\right)^{-1}\right|\right|\,||\boldsymbol{\sigma}||d\zeta\,.\end{aligned} \quad (2.92)$$

The solution that describes the actual evolution is bounded in the interval $[0,\,T]$. Moreover, (2.85) in hypothesis 4 holds, and one has

$$\|\boldsymbol{x}(t)\| \le \|\boldsymbol{x}(0)\| + MT + \int_0^t N\|\boldsymbol{x}(\zeta)\|d\zeta\,. \quad (2.93)$$

By applying the so-called *Bellman–Gronwall's Lemma*[1], one has

$$\|\boldsymbol{x}(t)\| \le (\|\boldsymbol{x}(0)\| + MT)e^{NT} \quad (2.94)$$

in $[0,\,T]$. Taking into account that $\boldsymbol{\sigma}$ is bounded and hypothesis 1, 2 and 3 hold, it yields

$$\|\boldsymbol{x}(t)-\boldsymbol{x}^\star(t)\| \le S\Delta + L\int_0^t \|\boldsymbol{x}(\zeta)-\boldsymbol{x}^\star(\zeta)\|d\zeta \quad (2.95)$$

where S is a positive constant which depends on (2.88), T, the initial conditions $\boldsymbol{x}(0)$ and P. By applying again the Bellman–Gronwall Lemma to inequality (2.95), one has

$$\|\boldsymbol{x}(t)-\boldsymbol{x}^\star(t)\| \le Se^{LT}\Delta = H\Delta \quad (2.96)$$

which proves the theorem. □

[1]

Lemma 2.1 (Bellman–Gronwall). Given $y(t)$ such that $y(t) \le \int_0^t a(\zeta)y(\zeta)d\zeta + b(t)$, with $a(t)$ and $b(t)$ being real known functions, then $y(t) \le \int_0^t a(\zeta)b(\zeta)e^{\int_0^t a(\gamma)d\gamma}d\zeta + b(t)$. If $b(t)$ is a constant, $y(t) \le b(0)e^{\int_0^t a(\zeta)d\zeta}$.

The theorem implies that if the initial conditions $\boldsymbol{x}(0)$ and $\boldsymbol{x}^\star(0)$ are sufficiently close to each other, the corresponding solutions are close. Since $\boldsymbol{x}^\star(0)$ is such that $\boldsymbol{\sigma}(\boldsymbol{x}^\star) = \mathbf{0}$ one has that $\|\boldsymbol{x}(0) - \boldsymbol{x}^\star(0)\|$ is the distance from $\boldsymbol{x}(0)$ to some point on the sliding manifold $\boldsymbol{\sigma}(\boldsymbol{x}) = \mathbf{0}$. Finally, if the equivalent dynamics of the system in sliding mode is asymptotically stable, the results hold for $T \to \infty$.

2.6 Conclusions

In this chapter we have seen the design of different types of SMC laws and their properties to compensate the uncertainties and nonlinearities of the controlled systems. Furthermore, we have seen the so-called approximability property which guarantees the ultimately boundedness of the system state when a real sliding mode is enforced.

3

Advances in Higher Order Sliding Mode Control

Abstract. In this chapter the basic concepts of Higher Order Sliding Mode Control are recalled. After some preliminaries on the design of the control law, the second order case and the third order case are discussed. Novel algorithms are finally presented: the Adaptive Suboptimal Second Order Sliding Mode, and a Second Order Sliding Mode for systems with quantized uncertainty.

3.1 Higher Order Sliding Mode

Sliding Mode Control (SMC) is an appreciated control methodology for its robustness against a wide class of uncertainties. Yet, because of the discontinuous nature of the control law, it can produce the so-called chattering effect [Fri02, BFPU07, Lev10, Boi11], i.e., high frequency oscillations of the controlled variable, which can be disruptive for the controlled plant, or significantly limit the life cycle of the actuators.

A number of methods have been proposed in the literature to overcome this drawback. More precisely, high-gain control with saturation approximates the signum function and alleviates the chattering phenomenon, while on-line estimation of the so-called equivalent control [Utk92] is used to reduce the discontinuous control component [SL91]. A well-established method to perform chattering alleviation is that consisting of shifting the discontinuity (which is necessary to ensure the finite time reaching to the sliding manifold) into some time derivative of the control variable, so that the control signal actually fed into the plant is indeed continuous. This approach, called Higher Order Sliding Mode (HOSM) control [BFUZ97, BFU97, BFUU00, Lev03, FBP03, Lev05, DF09], enforces in a finite time a sliding mode involving not only the sliding function, but also its time derivatives up to the order $r-1$ (the mode is accordingly called r-sliding mode). Because of the continuous nature of the control action, the HOSM control approach is appropriate to be applied even to electromechanical or mechanical systems [UGS99, BPPU03], as testified, for instance, by [CFM09, CFF10, CF12].

3.2 Preliminaries on Higher Order Sliding Mode

Consider the smooth dynamic system

$$\dot{\boldsymbol{x}} = \boldsymbol{a}(\boldsymbol{x}) + \boldsymbol{b}(\boldsymbol{x})\boldsymbol{u}, \tag{3.1}$$

where $\boldsymbol{x} \in \mathbb{R}^n$, $\boldsymbol{u} \in \mathbb{R}^m, \boldsymbol{a} : \mathbb{R}^n \to \mathbb{R}^n, \boldsymbol{b} : \mathbb{R}^n \to \mathbb{R}^{n\times m}$.

Definition 3.1 (Sliding function[2]). The sliding function $\boldsymbol{\sigma}(\boldsymbol{x}) : \mathbb{R}^n \to \mathbb{R}^m$ is a sufficiently smooth output function of system (3.1).

Definition 3.2 (r–sliding manifold). The r–sliding manifold[3] is given by

$$\begin{aligned}\{\boldsymbol{x} \in \mathbb{R}^n, \boldsymbol{u} \in \mathbb{R}^m : \boldsymbol{\sigma}(\boldsymbol{x}) &= L_{\boldsymbol{a}}\boldsymbol{\sigma}(\boldsymbol{x}) + L_{\boldsymbol{b}}\boldsymbol{\sigma}(\boldsymbol{x})\boldsymbol{u} \\ &= \dots \\ &= L_{\boldsymbol{a}}^{(r-1)}\boldsymbol{\sigma}(\boldsymbol{x}) + L_{\boldsymbol{b}}L_{\boldsymbol{a}}^{(r-2)}\boldsymbol{\sigma}(\boldsymbol{x})\boldsymbol{u} = \boldsymbol{0}\},\end{aligned} \tag{3.2}$$

where $L_{\boldsymbol{a}}^{(r-1)}\boldsymbol{\sigma}(\boldsymbol{x})$ is the $(r-1)$-th order Lie derivative of $\boldsymbol{\sigma}(\boldsymbol{x})$ along the vector field $\boldsymbol{a}(\boldsymbol{x})$. With a slight abuse of notation we also write $L_{\boldsymbol{a}}\boldsymbol{\sigma}(\boldsymbol{x}) + L_{\boldsymbol{b}}\boldsymbol{\sigma}(\boldsymbol{x})\boldsymbol{u} = \dot{\boldsymbol{\sigma}}$.

Definition 3.3 (r–sliding mode). A r–order sliding mode is enforced from $t = T_r \geq 0$, when, starting from an initial condition $x(t_0) = x_0$, the state of (3.1) reaches the r–sliding manifold (3.2), and remains there for all $t \geq T_r$.

Furthermore, the order of a sliding mode controller is identical to the order of the sliding mode that it is aimed at enforcing.

Definition 3.4. (**Equivalent control**) Consider system (3.1) and the sliding function $\boldsymbol{\sigma}(\boldsymbol{x})$. Assume that a r–order sliding mode exists on the sliding manifold (3.2). Assume also that a solution to system $\boldsymbol{\sigma}^{(r)} = L_{\boldsymbol{\zeta}}^{(r)}\boldsymbol{\sigma} = \boldsymbol{0}$, with respect to the control input $\boldsymbol{u}$, exists. This solution is called equivalent control and is denoted by $\boldsymbol{u}_{eq}$ [Utk92].

3.2.1 Design of a Higher Order Sliding Mode Control

Consider, for the sake of simplicity, a SISO dynamic system of the form

$$\begin{aligned}\dot{\boldsymbol{x}} &= \boldsymbol{a}(\boldsymbol{x}, t) + \boldsymbol{b}(\boldsymbol{x}, t)u \\ \sigma &= \sigma(\boldsymbol{x}, t),\end{aligned} \tag{3.3}$$

where $\boldsymbol{x} \in \mathbb{R}^n$, $u \in \mathbb{R}$ and $\sigma : \mathbb{R}^n \times \mathbb{R} \to \mathbb{R}$ ia a sufficiently smooth output function. We assume that (3.3) is an *uncertain* system, i.e., we assume that the system order n and the functions $\boldsymbol{a} : \mathbb{R}^n \times \mathbb{R} \to \mathbb{R}^n, \boldsymbol{b} : \mathbb{R}^n \times \mathbb{R} \to \mathbb{R}^n$ are unknown. However, we assume that the relative degree of the system is globally well defined, uniform, time-invariant, and equal to r. With reference to system (3.3), relative degree equal to r implies that u

[2]The sliding function is also called sliding variable

[3]For the sake of simplicity, the order r of the sliding manifold is omitted in the following.

first appears explicitly in the r-th time derivative of σ, i.e., $(\partial/\partial u)\sigma^{(r)} \neq 0$. Then, for suitable functions $h(\boldsymbol{x}, t) : \mathbb{R}^n \times \mathbb{R} \to \mathbb{R}$ and $g(\boldsymbol{x}, t) : \mathbb{R}^n \times \mathbb{R} \to \mathbb{R}$, one has

$$\sigma^{(r)} = h(\boldsymbol{x}, t) + g(\boldsymbol{x}, t)u. \tag{3.4}$$

Functions h and g are assumed to be bounded. More precisely, we assume the existence of positive constants H, $g_{\min}$, $g_{\max}$, such that

$$|h(\boldsymbol{x}, t)| \leq H \tag{3.5}$$

$$0 < g_{\min} \leq \ g(\boldsymbol{x}, t) \ \leq g_{\max} \,. \tag{3.6}$$

Note that instead of (3.6), one could analogously have the opposite inequality

$$-\, g_{\max} \leq g(\boldsymbol{x}, t) \leq -g_{\min} < 0, \tag{3.7}$$

i.e., it is required that function g has constant known sign. Since the information about the bounds of h and g are assumed to be available, the original dynamical system (3.12) implies the differential inclusion [AC84]

$$\sigma^{(r)} = f_1 + f_2 u, \tag{3.8}$$

with $f_1 \in [-H, H]$ and $f_2 \in [g_{\min}, g_{\max}]$. In the literature, it has been shown that the problem of making the r-sliding manifold associated with (3.8) finite-time attractive, generating a sliding mode of order r (r-sliding mode), can be solved by any r-sliding mode controller of the type

$$u(t) = K\Psi\left(\sigma,\, \dot{\sigma},\, \ldots,\, \sigma^{(r-1)}\right), \tag{3.9}$$

(see for instance [BFUZ97, BFUU00, Lev03, FBP03, Lev05, DF09]), where Ψ is a discontinuous function, and $K > 0$ is chosen so as to ensure the finite time convergence of the state trajectories. For the reader's convenience, few examples of HOSM controllers proposed in [Lev03] are reported for $r = 1, 2$, respectively:

$$\begin{aligned} u &= -K \operatorname{sign}(\sigma)\,, \\ u &= -K \operatorname{sign}\left(\dot{\sigma} + |\sigma|^{\frac{1}{2}} \operatorname{sign}(\sigma)\right). \end{aligned} \tag{3.10}$$

Note that, in order to alleviate the chattering phenomenon, a r-sliding controller can be applied to a system with relative degree $k < r$. Introducing successive time derivatives $u, \dot{u}, \ldots, u^{(r-k-1)}$ as a new auxiliary variables and $u^{(r-k)} = w$ as a new control variable, the relative degree of the resulting *auxiliary system* with respect to w is r. Then, the control actually fed into the plant u is a $(r-k-1)$-smooth function of time with $k < r-1$, a Lipschitz function with $k = r-1$, and a bounded 'infinite-frequency switching' (discontinuos) function with $k = r$ [Lev03]. In this thesis, in order to alleviate the chattering effect, the case with $k = r-1$ will be adopted when requested.

Note also that controllers (3.10), and generally (3.9), require the availability of σ, $\dot{\sigma}, \ldots, \sigma^{(r-1)}$. That requirement can be relaxed by implementing the well known Levant's differentiator.

3.2.2 Levant's Differentiator

Let $\psi(t)$ be a function defined on $[0, \infty)$. Assume that it is a bounded Lebesgue-measurable noise with unknown features and with the n-th derivative having a known Lipschitz constant $L > 0$. The n-order Levant's differentiator has the following form [Lev03]:

$$\begin{aligned}
\dot{z}_0 &= -\lambda_0 \left| z_0 - \psi \right|^{\frac{n}{n+1}} \operatorname{sign}(z_0 - \psi) + z_1 \\
\dot{z}_1 &= -\lambda_1 \left| z_1 - \dot{z}_0 \right|^{\frac{n-1}{n}} \operatorname{sign}(z_1 - \dot{z}_0) + z_2 \\
&\vdots \\
\dot{z}_{n-1} &= -\lambda_{n-1} \left| z_{n-1} - \dot{z}_{n-2} \right|^{\frac{1}{2}} \operatorname{sign}(z_{n-1} - \dot{z}_{n-2}) + z_n \\
\dot{z}_n &= -\lambda_n \operatorname{sign}(z_n - \dot{z}_{n-1}),
\end{aligned} \tag{3.11}$$

where $z_i, i = 0, 1, \ldots, n$, are the estimations of $\psi, \dot{\psi}, \ldots, \psi^{(n)}$, respectively, while $\lambda_i, i = 0, 1, \ldots, n$ are positive constant depending on the Lipschitz constant L (see [Lev03] for more details about the choice of $\lambda_i, i = 0, 1, \ldots, n$).

In the next section we discuss a particular second order sliding mode control that, in contrast to (3.9), does not require to measure $\dot{\sigma}$, avoiding the implementation of a Levant's differentiator: the well known Suboptimal second order sliding mode control [BFU98a]. More precisely, it is explained the procedure to perform the so-called chattering alleviation in case with $k = r - 1$ (see Subsection 3.2.1), i.e., $k = 1$ and $r = 2$.

3.3 Suboptimal Second Order Sliding Mode

Consider the SISO system given by

$$\begin{aligned}
\dot{x}_i(t) &= x_{i+1}(t) \\
\dot{x}_n(t) &= f(\boldsymbol{x}(t), t) + g(\boldsymbol{x}(t), t) u(t) \\
y(t) &= \sigma(\boldsymbol{x}(t)),
\end{aligned} \tag{3.12}$$

where $i = 1, \ldots, n-1$, $\boldsymbol{x} \in \mathbb{R}^n$ is the state vector, $u \in \mathbb{R}$ is the control variable, $\sigma : \mathbb{R}^n \to \mathbb{R}$ is a smooth output function. System (3.12) is an *uncertain system* since $f : \mathbb{R}^n \times \mathbb{R} \to \mathbb{R}$ and $g : \mathbb{R}^n \times \mathbb{R} \to \mathbb{R}$ are assumed to be unknown smooth functions. The relative degree k of the system is considered well defined, uniform and time invariant. In the following, the dependence of σ on $\boldsymbol{x}$ and of all the variables on t is omitted in some cases, when it is obvious, for the sake of simplicity.

Second Order Sliding Mode (SOSM) control is a particular case of HOSM control. Assume that the sliding variable is chosen as

$$\sigma = x_n + \sum_{i=1}^{n-1} c_i x_i, \tag{3.13}$$

where c_i, $i = 1, \ldots, n-1$ are real positive constants such that the characteristic equation $\sum_{i=1}^{n-1} c_i \, z^{\,i-1} + z^{\,n-1} = 0$ has distinct roots with negative real part. From (3.13) it clearly follows that the relative degree of system (3.12) is $k = 1$. Yet, the use of a control law (3.9) discontinuous on $\sigma = 0$ is not appropriate for an electromechanical application, due to the chattering effect (see [UGS99]). Then, it is convenient to artificially increase the relative degree of the auxiliary system as suggested in [BFU97]. To this end, one has to consider the first-time derivative of the sliding variable, i.e.,

$$\dot{\sigma} = f + gu + \sum_{i=1}^{n-1} c_i x_{i+1}, \tag{3.14}$$

and the second-time derivative,

$$\ddot{\sigma} = \underbrace{\frac{df}{dt} + \frac{dg}{dt}u + c_{n-1}\left(f + gu\right) + \sum_{i=1}^{n-2} c_i x_{i+2}}_{h} + g\dot{u} \, . \tag{3.15}$$

By defining $\xi_1 = \sigma$ and $\xi_2 = \dot{\sigma}$, it yields

$$\begin{aligned} \dot{\xi}_1(t) &= \xi_2(t) \\ \dot{\xi}_2(t) &= h(\boldsymbol{x}(t), u(t), t) + g(\boldsymbol{x}(t), t)w(t) \\ \dot{u}(t) &= w(t), \end{aligned} \tag{3.16}$$

where ξ_2 is assumed to be unmeasurable, functions h and g have the bounds indicated in (3.5) and (3.6), w is the auxiliary control law which has to be designed so that ξ_1 and ξ_2 are steered to zero in a finite time in spite of the uncertainties, thus enforcing a second order sliding mode (i.e., $r = k + 1 = 2$). Note that, h in (3.15) depends on the state $x_3, \ldots, x_n$, so that it is only locally bounded, which is true in most practical cases, since the operational region is always bounded. Moreover, according to (3.9), the control $w = \dot{u}$ is discontinuous. Yet, by virtue of the artificial increment of the relative degree, the control actually fed into the plant is the output of an integrator having as input $w(t)$, making $u(t)$ continuous, which is highly appreciable in case of mechanical or electromechanical plants. Note that in the literature, several algorithms have been proposed to solve second order sliding mode control problems, such as the Twisting and Super Twisting algorithms [Lev03], and the Suboptimal algorithm [BFU97, BFU98a]. For the reader's convenience, the Suboptimal SOSM (SSOSM) algorithm is reported.

The *extremal* values $\xi_{\max}$ in Algorithm 1 corresponds to the local minima/maxima of the sliding variable (see Fig. 3.1) and they can be detected by implementing for instance a peak detector as in [BFU98b]. It can be proved (see [BFU97, BFU98a] for the details of the proof) that, with the constraints (3.17) and (3.18), the control law (3.19) enforces the generation of a sequence of states with coordinates featuring the contraction property expressed by $|\xi_{\max_{i+1}}| < |\xi_{\max_i}|$, $i \in \mathbb{N}^+$. Finally, note that, h linearly depends on u, which, in principle, does not ensure its boundedness. Since, in the present approach, a second order sliding mode $\sigma = \dot{\sigma} = 0$ is enforced, the control u is close to the so-called equivalent control $u_{eq}(\boldsymbol{x}, t)$, obtained by posing $\dot{\sigma}(\boldsymbol{x}, u_{eq}, t) = 0$ [Utk92, BFU98b], and one can conclude that the control law (3.19), (3.17), (3.18) is locally applicable.

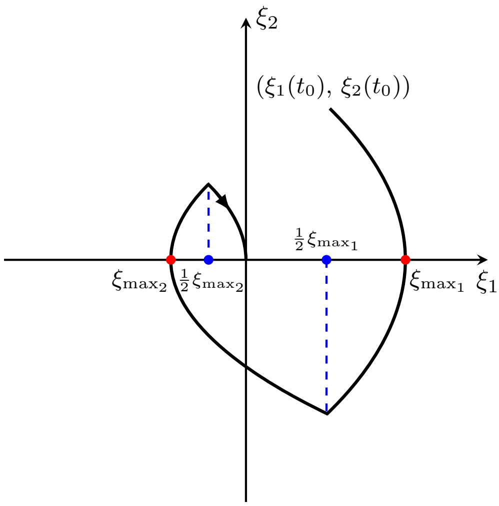

Fig. 3.1. Schematic view of the auxiliary state trajectory with the extremal values (red circles).

Algorithm 1 SSOSM algorithm

---

procedure SSOSM($g_{\min}$, $g_{\max}$, H, K)
  set $\xi_1(t) = \sigma(t)$
  while $t \geq t_0$ **do**
    set
$$\alpha^* \in (0,\, 1] \cap \left(0,\, \frac{3g_{\min}}{g_{\max}}\right) \tag{3.17}$$
    set $\xi_{\max} = \xi_1(t_0)$
    if $\left[\xi_1(t) - \frac{1}{2}\xi_{\max}\right][\xi_{\max} - \xi_1(t)] > 0$ **then**
      set $\alpha = \alpha^*$
    else
      set $\alpha = 1$
    end if
    if $\xi_1(t)$ is extremal **then**
      set $\xi_{\max}(t) = \xi_1(t)$
    end if
    set
$$K > \max\left(\frac{H}{\alpha^* g_{\min}};\, \frac{4H}{3g_{\min} - \alpha^* g_{\max}}\right) \tag{3.18}$$
    apply the control law
$$w(t) = -\alpha K \,\mathrm{sign}\left(\xi_1(t) - \frac{1}{2}\xi_{\max}(t)\right) \tag{3.19}$$
  end while
end procedure

3.4 Adaptive Suboptimal Second Order Sliding Mode

In this section, in order to relax the assumption on the a priori knowledge of the constants $H, g_{\min}$ and $g_{\max}$ in (3.5), (3.6), the design of Adaptive Suboptimal Second Order Sliding Mode (ASSOSM) control laws is addressed.

3.4.1 The Proposed Control Strategies

In particular, four control strategies are designed and analyzed. The first two techniques are adaptive versions of the Suboptimal SOSM (SSOSM) control [BFU98a] discussed in Section 3.3, in which during the reaching phase, the control amplitude is continuously adjusted, so as to arrive at dominating the effect of the uncertainties, in spite of the ignorance of their bounds. When a suitable control amplitude is attained, the origin of the state-space of the auxiliary system (3.16) (i.e., the second order system with states coinciding with the sliding variable and its first time derivative) becomes finite time attractive. The other two control strategies are oriented to reduce the control amplitude in steady-state by applying an additional component to the discontinuous adaptive law, based on the *average control*, obtained at the output of a first order low pass filter, in analogy with [BFPU98].

3.4.1.1 Strategy 1

Making reference to the auxiliary system (3.16), the first ASSOSM control strategy, proposed to steer ξ_1 and ξ_2 to zero in a finite time in spite of the uncertainties and the ignorance of their bounds, is very simple but effective. It allows the amplitude of the discontinuous Suboptimal control law to grow until the sliding manifold becomes an attractive subspace of the controlled system state-space. In analogy with [BFU98a], the control law can be first expressed as follows

$$w(t) = w_{ad}(t) = -W_{ad}(t)\,\mathrm{sign}\left(\xi_1(t) - \frac{1}{2}\xi_{\max}\right). \tag{3.20}$$

This law does not require to measure ξ_2 (this variable is unmeasurable by assumption). In fact, the extremal values $\xi_{\max}$ can be detected by implementing for instance a peak detector as in [BFU98b]. Furthermore, let

$$\Xi_{\max} = \max\left\{|\xi_{\max_i}|\right\} \tag{3.21}$$

denote the maximum of the sequence of the values of ξ_1 stored as $\xi_{\max}$. Then, the design parameter W_{ad} can be chosen according to the following adaptation mechanism

$$\dot{W}_{ad}(t) = \begin{cases} \gamma_1|\xi_1(t)| & \text{if } |\xi_1(t)| > \Xi_{\max} \\ 0 & \text{otherwise,} \end{cases} \tag{3.22}$$

where γ_1 is a positive constant arbitrarily set, and $W_{ad}(t_0) = W_{ad_0}$. Note that in (3.22), the increment of the control amplitude is activated only when the sliding variable tends to increase with respect to the value $\Xi_{\max}$, otherwise the previous value of W_{ad} is kept.

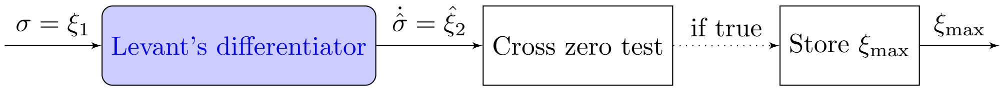

Fig. 3.2. Peak detection scheme to evaluate the extremal value $\xi_{\max}$.

An alternative implementation of Strategy 1 can be based on the use of the Levant's differentiator [Lev03] discussed in Subsection 3.2.2. A first advantage of this version is that the peak detector in [BFU98b] is no more necessary, which improves the stability properties of the controlled system as will be clarified in Subsection 3.4.2. A second advantage is that the estimate of ξ_2 (denoted by $|\hat{\xi}_2|$), obtained with high (theoretically ideal) accuracy after a finite time, can be used to improve the response promptness of the adaptive mechanism, by introducing a term depending on $|\hat{\xi}_2|$. The new formulation of (3.22) can be expressed as

$$\dot{W}_{ad}(t) = \begin{cases} \gamma_1 |\xi_1(t)| + \gamma_2 |\hat{\xi}_2(t)| & \text{if } |\xi_1(t)| > \Xi_{\max} \\ 0 & \text{otherwise,} \end{cases} \tag{3.23}$$

where γ_2 is a positive constant arbitrarily set.

Remark 3.1. Since the Levant's differentiator is used to determine ξ_2, the extremal values $\xi_{\max_i}$ can be evaluated by using, as an alternative with respect to the peak detector in [BFU98b], the scheme in Fig. 3.2. That is, $\xi_{\max}$ is stored at the time instants when $\hat{\xi}_2$ changes its sign.

Remark 3.2. The adaptation mechanism in (3.23) has the advantages previously mentioned. Its disadvantage with respect to the strategy proposed in (3.22) is the introduction of additional parameters to set (those of the Levant's differentiator and γ_2). Moreover, it is necessary to provide sufficient time for the differentiator to converge (the differentiator proves to converge in a finite time), to get a usable estimate of ξ_2.

3.4.1.2 Strategy 2

The adaptation mechanism (3.22) or (3.23) proposed in Strategy 1 transforms the AS-SOSM control law into a plain SSOSM law after a transient, which is necessary for the adaptive gain to reach the appropriate size. For this reason, Strategy 1 has the same conservativeness features of the original SSOSM control algorithm. In order to decrease the control amplitude whenever the sliding variable tends towards the sliding manifold, a second adaptive SOSM control strategy can be proposed. As for Strategy 1, one could write a first version based on the peak detector in [BFU98b], and a second version based on the Levant's differentiator. To keep the treatment concise, we will report hereafter only the version based on the Levant's differentiator. Specifically, the following adaptive mechanism is designed

$$\dot{W}_{ad}(t) = \begin{cases} \gamma_1 |\xi_1(t)| \operatorname{sign}(\xi_1(t)) \operatorname{sign}(\hat{\xi}_2(t)) & \text{if } W_{ad}(t) \geq 0 \\ -\gamma_1 |\xi_1(t)| \operatorname{sign}(\xi_1(t)) \operatorname{sign}(\hat{\xi}_2(t)) & \text{otherwise,} \end{cases} \tag{3.24}$$

where γ_1 is a positive constant arbitrarily set.

Remark 3.3. Also in this case the promptness of the adaptation mechanism (3.24) can be increased adding a term depending on $|\hat{\xi}_2|$, i.e.,

$$\dot{W}_{ad}(t) = \begin{cases} (\gamma_1|\xi_1(t)| + \gamma_2|\hat{\xi}_2(t)|)\,\mathrm{sign}(\xi_1(t))\,\mathrm{sign}(\hat{\xi}_2(t)) & \text{if } W_{ad}(t) \geq 0 \\ -(\gamma_1|\xi_1(t)| + \gamma_2|\hat{\xi}_2(t)|)\,\mathrm{sign}(\xi_1(t))\,\mathrm{sign}(\hat{\xi}_2(t)) & \text{otherwise,} \end{cases} \tag{3.25}$$

where γ_2 is a positive constant arbitrarily set.

3.4.1.3 Strategy 3

As shown in [BFPU98], the estimate of the equivalent control associated with the second order sliding mode control law can be used to compensate the uncertain terms. Yet, only an approximate cancellation of the uncertainties can be performed, which allows for a reduction of the control effort. This approach is now used to design alternative strategies oriented to improve the performance of Strategies 1 and 2.

Let the discontinuous control input be expressed as

$$w(t) = \gamma_3 w_{ad}(t) + \gamma_4 w_{av}(t), \tag{3.26}$$

where γ_3, γ_4 are positive definite functions, w_{ad} is chosen as (3.22) or (3.23) in Strategy 1, and w_{av} is the average control obtained at the output of a first order filter having the discontinuous signal w_{ad} as input, i.e.,

$$\tau_1 \dot{w}_{av}(t) + w_{av}(t) = w_{ad} \tag{3.27}$$

τ_1 being a suitably chosen time constant. Note that, according to the theory introduced in [Utk92], and the definition of *equivalent control* for systems controlled via SOSM control strategies [BFU98b], w_{av} asymptotically tends to the equivalent control when a second order sliding mode is enforced. In this strategy, γ_3 and γ_4 are selected through a weight tuning mechanism analogous to that in [BFPU98], i.e.,

$$\gamma_3(t) = \begin{cases} 1 & \text{if } |z(t)| \geq 1 \\ |z(t)| & \text{if } \gamma_{3_{\min}} < |z(t)| < 1 \\ \gamma_{3_{\min}} & \text{if } |z(t)| \leq \gamma_{3_{\min}}, \end{cases} \tag{3.28}$$

$$\gamma_4 = 1 - \gamma_3, \tag{3.29}$$

where z is the output of a first order filter designed as

$$\tau_2 \dot{z}(t) + z(t) = \gamma_3(t)\left(w(t) - w_{av}(t)\right), \tag{3.30}$$

with τ_2 being a suitably chosen time constant. Note that, the value $\gamma_3 = 1$ corresponds to the case in which only the adaptive discontinuous control law of Strategy 1 is applied. Further, note that $\gamma_{3_{\min}}$ is set on the basis of the various error sources in filtering which can be a priori evaluated. In practice, Strategy 3 tends to coincide with Strategy 1 when the controlled system is far from being in sliding mode. On the other hand, when the sliding mode is almost reached or even enforced, the major component of the control law (3.26) is the estimate of the equivalent control. The suitable blend between the adaptive SOSM control law of Strategy 1 and its filtered version according to (3.27) is realized by the peculiar switching logic in (3.28), (3.29).

3.4.1.4 Strategy 4

A further adaptive SOSM control strategy can be attained by composing Strategy 2 with the mechanism to estimate the equivalent control described in Strategy 3. Let the discontinuous control input be expressed as in (3.26), where w_{ad} is chosen as (3.24) or (3.25) in Strategy 2, and w_{av} is the average control obtained as in (3.27). Moreover, also in this case, γ_3 and γ_4 are selected as in (3.28)-(3.30).

3.4.2 Stability Analysis

In this section, the ASSOSM control strategies previously introduced are theoretically analyzed. Theorems are provided for Strategies 1 and 3. Moreover, comments on the stability features of Strategy 2 and 4 are also reported.

Making reference to the auxiliary system (3.16), let $\{H_i\}$, $\{g_{\min_i}\}$ and $\{g_{\max_i}\}$, $i \in \mathbb{N}$ denote the sequences of relative unknown extremal values of functions h and g, such that

$$|H_i| \leq H, \quad g_{\min_i} \geq g_{\min}, \quad g_{\max_i} \leq g_{\max}, \tag{3.31}$$

with H being the unknown upper bound of function h, and $g_{\min}$, $g_{\max}$ being the unknown lower bound and upper bound of function g, respectively. Let t_{d_i} be the time instants when

$$W_{ad} > \max\left(\frac{|H_i|}{g_{\min_i}}; \frac{4|H_i|}{3g_{\min_i} - g_{\max_i}}\right) \quad i \in \mathbb{N}, \tag{3.32}$$

and t_d be the time instant when (3.32) holds, with $|H_i| = H$, $g_{\min_i} = g_{\min}$ and $g_{\max_i} = g_{\max}$. Moreover, let t_{r_δ} be the time instant when the sliding variable reaches a δ-vicinity of the origin of the auxiliary state-space, and t_r be the time instant when the sliding manifold is finally reached, i.e., $\sigma(t) = \dot{\sigma}(t) = 0$, $\forall\, t \geq t_r$.

With reference to the ASSOSM control strategies proposed in the previous section, the following results can be proved.

Theorem 3.1. *Given the auxiliary system* (3.16)*, applying Strategy 1 with the control law* (3.20)*, the peak dector in [BFU98b] and the adaptive mechanism in* (3.22)*, then, in a finite time* $t_{r_\delta} \geq t_d$*, the auxiliary system state variables* ξ_1 *and* ξ_2 *are ultimately bounded in a* δ*-vicinity of the origin of the auxiliary system state-space.*

Proof. Two different cases can occur.
Case 1 ($|H_i| = H$, $g_{\min_i} = g_{\min}$ and $g_{\max_i} = g_{\max}$, $i \in \mathbb{N}$): In this case, one can distinguish between two subcases:

Subcase 1.1: $W_{ad}(t_0) = W_{ad_0}$ is such that

$$W_{ad_0} > \max\left(\frac{H}{g_{\min}}; \frac{4H}{3g_{\min} - g_{\max}}\right), \tag{3.33}$$

which implies that $t_d = t_0$. Then, since the standard convergence condition for the SSOSM algorithm [BFU98a] is satisfied, the control law (3.20) enforces the generation of a sequence of states with coordinates featuring the contraction property expressed by

$$|\xi_{\max_{i+1}}| < |\xi_{\max_i}|, \tag{3.34}$$

where $\xi_{\max_i}$ is the i-th extremal value of variable ξ_1. According to [BFU98b], the actual evolutions of ξ_1 and ξ_2 differ of $\mathcal{O}(\delta^2)$ and $\mathcal{O}(\delta)$, respectively, with respect to the ideal evolutions. This implies that in a finite time $t_{r_\delta} \geq t_d$ the distance of the sliding variable and its first time derivative from the origin of the auxiliary state-space is of $\mathcal{O}(\delta)$.

Subcase 1.2: $W_{ad}(t_0) = W_{ad_0}$ does not satisfy (3.33). Then, the adaptive mechanism (3.22) makes the adaptive gain $W_{ad}(t)$ grow, while the sliding variable increases. This process lasts until the time instant $t_{d_i} = t_d$, when the adaptive gain is such that (3.33) holds. At this point, Subcase 1.1 occurs.

Case 2 ($|H_i| < H$, $g_{\min_i} > g_{\min}$ and $g_{\max_i} < g_{\max}$, $i \in \mathbb{N}$): Also in this case two subcases can be distinguished.

Subcase 2.1: $W_{ad}(t_0) = W_{ad_0}$ is such that (3.32) holds. In this subcase, until $|h(\cdot)| \leq |H_i|$ and $g_{\min_i} \leq g(\cdot) \leq g_{\max_i}$, the control amplitude is sufficient to dominate the uncertain terms, so that a contraction, analogous to that described in (3.34) for Subcase 1.1, occurs. Yet, when $|h(\cdot)| > |H_i|$ and/or $g(\cdot) < g_{\min_i}$ or $g(\cdot) > g_{\max_i}$, the auxiliary variable $\xi_1(t)$ tends to increase. If $|\xi_1(t)| > \Xi_{\max}(t)$, $\Xi_{\max}(t)$ as in (3.21), the adaptive mechanism (3.22) makes the adaptive gain $W_{ad}(t)$ grow until the time instant $t_{d_{i+1}}$ when

$$W_{ad} > \max\left(\frac{|H_{i+1}|}{g_{\min_{i+1}}}; \frac{4|H_{i+1}|}{3g_{\min_{i+1}} - g_{\max_{i+1}}}\right) \quad i \in \mathbb{N}. \tag{3.35}$$

So, a contraction as in (3.34) occurs again. This mechanism iterates until $H_j = H$, $g_{\min_j} = g_{\min}$ and $g_{\max_j} = g_{\max}$, $j \geq i+1$, when Subcase 1.1 occurs.

Subcase 2.2: $W_{ad}(t_0) = W_{ad_0}$ does not satisfy (3.32). Then, $\xi_1(t)$ tends to increase until the time instant t_{d_i} when the adaptive gain W_{ad} is such that (3.32) holds. At this point, Subcase 2.1 occurs. □

Theorem 3.2. *Given the auxiliary system (3.16), applying Strategy 1 with the control law (3.20), the adaptive mechanism in (3.23), and the Levant's differentiator, assume that $t_0 \geq t_{Ld}$, t_{Ld} being the finite time necessary for the differentiator convergence, then, in a finite time $t_r \geq t_d \geq t_0$, the auxiliary system state variables ξ_1 and ξ_2 are steered to the origin of the auxiliary system state-space.*

Proof. The proof is analogous to that of Theorem 3.1. The only difference is that the Levant's differentiator is used instead of the peak detector in [BFU98b] to detect $\xi_{\max_i}$ with ideal accuracy. This implies that the auxiliary system reaches in a finite time the origin of the auxiliary state-space, enforcing a second order sliding mode. □

Remark 3.4. Note that, also in case of Strategy 2, Theorem 3.1 and Theorem 3.2 hold. The proofs are analogous to the previous ones, with the difference in the mechanism to tune the amplitude W_{ad}.

Now, by virtue of Theorem 3.1 and Theorem 3.2 also the following result can be proved.

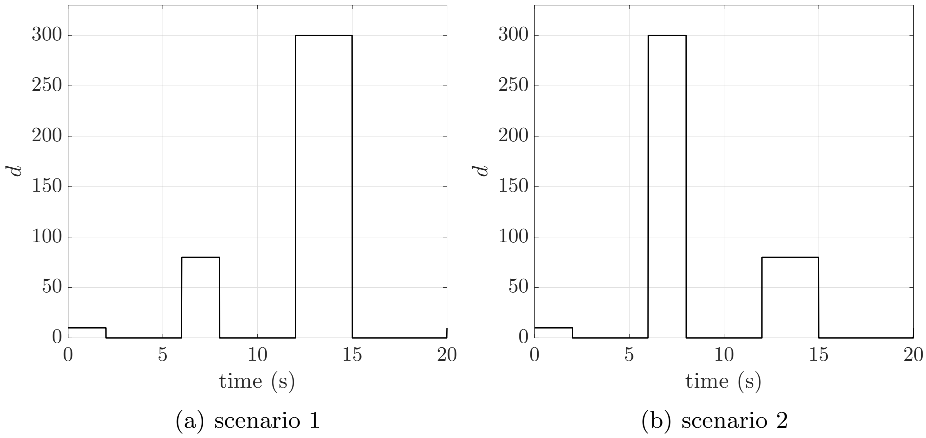

Fig. 3.3. The two instances of the matched disturbances d used in the example: **(a)** Scenario 1. **(b)** Scenario 2.

Theorem 3.3. *Given the auxiliary system* (3.16)*, applying Strategy 3 with the control law* (3.26)*-*(3.30) *and* (3.20)*, the peak detector in [BFU98b] and the adaptive mechanism* (3.22)*, then, in a finite time* $t_{r_\delta} \geq t_d$*, the auxiliary system state variables* ξ_1 *and* ξ_2 *are ultimately bounded in a* δ*-vicinity of the origin of the auxiliary system state-space.*

Proof. The proof is analogous to that of Theorem 3.1, observing that the saturation level $\gamma_3 = \gamma_{3_{\min}}$ in the weight tuning mechanism (3.28)-(3.29) corresponds to the fact that the discontinuous control (3.20) is never switched off, so that it again guarantees, in a finite time $t_{r_\delta} \geq t_d$, the reaching of a δ-vicinity of the sliding manifold. □

Theorem 3.4. *Given the auxiliary system* (3.16)*, applying Strategy 3 with the control law* (3.26)*-*(3.30) *and* (3.20)*, the adaptive mechanism in* (3.23)*, and the Levant's differentiator, assume that* $t_0 \geq t_{Ld}$*,* t_{Ld} *being the finite time necessary for the differentiator convergence, then, in a finite time* $t_r \geq t_d \geq t_0$*, the auxiliary system state variables* ξ_1 *and* ξ_2 *are steered to the origin of the auxiliary system state-space, i.e., a second order sliding mode is enforced.*

Proof. The proof is analogous to that of Theorem 3.2, observing again that the saturation level $\gamma_3 = \gamma_{3_{\min}}$ in the weight tuning mechanism (3.28)-(3.29) corresponds to the fact that the discontinuous control (3.20) is never switched off, so that it guarantees that, in a finite time $t_r \geq t_d$ ($t_d \geq t_0 \geq t_{Ld}$), the reaching of the sliding manifold is attained. This is true even if the predominant control component, to reduce the control amplitude in steady-state, is the average control obtained at the output of the first order filter (3.27). □

Remark 3.5. Theorems 3.3 and 3.4 are valid also for Strategy 4 which differs only for the adaptive mechanism to tune W_{ad}.

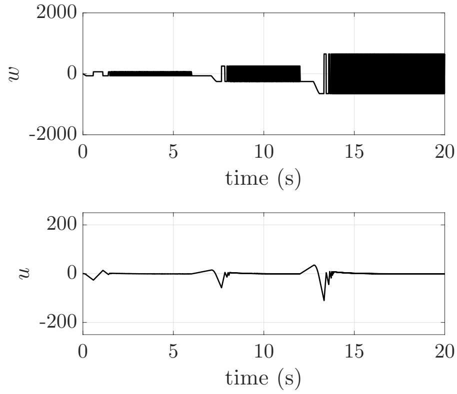

(a) scenario 1

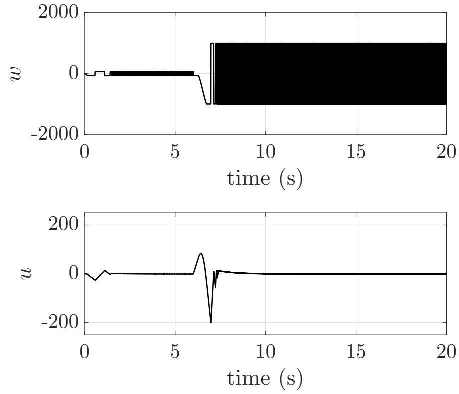

(b) scenario 2

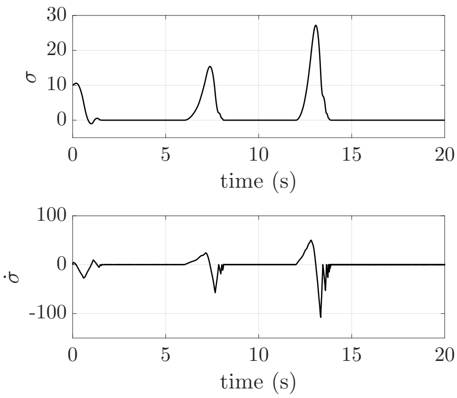

(c) scenario 1

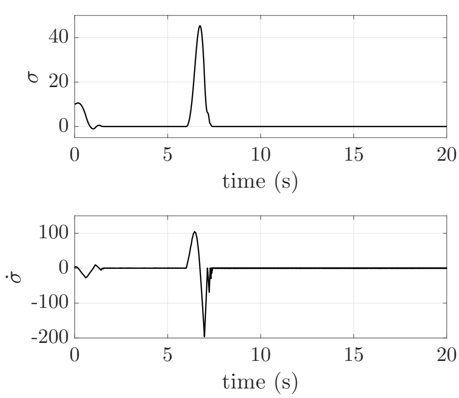

(d) scenario 2

Fig. 3.4. Strategy 1. **(a)**, **(b)** Time evolution of the discontinuous auxiliary control w (top) and of the continuous input u (bottom) in Scenario 1 and 2, respectively. **(c)**, **(d)** Time evolution of σ (top) and $\dot{\sigma}$ (bottom) in Scenario 1 and 2, respectively.

3.4.3 Illustrative Example

Consider the following uncertain auxiliary system

$$\begin{aligned} \dot{\xi}_1(t) &= \xi_2(t) \\ \dot{\xi}_2(t) &= \cos(\xi_1(t)) - \sin(\xi_1(t))\xi_2(t) + d(t) + u(t) + w(t) \end{aligned} \tag{3.36}$$

where $d(t)$ represents an exogenous bounded disturbance. Two instances of $d(t)$ are considered, namely Scenario 1 and Scenario 2, as illustrated in Fig. 3.3. Note that (3.36) is a system analogous to (3.16), since it can be written as

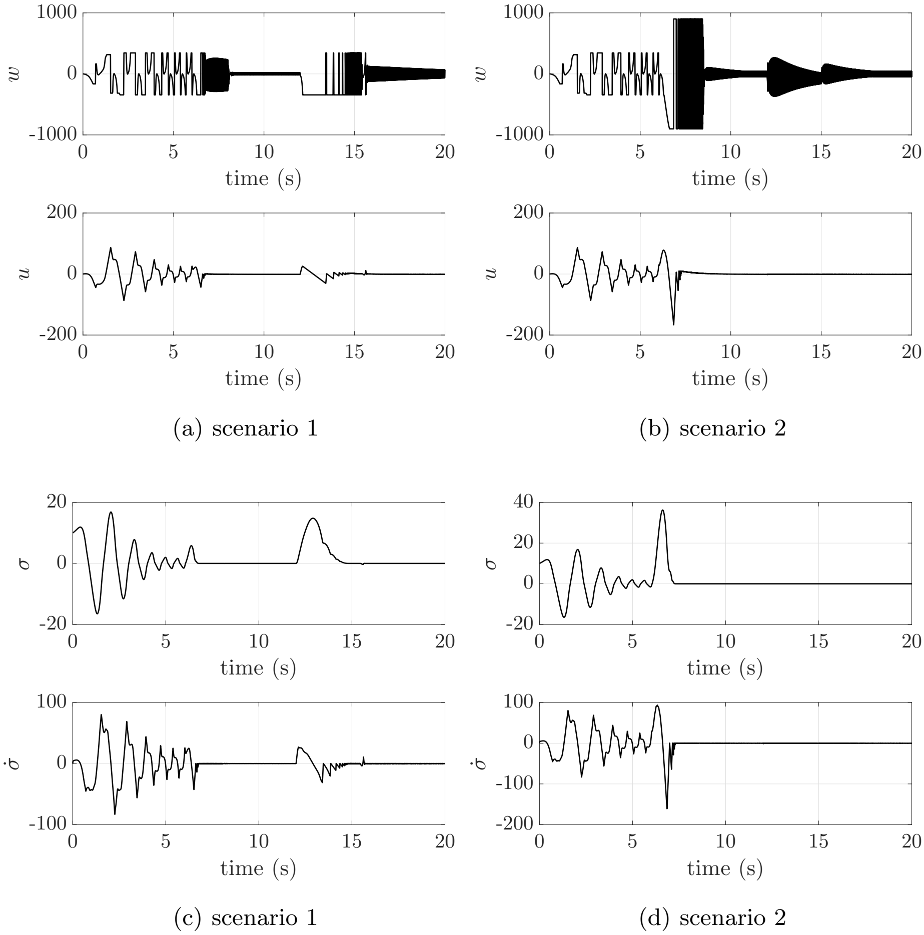

(a) scenario 1 (b) scenario 2

(c) scenario 1 (d) scenario 2

Fig. 3.5. Strategy 3. **(a)**, **(b)** Time evolution of the discontinuous auxiliary control w (top) and of the continuous input u (bottom) in Scenario 1 and 2, respectively. **(c)**, **(d)** Time evolution of σ (top) and $\dot{\sigma}$ (bottom) in Scenario 1 and 2, respectively.

$$
\begin{aligned}
\dot{\xi}_1(t) &= \xi_2(t) \\
\dot{\xi}_2(t) &= h(\boldsymbol{x}(t), u(t), d(t)) + gw(t) \\
\dot{u}(t) &= w(t)
\end{aligned}
\tag{3.37}
$$

with $h(\boldsymbol{x}(t), u(t), d(t)) = \cos(\xi_1(t)) - \sin(\xi_1(t))\xi_2(t) + d(t) + u(t)$, $\boldsymbol{x}(t) = [\xi_1, \xi_2]^T$, and $g = 1$. For the sake of exposition we illustrate the results obtained by applying only Strategy 1 (in the version expressed by (3.23) with $\gamma_1 = 30$ and $\gamma_2 = 15$), and Strategy 3 (with $\gamma_{3_{\min}} = 0.05$, $\tau_1 = 0.5$, $\tau_2 = 10$, and the same parameters used for Strategy 1). Figs. 3.4 and 3.5 show the time evolution of the discontinuous control $w(t)$, the continuous input $u(t)$, the sliding variable σ and its first time derivative $\dot{\sigma}$, for both the scenarios when Strategy 1 and Strategy 3 are applied, respectively.

3.5 Higher Order Sliding Modes with Optimal Reaching

Taking into account the results presented in [DF09] and referring to the auxiliary system

$$\begin{aligned}\dot{\xi}_1(t) &= \xi_2(t)\\ \dot{\xi}_2(t) &= \xi_3(t)\\ \dot{\xi}_3(t) &= h(\boldsymbol{x}(t),t) + g(\boldsymbol{x}(t),t)u(t),\end{aligned} \tag{3.38}$$

where $\xi_3 = \ddot{\sigma}$, then the so-called *robust Fuller's problem* can be formulated as follows

$$\min_u \left\{ \max_{h,g} \int_{t_0}^{+\infty} |\sigma(t)|^\nu dt \right\}, \tag{3.39}$$

subject to (3.38), (3.5)-(3.6). Assume bounded control $|u|_\infty \le \alpha$, and ν being a positive constant. The underlying idea is that the control law guarantees the best control action for the worst-case realization of the uncertain terms.

Let

$$\alpha_r := \alpha g_{\min} - H > 0 \tag{3.40}$$

denote the so-called *reduced control amplitude*, i.e., the minimum possible amplitude of $|\dot{\xi}_3|$, for any possible realization of the uncertain terms, with $\alpha > 0$. The solution to the robust Fuller's problem with $\nu \to 0^+$, in case of Third Order Sliding Mode (3SM) control, is given by

$$u = -\alpha \begin{cases} u_0 := 0 & (\sigma,\,\dot{\sigma},\,\ddot{\sigma}) \in \mathcal{M}_0 \\ u_1 := \operatorname{sign}(\ddot{\sigma}) & (\sigma,\,\dot{\sigma},\,\ddot{\sigma}) \in \mathcal{M}_1 \setminus \mathcal{M}_0 \\ u_2 := \operatorname{sign}\left(\dot{\sigma} + \frac{\ddot{\sigma}^2 u_1}{2\alpha_r}\right) & (\sigma,\,\dot{\sigma},\,\ddot{\sigma}) \in \mathcal{M}_2 \setminus \mathcal{M}_1 \\ u_3 := \operatorname{sign}(s(\sigma,\dot{\sigma},\ddot{\sigma})) & \text{else,} \end{cases} \tag{3.41}$$

where

$$s(\sigma,\dot{\sigma},\ddot{\sigma}) := \sigma + \frac{\ddot{\sigma}^3}{3\alpha_r^2} + u_2 \left[\frac{1}{\sqrt{\alpha_r}} \left(u_2\dot{\sigma} + \frac{\ddot{\sigma}^2}{2\alpha_r} \right)^{\frac{3}{2}} + \frac{\dot{\sigma}\ddot{\sigma}}{\alpha_r} \right], \tag{3.42}$$

while $\mathcal{M}_0$, $\mathcal{M}_1$, $\mathcal{M}_2$ are defined as

$$\begin{aligned}\mathcal{M}_0 &:= \left\{ (\sigma,\dot{\sigma},\ddot{\sigma}) \in \mathbb{R}^3 \,:\, \sigma = \dot{\sigma} = \ddot{\sigma} = 0 \right\}\\ \mathcal{M}_1 &:= \left\{ (\sigma,\dot{\sigma},\ddot{\sigma}) \in \mathbb{R}^3 \,:\, \sigma - \tfrac{\ddot{\sigma}^3}{6\alpha_r^2} = 0,\ \dot{\sigma} + \tfrac{\ddot{\sigma}|\ddot{\sigma}|}{2\alpha_r} = 0 \right\}\\ \mathcal{M}_2 &:= \left\{ (\sigma,\dot{\sigma},\ddot{\sigma}) \in \mathbb{R}^3 \,:\, s(\sigma,\dot{\sigma},\ddot{\sigma}) = 0 \right\}.\end{aligned} \tag{3.43}$$

The set $\mathcal{M}_1$ is the switching line, while the surface $\mathcal{M}_2$ is referred to as *switching manifold* (see Fig. 3.6).

Remark 3.6 (Second order sliding mode controller with optimal reaching). In [DF09] it is also provided an optimal family of second order switching curves that allow to make the state of the auxiliary system (e.g. (3.16)) reach, in a finite time, the origin of the auxiliary state-space, i.e.,

$$u = -\alpha \operatorname{sign}\left(\sigma + \frac{\beta(\nu)}{\alpha_r} \dot{\sigma} |\dot{\sigma}| \right), \quad \beta(\nu) \in \left[\frac{1}{4}, \frac{1}{2} \right]. \tag{3.44}$$

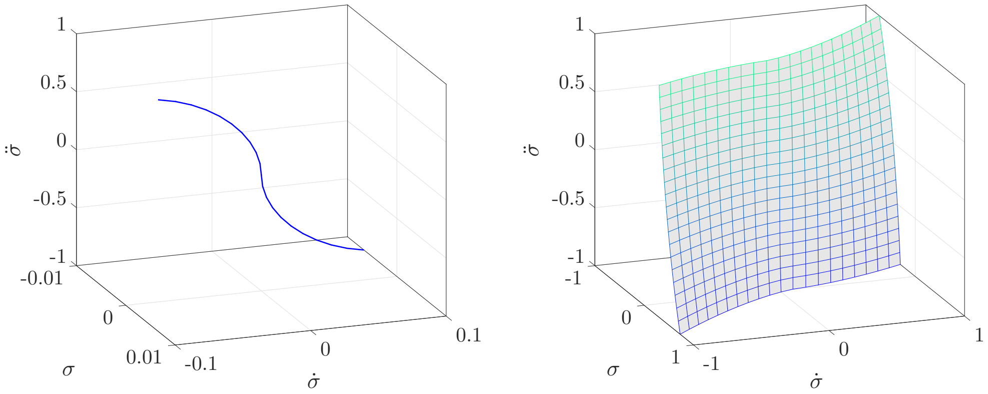

(a) set $\mathcal{M}_1$ (b) set $\mathcal{M}_2$

Fig. 3.6. Sets in case of 3SM algorithm with $\alpha_r = 1$. **a** switching line $\mathcal{M}_1$. **b** switching manifold $\mathcal{M}_2$.

3.6 Second Order Sliding Mode Control with Quantized Uncertainty

This section deals with the design of a Second-Order Sliding Mode (SOSM) control algorithm. The novelty of the proposed approach is the design of a nonsmooth switching line, based on the quantization of the uncertainties affecting the system. The quantized uncertainty levels allow one to define nested box sets in the auxiliary state space, i.e., the space of the sliding variable and its first time derivative, and select suitable control amplitudes for each set, in order to guarantee the convergence of the sliding variable to the sliding manifold in a finite time. The proposed algorithm is theoretically analyzed, proving the existence of an upperbound of the reaching time to the origin through the considered quantization levels.

3.6.1 Problem Formulation

Consider the single-input system (3.3) affine in the control variable, i.e.,

$$\begin{aligned} \dot{\boldsymbol{x}} &= \boldsymbol{a}(\boldsymbol{x},t) + \boldsymbol{b}(\boldsymbol{x},t)u \\ \sigma &= \sigma(\boldsymbol{x},t), \end{aligned} \tag{3.45}$$

where $\boldsymbol{x} \in \Omega$ ($\Omega \subset \mathbb{R}^n$ bounded) is the state vector, the value of which at the initial time instant t_0 is $\boldsymbol{x}(t_0) = \boldsymbol{x}_0$, and $u \in \mathbb{R}$ is a scalar input subject to the saturation $[-\alpha, \alpha]$, while $\boldsymbol{a}(\boldsymbol{x}(t)) : \Omega \to \mathbb{R}^n$, $\boldsymbol{b}(\boldsymbol{x}(t)) : \Omega \to \mathbb{R}^n$ are uncertain functions of class $C^1(\Omega)$, and $\sigma(\boldsymbol{x}(t)) : \Omega \to \mathbb{R}$ of class $C^2(\Omega)$ is a suitable output function. This function will play the role of sliding function in the following, that is $\sigma(\boldsymbol{x}(t))$ is the variable to steer to zero in a finite time in order to solve the control problem, according to classical sliding mode control theory [Utk92]. The sliding function $\sigma(\boldsymbol{x}(t))$ has to be selected such that the following assumption holds.

Assumption 3.1 (Sliding function). If $u(t)$ in (3.45) is designed so that, in a finite time t_r (ideal reaching time), $\sigma(\boldsymbol{x}(t_r)) = 0 \ \forall \boldsymbol{x}_0 \in \Omega$ and $\sigma(\boldsymbol{x}(t)) = 0 \ \forall t > t_r$, then $\forall t \geq t_r$ the origin is an asymptotically stable equilibrium point of (3.45) constrained to $\sigma(\boldsymbol{x}(t)) = 0$.

Assume that (3.45) is complete in Ω and has a uniform relative degree equal to 2. Moreover, assume that system (3.45) admits a global normal form in Ω, i.e., there exists a global diffeomorphism of the form $\boldsymbol{\Phi}(\boldsymbol{x}) : \Omega \to \Phi_\Omega \subset \mathbb{R}^n$,

$$\boldsymbol{\Phi}(\boldsymbol{x}) = \begin{pmatrix} \boldsymbol{\Psi}(\boldsymbol{x}) \\ \sigma(\boldsymbol{x}) \\ \boldsymbol{a}(\boldsymbol{x}) \cdot \nabla\sigma(\boldsymbol{x}) \end{pmatrix} = \begin{pmatrix} \boldsymbol{x_r} \\ \boldsymbol{\xi} \end{pmatrix}$$
$$\boldsymbol{\Psi} : \Omega \to \mathbb{R}^{n-2}, \quad \boldsymbol{x}_r \in \mathbb{R}^{n-2}, \quad \boldsymbol{\xi} = \begin{pmatrix} \sigma(\boldsymbol{x}) \\ \dot{\sigma}(\boldsymbol{x}) \end{pmatrix} \in \mathbb{R}^2 ,$$

such that,

$$\begin{aligned} \dot{\boldsymbol{x}}_{\boldsymbol{r}} &= \boldsymbol{a_r}(\boldsymbol{x_r}\,, \boldsymbol{\xi}) \\ \dot{\xi}_1 &= \xi_2 \\ \dot{\xi}_2 &= h(\boldsymbol{x_r}\,, \boldsymbol{\xi}) + g(\boldsymbol{x_r}\,, \boldsymbol{\xi})u \\ y &= \xi_1 \\ \boldsymbol{\xi}(t_0) &= \boldsymbol{\xi}_0, \end{aligned} \tag{3.46}$$

with

$$\begin{aligned} \boldsymbol{a_r} &= \frac{\partial \boldsymbol{\Psi}}{\partial \boldsymbol{x}}(\boldsymbol{\Phi}^{-1}(\boldsymbol{x_r}, \xi))\boldsymbol{a}(\boldsymbol{\Phi}^{-1}(\boldsymbol{x_r}, \boldsymbol{\xi})) \\ h &= \boldsymbol{a}(\boldsymbol{\Phi}^{-1}(\boldsymbol{x_r}, \boldsymbol{\xi})) \cdot \nabla \left(\boldsymbol{a}(\boldsymbol{\Phi}^{-1}(\boldsymbol{x_r}, \boldsymbol{\xi})) \cdot \nabla\sigma(\boldsymbol{\Phi}^{-1}(\boldsymbol{x_r}, \boldsymbol{\xi}))\right) \\ g &= \boldsymbol{b}(\boldsymbol{\Phi}^{-1}(\boldsymbol{x_r}, \boldsymbol{\xi})) \cdot \nabla \left(\boldsymbol{a}(\boldsymbol{\Phi}^{-1}(\boldsymbol{x_r}, \boldsymbol{\xi})) \cdot \nabla\sigma(\boldsymbol{\Phi}^{-1}(\boldsymbol{x_r}, \boldsymbol{\xi}))\right), \end{aligned}$$

where the obvious dependence on time is omitted. Note that, as a consequence of the uniform relative degree assumption, it yields

$$g(\boldsymbol{x_r},\, \boldsymbol{\xi}) \neq 0, \quad \forall\, (\boldsymbol{x_r}, \boldsymbol{\xi}) \in \Phi_\Omega \,. \tag{3.47}$$

Since $\boldsymbol{a_r}$, h, g (the latter is assumed to be positive definite, for the sake of simplicity) are continuous functions and Φ_Ω is a bounded set, one has that (3.5), (3.6) hold. Moreover, the following assumption on the internal dynamics $\boldsymbol{x_r}$ is introduced.

Remark 3.7 (Zero dynamics). From Assumption 3.1 it follows that the zero dynamics $\dot{\boldsymbol{x}}_{\boldsymbol{r}} = \boldsymbol{a_r}(\boldsymbol{x_r}\,, \boldsymbol{0})$ of system (3.46) is globally asymptotically stable.

Let Assumption 3.1 hold. Relying on (3.46), the control problem to solve is the design of a feedback control law

$$u(t) = \kappa\left(\sigma(\boldsymbol{x}(t)),\, \dot{\sigma}(\boldsymbol{x}(t))\right), \tag{3.48}$$

such that $\forall\, \boldsymbol{x}_0 \in \Omega, \exists\, t_r \geq 0 \,:\, \sigma(\boldsymbol{x}(t)) = \dot{\sigma}(\boldsymbol{x}(t)) = 0, \forall\, t \geq t_r$ in spite of the uncertainties.

3.6.2 The Proposed Control Strategy

Making reference to the SOSM control law (3.44) with α_r as in (3.40), and $\beta(\nu) = \frac{1}{2}$, we define a new *nonsmooth* switching line. The idea is based on the fact that the uncertain terms h and g, depending on $\boldsymbol{\xi}$, are quantized relaying on a partition of the auxiliary system state space into m stripes $\mathcal{B}_i$, $i = 1, \ldots, m$, with

$$\mathcal{B}_i := \left\{(\sigma, \dot{\sigma}) \in \mathbb{R}^2 \,:\, \underline{\sigma}_i \le \sigma \le \overline{\sigma}_i\right\}, \tag{3.49}$$

where $\underline{\sigma}_i < 0$ and $\overline{\sigma}_i > 0$ are constants, with $\underline{\sigma}_i < \underline{\sigma}_{i+1} < 0$ and $\overline{\sigma}_i > \overline{\sigma}_{i+1} > 0$, $i = 1, 2, \ldots, m-1$. Then, instead of considering unique functions h and g, we can consider the instances of h and g in the stripes, hereafter denoted as

$$\begin{aligned} h_{\mathcal{B}_i}(\boldsymbol{x_r}, \boldsymbol{\xi}) &= \{h(\boldsymbol{x_r}, \boldsymbol{\xi}) : \boldsymbol{\xi} \in \mathcal{B}_i\} \\ g_{\mathcal{B}_i}(\boldsymbol{x_r}, \boldsymbol{\xi}) &= \{g(\boldsymbol{x_r}, \boldsymbol{\xi}) : \boldsymbol{\xi} \in \mathcal{B}_i\}\ , \end{aligned} \tag{3.50}$$

with $i = 1, \ldots, m$. Let $\partial\mathcal{B}_i$ be the boundaries of the sets $\mathcal{B}_i$, and consider the switching line included in the ith level as

$$\mathcal{S}_i = \mathcal{S}_i^+ \cup \mathcal{S}_i^- := \left\{(\sigma, \dot{\sigma}) \in \mathbb{R}^2 \,:\, \sigma = -\frac{\dot{\sigma}|\dot{\sigma}|}{2\alpha_{r,i}}\right\}, \tag{3.51}$$

where $\mathcal{S}_i^+$ and $\mathcal{S}_i^-$ are the sets of points belonging to $\mathcal{S}_i$ with $\dot{\sigma} > 0$ and $\dot{\sigma} < 0$, respectively. For each level i, in order to define the corresponding switching line, one has

$$\alpha_{r,i} = \mathcal{G}_{\min,i}\alpha_i - \mathcal{H}_i > 0 \tag{3.52}$$

where $\mathcal{H}_i$ and $\mathcal{G}_{\min,i}$ are positive constants such that

$$\begin{aligned} |h_{\mathcal{B}_i}(\boldsymbol{x_r}, \boldsymbol{\xi})| &\le \mathcal{H}_i \\ g_{\mathcal{B}_i}(\boldsymbol{x_r}, \boldsymbol{\xi}) &\ge \mathcal{G}_{\min,i} > 0, \end{aligned} \tag{3.53}$$

with $i = 1, \ldots, m$.

Assumption 3.2 (Quantized uncertainty). The bounds $\mathcal{H}_i$, $\mathcal{G}_{\min,i}$ are known, with $\mathcal{H}_i \ge \mathcal{H}_{i+1}$, and $\mathcal{G}_{\min,i} \le \mathcal{G}_{\min,i+1}$, $i = 1, \ldots, m-1$.

Then, we select $\alpha_{r,i} > \alpha_{r,i+1}$, and

$$\alpha_i > \frac{\mathcal{H}_i}{\mathcal{G}_{\min,i}}\ , \tag{3.54}$$

such that $\alpha_i > \alpha_{i+1}$, $i = 1, \ldots, m-1$.

Remark 3.8 (Control effort). The inequalities $\alpha_i > \alpha_{i+1}$, $i = 1, \ldots, m-1$, imply that the effort of the control input fed into the plant is reduced when the auxiliary state trajectory moves towards the inner levels.

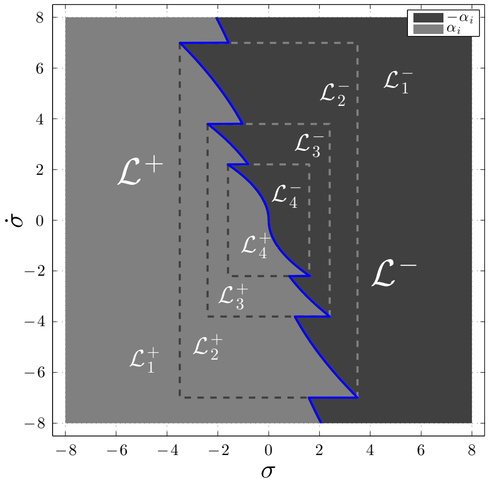

Fig. 3.7. Switching line $\mathcal{S}$ in case of the proposed SOSM algorithm, and the quantization levels.

Define now the box sets as

$$\mathcal{Z}_i := \mathcal{B}_i \cap \left\{(\sigma,\,\dot{\sigma}) \in \mathbb{R}^2 \,:\, \underline{\dot{\sigma}}_i \le \dot{\sigma} \le \overline{\dot{\sigma}}_i\right\}, \tag{3.55}$$

where $\underline{\dot{\sigma}}_i$ and $\overline{\dot{\sigma}}_i$ are obtained as the ordinates of the points given by the intersection between the boundaries of the set $\mathcal{B}_i$ and the switching line of the ith level, i.e., $\{(\overline{\sigma}_i,\,\underline{\dot{\sigma}}_i)\,(\underline{\sigma}_i,\,\overline{\dot{\sigma}}_i)\} = \mathcal{S}_i \bigcap \partial\mathcal{B}_i$. Finally, the proposed *nonsmooth switching line*, as illustrated in Fig. 3.7, is defined as

$$\mathcal{S} := \left(\bigcup_{i=1}^{m-1} \mathcal{S}_i \cap (\mathcal{Z}_i \setminus \mathcal{Z}_{i+1})\right) \cup (\mathcal{S}_m \cap \mathcal{Z}_m)\,, \tag{3.56}$$

while the quantization levels are

$$\mathcal{L}_i = \mathcal{L}_i^+ \cup \mathcal{L}_i^- := \mathcal{Z}_i \setminus \mathcal{Z}_{i+1}, \tag{3.57}$$

with $i = 1, \ldots, m-1$, $\mathcal{L}_m = \mathcal{Z}_m$, and $\mathcal{L}_i^+$ and $\mathcal{L}_i^-$ being the regions on the left and on the right of the switching line (3.56), respectively (see Fig. 3.7), i.e.,

$$\begin{aligned} \mathcal{L}_i^+ &:= \left\{(\sigma,\,\dot{\sigma}) \in \mathcal{L}_i \,:\, \sigma < -\frac{\dot{\sigma}|\dot{\sigma}|}{2\alpha_{r,i}}\right\} \cup \mathcal{S}_i^+ \\ \mathcal{L}_i^- &:= \left\{(\sigma,\,\dot{\sigma}) \in \mathcal{L}_i \,:\, \sigma > -\frac{\dot{\sigma}|\dot{\sigma}|}{2\alpha_{r,i}}\right\} \cup \mathcal{S}_i^- \,. \end{aligned} \tag{3.58}$$

Consider now system (3.46), with the auxiliary state space partitioned as in (3.57). Assume also that, for $(\sigma,\,\dot{\sigma}) \in \mathcal{L}_i$, h, g satisfy constraints (3.53). The control parameters α_i are chosen so as to satisfy the constraint (3.54). Then, the control law is defined as

$$u(t) = \alpha_i \operatorname{sign}_{\mathcal{L}_i^{\pm}} \tag{3.59}$$

where

$$\operatorname{sign}_{\mathcal{L}_i^{\pm}} = \begin{cases} +1 & \text{if } (\sigma,\, \dot{\sigma}) \in \mathcal{L}_i^{+} \\ -1 & \text{if } (\sigma,\, \dot{\sigma}) \in \mathcal{L}_i^{-} \end{cases} \tag{3.60}$$

with $i = 1, \dots, m$.

3.6.3 Stability Analysis

In the next Lemma the existence of m invariant regions $\mathcal{L}_{I,i}$ is demonstrated.

Lemma 3.1 (Invariant sets). Consider the state-space partitioned into the m regions defined in (3.57). Assume that the bounds (3.53) hold. Then, all the quantization regions $\mathcal{L}_i$ of the auxiliary state-space contain invariant sets $\mathcal{L}_{I,i} \subset \mathcal{L}_i$ of the form

$$\mathcal{L}_{I,i} := \mathcal{L}_i \setminus \{\mathcal{L}_{0,i} \cup \mathcal{L}_{1,i}\} \tag{3.61}$$

where

$$\begin{aligned} \mathcal{L}_{0,i} &:= \left\{ (\sigma, \dot{\sigma}) \,:\, \sigma > -\frac{\dot{\sigma}|\dot{\sigma}|}{2\alpha_{r,i}} + \overline{\sigma}_i,\ \dot{\sigma} > 0 \right\} \\ \mathcal{L}_{1,i} &:= \left\{ (\sigma, \dot{\sigma}) \,:\, \sigma < -\frac{\dot{\sigma}|\dot{\sigma}|}{2\alpha_{r,i}} + \underline{\sigma}_i,\ \dot{\sigma} < 0 \right\} \ . \end{aligned} \tag{3.62}$$

Moreover, the sets $\mathcal{L}_{I,i}$ are the maximum obtainable domains of attraction for the given switching sets.

Proof. The proof of the Lemma follows from [IRF16], where it is proved that, assuming $\sigma(t_0) = \sigma_0 \in \mathcal{L}_{0,i}$, in presence of the maximum realization of the uncertainties, the system will move on a parabolic arc, the equation of which is the following

$$\sigma = \frac{\dot{\sigma}|\dot{\sigma}|}{2\alpha_{r,i}} + \overline{\sigma}_i + \varepsilon \tag{3.63}$$

with $\varepsilon > 0$ (the case with $\sigma_0 \in \mathcal{L}_{1,i}$ is specular). Then, it is easy to see that starting inside $\mathcal{L}_{0,i}$ or $\mathcal{L}_{1,i}$, this arc intersects the σ-axis outside $\mathcal{L}_i$, and one can conclude that $\mathcal{L}_{I,i}$ are the maximum regions of attraction. □

In the next Theorem, the finite-time stability property of the controlled auxiliary system is proved by exploiting the bang-bang principle [AF66]. Specifically, an explicit expression for the convergence time of the auxiliary trajectory to the origin of the auxiliary state space is found.

Theorem 3.5 (Finite time convergence). *Given system (3.45) controlled via (3.59), such that for the worst possible realization of the disturbance terms Lemma 3.1 holds and the trajectory $(\sigma, \dot{\sigma}) \in \mathcal{L}_{I,i}$, $\forall\, i = 1, \dots, m$ and $\forall\, t \geq t_0$, then, the sliding function σ and its first time derivative $\dot{\sigma}$, i.e., ξ_1 and ξ_2 in the auxiliary system (3.46), are steered to zero in a finite time t_r.*

Proof. The proof of the convergence of the system trajectory to the origin of the auxiliary state space does not depend on the number of box sets, but directly follows from the results presented in [DF09, Theorem 2]. More specifically, when the system trajectory reaches the inner level $\mathcal{L}_m$, the control law (3.59) coincides with the second order sliding mode control law with optimal reaching introduced in [DF09], so that the finite time convergence to the origin of the controlled system is guaranteed as shown in [DF09]. Consider the auxiliary system (3.46) with the worst-case realization of the uncertain terms and controlled by applying the control input (3.59), then the system dynamics can be written as the following double integrator plant, i.e.,

$$\begin{aligned} \dot{\xi}_1(t) &= \xi_2(t) \\ \dot{\xi}_2(t) &= u_r(t) \end{aligned} \tag{3.64}$$

in which $u_r = (\alpha_{r,i}/\alpha_i)u$ implicitly takes into account the effect of the disturbance terms in the generic region $\mathcal{L}_i$. Let $(0, 0) = (\xi_1(t_r),\ \xi_2(t_r))$, where t_r is the reaching time to the origin, given a certain initial condition, by using the control law (3.59). From system (3.64), integrating backward from τ_i to t, τ_i being the initial time instant within the ith region, since the control law assumes constant value inside each region $\mathcal{L}_i$, one has

$$\xi_2(t) = \xi_2(\tau_i) + u_r(t - \tau_i) \tag{3.65}$$

$$\xi_1(t) = \xi_1(\tau_i) + \xi_2(\tau_i)(t - \tau_i) + \frac{1}{2}u_r(t^2 + \tau_i^2) - u_r\tau_i t. \tag{3.66}$$

Consider to start from the external region $\mathcal{L}_1$ and to reach $\mathcal{S}_1^-$. For the sake of brevity only the cases starting on the right of the nonsmooth switching line will be considered, that is the case in which the initial sign of the control law is negative (the opposite case is specular). Three different steps can be distinguished.

Step 1, Case 1 ($(\sigma, \dot{\sigma}) \in \mathcal{L}_1^- \setminus \mathcal{S}_1^-$). The initial control $u_r = -\alpha_{r,1}$ is applied to drive the state starting from $(\xi_1(t_0),\ \xi_2(t_0))$ to the switching line $\mathcal{S}_1^-$. Let $\tau_{s,1}$ denote the time instant when $\mathcal{S}_1^-$ is attained and the control switches to $u_r = \alpha_{r,1}$. Note that for $\xi_2 < 0$ the switching line has the form $\xi_1 = \xi_2^2/(2\alpha_{r,1})$. From equation (3.65), squaring and dividing for $2\alpha_{r,1}$, one has

$$\frac{\xi_2^2(t)}{2\alpha_{r,1}} = \frac{\xi_2^2(\tau_1)}{2\alpha_{r,1}} + \frac{\alpha_{r,1}}{2}(t^2 + \tau_i^2 - 2\tau_1 t) - \xi_2(\tau_1)(t - \tau_1). \tag{3.67}$$

Instead from equation (3.66) one has

$$\xi_1(t) = \xi_1(\tau_1) + \xi_2(\tau_1)(t - \tau_1) - \frac{\alpha_{r,1}}{2}(t^2 + \tau_i^2) + \alpha_{r,1}\tau_1 t. \tag{3.68}$$

Subtracting (3.67) to (3.68), one has

$$\frac{\xi_2^2(\tau_1)}{2\alpha_{r,1}} = \xi_1(\tau_1) + 2\xi_2(\tau_1)(t - \tau_1) - \alpha_{r,1}(t^2 + \tau_i^2) + 2\alpha_{r,1}\tau_1 t. \tag{3.69}$$

From equation (3.69), one obtains

$$\alpha_{r,1}t^2 - 2(\xi_2(\tau_1) + \alpha_{r,1}\tau_1)t + \left(2\xi_2(\tau_1)\tau_1 + \alpha_{r,1}\tau_i^2 - \xi_1(\tau_1) + \frac{\xi_2^2(\tau_1)}{2\alpha_{r,1}}\right) = 0\,. \tag{3.70}$$

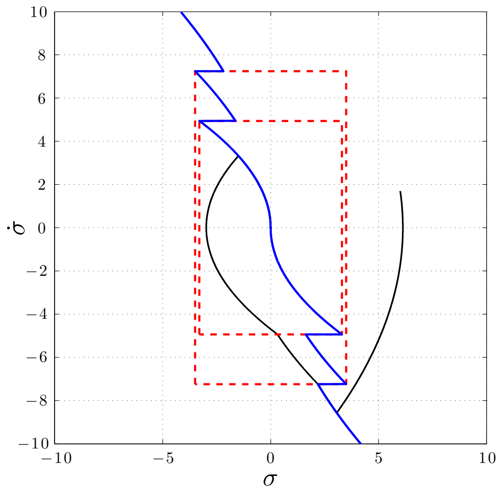

Fig. 3.8. Performance of a perturbed double integrator controlled via the proposed nonsmooth switching line based SOSM algorithm. The bounds of the uncertainties are $\mathcal{H}_1 = 8$, $\mathcal{H}_2 = 3.5$, $\mathcal{H}_3 = 3.3$, $\mathcal{G}_{\min,1} = \mathcal{G}_{\min,2} = \mathcal{G}_{\min,3} = 1$, while the initial conditions are $\xi_0 = [\xi_1(0),\, \xi_2(0)] = [6,\, 1.7]^T$.

Solving (3.70) and considering the positive root to make $\tau_{s,1}$ positive for all $\xi_2(\tau_1)$, the switching time $\tau_{s,1}$ is

$$\tau_{s,1} = \frac{\xi_2(\tau_1)}{\alpha_{r,1}} + \tau_1 + \sqrt{\frac{\xi_1(\tau_1)}{\alpha_{r,1}} + \frac{\xi_2^2(\tau_1)}{2\alpha_{r,1}^2}} \,. \tag{3.71}$$

From equation (3.65), one has that

$$\xi_2(\tau_{s,1}) = \xi_2(\tau_1) - \alpha_{r,1}(\tau_{s,1} - \tau_1) \,. \tag{3.72}$$

Assume now to reach the border of the region $\mathcal{L}_2$, that is $\underline{\dot{\sigma}}_2$, with $u_r = \alpha_{r,1}$ so as to have

$$\xi_2(T_1) = \xi_2(\tau_{s,1}) + \alpha_{r,1}(T_1 - \tau_{s,1}) = \underline{\dot{\sigma}}_2 \,. \tag{3.73}$$

Finally, with $\tau_1 = t_0$, the reaching time is

$$T_1 = \frac{\underline{\dot{\sigma}}_2}{\alpha_{r,1}} + \frac{\dot{\sigma}(t_0)}{\alpha_{r,1}} + t_0 + 2\sqrt{\frac{\sigma(t_0)}{\alpha_{r,1}} + \frac{\dot{\sigma}^2(t_0)}{2\alpha_{r,1}^2}} \,. \tag{3.74}$$

Step 1, Case 2 ($(\sigma, \dot{\sigma}) \in \mathcal{S}_1^-$). From equation (3.65), one has that, by applying $u_r = \alpha_{r,1}$,

$$\xi_2(T_1) = \xi_2(\tau_1) + \alpha_{r,1}(T_1 - \tau_1) \,. \tag{3.75}$$

Assume now to reach the border of the region $\mathcal{L}_2$, that is $\underline{\dot{\sigma}}_2$, so as to have

$$\xi_2(T_1) = \xi_2(\tau_1) + \alpha_{r,1}(T_1 - \tau_1) = \underline{\dot{\sigma}}_2 \,. \tag{3.76}$$

Then, with $\tau_1 = t_0$, the reaching time is

$$T_1 = \frac{\underline{\dot{\sigma}}_2}{\alpha_{r,1}} - \frac{\dot{\sigma}(t_0)}{\alpha_{r,1}} + t_0 \; . \tag{3.77}$$

Step 2 ($(\sigma, \dot{\sigma}) \in \mathcal{L}_2^+$). From equation (3.65), one has that, by applying $u_r = \alpha_{r,2}$,

$$\xi_2(T_2) = \xi_2(\tau_2) + \alpha_{r,2}(T_2 - \tau_2) \; . \tag{3.78}$$

Assume now to reach the border of the region $\mathcal{L}_3$, that is $\underline{\dot{\sigma}}_3$, so as to have

$$\xi_2(T_2) = \xi_2(\tau_2) + \alpha_{r,2}(T_2 - \tau_2) = \underline{\dot{\sigma}}_3 \; . \tag{3.79}$$

Consider that $\tau_2 = T_1$ so that $\xi_2(T_1) = \underline{\dot{\sigma}}_2$, then the reaching time is

$$T_2 = \frac{\underline{\dot{\sigma}}_3}{\alpha_{r,2}} - \frac{\underline{\dot{\sigma}}_2}{\alpha_{r,2}} + T_1 \; . \tag{3.80}$$

Then, for all the regions $\mathcal{L}_i$ $i = 2, \ldots, m-1$, it is possible to write

$$T_i = \frac{\underline{\dot{\sigma}}_{i+1}}{\alpha_{r,i}} - \frac{\underline{\dot{\sigma}}_i}{\alpha_{r,i}} + \sum_{j=1}^{i-1} T_j \; . \tag{3.81}$$

Step 3 ($(\sigma, \dot{\sigma}) \in \mathcal{L}_m^+ \setminus \mathcal{S}_m^+$). Since the target is the origin, the net time is

$$T_m = -\frac{\dot{\sigma}(T_{m-1})}{\alpha_{r,1}} + T_{m-1} + 2\sqrt{-\frac{\sigma(T_{m-1})}{\alpha_{r,m}} + \frac{\dot{\sigma}^2(T_{m-1})}{2\alpha_{r,m}^2}} \; . \tag{3.82}$$

Note that $\dot{\sigma}(T_{m-1}) = \overline{\dot{\sigma}}_m$, so that one has

$$T_m = -\frac{\overline{\dot{\sigma}}_m}{\alpha_{r,m}} + T_{m-1} + 2\sqrt{-\frac{\sigma(T_{m-1})}{\alpha_{r,m}} + \frac{\overline{\dot{\sigma}}_m^2}{2\alpha_{r,m}^2}} \; . \tag{3.83}$$

Finally, one can conclude that the convergence to the origin, in the worst case of uncertainty, occurs in a finite time T_m. In general, this implies a finite convergence time $t_r \leq T_m$, which concludes the proof. □

Note that, the finite time t_r is given by summing the time intervals needed to pass from the external region to the inner one. Given T_i, $i = 1, \ldots, m-1$ as the minimum time inside each quantization region, the whole convergence time is not the minimum one but an upperbound in case of the maximum realization of the uncertainty. Fig. 3.8 shows the performance of a perturbed chain of integrators in the case of the worst realization of the uncertainties. The state trajectory belongs to each region at most in one switch, and the convergence time can be explicitly estimated according to Theorem 3.5, resulting in 4.403 s compared to the actual one equal to 4.404 s. Since Theorem 3.5 has been proved in the continuous time, implying infinite frequency in the switched signals, the difference between the theoretical convergence time and the practical one is due to the use of the fixed step solver in simulation, which instead allows only for finite switching frequency. This slows down the sliding motion on the switching line of the innermost set.

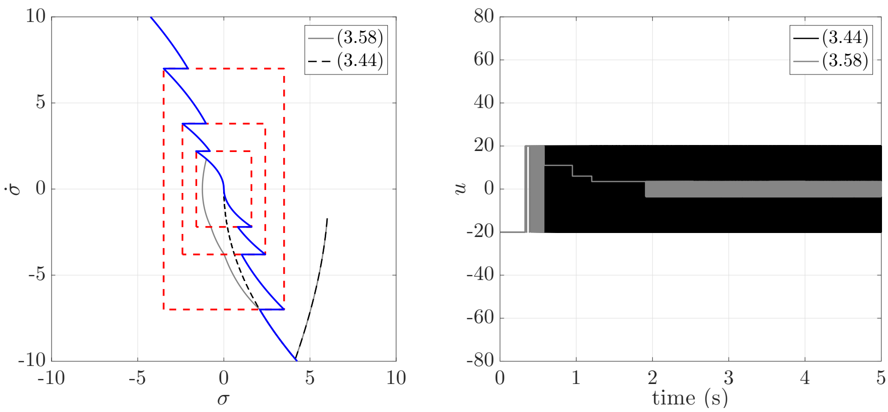

(a) auxiliary state space (b) control input

Fig. 3.9. Illustrative example. **(a)** Auxiliary state space trajectory and **(b)** time evolution of the control law u when the proposed nonsmooth algorithm (3.59) is applied (gray) and when the control algorithm (3.44) is used (black).

3.6.4 Illustrative Example

In this section, in order to assess the properties of the proposed nonsmooth SOSM control strategy, an illustrative example is briefly discussed. Consider the nonlinear uncertain system,

$$\begin{aligned}\dot{x}_1(t) &= x_2(t) + x_3(t)\\ \dot{x}_2(t) &= x_3(t)\\ \dot{x}_3(t) &= 0.5\cos(x_2(t)) + u(t)\\ y(t) &= x_1(t),\end{aligned} \tag{3.84}$$

where the initial condition is $x(0) = [6\ 0.1\ \ -1.8]^T$. Then, the system is stabilized by choosing the sliding variable $\sigma(x(t))$ as the controlled variable $y(t)$. Note that, (3.84) has a uniform relative degree equal to 2, and it admits a global normal form, i.e., there exists the global diffeomorphism

$$\boldsymbol{\Phi}(\boldsymbol{x}(t)) = \begin{pmatrix} x_2(t) \\ x_1(t) \\ x_2(t) + x_3(t) \end{pmatrix} = \begin{pmatrix} x_r(t) \\ \xi_1(t) \\ \xi_2(t) \end{pmatrix},$$

such that

$$\begin{aligned}\dot{x}_r(t) &= \xi_2(t) - x_r(t)\\ \dot{\xi}_1(t) &= \xi_2(t)\\ \dot{\xi}_2(t) &= \xi_2(t) - x_r(t) + 0.5\cos(x_r(t)) + u(t)\\ y(t) &= \xi_1(t)\\ \xi(0) &= \xi_0,\end{aligned} \tag{3.85}$$

$\xi_0 = [6\ -1.7\,]^T$ being the initial condition. Relying on systems (3.84)-(3.85) it is possible to set the bounds in (3.5)-(3.6) equal to $H = 8$, $g_{\min} = g_{\max} = 1$. We assume to known that the uncertainty is quantized in 4 levels, so that $m = 4$ with $\mathcal{H}_1 = 8$, $\mathcal{H}_2 = 4$, $\mathcal{H}_3 = 3$, $\mathcal{H}_4 = 2$, $\mathcal{G}_{\min,1} = \mathcal{G}_{\min,2} = \mathcal{G}_{\min,3} = \mathcal{G}_{\min,4} = 1$, and the corresponding nonsmooth switching line (see Fig. 3.9) is derived as in (3.56), with $\alpha_1 = 20$, $\alpha_2 = 11$, $\alpha_3 = 6$ and $\alpha_4 = 3.5$, respectively.

It is useful to compare the proposed algorithm with the already published control law with optimal reaching (3.44). The trajectory of the auxiliary system and the time evolution of the control signal are reported in Fig. 3.9. More specifically, in Fig. 3.9 **(b)** the main advantage of the proposed approach with respect to (3.44) clearly appears, in terms of control effort which is progressively reduced, according to the quantized levels. Of course, this implies that the convergence finite time is longer. Hence, although the reaching time is increased, the sliding mode is ensured even progressively reducing the gain through the levels, which is beneficial in many practical mechanical and electromechanical cases.

3.7 Conclusions

In this chapter we have seen the design of HOSM control laws and, in particular, the explicit forms of second order and third order sliding mode already published in the literature. After some preliminaries, the ASSOSM has been presented. This algorithm represents one of the contribution of the present work, fulfilling the requirement of relaxing the typical assumption on the knowledge of the bounds of the uncertainties. Moreover, a novel SOSM characterized by a nonsmooth switching line, based on the quantization of the uncertainties has been presented.

4

Practical Sliding Modes in Networked Control Systems

Abstract. This chapter presents novel SMC strategies of Event-Triggered (ET) type for a class of nonlinear systems affected by uncertainties and external disturbances. By virtue of its ET nature, the proposed control strategies are particularly appropriate for Networked Control Systems (NCSs), i.e., feedback systems including communication networks. The objective of the proposed control schemes is indeed to reduce the number of data transmissions over the communication network, in order to avoid problems typically due to the network congestion such as jitter and packet loss. In particular, an ET-SM control scheme and an ET-SOSM control scheme are designed for a class of nonlinear uncertain NCSs, guaranteeing satisfactory performance of the controlled system even in presence of delayed transmissions, and avoiding the notorious Zeno behaviour.

4.1 Preliminaries on Event-Triggered Control

As discussed in the previous chapters, SMC is considered a powerful strategy able to guarantee satisfactory performance in terms of robustness of the controlled system even in presence of unavoidable modelling uncertainties and external disturbances [Utk92, Utk93, ES98, UGS99]. The same robustness property holds for SOSM control methodology [BFU97, BFPU98, SEFL14a, BFLU99, BFU98b, DF09, BFU98a, RF10], in which not only the sliding function but also its first time derivative are steered to zero in a finite time. Moreover, by virtue of its low complexity, SMC methodology represents a very easy to implement solution adequate also for Networked Control Systems (NCSs), i.e., feedback systems including communication networks [HNX07, WL08, LXC+07, GC10, ZBP01].

In Networked Control Systems (NCSs), critical problems such as jitter, packet loss and delayed transmissions can occur specially when the network is congested [LR90, NB96], so determining the worsening of the performance of the controlled system. For these reasons, the need of designing robust control schemes able to reduce data transmissions over the network, while guaranteeing satisfactory performance of the controlled system even in presence of uncertainties and delayed transmissions becomes mandatory.

In the literature, a methodology which is very valued in designing control schemes capable of reducing data transmission effort over communication networks is the so-called

Event-Triggered (ET) control [Tab07, MT08, Ast08, HSVDB08, YA11, YX13, HJT12, PSW13, DTPH17]. Differently from traditional time-triggered control implementation, where periodic data transmissions occur, ET control schemes enable the communication between the plant and the controller (feedback path), and between the controller and the actuator (direct path) only when some triggering condition is satisfied (or violated depending on the adopted logic). For this reason, ET control approach can significantly reduce the number of data transmissions, avoiding the congestion of the network and its possible unavailability. Obviously, there exists a trade-off between the performance of the controlled system and the communication rate [DGJ13]. However, in spite of aperiodic data transmissions, satisfactory stability properties of the controlled system have been studied in the literature. Specifically, in [Tab07], it was proved that in case of nonlinear systems, relying on threshold-based ET algorithm, the Input-to-State Stability of the controlled system can be guaranteed by ensuring a certain decrease in a suitable Lyapunov function.

Recently, in the literature, the basic ET approach has been developed so as to take into account the knowledge of the nominal model of the plant. This has given raise to the so-called Model-Based ET (MB-ET) control [GA13, MA04]. This methodology has been also exploited together with SMC, and Model Predictive Control (MPC), [IF16, FIM14, FSS15], even in case of Mixed Logical Dynamical (MLD) systems [FSS14]. In particular, the use of SMC in conjunction with ET implementation is justified by the necessity of robustness in front of modelling uncertainties and external disturbances which can naturally affect the system [BB16].

4.2 Event-Triggered Sliding Mode Control

First, an ET-SMC scheme is presented for nonlinear uncertain systems with relative degree equal to one, including communication networks that can be unavailable. The proposed ET-SMC strategy is based on a triggering condition that depends on the sliding function associated with the controlled system and on the size of a pre-specified boundary layer of the sliding manifold. The proposed control scheme is theoretically analyzed in the chapter, proving that the sliding function is ultimately bounded in the desired boundary layer, even in presence of delayed transmissions. Moreover, in order to avoid the notorious Zeno behaviour [JLSE99, ATS06], the existence of a lower bound for the time elapsed between consecutive triggering events is proved.

4.2.1 Problem Formulation

Consider a plant[4] (process and actuator) which can be modelled as

$$\dot{\boldsymbol{x}} = \boldsymbol{a}(\boldsymbol{x}) + \boldsymbol{b}(\boldsymbol{x})u + \boldsymbol{d_m}(\boldsymbol{x}), \tag{4.1}$$

where $\boldsymbol{x} \in \Omega$ ($\Omega \subset \mathbb{R}^n$ bounded) is the state vector, the value of which at the initial time instant t_0 is $\boldsymbol{x}(t_0) = \boldsymbol{x}_0$, and $u \in \mathbb{R}$ is the control variable, while $\boldsymbol{a} : \Omega \to \mathbb{R}^n$ and

[4] For the sake of simplicity the dependence of all the variables on time t is omitted when obvious.

$\boldsymbol{b} : \Omega \to \mathbb{R}^n$ are uncertain functions of class C^0. Moreover, system (4.1) is subject to the external disturbance $\boldsymbol{d_m} : \Omega \times \mathbb{R} \to \mathbb{R}^n$. To permit the controller design in the next sections, the following assumption is made on $\boldsymbol{d_m}$.

Assumption 4.1 (Matched uncertainty). The external disturbance $\boldsymbol{d_m}$ is matched, i.e.,

$$\boldsymbol{d_m}(\boldsymbol{x}) = \boldsymbol{b}(\boldsymbol{x})d,$$

where d is unknown but bounded as

$$d \in \mathcal{D} \subset \mathbb{R},$$

$\mathcal{D}^{\text{sup}}$ being a known positive constant.

Define now a suitable output function: the so-called *sliding function*.

Definition 4.1 (Sliding function). $\sigma : \Omega \to \mathbb{R}$ of class C^1 is a sliding function for system (4.1) provided that the pair (σ, u) has the following property: if u in (4.1) is designed so that, in a finite time $t_r^\star \geq t_0$, $\forall\, \boldsymbol{x}_0 \in \Omega, \sigma = 0 \quad \forall\, t \geq t_r^\star$, then $\forall\, t \geq t_r^\star$ the origin is an asymptotically stable equilibrium point of (4.1) constrained to the sliding manifold $\sigma = 0$.

Now, regarding the sliding function σ as the controlled variable associated with system (4.1), assume that system (4.1) is complete in Ω and has a uniform relative degree equal to 1. The following definitions are introduced.

Definition 4.2 (Ideal sliding mode). Given $t_r^\star \geq t_0$ (ideal reaching time), if $\forall\, \boldsymbol{x}_0 \in \Omega, \sigma = 0 \quad \forall\, t \geq t_r^\star$, then an *ideal sliding mode* of system (4.1) is enforced on the sliding manifold $\sigma = 0$.

Definition 4.3 (Practical sliding mode). Given $t_r \geq t_0$ (practical reaching time), if $\forall\, \boldsymbol{x}_0 \in \Omega,\ |\sigma| \leq \delta \quad \forall\, t \geq t_r$, then a *practical sliding mode* of system (4.1) is enforced in a vicinity of the sliding manifold $\sigma = 0$.

Moreover, assume that system (4.1) admits a global normal form in Ω, i.e., there exists a global diffeomorphism (see [Kha96]) of the form $\boldsymbol{\Phi} = [\boldsymbol{\Psi}, \sigma]^T = [\boldsymbol{x_r}, \xi]^T$, with $\boldsymbol{\Phi} : \Omega \to \Phi_\Omega$ ($\Phi_\Omega \subset \mathbb{R}^n$ bounded), and $\boldsymbol{\Psi} : \Omega \to \mathbb{R}^{n-1}$, $\boldsymbol{x_r} \in \mathbb{R}^{n-1}$, $\xi \in \mathbb{R}$, such that

$$\dot{\boldsymbol{x}}_{\boldsymbol{r}} = \boldsymbol{a_r}(\boldsymbol{x_r}, \xi) \tag{4.2}$$

$$\dot{\xi} = h(\boldsymbol{x_r}, \xi) + g(\boldsymbol{x_r}, \xi)(u + d), \tag{4.3}$$

with

$$
\begin{aligned}
\boldsymbol{a}_{\boldsymbol{r}}\left(\boldsymbol{x}_{\boldsymbol{r}},\xi\right) &= \frac{\partial \boldsymbol{\Psi}}{\partial \boldsymbol{x}}\left(\boldsymbol{\Phi}^{-1}\left(\boldsymbol{x}_{\boldsymbol{r}},\xi\right)\right)\,\boldsymbol{a}\left(\boldsymbol{\Phi}^{-1}\left(\boldsymbol{x}_{\boldsymbol{r}},\xi\right)\right)\\
h\left(\boldsymbol{x}_{\boldsymbol{r}},\xi\right) &= \boldsymbol{a}\left(\boldsymbol{\Phi}^{-1}\left(\boldsymbol{x}_{\boldsymbol{r}},\xi\right)\right)\cdot\nabla\sigma\left(\boldsymbol{\Phi}^{-1}\left(\boldsymbol{x}_{\boldsymbol{r}},\xi\right)\right)\\
g\left(\boldsymbol{x}_{\boldsymbol{r}},\xi\right) &= \boldsymbol{b}\left(\boldsymbol{\Phi}^{-1}\left(\boldsymbol{x}_{\boldsymbol{r}},\xi\right)\right)\cdot\nabla\sigma\left(\boldsymbol{\Phi}^{-1}\left(\boldsymbol{x}_{\boldsymbol{r}},\xi\right)\right).
\end{aligned}
$$

Note that, as a consequence of the uniform relative degree assumption, one has that $g \neq 0$. Since $\boldsymbol{a}_{\boldsymbol{r}}$, h, g are continuous functions and Φ_{Ω} is a bounded set, one has also that

$$
\begin{aligned}
|h(\boldsymbol{x}_{\boldsymbol{r}},\xi))| &\leq H\\
g(\boldsymbol{x}_{\boldsymbol{r}},\xi)) &\leq g_{\max},
\end{aligned} \tag{4.4}
$$

H and $g_{\max}$ being known positive constants. Moreover, the following assumption is made on the uncertain function g.

Assumption 4.2 (Bounded uncertainty). The uncertain function g can be lower bounded as

$$
g(\boldsymbol{x}_{\boldsymbol{r}},\xi)) \geq g_{\min}, \tag{4.5}
$$

$g_{\min}$ being a known positive constant.

Now, a preliminary control problem can be formulated.

Problem 4.1. Let Assumptions 4.1 and 4.2 hold. Relying on (4.1)-(4.5), design a feedback control law

$$
u^{\star} = \kappa(\sigma), \tag{4.6}
$$

with the following property: $\forall\, \boldsymbol{x}_0 \in \Omega$, $\exists\, t_r^{\star} \geq t_0$ such that $\sigma = 0 \;\; \forall\, t \geq t_r^{\star}$, in spite of the uncertainties.

Note that the solution to Problem 4.1 is a control law capable of robustly enforcing an *ideal sliding mode* of system (4.1) in a finite time, according to Definition 4.2.

In practical implementation the state is sampled at certain time instants $t = \{t_0, t_1, \ldots, t_k, \ldots\}$, $k \in \mathbb{N}$, and the control law, computed as $u(t_k) = \kappa(\sigma(t_k))$, is held constant between two successive samplings. This kind of implementation, called sample-and-hold, can be expressed as

$$
u = u(t_k) \quad \forall\, t \in [t_k,\, t_{k+1}[\,,\;\; k \in \mathbb{N}, \tag{4.7}
$$

where t_k, $t_{k+1} \in \mathcal{T}$, $\mathcal{T}$ being the set of the triggering time instants. In conventional implementation, the sequence $\{t_k\}_{k\in\mathbb{N}}$ is typically periodic and the time interval $t_{k+1} - t_k$, is a priori fixed. The control approach, in that case, is classified as *time-triggered*.

In this chapter, instead of relying on time-triggered executions, we introduce a triggering condition which depends on the sliding function, so that the state of the auxiliary system is transmitted over the communication network only when such a condition is verified. This implies that also the control law is updated and sent to the actuator of the plant only at the triggering time instants. In the literature, this control approach is known as Event-Triggered (ET) control approach. Note that, in this work, we do not adopt a mathematical model of the network, but we design the control strategy aiming at reducing data transmission. This in order to avoid the network congestion and limit its negative consequences, such as packets drop. However, in order to take into account possible malfunctions, we suppose that the presence of the communication network can cause delayed transmissions due to the network unavailability. More precisely, we suppose that data transmissions could occur with time-varying delay Δ_d and Δ_f in the direct and feedback path, respectively. Let the overall time delay be $\Delta = \Delta_d + \Delta_f$. The following assumption is made on Δ.

Assumption 4.3 (Time delay). The overall time-varying delay Δ can be bounded as

$$\Delta \leq \Delta_{\max}, \tag{4.8}$$

$\Delta_{\max}$ being a known positive constant.

Moreover, we suppose that the plant is equipped with a particular zero-order-hold (indicated in Fig. 4.1 with ZOH*), such that the control variable computed at the last triggering time instant t_k is held constant $\forall\, t \in [t_k,\, t_{k+1}[$. Then, this approach tends to reduce the transmissions over the network both in the direct path (from the controller to the plant) and in the feedback path (from the sensor to the controller).

Taking into account the previous considerations, we can now move from Probelm 4.1 and formulate the problem which will be actually solved in this chapter.

Problem 4.2. Let Assumptions 4.1-4.3 hold. Relying on (4.1)-(4.5), design a feedback control law

$$u = u(t_k) = \kappa(\sigma(t_k)) \quad \forall\, t \in [t_k,\, t_{k+1}[,\;\; k \in \mathbb{N}, \tag{4.9}$$

with the following property: $\forall\, \boldsymbol{x}_0 \in \Omega$, $\exists\, t_r \geq t_0$ such that $|\sigma| \leq \delta \quad \forall\, t \geq t_r$, in spite of the uncertainties, δ being a positive constant arbitrarily set.

Note that the solution to Problem 4.2 is an ET control law capable of enforcing a *practical sliding mode* of system (4.1) in a finite time, according to Definition 4.3.

Before illustrating the features of the proposed control scheme, relying on Problem 4.2 let us introduce the following definition.

Definition 4.4 (Boundary layer). The *boundary layer* for the sliding function is

$$\mathcal{B}_\delta := \big\{\sigma \in \mathbb{R} : |\sigma| \leq \delta\big\}, \tag{4.10}$$

δ being a positive constant arbitrarily set.

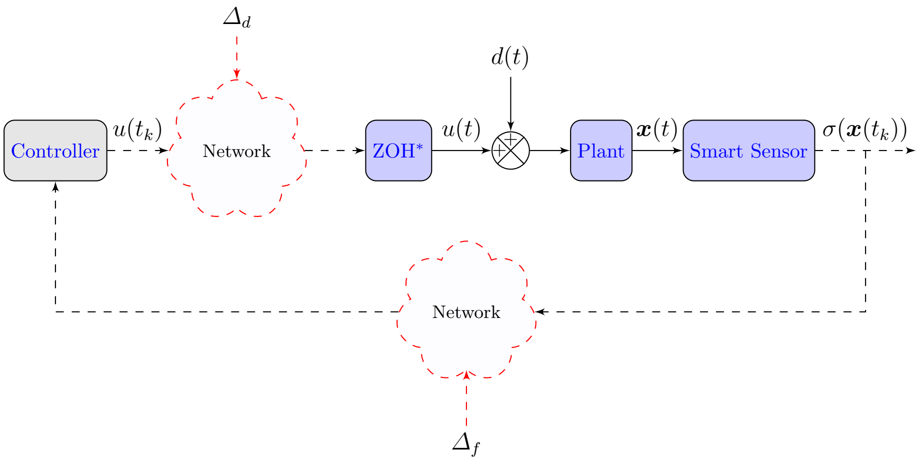

Fig. 4.1. The proposed event-triggered sliding mode control scheme.

4.2.2 The Proposed Control Scheme

The control scheme proposed to solve Problem 4.2 is reported in Fig. 4.1, where the dashed path means that the corresponding signals are transmitted over the network only at the triggering time instants t_k. The control scheme contains two key blocks: the *Smart Sensor* and the *Controller*.

The Smart Sensor

The considered sensor is smart in the sense that it has some computation capability, i.e., it is able to compute the sliding function and verify the following *triggering condition*:

$$|\sigma| = \delta, \tag{4.11}$$

δ being a positive constant arbitrarily set (see Definition 4.4).

The dashed path in Fig. 4.1 is enabled only when (4.11) holds, i.e., when the Smart Sensor generates a triggering signal. More precisely, when (4.11) is verified, the actual value of the sliding function σ is transmitted by the sensor over the network, so that the control law u is updated and sent to the plant.

The Controller

Relying on (4.9)-(4.11), the control law that we propose to solve Problem 4.2 can be expressed as

$$u = u(t_k) = -U_{\max}\,\mathrm{sign}(\sigma(t_k)) \quad \forall\, t \in [t_k,\, t_{k+1}[,\;\; k \in \mathbb{N}, \tag{4.12}$$

where

$$U_{\max} > \frac{F}{G_{\min}} + \mathcal{D}^{\sup} \tag{4.13}$$

is a positive value suitably selected in order to enforce a sliding mode. Note that the control signal is transmitted by the Controller to the plant (through the communication network) only when (4.11) holds.

4.2.3 Stability Analysis

In this section, the stability properties of system (4.1) controlled via the proposed ET-SM control strategy are analyzed. To this end, it is convenient to introduce the following definitions.

Definition 4.5 (Attractiveness). The set $\mathcal{B}_\delta$ is said to be attractive if the solution to the auxiliary system (4.3), $\forall\, \sigma \in \mathbb{R} \setminus \mathcal{B}_\delta$, satisfies the so-called η-reachability condition [Utk92, ES98] (see Subsection 2.2.5)

$$\sigma\dot{\sigma} \leq -\eta|\sigma|\,. \tag{4.14}$$

Definition 4.6 (Ultimately boundedness). The solution σ to the auxiliary system (4.3) is said to be ultimately bounded with respect to the set $\mathcal{B}_\delta$ if

$$\forall\, \boldsymbol{x}_0 \in \Omega,\ \exists\, t_r \geq t_0\ : \sigma \in \mathcal{B}_\delta \qquad \forall\, t \geq t_r\,. \tag{4.15}$$

Definition 4.7 (Positively invariant set). Let σ be the solution to the auxiliary system (4.3) starting from the initial condition $\sigma(t_0)$. The set $\mathcal{B}_\delta$ is said to be positively invariant if

$$\sigma(t_0) \in \mathcal{B}_\delta \Rightarrow \sigma \in \mathcal{B}_\delta \qquad \forall\, t \geq t_0\,. \tag{4.16}$$

Definition 4.8 (Practical stability). In analogy with [LSL12], given the bounded sets Ω, $\Omega_\delta \subset \Omega$, then, the origin of system (4.1) is said to be practically stable with respect to $(t_r^\star, t_{r,x}, \Omega, \Omega_\delta, \mathcal{D})$ if

$$\forall\, t_r^\star \geq t_0,\ \forall\, d \in \mathcal{D},\ \forall\, \boldsymbol{x}_0 \in \Omega,\ \exists\, t_{r,x} \geq t_r^\star : \boldsymbol{x} \in \Omega_\delta \quad \forall\, t \geq t_{r,x}\,. \tag{4.17}$$

Before showing the theoretical results, the following assumption is made on the initial condition of the auxiliary system (4.3).

Assumption 4.4 (Initial conditions). Given the auxiliary system (4.3), let the sign of the initial condition $\sigma(t_0)$ be known.

Now, making reference to the auxiliary system (4.3) the following results can be proved.

Lemma 4.1 (Finite time convergence to $\mathcal{B}_\delta$). Let Assumptions 4.1, 4.2 and 4.4 hold with $|\sigma(t_0)| > \delta$, δ being a positive constant arbitrarily set. Given the auxiliary system (4.3) controlled by (4.12), (4.13) with the triggering condition (4.11), then, the boundary layer $\mathcal{B}_\delta$ is attractive for the solution σ to (4.3).

Proof. Consider the η-reachability condition (4.14). Since Assumption 4.4 holds, one has that $\operatorname{sign}(\sigma) = \operatorname{sign}(\sigma(t_0)), \forall\, t \in [t_0, t_1]$, t_1 being the first triggering time instant. Making reference to system (4.3), since $\sigma \operatorname{sign}(\sigma) = |\sigma|$, it yields

$$\begin{aligned}\sigma\dot{\sigma} &= \sigma\left(h - gU_{\max}\operatorname{sign}(\sigma) + gd\right)\\ &\leq \left(H - g_{\min}(U_{\max} - \mathcal{D}^{\sup})\right)|\sigma|,\end{aligned} \tag{4.18}$$

By virtue of inequality (4.13), one can easily verify that (4.14) holds with $\eta = -(H - g_{\min}(U_{\max} - \mathcal{D}^{\sup})) > 0$. Then, integrating the inequality $\sigma\dot{\sigma} \leq -\eta|\sigma|$ from $t_0 = 0$ to t_r, one has

$$t_r \leq \frac{|\sigma(0)| - \delta}{\eta}, \tag{4.19}$$

implying the finite time convergence of the sliding function to $\mathcal{B}_\delta$. Moreover, one can also conclude that the first transmission over the network is executed at the triggering time instant $t_1 = t_r$. □

Remark 4.1. Note that, by virtue of Lemma 4.1, the proposed control solution avoids to transmit the value of σ and u over the network during the entire reaching phase, i.e., till the sliding function enters the boundary layer $\mathcal{B}_\delta$ at the time instant $t_1 = t_r$.

Lemma 4.2 (Invariance of $\mathcal{B}_\delta$). Let Assumptions 4.1, 4.2 and 4.4 hold with $|\sigma(t_0)| \leq \delta$, δ being a positive constant arbitrarily set. Given the auxiliary system (4.3) controlled by (4.12), (4.13) with the triggering condition (4.11), then, the boundary layer $\mathcal{B}_\delta$ is a positively invariant set for the solution σ to (4.3).

Proof. Consider two different cases in order to prove the result.

Case 1 ($|\sigma| < \delta$). In this case, according to the proposed ET-SMC strategy, $\forall\, t \in [t_k, t_{k+1}[$ the control law is not updated, i.e., its sign does not change. This implies that the sliding function evolves in the boundary layer $\mathcal{B}_\delta$ until it reaches its border, so that Case 2 occurs.

Case 2 ($|\sigma| = \delta$). In this second case, the triggering condition is verified. Then, the value of σ is sent to the controller and the control law is updated. In particular, the sign of the control law changes, and the sliding function is steered towards the interior of $\mathcal{B}_\delta$, so that Case 1 occurs again. This implies that $\forall\, \sigma(t_0) \in \mathcal{B}_\delta$, then, $\forall\, t \geq t_0$, $\sigma \in \mathcal{B}_\delta$, i.e., $\mathcal{B}_\delta$ is a positively invariant set, according to Definition 4.7. □

Now, relying on Lemmas 4.1 and 4.2, one can prove the major result concerning the evolution of the auxiliary system (4.3) controlled via the proposed strategy.

Theorem 4.1 (Evolution of the auxiliary system). *Let Assumptions 4.1, 4.2 and 4.4 hold, and let δ be a positive constant arbitrarily set. Given the auxiliary system (4.3) controlled by (4.12), (4.13) with the triggering condition (4.11), then, the solution σ to (4.3) is ultimately bounded with respect to $\mathcal{B}_\delta$.*

Proof. The proof is a straightforward consequence of Lemma 4.1 and Lemma 4.2. In fact, by virtue of Lemma 4.1, applying the control law (4.12), (4.13) there exists a time instant t_r when σ enters $\mathcal{B}_\delta$, i.e., the triggering condition (4.11) is verified. Then, by virtue of Lemma 4.2, $\forall t \geq t_r$, σ remains in $\mathcal{B}_\delta$, which implies that it is ultimately bounded with respect to $\mathcal{B}_\delta$. □

Remark 4.2 (Approximability property). Note that the proposed control scheme, because of its ET nature, cannot generate an ideal sliding mode (see Definition 4.2), but only a practical sliding mode (see Definition 4.3). However, by virtue of the Approximability Theorem 2.1, it can be proved that also the state of system (4.1) is ultimately bounded. This implies that Problem 4.2 is equivalent to the problem of designing a bounded control such that, according to Definition 4.8, the origin of system (4.1) is practically stable.

Now, since the triggering time instants are implicitly defined and only known at the execution times, we prove the existence of a lower bound for the so-called *inter-execution* or *inter-event* times [Tab07]. More specifically, let $\tau_{\min}$ be the minimum inter-event time, such that $t_{k+1} - t_k \geq \tau_{\min}$ for any $k \in \mathbb{N}^+$.

Theorem 4.2 (Minimum inter-event time). *Let Assumptions 4.1, 4.2 and 4.4 hold, and let δ be a positive constant arbitrarily set. Given the auxiliary system (4.3) controlled by (4.12), (4.13) with the triggering condition (4.11), then, $\forall t > t_r$ the inter-event times are lower bounded by*

$$\tau_{\min} = \frac{2\delta}{H + g_{\max}(U_{\max} + \mathcal{D}^{\sup})}. \tag{4.20}$$

Proof. Since the value of σ and u are transmitted over the network only when the triggering condition (4.11) is verified, the theorem will be proved by computing the time interval $t_{k+1} - t_k$ that σ takes to evolve from $-\delta$ to δ with the maximum velocity, i.e., $\dot{\sigma}_{\max} = H + g_{\max}(U_{\max} + \mathcal{D}^{\sup})$. Then, one has

$$\begin{aligned} \sigma(t_{k+1}) - \sigma(t_k) &= \int_{t_k}^{t_{k+1}} \dot{\sigma}_{\max}\, d\tau \\ \delta - (-\delta) &= \dot{\sigma}_{\max}(t_{k+1} - t_k) \\ 2\delta &= (H + g_{\max}(U_{\max} + \mathcal{D}^{\sup}))\tau_{\min}, \end{aligned} \tag{4.21}$$

where the equality $t_{k+1} - t_k = \tau_{\min}$ follows from the assumption that σ evolves with constant maximum velocity $\dot{\sigma}_{\max}$. Finally, from (4.21) one obtains (4.20), which proves the theorem. □

Remark 4.3 (Zeno behaviour). Note that Theorem 4.2 guarantees that the time elapsed between consecutive triggering events does not become arbitrarily small, avoiding the notorious Zeno behaviour [JLSE99, ATS06]. In practical cases, this result is very useful to assess the feasibility of the proposed scheduling policy.

Taking now into account the possible occurrence of delayed data transmissions, due to the presence of communication networks, the following result can be proved. More precisely, relying on Problem 4.2 we will prove that by modifying the triggering condition (4.11), the auxiliary state-space trajectory is ultimately bounded with respect to the desired boundary layer $\mathcal{B}_\delta$.

Theorem 4.3 (Delayed communications). *Let Assumptions 4.1-4.4 hold. Given the auxiliary system* (4.3) *controlled by* (4.12), (4.13) *with the triggering condition* (4.11), *then, for any desired*

$$\delta > (H + g_{\max}(U_{\max} + \mathcal{D}^{\sup}))\Delta_{\max},$$

the triggering condition

$$|\sigma| = \delta',$$

with

$$\delta' = \delta - (H + g_{\max}(U_{\max} + \mathcal{D}^{\sup}))\Delta_{\max},$$

enforces the following inequality

$$|\sigma| \leq \delta \quad \forall\, t \geq t_r', \tag{4.22}$$

t_r' *being the reaching time instant of the boundary layer*

$$\mathcal{B}_{\delta'} := \left\{\sigma \in \mathbb{R} : |\sigma| \leq \delta'\right\}.$$

Proof. In analogy with Lemma 4.1, one can easily prove that there exists a time instant t_r' when σ enters the inner boundary layer $\mathcal{B}_{\delta'}$. Suppose now that the transmission of $\sigma(t_k) = \delta'$ occurs with the maximum possible time delay $\Delta_{\max}$. Moreover, assume that the sliding function evolves with constant maximum velocity $\dot{\sigma}_{\max} = H + g_{\max}(U_{\max} + \mathcal{D}^{\sup})$. In order to enforce inequality (4.22), we impose that $\sigma(t_k + \Delta_{\max}) = \delta$. Then, one has

$$\begin{aligned}
\sigma(t_k + \Delta_{\max}) - \sigma(t_k) &= \int_{t_k}^{t_k+\Delta_{\max}} \dot{\sigma}_{\max}\, d\tau \\
\delta - \delta' &= \dot{\sigma}_{\max}\Delta_{\max} \\
\delta' &= \delta - (H + g_{\max}(U_{\max} + \mathcal{D}^{\sup}))\Delta_{\max},
\end{aligned} \tag{4.23}$$

which concludes the proof. □

Note that in case of delayed transmissions, the lower bound $\tau_{\min}$ can be obtained by using δ' instead of δ in Theorem 4.2.

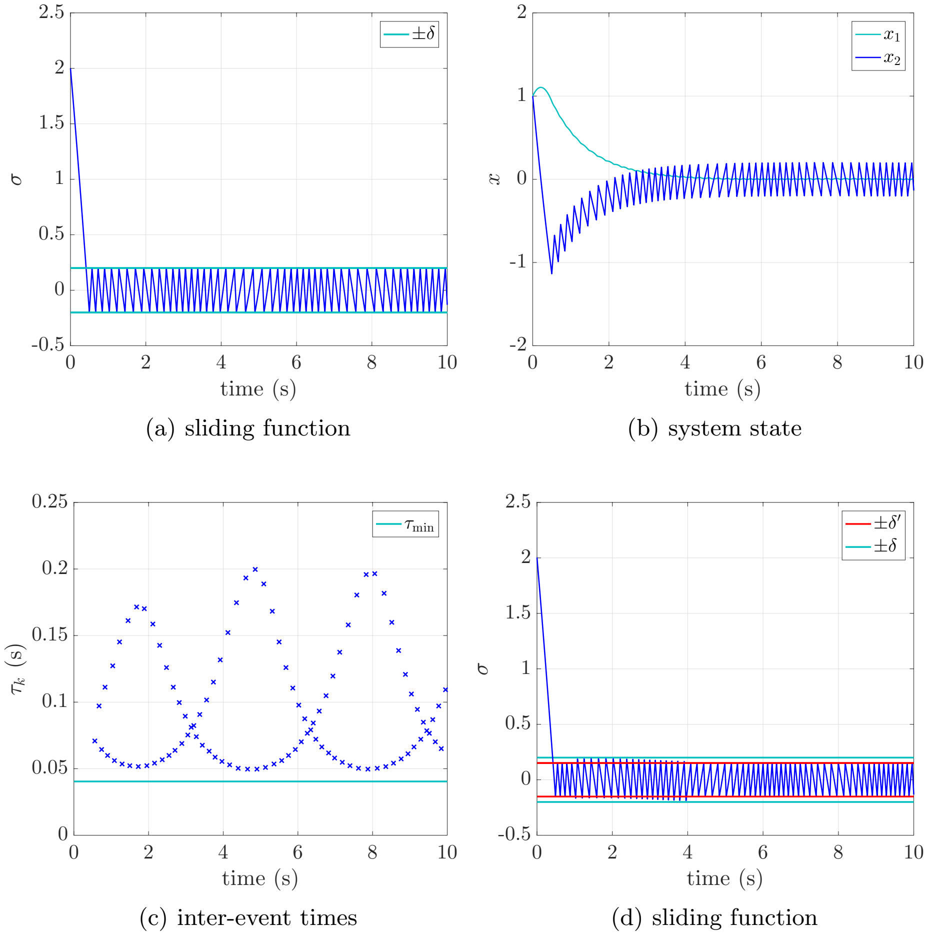

Fig. 4.2. Event-triggered sliding mode control. **(a)** Time evolution of the sliding function, with visualization of the boundary layer $\mathcal{B}_\delta$ of size δ. **(b)** Time evolution of the system states x_1 and x_2. **(c)** Inter-event times $\tau_k = t_{k+1} - t_k$, with visualization of the minimum inter-event time $\tau_{\min}$. **(d)** Time evolution of the sliding function in presence of delayed transmissions, with visualization of both the desired boundary layer $\mathcal{B}_\delta$ of size δ, and the boundary layer $\mathcal{B}_{\delta'}$ of size δ' adopted for the triggering condition.

4.2.4 Illustrative Example

In this section, an illustrative example is briefly discussed. Consider the perturbed double integrator

$$\begin{aligned} \dot{x}_1 &= x_2 \\ \dot{x}_2 &= u + d\,. \end{aligned} \tag{4.24}$$

with $d = \mathcal{D}^{\text{sup}} \sin(t)$, $\mathcal{D}^{\text{sup}} = 3$. Let the initial condition be $x(0) = \begin{bmatrix} 1 \ 1 \end{bmatrix}^T$, and the sliding function be $\sigma = x_1 + x_2$. In the triggering condition (4.11) the threshold is $\delta = 0.2$.

Then, the control amplitude $U_{\max}$ is selected equal to 5. In Fig. 4.2 the time evolution of the sliding function σ is shown. Note that, according to Theorem 4.1, σ is ultimately bounded with respect to the boundary layer $\mathcal{B}_\delta$, the size of which is δ. In Fig. 4.2 the time evolution of the system states x_1, x_2, and the inter-event times $\tau_k = t_{k+1} - t_k$, are also shown. In particular, one can appreciate that the minimum inter-event time $\tau_{\min} = 0.0404\,\mathrm{s}$, according to Theorem 4.2, is a lower bound for the inter-event times. Moreover, considering a sampling time $T_s = 1 \times 10^{-4}\,\mathrm{s}$, and a simulation time $T = 10\,\mathrm{s}$, the number of transmissions is 101, i.e., 99.9% less than the number required by the conventional (i.e., time-driven) SMC implementation. Obviously, reducing the size of the boundary layer implies the improvement of the convergence accuracy. Yet, a larger number of transmissions could be required. The correct balance between convergence accuracy and transmission load has to be searched depending on the specific application. Finally, in Fig. 4.2 the time evolution of the sliding function σ in presence of transmissions with maximum time delay $\Delta_{\max} = 0.005\,\mathrm{s}$ acting from $t = 1\,\mathrm{s}$ to $t = 4\,\mathrm{s}$ is shown. Note that, by selecting $\delta' = 0.151$ (see Theorem 4.3), even in presence of maximum time delay, σ is ultimately bounded with respect to the desired boundary layer $\mathcal{B}_\delta$. In this case, the number of transmissions is 127.

4.3 Event-Triggered Second Order Sliding Mode Control

The ET-SOSM control scheme that we propose now is based on two triggering conditions and two control laws that depend not only on the sliding function, but also on its first time derivative. The stability properties of this control strategy are theoretically analyzed proving that the sliding function and its first time derivative are ultimately bounded in a desired vicinity of the origin, even in presence of delayed transmissions. These results imply the ultimately boundedness of the state of the original uncertain nonlinear system as well. Moreover, in order to avoid the notorious Zeno behaviour [JLSE99, ATS06], the existence of a lower bound for the time elapsed between consecutive triggering events is proved.

4.3.1 Problem Formulation

Consider the uncertain nonlinear system (4.1), where $\boldsymbol{x} \in \Omega$ ($\Omega \subset \mathbb{R}^n$ bounded) is the state vector, the value of which at the initial time instant t_0 is $x(t_0) = x_0$, and $u \in \mathbb{R}$ is the control variable, while $\boldsymbol{a} : \Omega \to \mathbb{R}^n$ and $\boldsymbol{b} : \Omega \to \mathbb{R}^n$ are uncertain functions of class C^1. Let Assumption 4.1 hold. Definition 4.1 is modified as follows.

Definition 4.9 (Sliding function). $\sigma : \Omega \to \mathbb{R}$ of class C^2 is a sliding function for system (4.1) provided that the pair (σ, u) has the following property: if u in (4.1) is designed so that, in a finite time $t_r^\star \geq t_0$, $\forall \boldsymbol{x}_0 \in \Omega$, $\sigma = \dot{\sigma} = 0 \quad \forall t \geq t_r^\star$, then $\forall t \geq t_r^\star$ the origin is an asymptotically stable equilibrium point of (4.1) constrained to the sliding manifold $\sigma = \dot{\sigma} = 0$.

Now, regarding the sliding variabile σ as the controlled variable associated with system (4.1), assume that system (4.1) is complete in Ω and has a uniform relative degree equal to 2. The following definitions are introduced.

Definition 4.10 (Ideal second order sliding mode). Given $t_r^\star \geq t_0$ (ideal reaching time), if $\forall \boldsymbol{x}_0 \in \Omega,\ \sigma = \dot{\sigma} = 0 \ \ \forall t \geq t_r^\star$, then an *ideal second order sliding mode* of system (4.1) is enforced on the sliding manifold $\sigma = \dot{\sigma} = 0$.

Definition 4.11 (Practical second order sliding mode). Given $t_r \geq t_0$ (practical reaching time), if $\forall \boldsymbol{x}_0 \in \Omega,\ |\sigma| \leq \delta_1,\ |\dot{\sigma}| \leq \delta_2 \ \ \forall t \geq t_r$, then a *practical second order sliding mode* of system (4.1) is enforced in a vicinity of the sliding manifold $\sigma = \dot{\sigma} = 0$.

Moreover, assume that system (4.1) admits a global normal form in Ω, i.e., there exists a global diffeomorphism of the form $\boldsymbol{\Phi} = [\boldsymbol{\Psi},\, \sigma,\, \boldsymbol{a} \cdot \nabla\sigma]^T = [\boldsymbol{x_r}, \boldsymbol{\xi}]^T$, with $\boldsymbol{\Phi} : \Omega \to \Phi_\Omega$ ($\Phi_\Omega \subset \mathbb{R}^n$ bounded), and $\boldsymbol{\Psi} : \Omega \to \mathbb{R}^{n-2}$, $\boldsymbol{x_r} \in \mathbb{R}^{n-2}$, $\boldsymbol{\xi} = [\sigma,\, \dot{\sigma}]^T \in \mathbb{R}^2$, such that

$$\dot{\boldsymbol{x}}_{\boldsymbol{r}} = \boldsymbol{a_r}(\boldsymbol{x_r}, \boldsymbol{\xi}) \tag{4.25}$$

$$\begin{aligned} \dot{\xi}_1 &= \xi_2 \\ \dot{\xi}_2 &= h(\boldsymbol{x_r}, \boldsymbol{\xi}) + g(\boldsymbol{x_r}, \boldsymbol{\xi})(u + d), \end{aligned} \tag{4.26}$$

with

$$\begin{aligned} \boldsymbol{a_r}\left(\boldsymbol{x_r}, \boldsymbol{\xi}\right) &= \frac{\partial \boldsymbol{\Psi}}{\partial \boldsymbol{x}} \left(\boldsymbol{\Phi}^{-1}\left(\boldsymbol{x_r}, \boldsymbol{\xi}\right)\right) \boldsymbol{a}\left(\boldsymbol{\Phi}^{-1}\left(\boldsymbol{x_r}, \boldsymbol{\xi}\right)\right) \\ h\left(\boldsymbol{x_r}, \boldsymbol{\xi}\right) &= \boldsymbol{a}\left(\boldsymbol{\Phi}^{-1}\left(\boldsymbol{x_r}, \boldsymbol{\xi}\right)\right) \cdot \nabla\left(\boldsymbol{a}\left(\boldsymbol{\Phi}^{-1}\left(\boldsymbol{x_r}, \boldsymbol{\xi}\right)\right) \cdot \nabla\sigma\left(\boldsymbol{\Phi}^{-1}\left(\boldsymbol{x_r}, \boldsymbol{\xi}\right)\right)\right) \\ g\left(\boldsymbol{x_r}, \boldsymbol{\xi}\right) &= \boldsymbol{b}\left(\boldsymbol{\Phi}^{-1}\left(\boldsymbol{x_r}, \boldsymbol{\xi}\right)\right) \cdot \nabla\left(\boldsymbol{a}\left(\boldsymbol{\Phi}^{-1}\left(\boldsymbol{x_r}, \boldsymbol{\xi}\right)\right) \cdot \nabla\sigma\left(\boldsymbol{\Phi}^{-1}\left(\boldsymbol{x_r}, \boldsymbol{\xi}\right)\right)\right) . \end{aligned}$$

Note that, as a consequence of the uniform relative degree assumption, one has that $g \neq 0$. Since $\boldsymbol{a_r}$, h, g are continuous functions and Φ_Ω is a bounded set, one has also that

$$\begin{aligned} |h(\boldsymbol{x_r}, \xi)| &\leq H \\ g(\boldsymbol{x_r}, \xi) &\leq g_{\max}, \end{aligned} \tag{4.27}$$

H and $g_{\max}$ being known positive constants. Moreover, the following assumption is made on the uncertain function g.

Assumption 4.5 (Bounded uncertainty). The uncertain function g can be lower bounded as

$$g(\boldsymbol{x_r}, \xi) \geq g_{\min}, \tag{4.28}$$

$g_{\min}$ being a known positive constant.

Now, a preliminary control problem can be formulated.

Problem 4.3. Let Assumptions 4.1 and 4.5 hold. Relying on (4.1) and (4.26)-(4.28), design a feedback control law

$$u^\star = \kappa(\sigma, \dot{\sigma}), \tag{4.29}$$

with the following property: $\forall \boldsymbol{x}_0 \in \Omega$, $\exists\, t_r^\star \geq t_0$ such that $\sigma = \dot{\sigma} = 0$, $\forall t \geq t_r^\star$, in spite of the uncertainties.

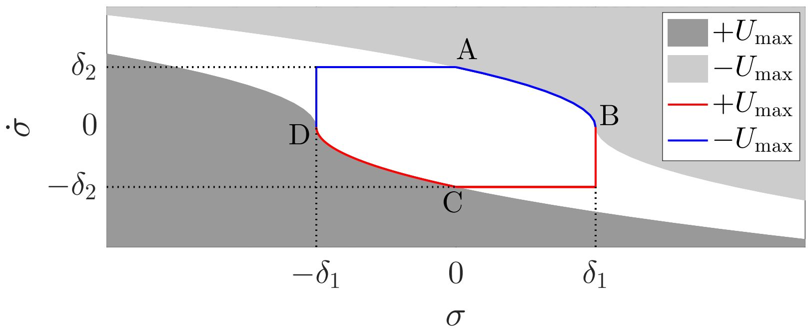

Fig. 4.3. Representation of the convergence set $\mathcal{B}$.

Note that the solution to Problem 4.3 is a control law capable of robustly enforcing an *ideal second order sliding mode* of system (4.1) in a finite time, according to Definition 4.10.

Taking into account the considerations made in Subsection 4.2.1, in the present chapter, instead of relying on time-triggered executions, we will introduce two different triggering conditions, transmitting data over the network only when such conditions are verified (*event-triggered* implementation).

Now, we can move from Problem 4.3 and formulate the problem which will be actually solved in this chapter.

Problem 4.4. Let Assumptions 4.1, 4.3 and 4.5 hold. Relying on (4.1) and (4.26)-(4.28), design a feedback control law

$$u = u(t_k) = \kappa(\sigma(t_k), \dot{\sigma}(t_k)) \quad \forall t \in [t_k,\, t_{k+1}[,\ \ k \in \mathbb{N}, \tag{4.30}$$

with the following property: $\forall\, \boldsymbol{x}_0 \in \Omega$, $\exists\, t_r \geq t_0$ such that $|\sigma| \leq \delta_1$, and $|\dot{\sigma}| \leq \delta_2, \forall\, t \geq t_r$, in spite of the uncertainties, δ_1 and δ_2 being positive constants arbitrarily set.

Note that the solution to Problem 4.4 is an ET control law capable of enforcing a *practical second order sliding mode* of system (4.1) in a finite time, according to Definition 4.11.

Before illustrating the features of the proposed control scheme, relying on Problem 4.4 let us introduce the following definition.

Definition 4.12 (Convergence set). The convergence set for the solution $(\sigma, \dot{\sigma})$ to (4.26) is

$$\mathcal{B} := \mathbb{R}^2 \setminus \{S_1 \cup S_2 \cup S_3 \cup S_4 \cup S_5\}, \tag{4.31}$$

where

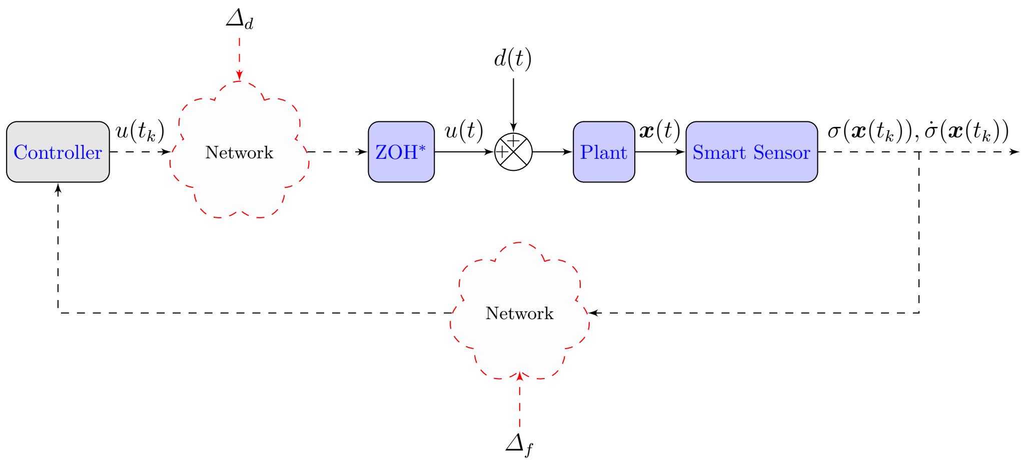

Fig. 4.4. The proposed event-triggered second order sliding mode control scheme.

$$
\begin{aligned}
S_1 &:= \left\{(\sigma,\, \dot{\sigma}) :\ |\dot{\sigma}| \geq \delta_2\right\}\\
S_2 &:= \left\{(\sigma,\, \dot{\sigma}) :\ \sigma \geq \delta_1\,,\ -\delta_2 < \dot{\sigma} \leq 0\right\}\\
S_3 &:= \left\{(\sigma,\, \dot{\sigma}) :\ \sigma \leq -\delta_1\,,\ 0 \leq \dot{\sigma} < \delta_2\right\}\\
S_4 &:= \left\{(\sigma,\, \dot{\sigma}) :\ \sigma \geq -\frac{\dot{\sigma}|\dot{\sigma}|}{2\alpha_r} + \delta_1\,,\ 0 < \dot{\sigma} < \delta_2\right\}\\
S_5 &:= \left\{(\sigma,\, \dot{\sigma}) :\ \sigma \leq -\frac{\dot{\sigma}|\dot{\sigma}|}{2\alpha_r} - \delta_1\,,\ -\delta_2 < \dot{\sigma} < 0\right\},
\end{aligned}
$$

δ_1, δ_2 being positive constants arbitrarily set, and α_r being a positive constant defined as

$$
\alpha_r := g_{\min}(U_{\max} - \mathcal{D}^{\sup}) - H > 0, \tag{4.32}
$$

where $U_{\max}$ is the control amplitude (see Fig. 4.3).

4.3.2 The Proposed Control Scheme

The control scheme proposed to solve Problem 4.4 is reported in Fig. 4.4, where the dashed path means that the corresponding signals are transmitted over the network only at the triggering time instants t_k. The control scheme contains two key blocks: the *Smart Sensor* and the *Controller*.

The Smart Sensor

The considered sensor is smart in the sense that it has some computation capability, i.e., it is able to compute $\sigma, \dot{\sigma}$, and verify two different triggering conditions. The first one being used only during the reaching of the convergence set (4.31), the second one being used for the rest of the control interval.

Triggering Condition 1: For any $(\sigma, \dot{\sigma}) \notin \{\mathcal{B} \cup \partial\mathcal{B}\}$ the adopted triggering condition is

$$\sigma = -\frac{\dot{\sigma}|\dot{\sigma}|}{2\alpha_r} \pm \delta_1, \tag{4.33}$$

δ_1 being a positive constant arbitrarily set (see Definition 4.12).

Note that the Smart Sensor checks the Triggering Condition 1 only during the reaching phase, i.e., before $(\sigma, \dot{\sigma})$ reaches $\partial\mathcal{B}$. For the rest of the control interval a second triggering condition is adopted.

Triggering Condition 2: For any $(\sigma, \dot{\sigma}) \in \{\mathcal{B} \cup \partial\mathcal{B}\}$ the adopted triggering condition is

$$(\sigma, \dot{\sigma}) \in \partial\mathcal{B}, \tag{4.34}$$

$\mathcal{B}$ being the desired convergence set for the solution $(\sigma, \dot{\sigma})$ (see Definition 4.12).

The dashed path in Fig. 4.4 is enabled only when (4.33) or (4.33) holds, i.e., when the Smart Sensor generates a triggering signal. More precisely, when (4.33) or (4.33) is verified, the actual values of the sliding function σ and its first time derivative $\dot{\sigma}$ are transmitted by the sensor over the network, so that the control law u is updated and sent to the plant.

The Controller

The proposed control strategy is based on two different control laws. The first one is used together with (4.33) only during the reaching phase, while the second one is used together with (4.34) for the rest of the control interval.

Control Law 1: In analogy with (3.44), and relaying on (4.30)-(4.33), for any $(\sigma(\boldsymbol{x}(t_k)), \dot{\sigma}(\boldsymbol{x}(t_k))) \notin \{\mathcal{B} \cup \partial\mathcal{B}\}$, the control law we propose to solve Problem 4.4 can be expressed as

$$u(t) = u(t_k) = -U_{\max} \operatorname{sign}\left(\sigma(\boldsymbol{x}(t_k)) + \frac{\dot{\sigma}(\boldsymbol{x}(t_k))|\dot{\sigma}(\boldsymbol{x}(t_k))|}{2\alpha_r}\right), \quad \forall t \in [t_k, t_{k+1}[, k \in \mathbb{N}, \tag{4.35}$$

where, according to (4.32), the control amplitude satisfies

$$U_{\max} > \frac{H}{g_{\min}} + \mathcal{D}^{\sup}. \tag{4.36}$$

Note that the control signal is transmitted by the Controller to the plant (through the communication network) only when (4.33) holds. When $(\sigma, \dot{\sigma})$ reaches $\partial\mathcal{B}$, a second control law is applied for the rest of the control interval.

Control Law 2: Relaying on (4.30)-(4.32) and (4.34), for any $(\sigma(\boldsymbol{x}(t_k)), \dot{\sigma}(\boldsymbol{x}(t_k))) \in \{\mathcal{B} \cup \partial\mathcal{B}\}$, the control law we propose to solve Problem 4.4 can be expressed as

$$u(t) = u(t_k) = -U_{\max} \operatorname{sign}(\dot{\sigma}(\boldsymbol{x}(t_k))) \qquad \forall\, t \in [t_k, t_{k+1}[, k \in \mathbb{N}\,, \tag{4.37}$$

with $U_{\max}$ as in (4.36). Note that the control signal is transmitted by the Controller to the plant (through the communication network) only when (4.34) holds.

Remark 4.4 (Chattering alleviation). Note that, when system (4.1) has unitary relative degree, in order to perform chattering alleviation, the foregoing control solution can be analogously applied by artificially increasing the relative degree of the system.

4.3.3 Stability Analysis

In this section, the stability properties of system (4.1) controlled via the proposed ET-SOSM control strategy are analyzed. To this end, it is convenient to introduce the following definitions.

Definition 4.13 (Ultimately boundedness). The solution $(\sigma, \dot{\sigma})$ to the auxiliary system (4.26) is said to be ultimately bounded with respect to the convergence set $\{\mathcal{B} \cup \partial\mathcal{B}\}$ if

$$\forall\, \boldsymbol{x}_0 \in \Omega,\ \exists\, t_r \geq t_0 \,:\, (\sigma, \dot{\sigma}) \in \{\mathcal{B} \cup \partial\mathcal{B}\} \quad \forall\, t \geq t_r\,. \tag{4.38}$$

Definition 4.14 (Positively invariant set). Let $(\sigma, \dot{\sigma})$ be the solution to the auxiliary system (4.26) starting from the initial condition $(\sigma(t_0), \dot{\sigma}(t_0))$. The set $\{\mathcal{B} \cup \partial\mathcal{B}\}$ is said to be positively invariant if

$$(\sigma(t_0),\, \dot{\sigma}(t_0)) \in \{\mathcal{B} \cup \partial\mathcal{B}\} \Rightarrow (\sigma, \dot{\sigma}) \in \{\mathcal{B} \cup \partial\mathcal{B}\}\ \ \forall\, t \geq t_0\,. \tag{4.39}$$

Before showing the theoretical results, the following assumption is made on the initial conditions of the auxiliary system (4.26).

Assumption 4.6 (Initial conditions). Given the auxiliary system (4.26), let the sign of the initial conditions $(\sigma(t_0), \dot{\sigma}(t_0))$ be known.

Now, making reference to the auxiliary system (4.26) the following results can be proved.

Lemma 4.3 (Finite time convergence to $\{\mathcal{B} \cup \partial\mathcal{B}\}$). Let Assumptions 4.1, 4.5 and 4.6 hold with $(\sigma(t_0), \dot{\sigma}(t_0)) \notin \{\mathcal{B} \cup \partial\mathcal{B}\}$, δ_1 and δ_2 in (4.31) being positive constants arbitrarily set. Given the auxiliary system (4.26) controlled by (4.35), (4.36) with the triggering condition (4.33), then, the solution $(\sigma, \dot{\sigma})$ to (4.26) is steered to the convergence set $\{\mathcal{B} \cup \partial\mathcal{B}\}$ in a finite time.

Proof. For the proof of this Lemma we refer to [DF09][Theorem 2]. □

Lemma 4.4 (Invariance of $\{\mathcal{B} \cup \partial\mathcal{B}\}$). Let Assumptions 4.1, 4.5 and 4.6 hold with $(\sigma(t_0), \dot{\sigma}(t_0)) \in \{\mathcal{B} \cup \partial\mathcal{B}\}$, δ_1 and δ_2 in (4.31) being positive constants arbitrarily set. Given the auxiliary system (4.26) controlled by (4.37), with the triggering condition (4.34), then, the convergence set $\{\mathcal{B} \cup \partial\mathcal{B}\}$ is a positively invariant set.

Proof. Since the value of $\dot{\sigma}$ and u are updated only when (4.34) holds, i.e., when $(\sigma, \dot{\sigma}) \in \partial\mathcal{B}$, the Lemma will be proved showing that for any $(\sigma(t_0), \dot{\sigma}(t_0)) \in \partial\mathcal{B}$, the vector field $(\dot{\sigma}, \ddot{\sigma})$ never points outside $\mathcal{B}$. Let $\partial\mathcal{B}^+$ denote $(\sigma, \dot{\sigma}) \in \partial\mathcal{B} : \dot{\sigma} > 0$, and $\partial\mathcal{B}^-$ denote $(\sigma, \dot{\sigma}) \in \partial\mathcal{B} : \dot{\sigma} < 0$ (in Fig. 4.3, $\partial\mathcal{B}^+$ is blue and $\partial\mathcal{B}^-$ is red). Assume that $(\sigma(t_0), \dot{\sigma}(t_0)) \in \partial\mathcal{B}^-$. The vector field is $(\dot{\sigma}, h + g(u + d))$ with $\dot{\sigma} < 0$ and, according to (4.37), $u = U_{\max}$. Then, $\ddot{\sigma} \geq \alpha_r > 0$, so that the vector field points up-left, that is inside $\mathcal{B}$. Note that, if $(\sigma(t_0), \dot{\sigma}(t_0)) \in \overline{CD}$ (all the points on this curve verify $\sigma = -\frac{\dot{\sigma}|\dot{\sigma}|}{2\alpha_r} - \delta_1$), then the vector field can be, at most, tangent to $\overline{CD}$, never pointing outside $\mathcal{B}$. Analogous considerations can be done if $(\sigma(t_0), \dot{\sigma}(t_0)) \in \partial\mathcal{B}^+$. □

Relying now on Lemmas 4.3 and 4.4, one can prove the major result concerning the evolution of the auxiliary system (4.26) controlled via the proposed strategy.

Theorem 4.4 (Evolution of the auxiliary system). *Let Assumptions 4.1, 4.5 and 4.6 hold. Given the auxiliary system (4.26) controlled by (4.35), (4.36) with the triggering condition (4.33) when $(\sigma, \dot{\sigma}) \notin \{\mathcal{B} \cup \partial\mathcal{B}\}$, and by (4.37) with the triggering condition (4.34) when $(\sigma, \dot{\sigma}) \in \{\mathcal{B} \cup \partial\mathcal{B}\}$, then, the solution $(\sigma, \dot{\sigma})$ to (4.26) is ultimately bounded with respect to the desired convergence set $\{\mathcal{B} \cup \partial\mathcal{B}\}$, δ_1 and δ_2 in (4.31) being positive constants arbitrarily set.*

Proof. The proof is a straightforward consequence of Lemmas 4.3 and 4.4. By virtue of Lemma 4.3, there exists a time instant t_r when the trajectory $(\sigma, \dot{\sigma})$ enters $\{\mathcal{B} \cup \partial\mathcal{B}\}$. Then, by virtue of Lemma 4.4, $\forall t \geq t_r$, $(\sigma, \dot{\sigma})$ is ultimately bounded with respect to the convergence set $\{\mathcal{B} \cup \partial\mathcal{B}\}$. □

Now, in order to prove the ultimately boundedness of the state of system (4.1), we show that in the convergence set an approximability property analogous to that of classical sliding mode control holds (see Theorem 2.1).

Theorem 4.5 (Approximability property). *Given the auxiliary system (4.26) controlled by (4.33), (4.35) and (4.36) when $(\sigma, \dot{\sigma}) \notin \{\mathcal{B} \cup \partial\mathcal{B}\}$, and by (4.34), (4.37) when $(\sigma, \dot{\sigma}) \in \{\mathcal{B} \cup \partial\mathcal{B}\}$, then, the origin of system (4.1) is practically stable if*

1. *exists a Lipschitz constant L for the right-hand side of (4.1) obtained with respect to $\boldsymbol{x}^\star$ by using the equivalent control $u_{eq} := -h(\boldsymbol{x}^\star)/g(\boldsymbol{x}^\star) - d$ (see Definition 3.4), i.e.,*

$$\dot{\boldsymbol{x}}^\star = \boldsymbol{a}(\boldsymbol{x}^\star) - \boldsymbol{b}(\boldsymbol{x}^\star)\frac{h(\boldsymbol{x}^\star)}{g(\boldsymbol{x}^\star)} \; ; \tag{4.40}$$

2. *the partial derivatives of the function $g(\boldsymbol{x})^{-1}\,\boldsymbol{b}(\boldsymbol{x})$, exist and they are bounded in any bounded domain;*
3. *exist positive constants M and N such that*

$$\|\boldsymbol{a}(\boldsymbol{x}) + \boldsymbol{b}(\boldsymbol{x})(u + d)\| \leq M + N\|\boldsymbol{x}\|. \tag{4.41}$$

Proof. In analogy with Theorem 2.1, we prove that for any pair of solutions $\boldsymbol{x}^\star$, $\boldsymbol{x}$ under the initial conditions $\|\boldsymbol{x}(t_r^\star) - \boldsymbol{x}^\star(t_r^\star)\| \le P\delta_2,\ P > 0$, there exists a positive number H such that $\|\boldsymbol{x} - \boldsymbol{x}^\star\| \le H\delta_2$ on a finite time interval $[t_r^\star, T]$, T being the control interval. More precisely, when a practical SOSM is generated, the control u in (4.26) differs from the equivalent control and can be expressed as follows

$$u = -\frac{h(\boldsymbol{x})}{g(\boldsymbol{x})} - d + \frac{\ddot{\sigma}(\boldsymbol{x})}{g(\boldsymbol{x})}. \tag{4.42}$$

Then, by substituting (4.42) in (4.1), the dynamics of the system becomes

$$\dot{\boldsymbol{x}} = \boldsymbol{a}(\boldsymbol{x}) - \boldsymbol{b}(\boldsymbol{x})\frac{h(\boldsymbol{x})}{g(\boldsymbol{x})} + \boldsymbol{b}(\boldsymbol{x})\frac{\ddot{\sigma}(\boldsymbol{x})}{g(\boldsymbol{x})}. \tag{4.43}$$

Now, relying on (4.40) and (4.43), one can compute the integral equations of $\boldsymbol{x}^\star$ and $\boldsymbol{x}$, respectively, i.e.,

$$\boldsymbol{x}^\star = \boldsymbol{x}^\star(t_r^\star) + \int_{t_r^\star}^{t} \left(\boldsymbol{a}(\boldsymbol{x}^\star(\zeta)) - \boldsymbol{b}(\boldsymbol{x}^\star(\zeta))\frac{h(\boldsymbol{x}^\star(\zeta))}{g(\boldsymbol{x}^\star(\zeta))}\right) d\zeta, \tag{4.44}$$

$$\boldsymbol{x} = \boldsymbol{x}(t_r^\star) + \int_{t_r^\star}^{t} \left(\boldsymbol{a}(\boldsymbol{x}(\zeta)) - \boldsymbol{b}(\boldsymbol{x}(\zeta))\frac{h(\boldsymbol{x}(\zeta))}{g(\boldsymbol{x}(\zeta))}\right) d\zeta + \int_{t_r^\star}^{t} \left(\boldsymbol{b}(\boldsymbol{x}(\zeta))\frac{\ddot{\sigma}(\boldsymbol{x}(\zeta))}{g(\boldsymbol{x}(\zeta))}\right) d\zeta. \tag{4.45}$$

Integrating the last term in (4.45) by parts and subtracting (4.44) to (4.45), it yields

$$\begin{aligned}\|\boldsymbol{x} - \boldsymbol{x}^\star\| \le \|\boldsymbol{x}(t_r^\star) - \boldsymbol{x}^\star(t_r^\star)\| + \Bigg\| &\int_{t_r^\star}^{t} \left(\boldsymbol{a}(\boldsymbol{x}(\zeta)) - \boldsymbol{b}(\boldsymbol{x}(\zeta))\frac{h(\boldsymbol{x}(\zeta))}{g(\boldsymbol{x}(\zeta))}\right) d\zeta \\ &- \int_{t_r^\star}^{t} \left(\boldsymbol{a}(\boldsymbol{x}^\star(\zeta)) - \boldsymbol{b}(\boldsymbol{x}^\star(\zeta))\frac{h(\boldsymbol{x}^\star(\zeta))}{g(\boldsymbol{x}^\star(\zeta))}\right) d\zeta \Bigg\| \\ &+ \left[\|\boldsymbol{b}(\boldsymbol{x}(\zeta))\| \left|\frac{\dot{\sigma}(\boldsymbol{x}(\zeta))}{g(\boldsymbol{x}(\zeta))}\right|\right]_{t_r^\star}^{t} + \int_{t_r^\star}^{t} \left\|\frac{d}{d\zeta}\frac{\boldsymbol{b}(\boldsymbol{x}(\zeta))}{g(\boldsymbol{x}(\zeta))}\right\| |\dot{\sigma}(\boldsymbol{x}(\zeta))| d\zeta.\end{aligned} \tag{4.46}$$

Taking into account assumption *(3)* in the theorem statement, and according to the Bellman-Gronwall lemma, the solution $\boldsymbol{x}$ is bounded on the finite time interval $[t_r^\star, T]$, i.e.,

$$\|\boldsymbol{x}\| \le \big(\|\boldsymbol{x}(t_r^\star)\| + M(T - t_r^\star)\big)e^{N(T - t_r^\star)}, \quad \forall\, t \in [t_r^\star, T]. \tag{4.47}$$

Then, by virtue of Theorem 4.4 (which implies that $|\dot{\sigma}| \le \delta_2$) and (4.47), taking into account assumptions *(1)*, *(2)* in the theorem statement, the inequality (4.46) can be expressed as

$$\|\boldsymbol{x} - \boldsymbol{x}^\star\| \le S\delta_2 + L\int_{t_r^\star}^{t} \|\boldsymbol{x}(\zeta) - \boldsymbol{x}^\star(\zeta)\| d\zeta \tag{4.48}$$

S being a positive constant that depends on the right-hand side of (4.43), $\boldsymbol{x}(t_r^\star)$, $\boldsymbol{x}^\star(t_r^\star)$, $t_r^\star$, T and P. Now, applying again the Bellman-Gronwall lemma to (4.48), one has that $\|\boldsymbol{x} - \boldsymbol{x}^\star\| \le H\delta_2$, with $H = Se^{L(T - t_r^\star)}$. Finally, since by Definition 4.9, $\forall\ t \ge t_r^\star$, the origin is an asymptotically stable equilibrium point of (4.1) constrained to $\sigma(\boldsymbol{x}^\star) = 0$, then there exists $\tau_r \ge t_r^\star$ such that $\boldsymbol{x} \in \Omega_\delta$, $\forall\, t \ge \tau_r$, which proves the theorem. □

Now, since the triggering time instants are known only at the execution times, we prove the existence of lower bounds for the inter-event times. Let $\tau_{\min,1}$ and $\tau_{\min,2}$ be the minimum inter-event time when $(\sigma,\dot\sigma)\notin\{\mathcal{B}\cup\partial\mathcal{B}\}$ and when $(\sigma,\dot\sigma)\in\{\mathcal{B}\cup\partial\mathcal{B}\}$, respectively.

Theorem 4.6 (Minimum inter-event time $\tau_{\min,1}$). *Let Assumptions 4.1, 4.5 and 4.6 hold, and let δ_1 and δ_2 in (4.31) be positive constants arbitrarily set. Given the auxiliary system (4.26) with $(\sigma(t_0),\dot\sigma(t_0))\notin\{\mathcal{B}\cup\partial\mathcal{B}\}$, controlled by (4.33), (4.35) and (4.36), then, for any $(\sigma,\dot\sigma)\notin\{\mathcal{B}\cup\partial\mathcal{B}\}$, the inter-event times are lower bounded.*

Proof. Assume $\sigma(t_0)>0$ and $\dot\sigma(t_0)>0$. Let t_1 be the first triggering time instant when $\sigma=-\dot\sigma|\dot\sigma|/(2\alpha_r)+\delta_1$ in (4.33) is verified. In order to compute the lower bound, we assume that the trajectory evolves with acceleration $-\alpha_r$ from $(\sigma(t_0),\dot\sigma(t_0))$ to $(\sigma(t_0'),\dot\sigma(t_0'))$, which lies on the $\dot\sigma=0$ axis, i.e.,

$$\sigma(t_0')=\sigma(t_0)+\frac{\dot\sigma^2(t_0)}{2\alpha_r},\quad \dot\sigma(t_0')=0\,. \tag{4.49}$$

Assume now that the trajectory evolves with acceleration $-\alpha_R:=-(g_{\max}(U_{\max}+\mathcal{D}^{\sup})+H)$ from (4.49) to $(\sigma(t_1),\dot\sigma(t_1))$, i.e.,

$$\begin{aligned}\sigma(t_1)&=\frac{\dot\sigma^2(t_1)}{2\alpha_r}+\delta_1\\ \dot\sigma(t_1)&=-\sqrt{\frac{2\alpha_R\alpha_r}{\alpha_R+\alpha_r}\left(\sigma(t_0')+\frac{\dot\sigma^2(t_0')}{2\alpha_R}-\delta_1\right)}\,.\end{aligned} \tag{4.50}$$

Finally, one can compute the time interval $\tau_{\min,1}=t_2-t_1$ that the trajectory takes to evolve with acceleration $-\alpha_R$ from (4.50) to $(\sigma(t_2),\dot\sigma(t_2))$ on the curve $\sigma=-\dot\sigma|\dot\sigma|/(2\alpha_r)-\delta_1$, i.e.,

$$\tau_{\min,1}=\frac{\gamma\,\dot\sigma(t_1)+\sqrt{\gamma^2\,\dot\sigma^2(t_1)-2\gamma\,\alpha_R\left(\frac{\dot\sigma^2(t_1)}{2\alpha_r}-\sigma(t_1)-\delta_1\right)}}{\gamma\,\alpha_R}, \tag{4.51}$$

with $\gamma=\frac{\alpha_R}{\alpha_r}+1$. Analogous considerations can be done starting from different initial condition $(\sigma(t_0),\dot\sigma(t_0))$. □

Theorem 4.7 (Minimum inter-event time $\tau_{\min,2}$). *Let Assumptions 4.1, 4.5 and 4.6 hold, and let δ_1 and δ_2 in (4.31) be positive constants arbitrarily set. Given the auxiliary system (4.26) with $(\sigma(t_0),\dot\sigma(t_0))\in\{\mathcal{B}\cup\partial\mathcal{B}\}$, controlled by (4.34) and (4.37), then, $\forall\,(\sigma,\dot\sigma)\in\{\mathcal{B}\cup\partial\mathcal{B}\}$, the inter-event times are lower bounded by*

$$\tau_{\min,2}=\frac{\delta_2}{H+g_{\max}(U_{\max}+\mathcal{D}^{\sup})}\,.$$

Proof. Since $(\sigma,\dot\sigma)$ and u are transmitted over the network only when the triggering condition (4.34) is verified, the theorem will be proved by computing the time interval $t_{k+1}-t_k$ that $\dot\sigma$ takes to evolve from 0 to δ_2 with acceleration $\alpha_R=H+g_{\max}(U_{\max}+\mathcal{D}^{\sup})$. Then, it yields

$$
\begin{aligned}
\dot\sigma(t_{k+1}) - \dot\sigma(t_k) &= \int_{t_k}^{t_{k+1}} \ddot\sigma_{\max}\, d\tau \\
\delta_2 - 0 &= \alpha_R\,(t_{k+1} - t_k) \\
\delta_2 &= (H + g_{\max}(U_{\max} + \mathcal{D}^{\sup}))\tau_{\min,2}\,.
\end{aligned} \tag{4.52}
$$

Analogous considerations can be done if we consider the evolution of $\dot\sigma$ from 0 to $-\delta_2$. □

Remark 4.5 (Zeno behaviour). Note that Theorems 4.6 and 4.7 guarantee that the time elapsed between two consecutive triggering events does not become arbitrarily small, avoiding the notorious Zeno behaviour [JLSE99, ATS06]. The minimum inter-vent times reasonably depend on the sizes of the desired convergence set $\mathcal{B}$, and on the bounds of the uncertanities. In practical cases, this result is very useful to assess the feasibility of the proposed control approach.

Taking now into account the possible occurrence of delayed data transmissions, due to the presence of the communication network, the following result can be proved. More precisely, relying on Problem 4.4 we will prove that by modifying the triggering condition (4.34), the auxiliary state-space trajectory is ultimately bounded with respect to the desired convergence set $\{\mathcal{B} \cup \partial\mathcal{B}\}$.

Theorem 4.8 (Delayed communications). *Let Assumptions 4.1, 4.3, 4.5 and 4.6 hold. Given the auxiliary system (4.26) controlled by (4.37) when $(\sigma, \dot\sigma) \in \{\mathcal{B} \cup \partial\mathcal{B}\}$, then, for any desired*

$$
\begin{aligned}
&\delta_2 > (H + g_{\max}(U_{\max} + \mathcal{D}^{\sup}))\varDelta_{\max} \\
&\delta_1 > \left(\frac{\delta_2^2}{2} - \frac{(\delta_2 - (H + g_{\max}(U_{\max} + \mathcal{D}^{\sup}))\varDelta_{\max})^2}{2}\right)\left(\frac{1}{\alpha_R} + \frac{1}{\alpha_r}\right),
\end{aligned}
$$

the triggering condition

$$
(\sigma, \dot\sigma) \in \partial\mathcal{B}'\,,
$$

with

$$
\mathcal{B}' := \mathbb{R}^2 \setminus \{S'_1 \cup S'_2 \cup S'_3 \cup S'_4 \cup S'_5\}
$$

and

$$
\begin{aligned}
S'_1 &:= \left\{(\sigma, \dot\sigma):\ |\dot\sigma| \ge \delta'_2\right\} \\
S'_2 &:= \left\{(\sigma, \dot\sigma):\ \sigma \ge \delta_1\,,\ -\delta'_2 < \dot\sigma \le 0\right\} \\
S'_3 &:= \left\{(\sigma, \dot\sigma):\ \sigma \le -\delta_1\,,\ 0 \le \dot\sigma < \delta'_2\right\} \\
S'_4 &:= \left\{(\sigma, \dot\sigma):\ \sigma \ge -\frac{\dot\sigma|\dot\sigma|}{2\alpha_r} + \delta'_1\,,\ 0 < \dot\sigma < \delta'_2\right\} \\
S'_5 &:= \left\{(\sigma, \dot\sigma):\ \sigma \le -\frac{\dot\sigma|\dot\sigma|}{2\alpha_r} - \delta'_1\,,\ -\delta'_2 < \dot\sigma < 0\right\} \\
\delta'_2 &:= \delta_2 - (H + g_{\max}(U_{\max} + \mathcal{D}^{\sup}))\varDelta_{\max} > 0 \\
\delta'_1 &:= \delta_1 - \left(\frac{\delta_2^2}{2} - \frac{(\delta'_2)^2}{2}\right)\left(\frac{1}{\alpha_R} + \frac{1}{\alpha_r}\right) > 0
\end{aligned}
$$

enforces the following relation

$$(\sigma, \dot{\sigma}) \in \{\mathcal{B} \cup \partial\mathcal{B}\} \quad \forall\, t \geq t_r', \tag{4.53}$$

t_r' *being the reaching time instant of* $\{\mathcal{B}' \cup \partial\mathcal{B}'\}$.

Proof. In analogy with Lemma 4.3, it follows that there exists a time instant t_r' when $(\sigma, \dot{\sigma})$ enters the inner convergence set $\{\mathcal{B}' \cup \partial\mathcal{B}'\}$. Suppose now that the transmission of $\dot{\sigma}(t_k) = \delta_2'$ occurs with the maximum time delay $\Delta_{\max}$. Moreover, assume that the sliding function evolves with constant maximum acceleration $\alpha_R := g_{\max}(U_{\max} + \mathcal{D}^{\sup}) + H$. In order to enforce relation (4.53), we impose that $\dot{\sigma}(t_k + \Delta_{\max}) = \delta_2$. Then, one has that

$$\begin{aligned} \dot{\sigma}(t_k + \Delta_{\max}) - \dot{\sigma}(t_k) &= \int_{t_k}^{t_k+\Delta_{\max}} \ddot{\sigma}_{\max}\, d\tau \\ \delta_2 - \delta_2' &= \alpha_R \Delta_{\max} \\ \delta_2' &= \delta_2 - \alpha_R \Delta_{\max}. \end{aligned} \tag{4.54}$$

Now, one can easily verify that the parabolic auxiliary state-space trajectory passing through point A in Fig. 4.3 with acceleration α_R is

$$\sigma = \frac{\dot{\sigma}|\dot{\sigma}|}{2\alpha_R} + \delta_1 - \frac{\delta_2^2}{2}\left(\frac{1}{\alpha_R} + \frac{1}{\alpha_r}\right).$$

Then, the intersection point of this curve with $\dot{\sigma} = \delta_2'$ is

$$\left(\sigma = \delta_1 + \frac{(\delta_2')^2}{2\alpha_R} - \frac{\delta_2^2}{2}\left(\frac{1}{\alpha_R} + \frac{1}{\alpha_r}\right),\ \dot{\sigma} = \delta_2'\right). \tag{4.55}$$

Finally, by imposing that the curve $\sigma = -\dot{\sigma}|\dot{\sigma}|/(2\alpha_r) + \delta_1'$ passes through the point (4.55), one can compute the value of δ_1'. □

Note that in case of delayed transmissions, the lower bound $\tau_{\min,2}$ can be obtained by using δ_2' instead of δ_2 in Theorem 4.7.

4.3.4 Illustrative Example

Consider the perturbed double integrator (4.24) with $d = \mathcal{D}^{\sup}\cos(t)$, $\mathcal{D}^{\sup} = 4.5$. Let the initial condition be $x(0) = \left[0.1\ 0\right]^T$, and the sliding variable be $\sigma = x_1$. Relying on system (4.24) it is possible to set the bounds in (4.27) and (4.28) equal to $H = 0$, $g_{\min} = g_{\max} = 1$. Then, according to (4.36), the control amplitude $U_{\max}$ is selected equal to 5, with $\alpha_r = 0.5$. Moreover, the convergence set $\mathcal{B}$ (see Definition 4.12) is chosen by selecting $\delta_1 = 0.01$, $\delta_2 = 0.1$.

In Fig. 4.5 the auxiliary state space trajectory is shown. Note that, according to Theorem 4.4, $(\sigma, \dot{\sigma})$ is ultimately bounded with respect to the convergence set $\mathcal{B}$. The inter-event times $\tau_k = t_{k+1} - t_k$ are also shown. In particular, one can appreciate that the minimum inter-event times $\tau_{\min,1} = 0.0032\,\mathrm{s}$ and $\tau_{\min,2} = 0.0105\,\mathrm{s}$ according to Theorems 4.6, 4.7, are lower bounds for the inter-event times. Note that, considering a sampling

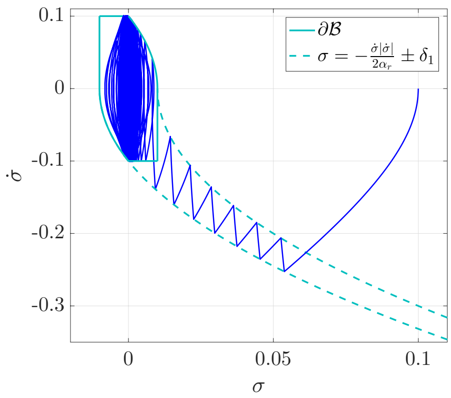

(a) auxiliary state space trajectory

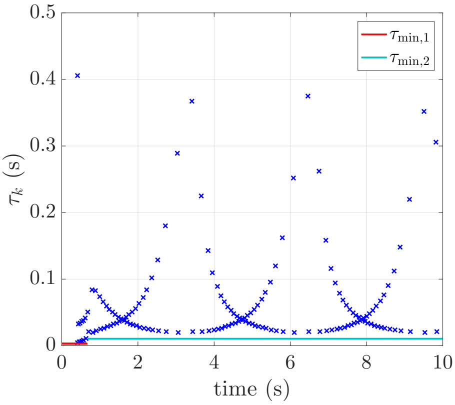

(b) inter-event times

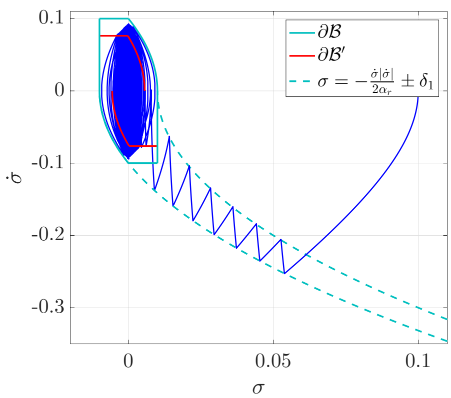

(c) auxiliary state space trajectory

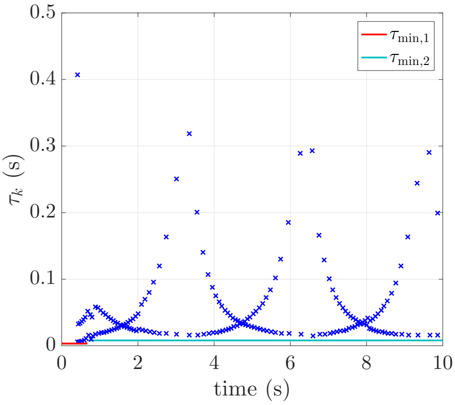

(d) inter-event times

Fig. 4.5. Event-triggered second order sliding mode control. **(a)** Auxiliary state space trajectory, with visualization of the sector around the switching line $\sigma = -\dot\sigma|\dot\sigma|/(2\alpha_r)$, and the convergence set $\mathcal{B}$. **(b)** Inter-event times $\tau_k = t_{k+1} - t_k$, with visualization of the minimum inter-event times $\tau_{\min,1}$ and $\tau_{\min,2}$. **(c)** Auxiliary state space trajectory, with visualization of the sector around the switching line $\sigma = -\dot\sigma|\dot\sigma|/(2\alpha_r)$, and the convergence sets $\mathcal{B}, \mathcal{B}'$, in presence of delayed transmissions. **(d)** Inter-event times $\tau_k = t_{k+1} - t_k$, with visualization of the minimum inter-event times $\tau_{\min,1}$ and $\tau_{\min,2}$, in presence of delayed transmissions.

time $T_s = 1 \times 10^{-4}$ s, and a simulation time $T = 10$ s, the number of transmissions is 156, i.e., 99.84% less than the number required by the conventional (i.e., time-driven) implementation. Obviously, reducing the size of the convergence set implies the improvement of the convergence accuracy. Yet, a larger number of transmissions could be required. The correct balance between convergence accuracy and transmission load has to be searched depending on the specific application. In Fig. 4.5 the auxiliary state space trajectory in presence of transmissions with maximum time delay $\varDelta_{\max} = 0.0025$ s acting from $t = 2$ s to $t = 8$ s is also shown. Note that, by selecting $\delta_1' = 0.0056$ and $\delta_2' = 0.0763$ (see

Theorem 4.8), even in presence of maximum time delay, $(\sigma, \dot{\sigma})$ is ultimately bounded with respect to the desired convergence set $\mathcal{B}$. The inter-event times, with $\tau_{\min,1} = 0.0032\,\mathrm{s}$ and $\tau_{\min,2} = 0.008\,\mathrm{s}$ are reported also in this case, where the number of transmissions is 190.

4.4 Conclusions

In this chapter, the Event-Triggered control approach and the Sliding Mode control methodology have been coupled to design robust control schemes for nonlinear uncertain systems including communication networks. The stability properties of the proposed control schemes have been theoretically analyzed, proving the ultimately boundedness of the auxiliary system state, which implies the ultimately boundedness of the solution of the controlled system even in presence of modelling uncertainties and delayed transmissions due to the network unavailability. Moreover, lower bounds for the time elapsed between consecutive triggering events have been provided, in order to guarantee the avoidance of the notorious Zeno behaviour.

PART 2

Part II

APPLICATION TO POWER SYSTEMS

5

Passivity Based Design of Sliding Modes

Abstract. In this chapter a distributed sliding mode control strategy is proposed for *optimal* Load Frequency Control (OLFC) in power networks, where besides frequency regulation also minimization of generation costs is achieved (economic dispatch). We study a nonlinear power network partitioned into control areas, where each area is modelled by an equivalent generator including voltage and second order turbine-governor dynamics. The turbine-governor dynamics suggest the design of a sliding manifold, such that the turbine-governor system enjoys a suitable passivity property, once the sliding manifold is attained. This work offers a new perspective on OLFC by means of sliding mode control, and in comparison with existing literature, we relax required dissipation conditions on the generation side and assumptions on the system parameters.

5.1 Preliminaries on Passivity

In this section, a minimum amount of preliminaries on passivity are provided. They are useful to the development of the various results appearing in this chapter.

We suppose the reader is familiar with standard notions for the analysis and control of nonlinear system, and foremost with dissipative systems [Wil07]. For detailed discussions on nonlinear systems, the textbooks [vdS00, HC08] and [SJK12], provide excellent starting points. We merely recall a few essential definitions and results for state-space systems of the form

$$\begin{aligned}\dot{\boldsymbol{x}} &= \boldsymbol{\zeta}(\boldsymbol{x}, \boldsymbol{u}) \\ \boldsymbol{y} &= \boldsymbol{h}(\boldsymbol{x}),\end{aligned} \tag{5.1}$$

with state $\boldsymbol{x} \in \mathbb{R}^n$, input $\boldsymbol{u}$, and output $\boldsymbol{y} \in \mathbb{R}^m$.

For physical systems of the form (5.1) the externally supplied (instantaneous) power can be represented as the scalar product of the system input $\boldsymbol{u}$ ('effort or 'flow')[5] and the system output $\boldsymbol{y}$ ('flow' or 'effort'), i.e., $\boldsymbol{u}^T\boldsymbol{y}$. Such a product is called the 'supply rate' of

[5]Recall that the effort and flow are voltages and currents in electrical systems or forces and velocities in mechanical systems, respectively.

the system. We start introducing the definitions of 'dissipation inequality' and 'passivity'.

Definition 5.1 (Dissipation inequality). System (5.1) is said to be dissipative with respect to the supply rate $s(t) \triangleq \boldsymbol{u}^T(t)\boldsymbol{y}(t)$ if there exists a function $S : \mathbb{R}^n \to \mathbb{R}^+$, called storage function, such that for all $\boldsymbol{x}(t_0) \in \mathbb{R}^n$, all $t_1 \geq t_0$, and all inputs $\boldsymbol{u}$

$$S(\boldsymbol{x}(t_1)) \leq S(\boldsymbol{x}(t_0)) + \int_{t_0}^{t_1} s(t)dt. \tag{5.2}$$

Let $d(t)$ be the dissipated energy, then, the energy-balance is given by

$$S(\boldsymbol{x}(t_1)) - S(\boldsymbol{x}(t_0)) = \int_{t_0}^{t_1} s(t)dt - d(t). \tag{5.3}$$

If (5.2) holds with equality for all $\boldsymbol{x}(t_0)$, and all $\boldsymbol{u}$, then (5.1) is lossless (i.e., $d(t) = 0$) with respect to $s(t)$.

Definition 5.2 (Passivity). System (5.1) is passive if it is dissipative with respect to the supply rate $s(t) = \boldsymbol{u}^T(t)\boldsymbol{y}(t)$. The system is said to be strictly input passive if there exists a $\delta > 0$ such that (5.1) is dissipative with respect to $s(t) = \boldsymbol{u}^T(t)\boldsymbol{y}(t) - \delta||\boldsymbol{u}(t)||^2$. On the other hand, the system is said to be strictly output passive if there exists a $\epsilon > 0$ such that (5.1) is dissipative with respect to $s(t) = \boldsymbol{u}^T(t)\boldsymbol{y}(t) - \epsilon||\boldsymbol{y}(t)||^2$. Finally, (5.1) is conservative if it is lossless (i.e., $d(t) = 0$) with respect to $s(t) = \boldsymbol{u}^T(t)\boldsymbol{y}(t)$.

We continue now recalling the definition of 'incremental passivity'.

Definition 5.3 (Incremental passivity). System (5.1) is incrementally passive if there exists a continuously differentiable, positive definite, radially unbounded, storage function $\mathcal{S}(\boldsymbol{x_1}, \boldsymbol{x_2}) : \mathbb{R}^{2n} \to \mathbb{R}_+$, such that for any two inputs $\boldsymbol{u_1}$, $\boldsymbol{u_2}$, and any two solutions to system (5.1), $\boldsymbol{x_1}$, $\boldsymbol{x_2}$ corresponding to these inputs, the respective outputs $\boldsymbol{y_1} = \boldsymbol{h}(\boldsymbol{x_1})$, $\boldsymbol{y_2} = \boldsymbol{h}(\boldsymbol{x_2})$ satisy the inequality

$$\dot{\mathcal{S}} = \frac{\partial \mathcal{S}}{\partial \boldsymbol{x_1}} \boldsymbol{\zeta}(\boldsymbol{x_1}, \boldsymbol{u_1}) + \frac{\partial \mathcal{S}}{\partial \boldsymbol{x_2}} \boldsymbol{\zeta}(\boldsymbol{x_2}, \boldsymbol{u_2}) \leq (\boldsymbol{y_1} - \boldsymbol{y_2})^T (\boldsymbol{u_1} - \boldsymbol{u_2}). \tag{5.4}$$

The following extension will be useful as well.

Definition 5.4 (Output strictly incremental passivity). System (5.1) is output strictly incrementally passive if in Definition 5.3, inequality (5.4) is replaced by

$$\dot{\mathcal{S}} = \frac{\partial \mathcal{S}}{\partial \boldsymbol{x_1}} \boldsymbol{\zeta}(\boldsymbol{x_1}, \boldsymbol{u_1}) + \frac{\partial \mathcal{S}}{\partial \boldsymbol{x_2}} \boldsymbol{\zeta}(\boldsymbol{x_2}, \boldsymbol{u_2}) \leq -\rho(\boldsymbol{y_1}, \boldsymbol{y_2}) + (\boldsymbol{y_1} - \boldsymbol{y_2})^T (\boldsymbol{u_1} - \boldsymbol{u_2}), \tag{5.5}$$

$\rho(\boldsymbol{y_1}, \boldsymbol{y_2}) : \mathbb{R}^{2n} \to \mathbb{R}_{\geq 0}$ being a positive definite function.

In case $\mathcal{S}$ is not radially unbounded, we introduce the following definition.

Definition 5.5 (Incremental cyclo-passivity). System (5.1) is incrementally cyclo-passive if in Definition 5.3, the incremental storage function $\mathcal{S}$ is not required to be radially unbounded.

Definition 5.5 is particularly useful, if we can only establish that the incremental storage function $\mathcal{S}(\boldsymbol{x_1}, \boldsymbol{x_2})$ is positive definite at a point $(\boldsymbol{x_1}, \boldsymbol{x_2})$. Often it is useful to establish incremental passivity with respect to a particular solution (often the steady state solution), and we introduce the following definition.

Definition 5.6 (Incremental passivity with respect to a particular solution). System (5.1) is incrementally passive with respect to a particular solution $\boldsymbol{x_2}$, with input $\boldsymbol{u_2}$ satisfying

$$\begin{aligned} \dot{\boldsymbol{x_2}} &= \boldsymbol{\zeta}(\boldsymbol{x_2}, \boldsymbol{u_2}) \\ \boldsymbol{y_2} &= \boldsymbol{h}(\boldsymbol{x_2}), \end{aligned} \tag{5.6}$$

if in Definition 5.3, the dissipation inequality holds with respect to the particular solution $\boldsymbol{x_2}$, instead of any solution to (5.1).

In case incremental passivity is established with respect to a steady state solution, (5.6) reads as

$$\begin{aligned} \boldsymbol{0} &= \boldsymbol{\zeta}(\overline{\boldsymbol{x}}, \overline{\boldsymbol{u}}) \\ \overline{\boldsymbol{y}} &= \boldsymbol{h}(\overline{\boldsymbol{x}}), \end{aligned} \tag{5.7}$$

We recall now three lemmas that will be essential to study the asymptotic behaviour of the closed loop system.

Lemma 5.1 (Stability). Let $\boldsymbol{x} = \boldsymbol{0}$ be an equilibrium of system

$$\dot{\boldsymbol{x}} = \boldsymbol{\zeta}(\boldsymbol{x}), \tag{5.8}$$

and suppose that $\boldsymbol{\zeta}$ is locally Lipschitz continuous. Let $\mathcal{S} : \mathbb{R}^n \to \mathbb{R}_+$ be a continuous differentiable, positive definite and radially unbounded function $\mathcal{S}(\boldsymbol{x})$ such that

$$\dot{\mathcal{S}} = \frac{\partial \mathcal{S}(\boldsymbol{x})}{\partial \boldsymbol{x}} \boldsymbol{\zeta}(\boldsymbol{x}) \leq 0, \qquad \forall \boldsymbol{x} \in \mathbb{R}^n. \tag{5.9}$$

Then, $\boldsymbol{x} = \boldsymbol{0}$ is globally stable and all solutions to (5.8) converge to the set E where $\dot{\mathcal{S}} = 0$. If $\dot{\mathcal{S}}$ is negative definite, then $\boldsymbol{x} = \boldsymbol{0}$ is globally asymptotically stable.

Lemma 5.2 (LaSalle's invariance principle). Let Ω be a positively invariant set of system (5.8). Suppose that every solution starting in Ω converges to a set $E \subset \Omega$ and let M be the largest invariant set contained in E. Then, every bounded solution starting in Ω converges to M as $t \to \infty$.

An application of LaSalle's invariance principle is the following asymptotic stability condition.

Corollary 5.1 (Asymptotic stability). Under the assumptions of Lemma 5.1, let $E = \{\boldsymbol{x} \in \mathbb{R}^n : \dot{\mathcal{S}}(\boldsymbol{x}) = 0\}$. If no solution other than $\boldsymbol{x} = \mathbf{0}$ can stay for all t in E, then the equilibrium $\boldsymbol{x} = \mathbf{0}$ is globally asymptotically stable.

Lemma 5.3 (Semistability). Consider system (5.8), and let Ω be an open neighborhood of $\boldsymbol{\zeta}^{-1}(\mathbf{0})$. Suppose that the trajectory of (5.8) is bounded for all $\boldsymbol{x} \in \Omega$, and assume that there exists a continuously differentiable function $\mathcal{S} : \Omega \to \mathbb{R}$ such that

$$\dot{\mathcal{S}} = \frac{\partial \mathcal{S}(\boldsymbol{x})}{\partial \boldsymbol{x}} \boldsymbol{\zeta}(\boldsymbol{x}) \leq 0, \qquad \forall \boldsymbol{x} \in \mathbb{R}^n. \tag{5.10}$$

If every point in the largest invariant subset M of $\{\boldsymbol{x} \in \Omega : \frac{\partial \mathcal{S}(\boldsymbol{x})}{\partial \boldsymbol{x}} \boldsymbol{\zeta}(\boldsymbol{x}) = 0\}$ is Lyapunov stable, then (5.8) is semistable, i.e., (5.8) converges to a constant vector.

5.2 Preliminaries on Power Systems

A power mismatch between generation and demand gives rise to a frequency in the power network that can deviate from its nominal value. Regulating the frequency back to its nominal value by Load Frequency Control (LFC) is challenging and it is uncertain if current implementations are adequate to deal with an increasing share of renewable energy sources [ADGS16]. Traditionally, the LFC is performed at each control area by a primary droop control and a secondary proportional-integral (PI) control. To cope with the increasing uncertainties affecting a control area and to improve the controller's performance, advanced control techniques have been proposed to redesign the conventional LFC schemes, such as model predictive control (MPC) [EIU16], adaptive control [ZARA05], fuzzy control [CF97] and sliding mode (SM) control. However, due to the predefined power flows through the tie-lines, the possibility of achieving economically optimal LFC is lost [RKTR07]. Besides improving the stability and the dynamic performance of power systems, new control strategies are additionally required to reduce the operational costs of LFC [Lai01]. In this work we propose a novel distributed *optimal* LFC (OLFC) scheme that incorporates the economic dispatch into the LFC loop, departing from the conventional tie-line requirements. An up-to-date survey on recent results on offline and online optimal power flows and OLFC can be found in [MDS$^+$17]. We restrict ourselves here to a brief overview of online solutions to OLFC that are close to the presented work. Particularly, we focus on distributed solutions, in contrast to more centralized control schemes that have been studied in e.g. [TD17a, DG17, XDLvS17]. In order to obtain

OLFC, the vast majority of distributed solutions appearing in the literature fit in one of two categories. First, the economic dispatch problem is distributively solved by a primal-dual algorithm converging to the solution of the associated Lagrangian dual problem [ZP15, LZC16, SDPvdS17, YC14, KDSL16, JLvdB09, MDC12, MF16, CMW15, ASDG15, YHL15, YHL16]. This approach generally requires measurements of the loads or the power flows, which is not always desirable in a LFC scheme. This issue is avoided by the second class of solutions, where a distributed consensus algorithm is employed to converge to a state of identical marginal costs, solving the economic dispatch problem in the unconstrained case [BDT14, TBD16, SD16, ZMD15, XLSvS17, MDPvdSS17, ADJS13, KH12, BDL+14, RAOZC14, YTX13, YWSL16, ZC12]. The proposed sliding mode controller design in this work is compatible with both approaches, although we put the emphasize on a distributed consensus based solution and remark on the primal-dual based approach.

Sliding mode control has been used to improve the conventional LFC schemes [VPP10], possibly together with disturbance observers [MFL+16]. However, the proposed use of SM to obtain a distributed OLFC scheme is new and can offer a few advantages over the previous results on OLFC. Foremost, it is possible to incorporate the widely used second order model for the turbine-governor dynamics that is generally neglected in the analytical OLFC studies. Since the generated control signals in OLFC schemes adjust continuously and in real-time the governor set points, it is important to incorporate the generation side in a satisfactory level of detail. In this work, we adopt a *nonlinear* model of a power network, including voltage dynamics, partitioned into control areas having an arbitrarily complex and meshed topology. The generation side is modelled by an equivalent generator including voltage dynamics and second order turbine-governor dynamics, which is standard in studies on conventional LFC schemes. We propose a *distributed* SM controller that is shown to achieve frequency control, while minimizing generation costs. This result is obtained by avoiding the measurement of the power demand and the use of observers, which is an element concurring to the ease of practical implementation of the proposed control strategy. The proposed control scheme continuously adjusts the governor set point. Conventional SM controllers can suffer from the notorious drawback known as chattering effect, due to the discontinuous control input. To alleviate this issue, we incorporate the well known Suboptimal Second Order Sliding Mode (SSOSM) control algorithm [BFU98a] leading to a continuous control input. To design the controllers obtaining OLFC, we recall an incremental passivity property of the power network [TBD16] that prescribes a suitable sliding manifold. Particularly, the non-passive turbine-governor system, constrained to this manifold, is shown to be incrementally passive allowing for a passive feedback interconnection, once the closed-loop system evolves on the sliding manifold. The proposed approach differs substantially from two notable exceptions that also incorporate the turbine-governor dynamics ([TD17b, KMDL17]) and shows some benefits. In contrast to [TD17b], we do not impose constraints on the permitted system parameters, and in contrast to [KMDL17] we do not impose dissipation assumptions on the generation side and allow for a higher relative degree (see also Remark 5.8). Furthermore, we believe that the chosen approach, where the design of the sliding manifold is inspired by desired passivity properties, offers new perspectives on the control of networks that have similar control objectives as the one presented, e.g. achieving power sharing in microgrids. As this work is (to the best of our knowledge) the first to use sliding mode control to obtain

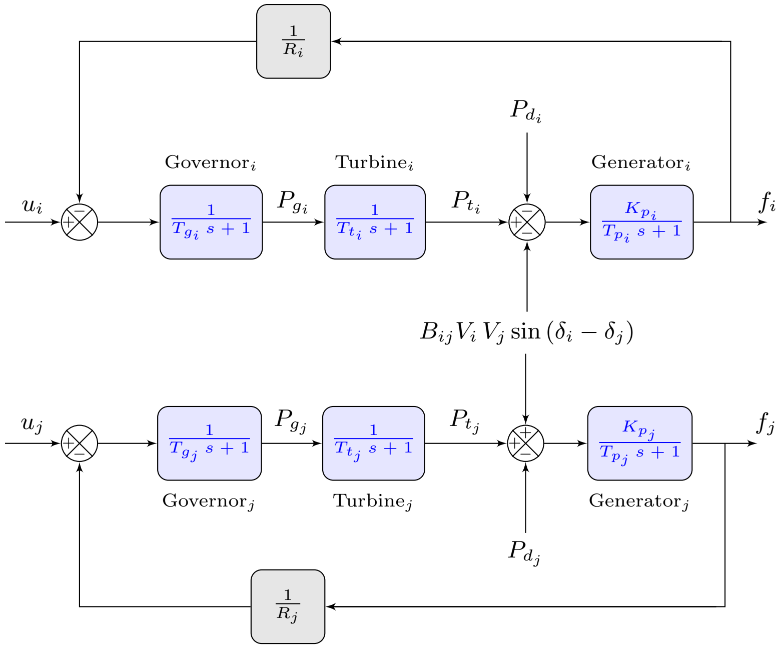

Fig. 5.1. Block diagram of two interconnected control areas. The voltage dynamics are omitted.

OLFC, it additionally enables further studies to compare the performance with respect to other approaches found in the literature.

5.3 Control Areas with Second Order Turbine-Governor Dynamics

Consider a power network consisting of n interconnected control areas. The network topology is represented by a connected and undirected graph $\mathcal{G} = (\mathcal{V}, \mathcal{E})$, where the nodes $\mathcal{V} = \{1, ..., n\}$, represent the control areas and the edges $\mathcal{E} = \{1, ..., m\}$, represent the transmission lines connecting the areas. The topology can be described by its corresponding incidence matrix $\boldsymbol{\mathcal{B}} \in \mathbb{R}^{n\times m}$. Then, by arbitrarily labeling the ends of edge k with a $+$ and a $-$, one has that

$$\mathcal{B}_{ik} = \begin{cases} +1 & \text{if } i \text{ is the positive end of } k \\ -1 & \text{if } i \text{ is the negative end of } k \\ 0 & \text{otherwise.} \end{cases}$$

A control area is represented by an equivalent generator and a load, where the governing dynamics of the i-th area are described by the so called ‘flux-decay’ or ‘single-axis model’ given as[6] [MBB08]:

[6] For notational simplicity, the dependency of the variables on time t is omitted throughout most of this chapter.

$$
\begin{aligned}
\dot{\delta}_i &= f_i \\
T_{p_i}\dot{f}_i &= -f_i + K_{p_i}\left(P_{t_i} - P_{d_i} + \sum_{j\in\mathcal{N}_i} V_iV_jB_{ij}\sin\left(\delta_i - \delta_j\right)\right) \\
T_{V_i}\dot{V}_i &= \overline{E}_{f_i} - \left(1 - \left(X_{d_i} - X'_{d_i}\right)B_{ii}\right)V_i - \left(X_{d_i} - X'_{d_i}\right)\sum_{j\in\mathcal{N}_i} V_jB_{ij}\cos\left(\delta_i - \delta_j\right),
\end{aligned}
\tag{5.11}
$$

where $\mathcal{N}_i$ is the set of control areas connected to the i-th area by transmission lines. Note that we assume that the network is lossless, which is generally valid in high voltage transmission networks where the line resistance is negligible. Moreover, P_{t_i} in (5.11) is the power generated by the i-th (equivalent) plant and can be expressed as the output of the following second order dynamical system that describes the behaviour of both the governor and the turbine

$$
\begin{aligned}
T_{t_i}\dot{P}_{t_i} &= -P_{t_i} + P_{gi} \\
T_{gi}\dot{P}_{gi} &= -\frac{1}{R_i}f_i - P_{gi} + u_i.
\end{aligned}
\tag{5.12}
$$

The symbols used in (5.11) and (5.12) are described in Table 5.1. To further illustrate the dynamics, a block diagram for a two area network is provided in Fig. 5.1. In this work we aim at the design of a continuous control input u_i to achieve both frequency regulation and economic efficiency (optimal Load Frequency Control). To study the power network we write system (5.11) compactly for all areas $i \in \mathcal{V}$ as

$$
\begin{aligned}
\dot{\boldsymbol{\eta}} &= \boldsymbol{\mathcal{B}}^T\boldsymbol{f} \\
\boldsymbol{T_p}\dot{\boldsymbol{f}} &= -\boldsymbol{f} + \boldsymbol{K_p}(\boldsymbol{P_t} - \boldsymbol{P_d} - \boldsymbol{\mathcal{B}\Gamma}(\boldsymbol{V})\mathbf{sin}(\boldsymbol{\eta})) \\
\boldsymbol{T_V}\dot{\boldsymbol{V}} &= -(\boldsymbol{X_d} - \boldsymbol{X'_d})\boldsymbol{E}(\boldsymbol{\eta})\boldsymbol{V} + \overline{\boldsymbol{E}}_{\boldsymbol{f}},
\end{aligned}
\tag{5.13}
$$

and the turbine-governor dynamics in (5.12) as

$$
\begin{aligned}
\boldsymbol{T_t}\dot{\boldsymbol{P}}_{\boldsymbol{t}} &= -\boldsymbol{P_t} + \boldsymbol{P_g} \\
\boldsymbol{T_g}\dot{\boldsymbol{P}}_{\boldsymbol{g}} &= -\boldsymbol{R}^{-1}\boldsymbol{f} - \boldsymbol{P_g} + \boldsymbol{u},
\end{aligned}
\tag{5.14}
$$

where $\boldsymbol{\eta} = \boldsymbol{\mathcal{B}}^T\boldsymbol{\delta} \in \mathbb{R}^m$ is vector describing the differences in voltage angles, while $\mathbf{sin}(\boldsymbol{\eta}) = [\sin(\eta_1), \ldots, \sin(\eta_m)]^T$. Furthermore, $\boldsymbol{\Gamma} = \mathrm{diag}\{\Gamma_1, \ldots, \Gamma_m\}$, where $\Gamma(\boldsymbol{V})_k = V_iV_jB_{ij}$, with $k \sim \{i, j\}$, i.e., line k connects areas i and j. The components of the matrix $\boldsymbol{E}(\boldsymbol{\eta}) \in \mathbb{R}^{n\times n}$ are defined as

$$
\begin{aligned}
E_{ii}(\boldsymbol{\eta}) &= \frac{1}{X_{d_i} - X'_{d_i}} - B_{ii} && i \in \mathcal{V} \\
E_{ij}(\boldsymbol{\eta}) &= B_{ij}\cos(\eta_k) = E_{ji}(\boldsymbol{\eta}) && k \sim \{i, j\} \in \mathcal{E} \\
E_{ij}(\boldsymbol{\eta}) &= 0 && \text{otherwise.}
\end{aligned}
\tag{5.15}
$$

The remaining symbols follow straightforwardly from (5.11) and (5.12), and are vectors and matrices of suitable dimensions.

Table 5.1. Description of the used symbols

	State variables
δ_i	Voltage angle
f_i	Frequency deviation
V_i	Voltage
P_{t_i}	Turbine output power
P_{gi}	Governor output
	Parameters
T_{p_i}	Time constant of the control area
T_{t_i}	Time constant of the turbine
T_{gi}	Time constant of the governor
T_{V_i}	Direct axis transient open-circuit constant
K_{p_i}	Gain of the control area
R_i	Speed regulation coefficient
X_{d_i}	Direct synchronous reactance
X'_{d_i}	Direct synchronous transient reactance
B_{ij}	Transmission line susceptance
	Inputs
u_i	Control input to the governor
$\overline{E}_{f_i}$	Constant exciter voltage
P_{d_i}	Unknown power demand

Remark 5.1 (Reactance and susceptance). For each (equivalent) generator $i \in \mathcal{V}$, the reactance is higher than the transient reactance, i.e. $X_{d_i} > X'_{d_i}$ [KBL94]. Furthermore, the self-susceptance of area $i \in \mathcal{V}$ is given by $B_{ii} = \sum_{j \in \mathcal{N}_i} B_{ij}$ and the susceptance of a line satisfies $B_{ij} = B_{ji} < 0$. Consequently, $\boldsymbol{E}(\boldsymbol{\eta})$ is a strictly diagonally dominant and symmetric matrix with positive elements on its diagonal and is therefore positive definite.

To permit the controller design in the next sections, the following assumption is made on the *unknown* demand (unmatched disturbance) and the available measurements.

Assumption 5.1 (Available information). The variables f_i, P_{t_i} and P_{gi} are locally available at control area i. The unmatched disturbance P_{d_i} is unknown, and can be bounded as $|P_{d_i}| \leq \mathcal{D}_i$, where $\mathcal{D}_i$ is a positive constant available at control area i.

In case not all variables are locally available, Assumption 5.1 can be relaxed by implementing observers that estimate the unmeasured states in a finite time (see Section 5.9).

5.4 Incremental passivity of the power network

In this section we recall a useful incremental passivity property of system (5.13) that has been established before in [TBD16]. Before we can establish this incremental passivity property for the considered power network model, we first need the following assumption on the existence of a steady state solution.

Assumption 5.2 (Steady state solution). The unknown power demand (unmatched disturbance) $\boldsymbol{P_d}$ is constant and for a given $\overline{\boldsymbol{P}}_{\boldsymbol{t}}$, there exist a $\overline{\boldsymbol{u}}$ and state $(\overline{\boldsymbol{\eta}}, \overline{\boldsymbol{f}}, \overline{\boldsymbol{V}}, \overline{\boldsymbol{P}}_{\boldsymbol{t}}, \overline{\boldsymbol{P}}_{\boldsymbol{g}})$ that satisfies

$$
\begin{aligned}
\mathbf{0} &= \boldsymbol{\mathcal{B}}^T \overline{\boldsymbol{f}} \\
\mathbf{0} &= -\overline{\boldsymbol{f}} + \boldsymbol{K_p}(\overline{\boldsymbol{P}}_{\boldsymbol{t}} - \boldsymbol{P_d} - \boldsymbol{\mathcal{B}} \boldsymbol{\Gamma}(\overline{\boldsymbol{V}}) \mathbf{sin}(\overline{\boldsymbol{\eta}})) \\
\mathbf{0} &= -(\boldsymbol{X_d} - \boldsymbol{X_d'}) \boldsymbol{E}(\overline{\boldsymbol{\eta}}) \overline{\boldsymbol{V}} + \overline{\boldsymbol{E}}_{\boldsymbol{f}},
\end{aligned}
\tag{5.16}
$$

and

$$
\begin{aligned}
\mathbf{0} &= -\overline{\boldsymbol{P}}_{\boldsymbol{t}} + \overline{\boldsymbol{P}}_{\boldsymbol{g}} \\
\mathbf{0} &= -\boldsymbol{R}^{-1} \overline{\boldsymbol{f}} - \overline{\boldsymbol{P}}_{\boldsymbol{g}} + \overline{\boldsymbol{u}}.
\end{aligned}
\tag{5.17}
$$

To state an incremental passivity property of (5.13), we make use of the following storage function [TBD16, DPM17]

$$
S_1(\boldsymbol{\eta}, \boldsymbol{f}, \boldsymbol{V}) = \frac{1}{2} \boldsymbol{f}^T \boldsymbol{T_p} \boldsymbol{f} + \frac{1}{2} \boldsymbol{V}^T \boldsymbol{E}(\boldsymbol{\eta}) \boldsymbol{V},
\tag{5.18}
$$

that can also be interpreted as a Hamiltonian function of the system [SDPvdS17].

Lemma 5.4 (Incremental cyclo-passivity of (5.13)). System (5.13) with input $\boldsymbol{P_t}$ and output $\boldsymbol{f}$ is an output strictly incrementally cyclo-passive system, with respect to the constant $(\overline{\boldsymbol{\eta}}, \overline{\boldsymbol{f}}, \overline{\boldsymbol{V}})$ satisfying (5.16).

Proof. For notational convenience we define $\boldsymbol{x} = (\boldsymbol{\eta}, \boldsymbol{f}, \boldsymbol{V})$. A tedious but straightforward evaluation of (note the use of a calligraphic $\mathcal{S}$)

$$
\mathcal{S}_1(\boldsymbol{x}) = S_1(\boldsymbol{x}) - S_1(\overline{\boldsymbol{x}}) - \nabla S_1(\overline{\boldsymbol{x}})^T (\boldsymbol{x} - \overline{\boldsymbol{x}}),
\tag{5.19}
$$

shows that $\mathcal{S}_1(\boldsymbol{x})$ satisfies [TBD16], [DPM17]

$$
\dot{\mathcal{S}}_1(\boldsymbol{x}) = -\boldsymbol{f}^T \boldsymbol{K_p}^{-1} \boldsymbol{f} - \dot{\boldsymbol{V}}^T \boldsymbol{T_V} (\boldsymbol{X_d} - \boldsymbol{X_d'})^{-1} \dot{\boldsymbol{V}} + (\boldsymbol{f} - \overline{\boldsymbol{f}})^T (\boldsymbol{P_t} - \overline{\boldsymbol{P}}_{\boldsymbol{t}}),
\tag{5.20}
$$

along the solutions to (5.13). □

For the stability analysis in Section 5.7 the following technical assumption is needed on the steady state that eventually allows us to infer boundedness of solutions.[7]

[7] In case boundedness of solutions can be inferred by other means, Assumption 5.3 can be omitted.

Assumption 5.3 (Steady state voltages and voltage angles). Let $\overline{\boldsymbol{V}} \in \mathbb{R}^n_{>0}$ and let differences in steady state voltage angles satisfy

$$\overline{\eta}_k \in (-\frac{\pi}{2}, \frac{\pi}{2}) \quad \forall k \in \mathcal{E}. \tag{5.21}$$

Furthermore, for all $i \in \mathcal{V}$ it holds that

$$\frac{1}{X_{d_i} - X'_{d_i}} - B_{ii} + \sum_{k \sim \{i,j\} \in \mathcal{E}} \frac{B_{ij}(\overline{V}_i + \overline{V}_j \sin^2(\overline{\eta}_k))}{\overline{V}_i \cos(\overline{\eta}_k)} > 0. \tag{5.22}$$

The assumption above holds if the generator reactances are small compared to the line reactances and the differences in voltage (angles) are small [DPM17]. It is important to note that this holds for typical operation points of the power network. The main consequence of Assumption 5.3 is that the incremental storage function $\mathcal{S}_1$ now obtains a strict local minimum at a steady state satisfying (5.16).

Lemma 5.5 (Local minimum of $\mathcal{S}_1$). Let Assumption 5.3 hold. Then, the incremental storage function $\mathcal{S}_1$ has a local minimum at $(\overline{\boldsymbol{\eta}}, \overline{\boldsymbol{f}}, \overline{\boldsymbol{V}})$ satisfying (5.16).

Proof. Under Assumption 5.3, the Hessian of (5.18), evaluated at $(\overline{\boldsymbol{\eta}}, \overline{\boldsymbol{f}}, \overline{\boldsymbol{V}})$, is positive definite [TBD16, Lemma 2], [DPM17, Proposition 1]. Consequently, S_1 is strictly convex around $(\overline{\boldsymbol{\eta}}, \overline{\boldsymbol{f}}, \overline{\boldsymbol{V}})$. The incremental storage function (5.19) is defined as a Bregman distance [Bre67] associated with (5.18) for the points $(\boldsymbol{\eta}, \boldsymbol{f}, \boldsymbol{V})$ and $(\overline{\boldsymbol{\eta}}, \overline{\boldsymbol{f}}, \overline{\boldsymbol{V}})$. Due to the strict convexity of S_1 around $(\overline{\boldsymbol{\eta}}, \overline{\boldsymbol{f}}, \overline{\boldsymbol{V}})$, (5.19) has a local minimum at $(\overline{\boldsymbol{\eta}}, \overline{\boldsymbol{f}}, \overline{\boldsymbol{V}})$. $\square$

Remark 5.2 (Different power network models). The focus of this work is to achieve OLFC by distributed sliding mode control for the nonlinear power network, explicitly taking into account the turbine-governor dynamics. Equations (5.13) adequately represent a power network for the purpose of frequency regulation and are often further simplified by assuming constant voltages, leading to the so called 'swing equations'. To the analysis in this work the incremental passivity property established above is essential, which has been derived for various other models, including microgrids. It is therefore expected that the presented approach can be straightforwardly applied to a wider range of models than the one we consider in this work.

5.5 Frequency Regulation and Economic Dispatch

In this section we formulate the control objectives of optimal load frequency control. Before doing so, we first note that the steady state frequency $\overline{\boldsymbol{f}}$, is generally different from zero without proper adjustments of $\overline{\boldsymbol{u}}$ [TBD16].

Lemma 5.6 (Steady state frequency). Let Assumption 5.2 hold, then necessarily $\overline{\boldsymbol{f}} = \mathbb{1}_n f^*$ with

$$f^* = \frac{\mathbb{1}_n^T(\overline{\boldsymbol{u}} - \boldsymbol{P_d})}{\mathbb{1}_n^T(\boldsymbol{K_p}^{-1} + \boldsymbol{R}^{-1})\mathbb{1}_n}, \tag{5.23}$$

where $\mathbb{1}_n \in \mathbb{R}^n$ is the vector consisting of all ones.

This leads us to the first objective, concerning the regulation of the frequency deviation.

Objective 5.1 (Frequency regulation).

$$\lim_{t\to\infty} \boldsymbol{f}(t) = \boldsymbol{0}. \tag{5.24}$$

From (5.23) it is clear that it is sufficient that $\mathbb{1}_n^T(\overline{\boldsymbol{u}} - \boldsymbol{P_d}) = 0$, to have zero frequency deviation at the steady state. Therefore, there is flexibility to distribute the total required generation optimally among the various control areas. To make the notion of optimality explicit we assign to every control area a strictly convex linear-quadratic cost function $C_i(P_{t_i})$ related to the generated power P_{t_i}

$$C_i(P_{t_i}) = \frac{1}{2}\mathcal{Q}_i P_{t_i}^2 + \mathcal{R}_i P_{t_i} + \mathcal{C}_i \quad \forall i \in \mathcal{V}. \tag{5.25}$$

Minimizing the total generation cost, subject to the constraint that allows for a zero frequency deviation can then be formulated as the following optimization problem:

$$\begin{aligned} &\min \sum_{i\in\mathcal{V}} C_i(P_{t_i}) \\ &\text{s.t.} \quad \mathbb{1}_n^T(\overline{\boldsymbol{u}} - \boldsymbol{P_d}) = 0. \end{aligned} \tag{5.26}$$

The lemma below makes the solution to (5.26) explicit [TBD16].

Lemma 5.7 (Optimal generation). The solution $\overline{\boldsymbol{P}}_{\boldsymbol{t}}^{opt}$ to (5.26) satisfies

$$\overline{\boldsymbol{P}}_{\boldsymbol{t}}^{opt} = \boldsymbol{\mathcal{Q}}^{-1}(\overline{\boldsymbol{\lambda}}^{opt} - \boldsymbol{\mathcal{R}}), \tag{5.27}$$

where

$$\overline{\boldsymbol{\lambda}}^{opt} = \mathbb{1}_n \frac{\mathbb{1}_n^T(\boldsymbol{P_d} + \boldsymbol{\mathcal{Q}}^{-1}\boldsymbol{\mathcal{R}})}{\mathbb{1}_n^T\boldsymbol{\mathcal{Q}}^{-1}\mathbb{1}_n}, \tag{5.28}$$

and $\boldsymbol{\mathcal{Q}} = \text{diag}(\mathcal{Q}_1, \dots, \mathcal{Q}_n)$, $\boldsymbol{\mathcal{R}} = (\mathcal{R}_1, \dots, \mathcal{R}_n)^T$.

Proof. To solve the optimization problem (5.26), the method of Lagrange multipliers is used. Specifically, let $C(\boldsymbol{P_t}) = \sum_{i\in\mathcal{V}} C_i(P_{t_i})$, the Lagrangian function associated to (5.26) can be expressed as

$$L(\boldsymbol{P_t}, \lambda) = C(\boldsymbol{P_t}) + \lambda(\mathbb{1}_n^T\overline{\boldsymbol{P}}_{\boldsymbol{t}} - \mathbb{1}_n^T\boldsymbol{P_d}), \tag{5.29}$$

λ being the Lagrangian multiplier. From the convexity property of the cost function $C(\boldsymbol{P_t})$, one can conclude that the solution to (5.26) is a saddle point, and it can be obtained by solving a max-min optimal problem, i.e., $\max_{\lambda} \min_{\boldsymbol{P}_t} L(\boldsymbol{P_t}, \lambda)$. Then, from the first order optimality conditions, it yields

$$\begin{aligned} \nabla C(\overline{\boldsymbol{P}}_{\boldsymbol{t}}^{opt}) + \overline{\boldsymbol{\lambda}}^{opt} &= \boldsymbol{0} \\ \mathbb{1}_n^T \overline{\boldsymbol{P}}_{\boldsymbol{t}}^{opt} - \mathbb{1}_n^T \boldsymbol{P_d} &= 0, \end{aligned} \tag{5.30}$$

where $\nabla C(\overline{\boldsymbol{P}}_{\boldsymbol{t}}^{opt}) = \boldsymbol{\mathcal{Q}}\overline{\boldsymbol{P}}_{\boldsymbol{t}}^{opt} + \boldsymbol{\mathcal{R}}$. To conclude the proof, equalities (5.27) and (5.28) are obtained by manipulating (5.30). □

From (5.27) it follows that the marginal costs $\boldsymbol{\mathcal{Q}}\overline{\boldsymbol{P}}_{\boldsymbol{t}}^{opt} + \boldsymbol{\mathcal{R}}$ are identical. Note that (5.27) depends explicitly on the *unknown* power demand $\boldsymbol{P_d}$. We aim at the design of a controller solving (5.26) without measurements of the power demand, leading to the second objective.

Objective 5.2 (Economic dispatch).

$$\lim_{t\to\infty} \boldsymbol{P_t}(t) = \overline{\boldsymbol{P}}_{\boldsymbol{t}}^{opt}, \tag{5.31}$$

with $\overline{\boldsymbol{P}}_{\boldsymbol{t}}^{opt}$ as in (5.27), without measurements of $\boldsymbol{P_d}$.

In order to achieve Objective 5.1 and Objective 5.2 we refine Assumption 5.2 that ensures the feasibility of the objectives.

Assumption 5.4 (Existence of a optimal steady state). Assumption 5.2 holds when $\overline{\boldsymbol{f}} = \boldsymbol{0}$ and $\overline{\boldsymbol{P}}_{\boldsymbol{t}} = \overline{\boldsymbol{P}}_{\boldsymbol{g}} = \overline{\boldsymbol{P}}_{\boldsymbol{t}}^{opt}$, with $\overline{\boldsymbol{P}}_{\boldsymbol{t}}^{opt}$ as in (5.27).

Remark 5.3 (Varying power demand). To allow for a steady state solution, the power demand (unmatched disturbance) is required to be constant. This is not needed to reach the desired sliding manifold introduced in the next section, but is required only to establish the asymptotic convergence properties in Objective 5.1 and Objective 5.2. Furthermore, the proposed solution shows ([TBD16, Remark 8]) the existence of a finite $\mathcal{L}_2$-to-$\mathcal{L}_\infty$ gain and a finite $\mathcal{L}_2$-to-$\mathcal{L}_2$ gain from a varying demand to the frequency deviation $\boldsymbol{f}$ [KPA+04], once the system evolves on the sliding manifold, introduced in the next section.

5.6 Distributed Sliding Mode Control

In Section 5.4 we discussed a passivity property of the power network (5.13), with input $\boldsymbol{P_t}$ and output $\boldsymbol{f}$. Unfortunately, the turbine-governor system (5.14) does not immediately allow for a passive interconnection, since (5.14) is a linear system with relative degree two, when considering $-\boldsymbol{f}$ as the input and $\boldsymbol{P_t}$ as the output[8]. To alleviate this issue we propose a *distributed* Suboptimal Second Order Sliding Mode (D–SSOSM) control algorithm that simultaneously achieves Objective 5.1 and Objective 5.2, by constraining (5.14) such that it enjoys a suitable passivity property, and by exchanging information on the marginal costs. As a first step (see also Remark 5.4 below), we augment the turbine-governor dynamics (5.14) with a distributed control scheme, resulting in:

$$\begin{aligned} \boldsymbol{T_t}\dot{\boldsymbol{P}}_{\boldsymbol{t}} &= -\boldsymbol{P_t} + \boldsymbol{P_g} \\ \boldsymbol{T_g}\dot{\boldsymbol{P}}_{\boldsymbol{g}} &= -\boldsymbol{R}^{-1}f - \boldsymbol{P_g} + \boldsymbol{u} \\ \boldsymbol{T_\theta}\dot{\boldsymbol{\theta}} &= -\boldsymbol{\theta} + \boldsymbol{P_t} - \boldsymbol{A}\boldsymbol{\mathcal{L}^{com}}(\boldsymbol{\mathcal{Q}\theta} + \boldsymbol{\mathcal{R}}). \end{aligned} \tag{5.32}$$

Here, $\boldsymbol{\mathcal{Q}\theta} + \boldsymbol{\mathcal{R}}$ reflects the 'virtual' marginal costs and $\boldsymbol{\mathcal{L}^{com}}$ is the Laplacian matrix corresponding to the topology of an underlying communication network. The diagonal matrix $\boldsymbol{T_\theta} \in \mathbb{R}^{n\times n}$ provides additional design freedom to shape the transient response and the matrix $\boldsymbol{A}$ is suggested later to obtain a suitable passivity property. We note that $\boldsymbol{\mathcal{L}^{com}}(\boldsymbol{\mathcal{Q}\theta} + \boldsymbol{\mathcal{R}})$ represents the exchange information on the marginal costs among the control areas. To guarantee an optimal coordination of generation among *all* the control areas the following assumption is made:

Assumption 5.5. (**Communication topology**) The graph corresponding to the communication topology is undirected and connected.

Remark 5.4. (**First order turbine-governor dynamics**) The rational behind this seemingly ad-hoc choice of the augmented dynamics is that for the controlled first order turbine-governor dynamics, where $\boldsymbol{u} = \boldsymbol{\theta}$ and $\boldsymbol{P_g} = -\boldsymbol{R}^{-1}\boldsymbol{f} + \boldsymbol{\theta}$, system

$$\begin{aligned} \boldsymbol{T_t}\dot{\boldsymbol{P}}_{\boldsymbol{t}} &= -\boldsymbol{P_t} - \boldsymbol{R}^{-1}\boldsymbol{f} + \boldsymbol{\theta} \\ \boldsymbol{T_\theta}\dot{\boldsymbol{\theta}} &= -\boldsymbol{\theta} + \boldsymbol{P_t} - \boldsymbol{R}^{-1}\boldsymbol{\mathcal{Q}}\boldsymbol{\mathcal{L}^{com}}(\boldsymbol{\mathcal{Q}\theta} + \boldsymbol{\mathcal{R}}), \end{aligned} \tag{5.33}$$

has been shown to be incrementally passive with input $-\boldsymbol{f}$ and output $\boldsymbol{P_t}$, and is able to solve Objective 5.1 and Objective 5.2 [TD17b]. We aim at the design of $\boldsymbol{u}$ and $\boldsymbol{A}$ in (5.32), such that (5.32) behaves similarly as (5.33). This is made explicit in Lemma 5.8 and Lemma 5.9.

We now propose a sliding function $\boldsymbol{\sigma}(\boldsymbol{f}, \boldsymbol{P_t}, \boldsymbol{P_g}, \boldsymbol{\theta})$ and a matrix $\boldsymbol{A}$ for system (5.32), which will allow us to prove convergence to the desired state. The choices are motivated by the stability analysis in the next section, but are stated here for the sake of exposition. First, the sliding function $\boldsymbol{\sigma} : \mathbb{R}^{4n} \to \mathbb{R}^n$ is given by

$$\boldsymbol{\sigma}(\boldsymbol{f}, \boldsymbol{P_t}, \boldsymbol{P_g}, \boldsymbol{\theta}) = \boldsymbol{M_1 f} + \boldsymbol{M_2 P_t} + \boldsymbol{M_3 P_g} + \boldsymbol{M_4 \theta}, \tag{5.34}$$

where $\boldsymbol{M_1} \succ \boldsymbol{0}$, $\boldsymbol{M_2} \succeq \boldsymbol{0}$, $\boldsymbol{M_3} \succ \boldsymbol{0}$ are diagonal matrices and $\boldsymbol{M_4} = -(\boldsymbol{M_2} + \boldsymbol{M_3})$. Therefore, $\sigma_i, i \in \mathcal{V}$, depends only on the locally available variables that are defined on

[8] A linear system with relative degree two is not passive, as follows e.g. from the Kalman-Yakubovich-Popov lemma.

node i, facilitating the design of a distributed controller (see Remark 5.6). Second, the diagonal matrix $\boldsymbol{A} \in \mathbb{R}^{n\times n}$ is defined as

$$\boldsymbol{A} = (\boldsymbol{M_2} + \boldsymbol{M_3})^{-1}\boldsymbol{M_1}\boldsymbol{\mathcal{Q}}. \tag{5.35}$$

By regarding the sliding function (5.34) as the output function of system (5.13), (5.32), it appears that the relative degree of the system is one. This implies that a first order sliding mode controller can be *naturally* applied [Utk92] in order to attain in a finite time, the sliding manifold defined by $\boldsymbol{\sigma} = \mathbf{0}$. However, the input $\boldsymbol{u}$ to the governor affects the first time derivative of the sliding function, i.e. $\boldsymbol{u}$ affects $\dot{\boldsymbol{\sigma}}$. Since sliding mode controllers generate a discontinuous signal, we additionally require $\dot{\boldsymbol{\sigma}} = \mathbf{0}$, to guarantee that the signal $\boldsymbol{u}$ is continuous. Therefore, we define the desired sliding manifold as

$$\{(\boldsymbol{\eta}, \boldsymbol{f}, \boldsymbol{V}, \boldsymbol{P_t}, \boldsymbol{P_g}, \boldsymbol{\theta}) : \boldsymbol{\sigma} = \dot{\boldsymbol{\sigma}} = \mathbf{0}\}. \tag{5.36}$$

We continue by discussing a possible controller attaining the desired sliding manifold (5.36) while providing a continuous control input $\boldsymbol{u}$.

5.6.1 Suboptimal Second Order Sliding Mode Controller

To prevent chattering, it is important to provide a continuous control input $\boldsymbol{u}$ to the governor. Since sliding mode controllers generate a discontinuous control signal, we adopt the procedure suggested in [BFU98a] and first integrate the discontinuous signal, yielding for system (5.32)

$$\begin{aligned}
\boldsymbol{T_t}\dot{\boldsymbol{P}}_{\boldsymbol{t}} &= -\boldsymbol{P_t} + \boldsymbol{P_g} \\
\boldsymbol{T_g}\dot{\boldsymbol{P}}_{\boldsymbol{g}} &= -\boldsymbol{R}^{-1}\boldsymbol{f} - \boldsymbol{P_g} + \boldsymbol{u} \\
\boldsymbol{T_\theta}\dot{\boldsymbol{\theta}} &= -\boldsymbol{\theta} + \boldsymbol{P_t} - \boldsymbol{A}\boldsymbol{\mathcal{L}^{com}}(\boldsymbol{\mathcal{Q}}\boldsymbol{\theta} + \boldsymbol{\mathcal{R}}) \\
\dot{\boldsymbol{u}} &= \boldsymbol{w},
\end{aligned} \tag{5.37}$$

where $\boldsymbol{w}$ is the new (discontinuous) input generated by a sliding mode controller discussed below. A consequence is that the system relative degree (with respect to the new control input $\boldsymbol{w}$) is now two, and we need to rely on a second order sliding mode control strategy to attain the sliding manifold (5.34) in a finite time [Lev03]. To make the controller design explicit, we discuss a specific second order sliding mode controller, the so-called 'Suboptimal Second Order Sliding Mode' (SSOSM) controller proposed in [BFU98a]. We introduce two auxiliary variables $\boldsymbol{\xi_1} = \boldsymbol{\sigma} \in \mathbb{R}^n$ and $\boldsymbol{\xi_2} = \dot{\boldsymbol{\sigma}} \in \mathbb{R}^n$, and define the so-called auxiliary system as

$$\begin{aligned}
\dot{\boldsymbol{\xi}}_{\boldsymbol{1}} &= \boldsymbol{\xi_2} \\
\dot{\boldsymbol{\xi}}_{\boldsymbol{2}} &= \boldsymbol{\phi}(\boldsymbol{\eta}, \boldsymbol{f}, \boldsymbol{V}, \boldsymbol{P_t}, \boldsymbol{P_g}, \boldsymbol{\theta}) + \boldsymbol{G}\boldsymbol{w}.
\end{aligned} \tag{5.38}$$

Bearing in mind that $\dot{\boldsymbol{\xi}}_{\boldsymbol{2}} = \ddot{\boldsymbol{\sigma}} = \boldsymbol{\phi} + \boldsymbol{G}\boldsymbol{w}$, the expressions for the mapping $\boldsymbol{\phi}$ and matrix $\boldsymbol{G}$ can be straightforwardly obtained from (5.34) by taking the second derivative of $\boldsymbol{\sigma}$ with respect to time, yielding for the latter[9] $\boldsymbol{G} = \boldsymbol{M_3}\boldsymbol{T_g}^{-1} \in \mathbb{R}^{n\times n}$. We assume that the entries of $\boldsymbol{\phi}$ and $\boldsymbol{G}$ have known bounds

[9] The expression for $\boldsymbol{\phi}$ is rather long and is omitted.

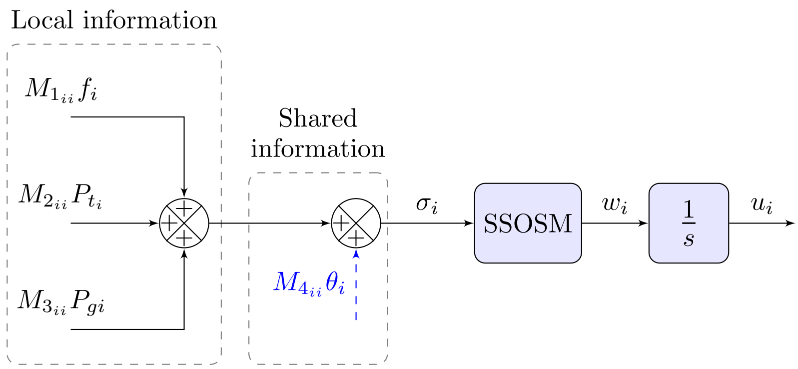

Fig. 5.2. Block diagram of the proposed Distributed Suboptimal Second Order Sliding Mode (D–SSOSM) control strategy.

$$\begin{aligned} &|\phi_i| \leq \Phi_i && \forall i \in \mathcal{V} \\ &0 < G_{\min_i} \leq G_{ii} \leq G_{\max_i} && \forall i \in \mathcal{V} \end{aligned} \tag{5.39}$$

with Φ_i, $G_{\min_i}$ and $G_{\max_i}$ being positive constants. Second, $\boldsymbol{w}$ is a discontinuous control input described by the SSOSM control algorithm [BFU98a], and consequently for each area $i \in \mathcal{V}$, the control law w_i is given by

$$w_i = -\alpha_i W_{\max_i} \operatorname{sign}\left(\xi_{1_i} - \frac{1}{2}\xi_{1,\max_i}\right), \tag{5.40}$$

with

$$W_{\max_i} > \max\left(\frac{\Phi_i}{\alpha_i^* G_{\min_i}}; \frac{4\Phi_i}{3G_{\min_i} - \alpha_i^* G_{\max_i}}\right), \tag{5.41}$$

$$\alpha_i^* \in (0, 1] \cap \left(0, \frac{3G_{\min_i}}{G_{\max_i}}\right), \tag{5.42}$$

α_i switching between α_i^* and 1, according to [BFU98a, Algorithm 1]. Note that indeed the input signal to the governor, $\boldsymbol{u}(t) = \int_0^t \boldsymbol{w}(\tau)d\tau$, is continuous, since the input $\boldsymbol{w}$ is piecewise constant. The extremal values $\xi_{1,\max_i}$ in (5.40) can be detected by implementing for instance a peak detection as in [BFU98b]. The block diagram of the proposed control strategy is depicted in Fig. 5.2.

Remark 5.5. (**Uncertainty of $\boldsymbol{\phi}$ and $\boldsymbol{G}$**) The mapping $\boldsymbol{\phi}$ and matrix $\boldsymbol{G}$ are uncertain due to the presence of the unmeasurable power demand $\boldsymbol{P_d}$ and voltage angle $\boldsymbol{\theta}$, and possible uncertainties in the system parameters. In practical cases the bounds in (5.39) can be determined relying on data analysis and physical insights. However, if these bounds cannot be a-priori estimated, the adaptive version of the SSOSM algorithm proposed in [ICF16] can be used to dominate the effect of the uncertainties.

Remark 5.6. (**Distributed control**) Given $\boldsymbol{A}$ in (5.35), the dynamics of θ_i in (5.32) read for node $i \in \mathcal{V}$ as

$$T_{\theta i}\dot{\theta}_i = -\theta_i + P_{t_i} - \frac{\mathcal{Q}_i M_{1_{ii}}}{M_{2_{ii}} + M_{3_{ii}}} \sum_{j \in \mathcal{N}_j^{com}} (\mathcal{Q}_i\theta_i + \mathcal{R}_i - \mathcal{Q}_j\theta_j - \mathcal{R}_j),$$

where $\mathcal{N}_j^{com}$ is the set of controllers connected to controller i. Furthermore, (5.40) depends only on σ_i, i.e. on states defined at node i. Consequently, the overall controller is indeed distributed and only information on marginal costs needs to be shared among connected controllers.

Remark 5.7. (**Alternative SOSM controllers**) In this work we rely on the SOSM control law proposed in [BFU98a]. However, to constrain system (5.13) augmented with dynamics (5.37) on the sliding manifold (5.36), where $\boldsymbol{\sigma} = \dot{\boldsymbol{\sigma}} = \mathbf{0}$, any other SOSM control law that does not need the measurement of $\dot{\boldsymbol{\sigma}}$ can be used (e.g. the super-twisting control [Lev93]). An interesting continuation of the presented results is to study the performance of various SOSM controllers within the setting of (optimal) LFC.

Remark 5.8. (**Comparison with [TD17b] and [KMDL17]**) The controller proposed in [TD17b] requires, besides a gain restriction in the controller, that

$$\begin{aligned} 4T_{gi}T_{t_i}^{-1} &> 1 \\ K_{p_i}^{-1}T_{gi}T_{t_i}^{-1} &> 1. \end{aligned} \tag{5.43}$$

In this work, we do not impose such restriction on the parameters. The result in [KMDL17] requires, besides some assumptions on the dissipation inequality related to the generation side, the existence of frequency dependent generation and load, where the generation/demand (output) depends directly (e.g. proportionally) on the frequency (input), avoiding complications arising from generation dynamics that have relative degree two when considering the input-output pair just indicated (see also Remark 5.10).

Remark 5.9. (**Primal-dual based approaches**) Although the focus in this work is to augment the power network with consensus-type dynamics in (5.32), it is equally possible to augment the power network with a continuous primal-dual algorithm that has been studied extensively to obtain optimal LFC. This work provides therefore also means to extend existing results on primal-dual based approaches to incorporate the turbine-governor dynamics, generating the control input by a higher order sliding mode controller. The required adjustments follow similar steps as discussed in [TD17b, Remark 9], and, for the sake of brevity, we directly state the resulting primal-dual based augmented system, replacing (5.32),

$$\begin{aligned} \boldsymbol{T_t}\dot{\boldsymbol{P}}_{\boldsymbol{t}} &= -\boldsymbol{P_t} + \boldsymbol{P_g} \\ \boldsymbol{T_g}\dot{\boldsymbol{P}}_{\boldsymbol{g}} &= -\boldsymbol{R}^{-1}\boldsymbol{f} - \boldsymbol{P_g} + \boldsymbol{u} \\ \boldsymbol{T_\theta}\dot{\boldsymbol{\theta}} &= -\boldsymbol{\theta} + \boldsymbol{P_t} - \boldsymbol{M_1}(\boldsymbol{M_2} + \boldsymbol{M_3})^{-1}\left(\nabla C(\boldsymbol{\theta}) - \boldsymbol{\psi}\right) \\ \dot{\boldsymbol{v}} &= -\boldsymbol{\mathcal{B}}^T\boldsymbol{\psi} \\ \dot{\boldsymbol{\psi}} &= \boldsymbol{\mathcal{B}}\boldsymbol{v} - \boldsymbol{\theta} + \boldsymbol{P_d}. \end{aligned} \tag{5.44}$$

In this case only strict convexity of $C(\boldsymbol{\theta})$ is required and the load $\boldsymbol{P_d}$ explicitly appears in (5.44). The stability analysis of the power network, including the augmented turbine-governor dynamics (5.44), follows *mutatis mutandis*, the same argumentation as in the next section where the focus is on the augmented system (5.32). Some required nontrivial modifications in the analysis are briefly discussed in Remark 5.13.

5.7 Stability Analysis

In this section we study the stability of the proposed control scheme, based on an enforced passivity property of (5.32) on the sliding manifold defined by (5.34). First, we establish that the second order sliding mode controller (5.38)–(5.42) constrains the system in finite time to the desired sliding manifold.

Lemma 5.8. (**Convergence to the sliding manifold**) Let Assumption 5.1 hold. The solutions to system (5.13), augmented with (5.37), in closed loop with controller (5.38)–(5.42) converge in a finite time T_r to the sliding manifold (5.36) such that

$$\boldsymbol{P_g} = -\,\boldsymbol{M_3}^{-1}(\boldsymbol{M_1 f} + \boldsymbol{M_2 P_t} + \boldsymbol{M_4 \theta}) \quad \forall t \geq T_r. \tag{5.45}$$

Proof. Following [BFU98a], the application of (5.38)–(5.42) to each control area guarantees that $\boldsymbol{\sigma} = \dot{\boldsymbol{\sigma}} = \mathbf{0}$, $\forall\, t \geq T_r$. The details are omitted, and are an immediate consequence of the used SSOSM control algorithm [BFU98a]. Then, from (5.34) one can easily obtain (5.45), where $\boldsymbol{M_3}$ is indeed invertible. □

Exploiting relation (5.45), on the sliding manifold where $\boldsymbol{\sigma} = \dot{\boldsymbol{\sigma}} = \mathbf{0}$, the so-called equivalent system is as follows

$$\begin{aligned} \boldsymbol{M_3 T_t \dot{P}_t} &= -(\boldsymbol{M_2} + \boldsymbol{M_3})\boldsymbol{P_t} - \boldsymbol{M_4 \theta} - \boldsymbol{M_1 f} \\ \boldsymbol{T_\theta \dot{\theta}} &= -\boldsymbol{\theta} + \boldsymbol{P_t} - \boldsymbol{A \mathcal{L}^{com}}(\boldsymbol{\mathcal{Q}\theta} + \boldsymbol{\mathcal{R}}). \end{aligned} \tag{5.46}$$

As a consequence of the feasibility assumption (Assumption 5.4), the system above admits the following steady state

$$\begin{aligned} \mathbf{0} &= -(\boldsymbol{M_2} + \boldsymbol{M_3})\overline{\boldsymbol{P}}_{\boldsymbol{t}}^{opt} - \boldsymbol{M_4}\overline{\boldsymbol{\theta}} - \boldsymbol{M_1}\mathbf{0} \\ \mathbf{0} &= -\overline{\boldsymbol{\theta}} + \overline{\boldsymbol{P}}_{\boldsymbol{t}}^{opt} - \boldsymbol{A \mathcal{L}^{com}}(\boldsymbol{\mathcal{Q}}\overline{\boldsymbol{\theta}} + \boldsymbol{\mathcal{R}}). \end{aligned} \tag{5.47}$$

Now, we show that system (5.46), with $\boldsymbol{A}$ as in (5.35), indeed possesses a passivity property with respect to the steady state (5.47). Note that, due to the discontinuous control law (5.40), the solutions to the closed loop system are understood in the sense of Filippov. Following the equivalent control method [Utk92], the solutions to the equivalent system are however continuously differentiable.

Lemma 5.9. (**Incremental passivity of (5.46)**) System (5.46) with input $-\boldsymbol{f}$ and output $\boldsymbol{P_t}$ is an incrementally passive system, with respect to the constant $(\overline{\boldsymbol{P}}_{\boldsymbol{t}}^{opt}, \overline{\boldsymbol{\theta}})$ satisfying (5.47).

Proof. Consider the following incremental storage function

$$\begin{aligned}\mathcal{S}_2 = &\frac{1}{2}(\boldsymbol{P_t} - \overline{\boldsymbol{P}}_{\boldsymbol{t}}^{opt})^T \boldsymbol{M_1}^{-1}\boldsymbol{M_3}\boldsymbol{T_t}(\boldsymbol{P_t} - \overline{\boldsymbol{P}}_{\boldsymbol{t}}^{opt}) \\ &+ \frac{1}{2}(\boldsymbol{\theta} - \overline{\boldsymbol{\theta}})^T \boldsymbol{M_1}^{-1}(\boldsymbol{M_2} + \boldsymbol{M_3})\boldsymbol{T_\theta}(\boldsymbol{\theta} - \overline{\boldsymbol{\theta}}),\end{aligned} \tag{5.48}$$

which is positive definite, since $\boldsymbol{M_1} \succ \boldsymbol{0}, \boldsymbol{M_2} \succeq \boldsymbol{0}$ and $\boldsymbol{M_3} \succ \boldsymbol{0}$. Then, we have that $\mathcal{S}_2$ satisfies along the solutions to (5.46)

$$\begin{aligned}\dot{\mathcal{S}}_2 &= \frac{1}{2}(\boldsymbol{P_t} - \overline{\boldsymbol{P}}_{\boldsymbol{t}}^{opt})^T \boldsymbol{M_1}^{-1}\boldsymbol{M_3}\boldsymbol{T_t}\dot{\boldsymbol{P}}_{\boldsymbol{t}} + \frac{1}{2}(\boldsymbol{\theta} - \overline{\boldsymbol{\theta}})^T \boldsymbol{M_1}^{-1}(\boldsymbol{M_2} + \boldsymbol{M_3})\boldsymbol{T_\theta}\dot{\boldsymbol{\theta}} \\ &= \frac{1}{2}(\boldsymbol{P_t} - \overline{\boldsymbol{P}}_{\boldsymbol{t}}^{opt})^T(-\boldsymbol{M_1}^{-1}(\boldsymbol{M_2} + \boldsymbol{M_3})\boldsymbol{P_t} - \boldsymbol{f} - \boldsymbol{M_1}^{-1}\boldsymbol{M_4}\boldsymbol{\theta}) \\ &\quad + \frac{1}{2}(\boldsymbol{\theta} - \overline{\boldsymbol{\theta}})^T \boldsymbol{M_1}^{-1}(\boldsymbol{M_2} + \boldsymbol{M_3})(\boldsymbol{P_t} - \boldsymbol{\theta} - \boldsymbol{A}\boldsymbol{\mathcal{L}^{com}}(\boldsymbol{\mathcal{Q}}\boldsymbol{\theta} + \boldsymbol{\mathcal{R}})).\end{aligned}$$

In view of $\boldsymbol{M_4} = -(\boldsymbol{M_2} + \boldsymbol{M_3})$, $\boldsymbol{A} = (\boldsymbol{M_2} + \boldsymbol{M_3})^{-1}\boldsymbol{M_1}\boldsymbol{\mathcal{Q}}$ and equality (5.47), it follows that

$$\begin{aligned}\dot{\mathcal{S}}_2 = &-(\boldsymbol{P_t} - \boldsymbol{\theta})^T \boldsymbol{M_1}^{-1}(\boldsymbol{M_2} + \boldsymbol{M_3})(\boldsymbol{P_t} - \boldsymbol{\theta}) \\ &-(\boldsymbol{\mathcal{Q}}\boldsymbol{\theta} + \boldsymbol{\mathcal{R}} - \boldsymbol{\mathcal{Q}}\overline{\boldsymbol{\theta}} - \boldsymbol{\mathcal{R}})\boldsymbol{\mathcal{L}^{com}}(\boldsymbol{\mathcal{Q}}\boldsymbol{\theta} + \boldsymbol{\mathcal{R}} - \boldsymbol{\mathcal{Q}}\overline{\boldsymbol{\theta}} - \boldsymbol{\mathcal{R}}) \\ &-(\boldsymbol{P_t} - \overline{\boldsymbol{P}}_{\boldsymbol{t}}^{opt})^T(\boldsymbol{f} - \boldsymbol{0}).\end{aligned}$$

□

Remark 5.10. (**Relative degree order reduction**) An important consequence of the proposed sliding mode controller (5.38)–(5.42) is that the relative degree of system (5.46) is one with input $-\boldsymbol{f}$ and output $\boldsymbol{P_t}$. This is in contrast to the 'original' system (5.14) that has relative degree two with the same input–output pair.

Now, relying on the interconnection of incrementally passive systems, we can prove the main result of this work concerning the evolution of the augmented system controlled via the proposed distributed SSOSM control strategy.

Theorem 5.1 (Main result). *Let assumptions 5.1–5.5 hold. Consider system (5.13) and (5.32), controlled via (5.38)–(5.42). Then, the solutions to the closed-loop system starting in a neighbourhood of the equilibrium* $(\overline{\boldsymbol{\eta}}, \overline{\boldsymbol{f}} = \boldsymbol{0}, \overline{\boldsymbol{V}}, \overline{\boldsymbol{P}}_{\boldsymbol{t}}^{opt}, \overline{\boldsymbol{P}}_{\boldsymbol{g}}, \overline{\boldsymbol{\theta}})$ *approach the set where* $\overline{\boldsymbol{f}} = \boldsymbol{0}$ *and* $\overline{\boldsymbol{P}}_{\boldsymbol{t}} = \overline{\boldsymbol{P}}_{\boldsymbol{t}}^{opt}$*, with* $\overline{\boldsymbol{P}}_{\boldsymbol{t}}^{opt}$ *given by (5.27).*

Proof. Following Lemma 5.8, we have that the SSOSM control enforces system (5.32) to evolve $\forall t \geq T_r$ on the sliding manifold (5.36), resulting in the reduced order system (5.46). To study the obtained closed loop system, consider the overall incremental storage function $\mathcal{S} = \mathcal{S}_1 + \mathcal{S}_2$, with $\mathcal{S}_1$ given by (5.19) and $\mathcal{S}_2$ given by (5.48). In view of Lemma 5.5, we have that $\mathcal{S}$ has a local minimum at $(\overline{\boldsymbol{\eta}}, \overline{\boldsymbol{f}} = \mathbf{0}, \overline{\boldsymbol{V}}, \overline{\boldsymbol{P}}_{\boldsymbol{t}}^{opt}, \overline{\boldsymbol{\theta}})$ and satisfies along the solutions to (5.13), (5.46)

$$\begin{aligned}\dot{\mathcal{S}} =& -\boldsymbol{f}^T\boldsymbol{K}_{\boldsymbol{p}}^{-1}\boldsymbol{f} - \dot{\boldsymbol{V}}^T\boldsymbol{T}_{\boldsymbol{V}}(\boldsymbol{X}_{\boldsymbol{d}} - \boldsymbol{X}_{\boldsymbol{d}}')^{-1}\dot{\boldsymbol{V}} - (\boldsymbol{P}_{\boldsymbol{t}} - \boldsymbol{\theta})^T\boldsymbol{M}_{\boldsymbol{1}}^{-1}(\boldsymbol{M}_{\boldsymbol{2}} + \boldsymbol{M}_{\boldsymbol{3}})(\boldsymbol{P}_{\boldsymbol{t}} - \boldsymbol{\theta})\\ &- (\boldsymbol{\mathcal{Q}}\boldsymbol{\theta} + \boldsymbol{\mathcal{R}} - \boldsymbol{\mathcal{Q}}\overline{\boldsymbol{\theta}} - \boldsymbol{\mathcal{R}})\boldsymbol{\mathcal{L}}^{\boldsymbol{com}}(\boldsymbol{\mathcal{Q}}\boldsymbol{\theta} + \boldsymbol{\mathcal{R}} - \boldsymbol{\mathcal{Q}}\overline{\boldsymbol{\theta}} - \boldsymbol{\mathcal{R}}) \leq \ 0,\end{aligned}$$

where $\dot{\boldsymbol{V}} = \boldsymbol{T}_{\boldsymbol{V}}^{-1}\big(-(\boldsymbol{X}_{\boldsymbol{d}} - \boldsymbol{X}_{\boldsymbol{d}}')\boldsymbol{E}(\boldsymbol{\eta})\boldsymbol{V} + \overline{\boldsymbol{E}}_{\boldsymbol{f}}\big)$. Consequently, there exists a forward invariant set Υ around $(\overline{\boldsymbol{\eta}}, \overline{\boldsymbol{f}} = \mathbf{0}, \overline{\boldsymbol{V}}, \overline{\boldsymbol{P}}_{\boldsymbol{t}}^{opt}, \overline{\boldsymbol{\theta}})$ and by LaSalle's invariance principle the solutions that start in Υ approach the largest invariant set contained in

$$\Upsilon \cap \{(\boldsymbol{\eta}, \boldsymbol{f}, \boldsymbol{V}, \boldsymbol{P}_{\boldsymbol{t}}, \boldsymbol{\theta}) : \boldsymbol{f} = \mathbf{0}, \boldsymbol{V} = \big((\boldsymbol{X}_{\boldsymbol{d}} - \boldsymbol{X}_{\boldsymbol{d}}')\boldsymbol{E}(\overline{\boldsymbol{\eta}})\big)^{-1}\overline{\boldsymbol{E}}_{\boldsymbol{f}}, \boldsymbol{P}_{\boldsymbol{t}} = \boldsymbol{\theta}, \boldsymbol{\theta} = \overline{\boldsymbol{\theta}} + \boldsymbol{\mathcal{Q}}^{-1}\mathbb{1}_n\alpha\},$$

where $\alpha \in \mathbb{R}$ is some scalar. On this invariant set the controlled power network satisfies

$$\begin{aligned}\dot{\boldsymbol{\eta}} &= \boldsymbol{\mathcal{B}}^T\mathbf{0}\\ \mathbf{0} &= \boldsymbol{K}_{\boldsymbol{p}}(\overline{\boldsymbol{\theta}} + \boldsymbol{\mathcal{Q}}^{-1}\mathbb{1}_n\alpha - \boldsymbol{P}_{\boldsymbol{d}} - \boldsymbol{\mathcal{B}}\boldsymbol{\Gamma}(\boldsymbol{V})\mathbf{sin}(\boldsymbol{\eta}))\\ \mathbf{0} &= -(\boldsymbol{X}_{\boldsymbol{d}} - \boldsymbol{X}_{\boldsymbol{d}}')\boldsymbol{E}(\boldsymbol{\eta})\boldsymbol{V} + \overline{\boldsymbol{E}}_{\boldsymbol{f}}\\ \boldsymbol{M}_{\boldsymbol{3}}\boldsymbol{T}_{\boldsymbol{t}}\dot{\boldsymbol{P}}_{\boldsymbol{t}} &= \mathbf{0}\\ \boldsymbol{T}_{\boldsymbol{\theta}}\dot{\boldsymbol{\theta}} &= \mathbf{0}.\end{aligned} \tag{5.49}$$

Pre-multiplying both sides of the second line of (5.49) with $\mathbb{1}_n^T\boldsymbol{K}_{\boldsymbol{p}}^{-1}$ yields $0 = \mathbb{1}_n^T(\overline{\boldsymbol{\theta}} + \boldsymbol{\mathcal{Q}}^{-1}\mathbb{1}_n\alpha - \boldsymbol{P}_{\boldsymbol{d}})$. Since $\overline{\boldsymbol{\theta}} = \overline{\boldsymbol{P}}_{\boldsymbol{t}}^{opt}$, $\mathbb{1}_n^T(\overline{\boldsymbol{P}}_{\boldsymbol{t}}^{opt} - \boldsymbol{P}_{\boldsymbol{d}}) = 0$ and $\boldsymbol{\mathcal{Q}}$ is a diagonal matrix with only positive elements, it follows that necessarily $\alpha = 0$. We can conclude that the solutions to the system (5.13) and (5.32), controlled via (5.38)–(5.42), indeed approach the set where $\overline{\boldsymbol{f}} = \mathbf{0}$ and $\overline{\boldsymbol{P}}_{\boldsymbol{t}} = \overline{\boldsymbol{P}}_{\boldsymbol{t}}^{opt}$, with $\overline{\boldsymbol{P}}_{\boldsymbol{t}}^{opt}$ given by (5.27). □

Remark 5.11. (**Robustness to failed communication**) The proposed control scheme is distributed and as such requires a communication network to share information on the marginal costs. However, note that the term $-\boldsymbol{A}\boldsymbol{\mathcal{L}}^{\boldsymbol{com}}(\boldsymbol{\mathcal{Q}}\boldsymbol{\theta} + \boldsymbol{\mathcal{R}})$ in (5.32) is not needed to enforce the passivity property established in Lemma 5.9, but is required to prove convergence to the economic efficient generation $\overline{\boldsymbol{P}}_{\boldsymbol{t}}^{opt}$. In fact, setting $\boldsymbol{A} = \mathbf{0}$ still permits to infer frequency regulation following the argumentation of Theorem 5.1.

Remark 5.12. (**Region of attraction**) LaSalle's invariance principle can be applied to all bounded solutions. As follows from Lemma 5.5, we have that the considered incremental storage function has a local minimum at the desired steady state, whereas the time to converge to the sliding manifold can be made arbitrarily small by properly choosing the gains of the SSOSM control. This guarantees that solutions starting in the vicinity of the steady state of interest remain bounded. A preliminary (numerical) assessment indicates that the region of attraction is large, but a thorough analysis is left as future endeavour.

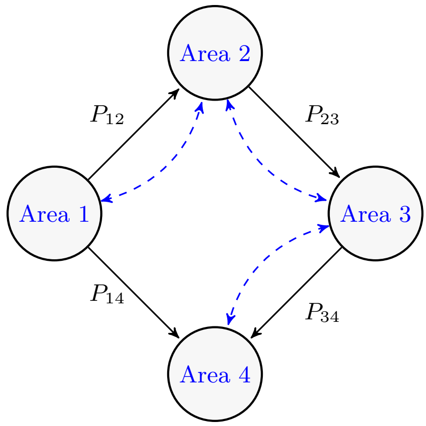

Fig. 5.3. Scheme of the considered power network partitioned into 4 control areas, where $P_{ij} = \frac{V_i V_j}{X_{ij}} \sin(\delta_i - \delta_j)$. The solid arrows indicate the positive direction of the power flows through the power network, while the dashed lines represent the communication network.

Remark 5.13. (**Stability of primal-dual based approaches**) To accommodate the additional dynamics of states $\boldsymbol{v}$ and $\boldsymbol{\psi}$ appearing in primal-dual based augmented system (5.44), an additional storage term is required in Lemma 5.9, namely:

$$\mathcal{S}_3 = \frac{1}{2}(\boldsymbol{v} - \overline{\boldsymbol{v}})^T(\boldsymbol{v} - \overline{\boldsymbol{v}}) + \frac{1}{2}(\boldsymbol{\psi} - \overline{\boldsymbol{\psi}})^T(\boldsymbol{\psi} - \overline{\boldsymbol{\psi}}), \tag{5.50}$$

where $\overline{\boldsymbol{v}}$ and $\overline{\boldsymbol{\psi}}$ satisfy the steady state equations

$$\begin{aligned} \mathbf{0} &= -\overline{\boldsymbol{\theta}} + \overline{\boldsymbol{P}}_{\boldsymbol{t}}^{opt} - \boldsymbol{M_1}(\boldsymbol{M_2} + \boldsymbol{M_3})^{-1}\left(\nabla C(\overline{\boldsymbol{\theta}}) - \overline{\boldsymbol{\psi}}\right) \\ \mathbf{0} &= -\boldsymbol{\mathcal{B}}^T\overline{\boldsymbol{\psi}} \\ \mathbf{0} &= \boldsymbol{\mathcal{B}}\overline{\boldsymbol{v}} - \overline{\boldsymbol{\theta}} + \boldsymbol{P_d}. \end{aligned} \tag{5.51}$$

Consequently, $\mathcal{S}_2 + \mathcal{S}_3$ satisfies along the solutions to the system, constrained to the manifold $\boldsymbol{\sigma} = \dot{\boldsymbol{\sigma}} = \mathbf{0}$,

$$\begin{aligned} \dot{\mathcal{S}}_2 + \dot{\mathcal{S}}_3 = &- (\boldsymbol{P_t} - \boldsymbol{\theta})^T\boldsymbol{M_1}^{-1}(\boldsymbol{M_2} + \boldsymbol{M_3})(\boldsymbol{P_t} - \boldsymbol{\theta}) \\ &- (\boldsymbol{\theta} - \overline{\boldsymbol{\theta}})^T(\nabla C(\boldsymbol{\theta}) - \nabla C(\overline{\boldsymbol{\theta}})) - (\boldsymbol{P_t} - \overline{\boldsymbol{P}}_{\boldsymbol{t}}^{opt})^T(\boldsymbol{f} - \mathbf{0}). \end{aligned}$$

Note that, as a result of the mean value theorem, $-(\boldsymbol{\theta} - \overline{\boldsymbol{\theta}})^T(\nabla C(\boldsymbol{\theta}) - \nabla C(\overline{\boldsymbol{\theta}})) = -(\boldsymbol{\theta} - \overline{\boldsymbol{\theta}})^T\nabla^2 C(\tilde{\boldsymbol{\theta}})(\boldsymbol{\theta} - \overline{\boldsymbol{\theta}}) \leq 0$, for some $\tilde{\theta}_i \in [\theta_i, \overline{\theta}_i]$, for all $i \in \mathcal{V}$. The matrix $\nabla^2 C(\tilde{\boldsymbol{\theta}}) \in \mathbb{R}^{n\times n}$ is positive definite due to the strict convexity of $C(\cdot)$. The proof of Theorem 5.1 can now be repeated using the incremental storage function $\mathcal{S} = \mathcal{S}_1 + \mathcal{S}_2 + \mathcal{S}_3$.

5.8 Case Study

In this section, the proposed control solution is assessed in simulation, by implementing a power network partitioned into four control areas (e.g. the IEEE New England 39-bus

Table 5.2. Network Parameters and Power Demand

		Area 1	Area 2	Area 3	Area 4
T_{p_i}	(s)	21.0	25.0	23.0	22.0
T_{t_i}	(s)	0.30	0.33	0.35	0.28
T_{gi}	(s)	0.080	0.072	0.070	0.081
T_{V_i}	(s)	5.54	7.41	6.11	6.22
K_{p_i}	(Hz p.u.$^{-1}$)	120.0	112.5	115.0	118.5
R_i	(Hz p.u.$^{-1}$)	2.5	2.7	2.6	2.8
X_{d_i}	(p.u.)	1.85	1.84	1.86	1.83
X'_{d_i}	(p.u.)	0.25	0.24	0.26	0.23
$\overline{E}_{f_i}$	(p.u.)	1.0	1.0	1.0	1.0
B_{ii}	(p.u.)	−13.6	−12.9	−12.3	−12.3
$T_{\theta i}$	(s)	0.33	0.33	0.33	0.33
$\mathcal{Q}_i$	(10^4 \$ h^{-1})	2.42	3.78	3.31	2.75
$\varDelta P_{d_i}$	(p.u.)	0.010	0.015	0.012	0.014

system [NC13]). The topology of the power network is represented in Fig. 5.3, together with the communication network (dashed lines). The line parameters are $B_{12} = -5.4$ p.u., $B_{23} = -5.0$ p.u., $B_{34} = -4.5$ p.u. and $B_{14} = -5.2$ p.u., while the network parameters and the power demand variation $\varDelta P_{d_i}$ of each area are provided in Table 5.2, where a base power of 1000 MW is assumed. The matrices in (5.34) are chosen as $\boldsymbol{M_1} = 3\mathbb{I}_4$, $\boldsymbol{M_2} = \mathbb{I}_4$, $\boldsymbol{M_3} = 0.1\mathbb{I}_4$ and $\boldsymbol{M_4} = -(\boldsymbol{M_2} + \boldsymbol{M_3})$, $\mathbb{I}_4 \in \mathbb{R}^{4\times 4}$ being the identity matrix, while the control amplitude $W_{\max_i}$ and the parameter α_i^*, in (5.40) are 10 and 1, respectively, for all $i \in \mathcal{V}$. For the sake of simplicity, in the cost function (5.25), we select $\mathcal{R}_i = \mathcal{C}_i = 0$ for all $i \in \mathcal{V}$. The system is initially at the steady state. Then, at the time instant $t = 1$ s, the power demand in each area is increased according to the values reported in Table 5.2. From Fig. 5.4, one can observe that the frequency deviations converge asymptotically to zero after a transient where the frequency drops because of the increasing load. Indeed, one can note that the proposed controllers increase the power generation in order to reach again a zero steady state frequency deviation. Moreover, the total power demand is shared among the areas, minimizing the total generation costs. More precisely, by applying the proposed D-SSOSM, the total generation costs are 10 % less than the generation costs when each area would produce only for its own demand.

5.9 Third Order Sliding Mode Observers

The control scheme proposed in Section 5.6 requires to acquire the measurements of all the state variables to compute the sliding function (5.34), and generate the control law (5.40). Yet, the necessity of a large number of sensors can significantly limit the applicability of this control approach. The use of an observer can be seen as a way to overcome this limitation, thus enhancing monitoring and control of power network. Few relevant works have proposed observers with application to power systems. For example, in [HIU$^+$12], an observer has been designed to estimate the electrical active power demand. In [JWW$^+$01],

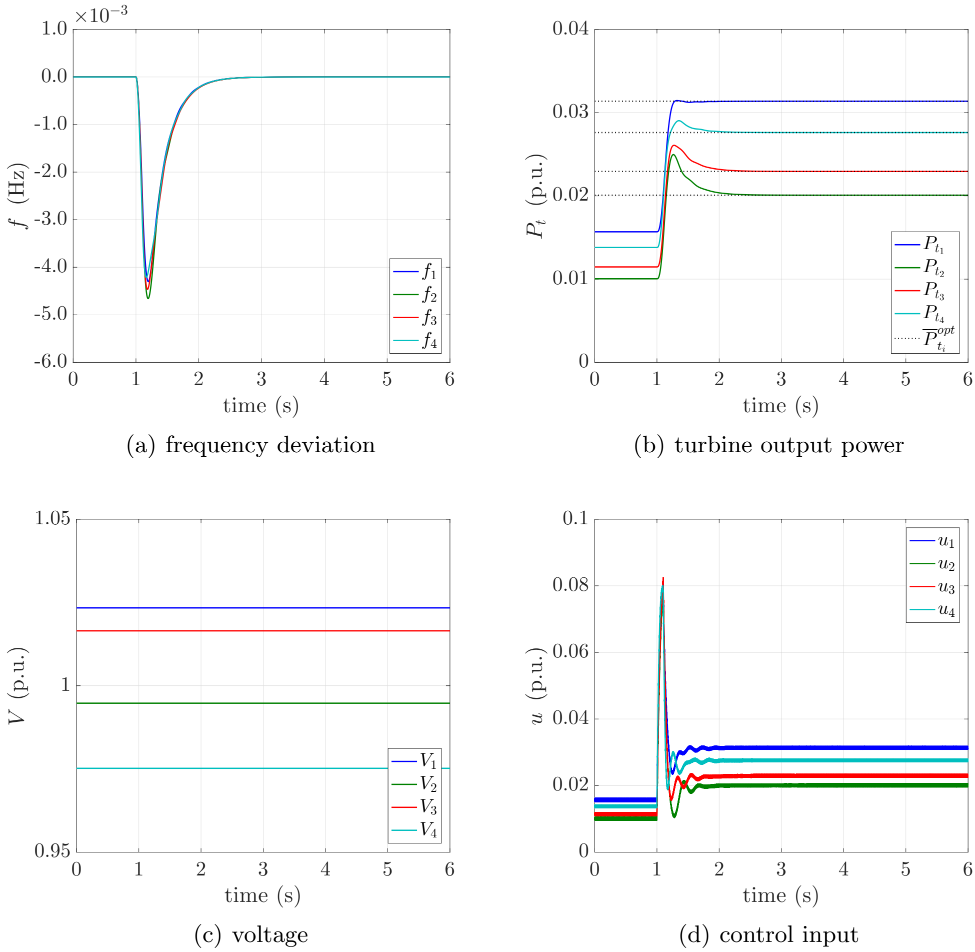

Fig. 5.4. Evolution of the controlled power system considering a power demand variation at the time instant $t = 1\,\text{s}$. **(a)** Frequency deviation in each control area. **(b)** Generated power at the output of each steam turbine. **(c)** Voltage dynamics in each node. **(d)** Control inputs to the governors.

a sliding mode observer has been used to estimate the states of each synchronous generator in multi-machines power systems. In [MMEF15], a sliding mode observer has been proposed to detect and reconstruct load alteration failures in power networks.

In this section, we adopt the model of a power network partitioned into control areas having an arbitrarily complex and meshed topology. The generation side is modeled by an equivalent generator including second-order turbine-governor dynamics. We assume to measure only the voltage angle variation and the turbine output power variation for each control area. The main contribution of this section is the design of two third order sliding mode observers capable of estimating, respectively, the frequency deviation and the governor output variation of each control area. The finite-time convergence to zero of the error system dynamics is proved.

The third order sliding mode observers have been designed having in mind the control strategy proposed in Section 5.6, which relies on the Suboptimal Second Order Sliding Mode (SSOSM) control algorithm [BFU98a], and on the design of the sliding manifold (5.34), where the controlled system exhibits an incremental passivity property that allows us to infer convergence to a zero steady state frequency deviation and minimize the generation costs. Differently from the control strategy proposed in Section 5.6, where the availability of all the state variables is assumed, in this section we assume that the sliding function, defined to solve the control problem, depends on unmeasurable states of the power network.

5.9.1 Problem Formulation

The following (standard) notation is used throughout this section. For a given state variable $\boldsymbol{x}$, $\tilde{\boldsymbol{x}}$ denotes its value after the change of coordinates $\tilde{\boldsymbol{x}} = \boldsymbol{E}\boldsymbol{x}$, while $\hat{\boldsymbol{x}}$ denotes the estimate of $\tilde{\boldsymbol{x}}$.

In addition to the Assumptions 5.2–5.5, in this section we adopt an assumption that is commonly used in the literature for the purposes of the design of monitoring and control algorithms (see e.g. [vdSS16]).

Assumption 5.6 (Constant Voltages). The voltage profile is flat, which means that the magnitude of voltage at each node of the power network is equal to 1 p.u. (i.e., $\boldsymbol{V} = \overline{\boldsymbol{V}} = 1$ p.u., where 1 p.u. is the expression of the actual value with respect to the base values).

For the reader's convenience, we rewrite the equivalent generator dynamics (5.13) for all nodes $i \in \mathcal{V}$ as

$$\begin{aligned} \dot{\boldsymbol{\delta}} &= 2\pi \boldsymbol{f} \\ \boldsymbol{T_p}\dot{\boldsymbol{f}} &= -\boldsymbol{f} + \boldsymbol{K_p}\left(\boldsymbol{P_t} - \boldsymbol{P_d} - \boldsymbol{\mathcal{B}\Gamma}(\overline{\boldsymbol{V}})\mathbf{sin}(\boldsymbol{\mathcal{B}}^T\boldsymbol{\delta})\right) \\ \boldsymbol{y_1} &= \boldsymbol{\delta}, \end{aligned} \tag{5.52}$$

and the turbine-governor dynamics (5.14) as

$$\begin{aligned} \boldsymbol{T_t}\dot{\boldsymbol{P}}_{\boldsymbol{t}} &= -\boldsymbol{P_t} + \boldsymbol{P_g} \\ \boldsymbol{T_g}\dot{\boldsymbol{P}}_{\boldsymbol{g}} &= -\boldsymbol{R}^{-1}\boldsymbol{f} - \boldsymbol{P_g} + \boldsymbol{u} \\ \boldsymbol{y_2} &= \boldsymbol{P_t}, \end{aligned} \tag{5.53}$$

where $\boldsymbol{\delta} \in \mathbb{R}^n$, $\boldsymbol{f} \in \mathbb{R}^n$, $\boldsymbol{P_t} \in \mathbb{R}^n$, $\boldsymbol{P_g} \in \mathbb{R}^n$, $\boldsymbol{\Gamma} = \mathrm{diag}\{\Gamma_1, \ldots, \Gamma_m\}$, with $\Gamma(\overline{\boldsymbol{V}})_k = \overline{V}_i\overline{V}_j/X_{ij}$, $\boldsymbol{P_d} \in \mathbb{R}^n$, $\boldsymbol{u} \in \mathbb{R}^n$, $\boldsymbol{y_1} \in \mathbb{R}^n$, and $\boldsymbol{y_2} \in \mathbb{R}^n$. Matrices $\boldsymbol{T_p}, \boldsymbol{T_t}, \boldsymbol{T_g}, \boldsymbol{K_p}, \boldsymbol{R}$ are suitable $n \times n$ diagonal matrices.

Moreover, Assumption 5.1 is modified as follows.

Assumption 5.7 (Available information). Variables P_{t_i} and δ_i are locally available at the i-th control area. The disturbance P_{d_i} is unknown, and both the disturbance itself and its first time derivative are bounded as follows

$$|P_{d_i}| \leq \Delta_{M_{d_i}}, \quad |\dot{P}_{d_i}| \leq \Delta_{\dot{M}_{d_i}}, \tag{5.54}$$

where $\Delta_{M_{d_i}}$ and $\Delta_{\dot{M}_{d_i}}$ are positive constants that can be determined relying on data analysis and engineering understanding. Furthermore, $T_{p_i}, T_{t_i}, T_{g_i}$ and K_{p_i} are assumed to be known at the i-th control area.

Assumption 5.7 implies that the variables P_{g_i} and f_i have to be estimated at the i-th control area.

5.9.1.1 Useful Changes of Coordinates

In this section we suggest changes of coordinates for the equivalent generator dynamics (5.52) and for the turbine-governor dynamics (5.53). These are useful for the purpose of the observers design. For the i-th control area, the generator dynamics can be written

as

$$\begin{aligned} \dot{\delta}_i &= 2\pi f_i \\ \dot{f}_i &= a_i f_i - K_{p_i} a_i P_{t_i} + \phi_i \\ y_{i_1} &= \delta_i, \end{aligned} \tag{5.55}$$

where $a_i \triangleq -1/T_{p_i}$, and

$$\phi_i \triangleq -\frac{K_{p_i}}{T_{p_i}} P_{d_i} - \frac{K_{p_i}}{T_{p_i}} \sum_{j \in \mathcal{N}_i} \frac{\overline{V}_i \overline{V}_j}{X_{ij}} \sin(\delta_i - \delta_j). \tag{5.56}$$

It is possible to introduce a linear change of coordinates $\tilde{\boldsymbol{x}}_i = \boldsymbol{E_1}_i \boldsymbol{x}_i$ for the system (5.55) in the form of

$$\begin{bmatrix} \tilde{\delta}_i \\ \tilde{f}_i \end{bmatrix} = \overbrace{\begin{bmatrix} 1 & 0 \\ 0 & 2\pi \end{bmatrix}}^{\boldsymbol{E_1}_i} \begin{bmatrix} \delta_i \\ f_i \end{bmatrix}. \tag{5.57}$$

The new coordinate system results in being

$$\begin{aligned} \dot{\tilde{\delta}}_i &= \tilde{f}_i \\ \dot{\tilde{f}}_i &= a_i \tilde{f}_i - 2\pi K_{p_i} a_i P_{t_i} + 2\pi \phi_i \\ \tilde{y}_{i_1} &= \tilde{\delta}_i. \end{aligned} \tag{5.58}$$

The coordinate system (5.58) is used as a basis to design a third order sliding mode observer with the aim of estimating f_i.

Analogously, equation (5.12) can be rewritten as

$$
\begin{aligned}
\dot{P}_{t_i} &= -b_i P_{t_i} + b_i P_{g_i} \\
\dot{P}_{g_i} &= d_i f_i + c_i P_{g_i} - c_i u_i \\
y_{i_2} &= P_{t_i},
\end{aligned}
\tag{5.59}
$$

where $b_i \triangleq 1/T_{t_i}$, $c_i \triangleq -1/T_{g_i}$, and $d_i \triangleq -1/(R_i T_{g_i})$. It is useful to introduce again a change of coordinates $\tilde{\boldsymbol{x}}_i = \boldsymbol{E_2}_i \boldsymbol{x}_i$, i.e.,

$$
\begin{bmatrix} \tilde{P}_{t_i} \\ \tilde{P}_{g_i} \end{bmatrix} = \overbrace{\begin{bmatrix} 1 & 0 \\ 0 & b_i \end{bmatrix}}^{\boldsymbol{E_2}_i} \begin{bmatrix} P_{t_i} \\ P_{g_i} \end{bmatrix}.
\tag{5.60}
$$

The new coordinate system results in being

$$
\begin{aligned}
\dot{\tilde{P}}_{t_i} &= -b_i \tilde{P}_{t_i} + \tilde{P}_{g_i} \\
\dot{\tilde{P}}_{g_i} &= c_i \tilde{P}_{g_i} + \frac{b_i d_i}{2\pi} \tilde{f}_i - b_i c_i u_i \\
\tilde{y}_{i_2} &= \tilde{P}_{t_i}.
\end{aligned}
\tag{5.61}
$$

The coordinate system (5.61) is used as a basis to design a third order sliding mode observer with the aim of estimating P_{g_i}.

In the next sections we present in detail the procedure for the design of the observers to estimate the unmeasured state variables of each control area, considering the few local available measurements indicated in Assumption 5.7. In particular, we design two third order sliding mode observers for each control area, which are capable of estimating respectively the frequency deviation and the governor output power variation. The introduced architectures for the observers rely on a decentralized computation, since no communication is introduced among observers belonging to different control areas.

5.9.2 Observer for Frequency Deviation Estimation

To locally estimate the frequency of each control area, it is possible to introduce a third order sliding mode observer according to the following proposition.

Proposition 5.1. The following third order sliding mode observer

$$
\begin{aligned}
\dot{\hat{\delta}}_i &= k_{1_i} |e_{\delta_i}|^{2/3} \operatorname{sign}(e_{\delta_i}) + \underline{a_i e_{\delta_i}} + \hat{f}_i \\
\dot{\hat{f}}_i &= k_{2_i} |e_{\delta_i}|^{1/3} \operatorname{sign}(e_{\delta_i}) - 2\pi K_{p_i} a_i P_{t_i} + a_i \hat{f}_i + \underline{a_i^2 e_{\delta_i}} + \underline{k_{1_i} a_i |e_{\delta_i}|^{2/3} \operatorname{sign}(e_{\delta_i})} + \hat{z}_i \\
\dot{\hat{z}}_i &= k_{3_i} \operatorname{sign}(e_{\delta_i}),
\end{aligned}
\tag{5.62}
$$

where $\hat{\delta}_i$ is the estimate of $\tilde{\delta}_i$, $e_{\delta_i} \triangleq \tilde{\delta}_i - \hat{\delta}_i$, $\hat{f}_i$ is the estimate of $\tilde{f}_i$, $\hat{z}_i$ is an auxiliary variable required in order to ensure that $\dot{\hat{f}}_i$ is continuous, and k_{1_i}, k_{2_i}, k_{3_i} are positive scalar design, leads to a correct estimation of the frequency deviation in each i-th control area in a finite time. Note that this observer differs from that in [CKF+16] because of the presence of additional terms. These terms have been underlined.

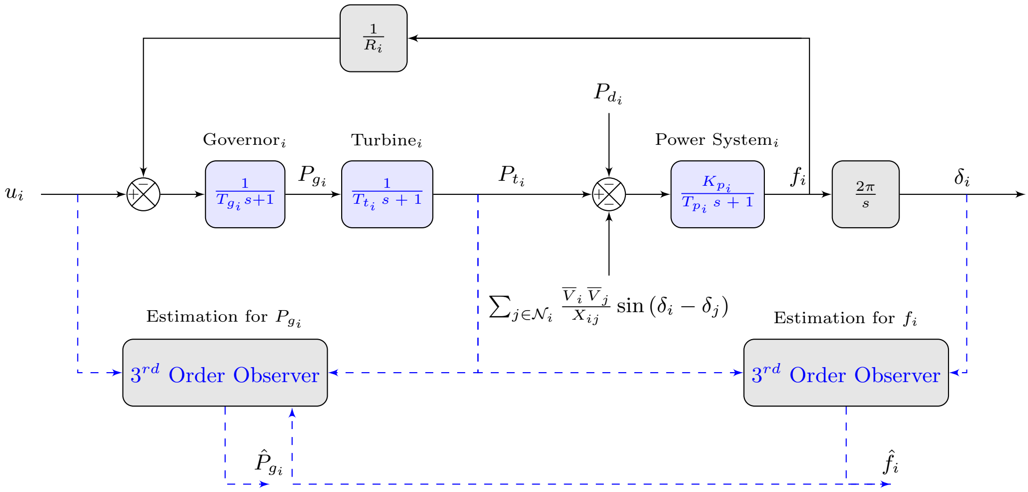

Fig. 5.5. The block diagram of the i-th control area dynamics of a power network with the designed observers.

Proof. By subtracting (5.62) from (5.58), it yields the error dynamics

$$
\begin{aligned}
\dot{e}_{\delta_i} &= -k_{1_i}|e_{\delta_i}|^{2/3}\operatorname{sign}(e_{\delta_i}) - a_i e_{\delta_i} + e_{f_i} \\
\dot{e}_{f_i} &= -k_{2_i}|e_{\delta_i}|^{1/3}\operatorname{sign}(e_{\delta_i}) + a_i e_{f_i} - a_i^2 e_{\delta_i} - k_{1_i}a_i|e_{\delta_i}|^{2/3}\operatorname{sign}(e_{\delta_i}) + 2\pi\phi_i - \hat{z}_i \\
\dot{\hat{z}}_i &= k_{3_i}\operatorname{sign}(e_{\delta_i}),
\end{aligned}
\tag{5.63}
$$

where $e_{f_i} \triangleq \tilde{f}_i - \hat{f}_i$. By defining $\overline{e}_{f_i} \triangleq e_{f_i} - a_i e_{\delta_i}$, the error system dynamics (5.63) can be rewritten as follows

$$
\begin{aligned}
\dot{e}_{\delta_i} &= -\,k_{1_i}|e_{\delta_i}|^{2/3}\operatorname{sign}(e_{\delta_i}) + \overline{e}_{f_i} \\
\dot{\overline{e}}_{f_i} &= -\,k_{2_i}|e_{\delta_i}|^{1/3}\operatorname{sign}(e_{\delta_i}) + a_i e_{f_i} - a_i^2 e_{\delta_i} - k_{1_i}a_i|e_{\delta_i}|^{2/3}\operatorname{sign}(e_{\delta_i}) + 2\pi\phi_i - \hat{z}_i \\
&\quad + \underbrace{k_{1_i}a_i|e_{\delta_i}|^{2/3}\operatorname{sign}(e_{\delta_i}) + a_i^2 e_{\delta_i} - a_i e_{f_i}}_{-a_i\dot{e}_{\delta_i}} \\
\dot{\hat{z}}_i &= k_{3_i}\operatorname{sign}(e_{\delta_i}).
\end{aligned}
\tag{5.64}
$$

Algebraic terms can be simplified in (5.64). This is possible thanks to the addition of the terms highlighted in Proposition 5.1. One gets

$$
\begin{aligned}
\dot{e}_{\delta_i} &= -k_{1_i}|e_{\delta_i}|^{2/3}\operatorname{sign}(e_{\delta_i}) + \overline{e}_{f_i} \\
\dot{\overline{e}}_{f_i} &= -k_{2_i}|e_{\delta_i}|^{1/3}\operatorname{sign}(e_{\delta_i}) + 2\pi\phi_i - \hat{z}_i \\
\dot{\hat{z}}_i &= k_{3_i}\operatorname{sign}(e_{\delta_i}).
\end{aligned}
\tag{5.65}
$$

Let $e_{z_i} \triangleq 2\pi\phi_i - \hat{z}_i$, then equation (5.65) can be rewritten as follows

$$
\begin{aligned}
\dot{e}_{\delta_i} &= -k_{1_i}|e_{\delta_i}|^{2/3}\operatorname{sign}(e_{\delta_i}) + \overline{e}_{f_i} \\
\dot{\overline{e}}_{f_i} &= -k_{2_i}|e_{\delta_i}|^{1/3}\operatorname{sign}(e_{\delta_i}) + e_{z_i} \\
\dot{e}_{z_i} &= -k_{3_i}\operatorname{sign}(e_{\delta_i}) + \Phi_i,
\end{aligned} \tag{5.66}
$$

where $\Phi_i \triangleq 2\pi\dot{\phi}_i$. Equation (5.66) is in the form of the standard third order sliding mode observer error dynamics [Lev03], or, equivalently, of the second order sliding mode differentiator error dynamics [ORM$^+$15].

According to Assumption 5.7 and recalling the definition of ϕ_i in (5.56), one has that the modulus of Φ_i in (5.66) is bounded as

$$
|\Phi_i| \leq \Delta_{M_{1_i}}, \tag{5.67}
$$

$\Delta_{M_{1_i}}$ being a positive constant. In order to steer the error dynamics (5.66) to the origin in a finite time, the gains k_{1_i}, k_{2_i}, and k_{3_i} can be tuned relying on the rules proposed in [ORM$^+$15], where a differentiable Lyapunov function for the second order sliding mode differentiator error dynamics is provided together with a new family of gains. In particular, the gains of the observer are designed during the Lyapunov function construction process by solving linear inequalities.

Furthermore, the convergence time $T(e_{0_i})$ to the origin for the system (5.66) can be expressed according to [ORM$^+$15] as

$$
T(e_{0_i}) \leq \frac{V^{1/5}(e_{0_i})}{\frac{1}{5}\gamma}, \tag{5.68}
$$

where e_{0_i} represents the initial conditions for the system (5.66), V is the candidate Lyapunov function in [ORM$^+$15], and $0 < \gamma \leq 2.8 \times 10^{-4}$. The following condition holds in a finite time

$$
e_{\delta_i} = \overline{e}_{f_i} = e_{f_i} = e_{z_i} = 0. \tag{5.69}
$$

It follows that $\hat{f}_i = \tilde{f}_i$ in a finite time, i.e., it is possible to locally estimate the frequency of each control area. □

5.9.3 Observer for Governor Output Variation Estimation

To locally estimate the governor output variation P_{g_i} of each control area, it is possible to introduce again a third order sliding mode observer.

Even though the design procedure is similar to Section 5.9.2, it is worth underlining the major aspects.

Proposition 5.2. The following third order sliding mode observer

$$
\begin{aligned}
\dot{\hat{P}}_{t_i} &= k_{4_i}|e_{P_{t_i}}|^{2/3}\operatorname{sign}(e_{P_{t_i}}) + \underline{(c_i - b_i)e_{P_{t_i}}} + \hat{P}_{g_i} - b_i\hat{P}_{t_i} \\
\dot{\hat{P}}_{g_i} &= k_{5_i}|e_{P_{t_i}}|^{1/3}\operatorname{sign}(e_{P_{t_i}}) + c_i\hat{P}_{g_i} + \underline{c_i^2 e_{P_{t_i}}} - b_i c_i u_i + \underline{k_{4_i}c_i|e_{P_{t_i}}|^{2/3}\operatorname{sign}(e_{P_{t_i}})} \\
&\quad + \frac{b_i d_i}{2\pi}\hat{f}_i + \hat{w}_i \\
\dot{\hat{w}}_i &= k_{6_i}\operatorname{sign}(e_{P_{t_i}}),
\end{aligned} \tag{5.70}
$$

where $\hat{P}_{t_i}$ is the estimate of $\tilde{P}_{t_i}$, $e_{P_{t_i}} \triangleq \tilde{P}_{t_i} - \hat{P}_{t_i}$, $\hat{P}_{g_i}$ is the estimate of $\tilde{P}_{g_i}$, $\hat{w}_i$ is an auxiliary variable required in order to ensure that $\dot{\hat{P}}_{g_i}$ is continuous, and k_{4_i}, k_{5_i}, and k_{6_i} are positive design constants, leads to a correct estimation of the governor output variation in each i-th control area in a finite time. Note that also this observer differs from that in [CKF+16] because of the presence of additional terms. These terms have been underlined.

Proof. By subtracting (5.70) from (5.61), it yields the error dynamics

$$
\begin{aligned}
\dot{e}_{P_{t_i}} &= -k_{4_i}|e_{P_{t_i}}|^{2/3}\,\mathrm{sign}(e_{P_{t_i}}) - (c_i - b_i)e_{P_{t_i}} + e_{P_{g_i}} - b_i e_{P_{t_i}}, \\
\dot{e}_{P_{g_i}} &= -k_{5_i}|e_{P_{t_i}}|^{1/3}\,\mathrm{sign}(e_{P_{t_i}}) + c_i e_{P_{g_i}} - c_i^2 e_{P_{t_i}} - k_{4_i} c_i |e_{P_{t_i}}|^{2/3}\,\mathrm{sign}(e_{P_{t_i}}) + \nu_i - \hat{w}_i \\
\dot{\hat{w}}_i &= k_{6_i}\,\mathrm{sign}(e_{P_{t_i}}),
\end{aligned}
\tag{5.71}
$$

where $e_{P_{g_i}} \triangleq \tilde{P}_{g_i} - \hat{P}_{g_i}$, and $\nu_i \triangleq \frac{b_i d_i}{2\pi} e_{f_i}$. The additional terms highlighted in Proposition 5.2 give rise to algebraic simplifications. System (5.71) becomes

$$
\begin{aligned}
\dot{e}_{P_{t_i}} &= -k_{4_i}|e_{P_{t_i}}|^{2/3}\,\mathrm{sign}(e_{P_{t_i}}) - c_i e_{P_{t_i}} + e_{P_{g_i}} \\
\dot{e}_{P_{g_i}} &= -k_{5_i}|e_{P_{t_i}}|^{1/3}\,\mathrm{sign}(e_{P_{t_i}}) + c_i e_{P_{g_i}} - c_i^2 e_{P_{t_i}} - k_{4_i} c_i |e_{P_{t_i}}|^{2/3}\,\mathrm{sign}(e_{P_{t_i}}) + \nu_i - \hat{w}_i \\
\dot{\hat{w}}_i &= k_{6_i}\,\mathrm{sign}(e_{P_{t_i}}).
\end{aligned}
\tag{5.72}
$$

It is worth noting that equation (5.72) and (5.63) have the same structure. By defining $\overline{e}_{P_{g_i}} \triangleq -c_i e_{P_{t_i}} + e_{P_{g_i}},$, it is possible to apply the same procedure explained in Subsection 5.9.2 to obtain again the error dynamics in the form of the standard third order sliding mode observer error dynamics[Lev03]

$$
\begin{aligned}
\dot{e}_{P_{t_i}} &= -k_{4_i}|e_{P_{t_i}}|^{2/3}\,\mathrm{sign}(e_{P_{t_i}}) + \overline{e}_{P_{g_i}} \\
\dot{\overline{e}}_{P_{g_i}}, &= -k_{5_i}|e_{P_{t_i}}|^{1/3}\,\mathrm{sign}(e_{P_{t_i}}) + e_{w_i} \\
\dot{e}_{w_i} &= -k_{6_i}\,\mathrm{sign}(e_{P_{t_i}}) + \Psi_i,
\end{aligned}
\tag{5.73}
$$

where $\Psi_i \triangleq \dot{\nu}_i = \frac{b_i d_i}{2\pi} \dot{e}_{f_i}$.

According to the developments in Subsection 5.9.2, the modulus of Ψ_i in (5.73) is bounded as

$$
|\Psi_i| \le \Delta_{M_{2_i}}, \tag{5.74}
$$

$\Delta_{M_{2_i}}$ being a positive constant. As explained in Subsection 5.9.2, the systems (5.73) converges to the origin in a finite time, allowing a correct state estimation of P_{g_i}. □

In order to illustrate the observer design presented in this section, in Fig. 5.5 we report the block diagram of the i-th control area together with the associated observers.

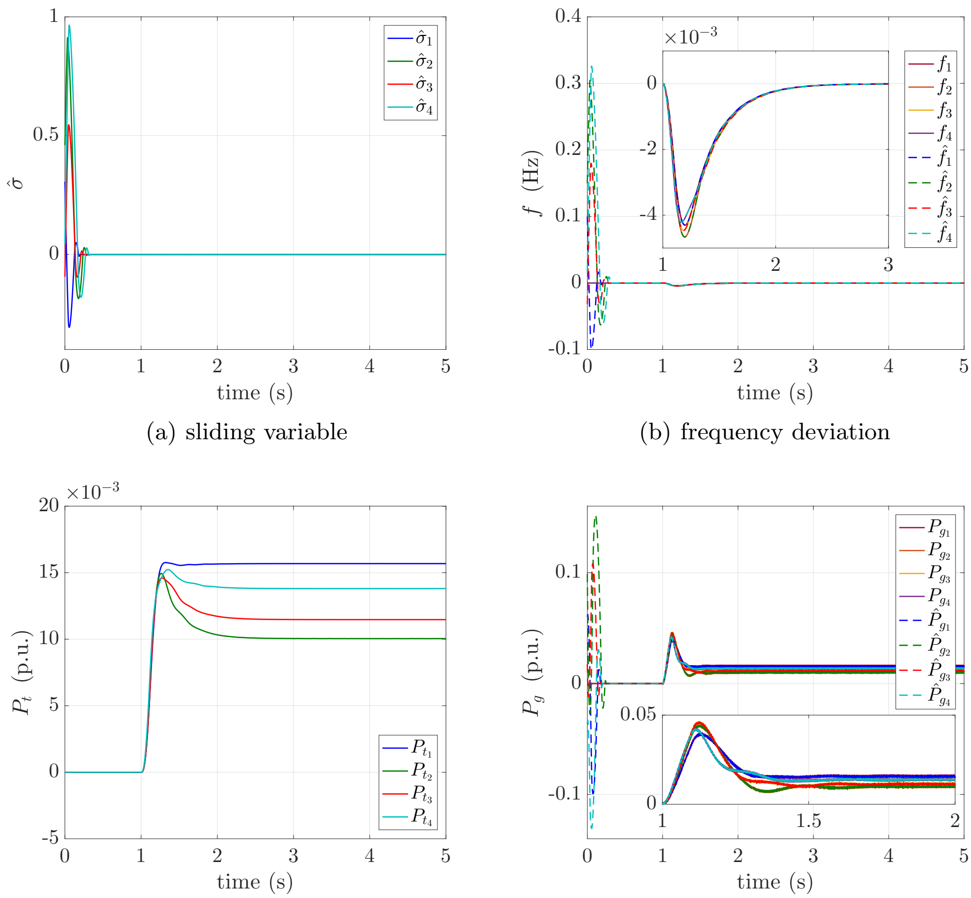

(a) sliding variable (b) frequency deviation

(c) turbine output power (d) governor output power

Fig. 5.6. Evolution of the controlled power system considering a power demand variation at the time instant $t = 1\,\mathrm{s}$. **(a)** Frequency deviation in each control area. **(b)** Generated power at the output of each steam turbine. **(c)** Voltage dynamics in each node. **(d)** Control inputs to the governors.

5.9.4 Case Study

In this section, the proposed observers-based distributed control approach is assessed in simulation by implementing a power network partitioned into four control areas.

The topology of the power network is represented in Fig. 5.3 together with the communication network (dashed lines). The relevant parameters of the power network and the power demand ΔP_{d_i} of each area are provided in Table 5.2, where a base power of 1000 MVA is assumed, while the line parameters are $\Gamma_1 = 5.4$ p.u., $\Gamma_2 = 5.0$ p.u., $\Gamma_3 = 4.5$ p.u. and $\Gamma_4 = 5.2$ p.u. The gains of the observers are selected as follows: $k_{1_i} = k_{4_i} = 20$; $k_{2_i} = k_{5_i} = 67$; $k_{3_i} = k_{6_i} = 250$, $\forall i = 1, \ldots, 4$. The matrices in (5.34) are chosen as

$\boldsymbol{M_1} = 3\mathbb{I}_4$, $\boldsymbol{M_2} = \mathbb{I}_4$, $\boldsymbol{M_3} = 0.1\mathbb{I}_4$ and $\boldsymbol{M_4} = -(\boldsymbol{M_2} + \boldsymbol{M_3})$, $\mathbb{I}_4 \in \mathbb{R}^{4\times 4}$, while, for the sake of simplicity, in the cost function (5.25), we select $\mathcal{R}_i = \mathcal{C}_i = 0$ for all $i \in \mathcal{V}$. In simulation, the system is initially at the steady state. At the instant $t = 1$ $[s]$, the power demand in each area is increased according to the values shown in Table 5.2. Fig. 5.6 shows, from the top, that the estimated sliding variables are steered to the sliding manifold after a transient due to the observers convergence. From figure 5.6 one can also notice a transient during which the frequency drops because of the increasing load. Then, in order to bring the frequency deviation back to zero, the proposed controllers increase the power generation.

5.10 Conclusions

A Distributed Suboptimal Second Order Sliding Mode (D-SSOSM) control scheme has been proposed to solve an optimal load frequency control problem in power systems. In this work, we have adopted a nonlinear model of a power network, including voltage dynamics, where each control area is represented by an equivalent generator including second order turbine-governor dynamics. Based on a suitable chosen sliding manifold, the controlled turbine-governor system, constrained to this manifold, possesses an incremental passivity property that is exploited to prove that the frequency deviation asymptotically approaches zero and an economic dispatch is achieved. An important feature of the proposed distributed control approach is that the controllers do not require the measurement of the power demand nor rely on load observers. Designing the sliding modes, based on passivity considerations, appears to be powerful and we will pursue this approach within different settings, such as achieving power sharing in microgrids. Additionally, we would like to compare the performance of the proposed sliding mode based control scheme with other approaches to OLFC appearing in the literature. Then, two third order sliding mode observers capable of estimating the frequency deviation and the governor output variation of each control area have been designed.

6

Energy Function Based Design of Sliding Modes

Abstract. This chapter proposes a decentralized Second Order Sliding Mode (SOSM) control strategy for Automatic Generation Control (AGC) in power networks, where frequency regulation is achieved, and power flows are controlled towards their desired values. This work considers a power network partitioned into control areas, where each area is modelled by an equivalent generator including second-order turbine-governor dynamics, and where the areas are nonlinearly coupled through the power flows. Asymptotic convergence to the desired state is established by constraining the state of the power network on a suitable sliding manifold. This is designed relying on stability considerations made on the basis of an incremental energy (storage) function. Simulation results confirm the effectiveness of the proposed control approach.

6.1 Preliminaries on Automatic Generation Control

As a result of power mismatch between generation and load demand, the frequency in a power system can deviate from its nominal value. Whereas primary droop control is utilized to prevent destabilization of the network, the frequency is controlled back to its nominal value by the so-called 'Automatic Generation Control' (AGC). In an AGC scheme, each Control Area (CA) determines its Area Control Error (ACE) and changes the setpoints to the governor accordingly to compensate for local load changes and to maintain the scheduled tie line power flows. Due to the increasing share of renewable energy sources, it is however unsure if the existing implementations are still adequate [ADGS16].

To cope with the increasing uncertainties affecting a CA and to improve the controllers performance, advanced control techniques have been proposed to redesign the conventional AGC schemes (see for instance [EIU16, ZARA05, CF97]). In this chapter we propose a new control strategy based on the SM control methodology, which has been previously used in the literature to improve the conventional AGC schemes [MFWW13, Don16, VPP10, MFL$^+$16, PPK15].

Although SM control in AGC has received a considerable amount of attention, the solution proposed in this chapter and the associated stability analysis differ substantially from the aforementioned works. Foremost, we consider a nonlinear coupling between the various control areas, induced by the nonlinear power flow equations, which poses new challenges in the design of the sliding manifold.

In this chapter, we adopt the model of a power network partitioned into control areas, having an arbitrarily complex and meshed topology. The generation side is modelled by an equivalent generator including second-order turbine-governor dynamics, where the proposed *decentralized* control scheme continuously adjusts the governor set point. To be able to control the power system using continuous control signals, which can be beneficial in field implementations, the well known Suboptimal SOSM (SSOSM) control algorithm [BFU98a] is exploited. Moreover, the convergence to the sliding manifold is obtained neither measuring the power demand, nor using load observers.

When the nonlinear power system is constrained to the designed sliding manifold, the convergence towards the desired state is established relying on a suitable incremental energy function [TBD16] and Lyapunov arguments. Indeed, an incremental energy function based stability analysis suggests the design of the sliding manifold. Finally, the case study considered in this chapter shows the effectiveness of the proposed controller and demonstrates that, besides the immediate application to AGC, the combined use of SM control and other nonlinear control techniques can provide new insights and control strategies.

6.2 Control Areas with Second Order Turbine-Governor Dynamics

In this section the dynamic model of a power network partitioned into control areas is presented (see Section 5.3). For the reader's convenience, we rewrite the equivalent generator dynamics (5.13), and the turbine-governor dynamics (5.14) for all nodes $i \in \mathcal{V}$ as

$$\begin{aligned} \dot{\boldsymbol{\eta}} &= \boldsymbol{\mathcal{B}}^T \boldsymbol{f} \\ \boldsymbol{T_p K_p^{-1}} \dot{\boldsymbol{f}} &= -\boldsymbol{K_p^{-1}} \boldsymbol{f} + \boldsymbol{P_t} - \boldsymbol{P_d} - \boldsymbol{\mathcal{B}\Gamma} \mathbf{sin}(\boldsymbol{\eta}) \\ \boldsymbol{T_t} \dot{\boldsymbol{P}}_{\boldsymbol{t}} &= -\boldsymbol{P_t} + \boldsymbol{P_g} \\ \boldsymbol{T_g} \dot{\boldsymbol{P}}_{\boldsymbol{g}} &= -\boldsymbol{R}^{-1} \boldsymbol{f} - \boldsymbol{P_g} + \boldsymbol{u}, \end{aligned} \tag{6.1}$$

where $\boldsymbol{\eta} = \boldsymbol{\mathcal{B}}^T \boldsymbol{\delta} \in \mathbb{R}^m$, $\boldsymbol{f} \in \mathbb{R}^n$, $\boldsymbol{P_t} \in \mathbb{R}^n$, $\boldsymbol{P_g} \in \mathbb{R}^n$, $\boldsymbol{\Gamma} = \operatorname{diag}\{\Gamma_1, \ldots, \Gamma_m\}$, with $\Gamma_k = \overline{V}_i \overline{V}_j / X_{ij}$, where line k connects areas i and j, $\mathbf{sin}(\boldsymbol{\eta}) = (\sin(\eta_1), \ldots, \sin(\eta_m))^T$, $\boldsymbol{P_d} \in \mathbb{R}^n$ and $\boldsymbol{u} \in \mathbb{R}^n$. Matrices $\boldsymbol{T_p}, \boldsymbol{T_t}, \boldsymbol{T_g}, \boldsymbol{K_p}, \boldsymbol{R}$ are suitable $n \times n$ diagonal matrices, e.g., $\boldsymbol{K_p} = \operatorname{diag}\{K_{p_1}, \ldots, K_{p_n}\}$.

To permit the controller design in the next sections, the following assumption is made on the disturbances (*unknown* loads) and the available measurements:

Assumption 6.1 (Available measurements). The variables f_i, P_{ti}, P_{gi} and the power flow $(\mathcal{B}\Gamma \sin(\eta))_i$ are locally available at control area i. The unmatched disturbance P_{di} is unknown, and can be bounded as $|P_{di}| \leq \mathcal{D}_i$ where $\mathcal{D}_i$ is a positive constant available at control area i.

6.3 Frequency Regulation and Power Flows Scheduling

In this section we formulate two objectives of automatic generation control. The first objective is concerned with the steady state frequency deviation, i.e. with $\lim_{t\to\infty} \boldsymbol{f}(t)$.

Objective 6.1 (Frequency regulation).

$$\lim_{t\to\infty} \boldsymbol{f}(t) = \mathbf{0}. \tag{6.2}$$

The second objective is to maintain the scheduled net power flows in a control area, where the net power flow is the total power flow exchanged by a control area.

Objective 6.2 (Maintaining scheduled net power flows).

$$\lim_{t\to\infty} \boldsymbol{\mathcal{B}\Gamma}\mathbf{sin}(\boldsymbol{\eta}(t)) = \boldsymbol{\mathcal{B}}\overline{\boldsymbol{P}}_{\boldsymbol{f}}, \tag{6.3}$$

where $\boldsymbol{\mathcal{B}}\overline{\boldsymbol{P}}_{\boldsymbol{f}}$ is the desired net power flow. In case the power network does not contain cycles, Objective 6.2 is equivalent to $\lim_{t\to\infty} \boldsymbol{\Gamma}\mathbf{sin}(\boldsymbol{\eta}(t)) = \overline{\boldsymbol{P}}_{\boldsymbol{f}}$, such that the power flow on every line is identical to its desired value (see Remark 6.6 in Section 6.5). To be able to satisfy Objectives 6.1 and 6.2, we make the following assumption on the feasibility of the control problem.

Assumption 6.2 (Feasibility). For a given constant $\boldsymbol{P_d}$, there exist a $\overline{\boldsymbol{u}}$ and state $(\overline{\boldsymbol{f}} = \mathbf{0}, \overline{\boldsymbol{\eta}}, \overline{\boldsymbol{P}}_{\boldsymbol{t}}, \overline{\boldsymbol{P}}_{\boldsymbol{g}})$ that satisfies

$$\begin{aligned}
\mathbf{0} &= \boldsymbol{\mathcal{B}}^T \mathbf{0} \\
\mathbf{0} &= -\boldsymbol{K}_{\boldsymbol{p}}^{-1}\mathbf{0} + \overline{\boldsymbol{P}_{\boldsymbol{t}}} - \boldsymbol{P_d} - \boldsymbol{\mathcal{B}\Gamma}\mathbf{sin}(\overline{\boldsymbol{\eta}}) \\
\mathbf{0} &= -\overline{\boldsymbol{P}_{\boldsymbol{t}}} + \overline{\boldsymbol{P}}_{\boldsymbol{g}} \\
\mathbf{0} &= -\boldsymbol{R}^{-1}\mathbf{0} - \overline{\boldsymbol{P}}_{\boldsymbol{g}} + \overline{\boldsymbol{u}},
\end{aligned} \tag{6.4}$$

where $\boldsymbol{\mathcal{B}\Gamma}\mathbf{sin}(\overline{\boldsymbol{\eta}}) = \boldsymbol{\mathcal{B}}\overline{\boldsymbol{P}}_{\boldsymbol{f}}$.

Remark 6.1 (Constant power demand). To satisfy Assumption 6.2, the power demand (unmatched disturbance) is required to be constant. This is not needed to reach the desired sliding manifold, but is required to establish the asymptotic convergence properties in Objective 6.1 and Objective 6.2. We make this assumption on the constant power demand explicit in the stability analysis in Section 6.5.

Furthermore we desire the controllers to be decentralized and able to provide a continuous control input. We are now in a position to formulate the control problem:

Problem 6.1. Let Assumptions 6.1 and 6.2 hold. Given system (6.1), design a decentralized control scheme, providing a continuous control input, capable of guaranteeing that the controlled system is asymptotically stable with zero steady state frequency deviation, maintaining, at the steady state, the scheduled (net) power flows.

6.4 Decentralized Sliding Mode Control

In this section a decentralized Suboptimal Second Order Sliding Mode (SSOSM) control algorithm is proposed to solve the aforementioned control problem. To do so, the well established SSOSM controller proposed in [BFU98a] is applied to the power network augmented with an additional state variable $\boldsymbol{\theta} \in \mathbb{R}^n$ with dynamics

$$\boldsymbol{T_\theta} \dot{\boldsymbol{\theta}} = -\boldsymbol{\theta} + \boldsymbol{P_t}. \tag{6.5}$$

We select the sliding function $\boldsymbol{\sigma} \in \mathbb{R}^n$ as

$$\boldsymbol{\sigma} = \boldsymbol{M_1 f} + \boldsymbol{M_2 P_t} + \boldsymbol{M_3 P_g} + \boldsymbol{M_4 \theta} + \boldsymbol{M_5} \boldsymbol{\mathcal{B}}(\boldsymbol{\Gamma} \mathbf{sin}(\boldsymbol{\eta}) - \overline{\boldsymbol{P}}_{\boldsymbol{f}}), \tag{6.6}$$

where $\boldsymbol{M_1}, \ldots \boldsymbol{M_5}$ are constant $n \times n$ diagonal matrices, suitable selected in order to assign the dynamics of the augmented system when $\boldsymbol{\sigma} = \mathbf{0}$. The permitted values for $\boldsymbol{M_1}, \ldots \boldsymbol{M_5}$ follow from the stability analysis in Section 6.5.

Remark 6.2 (Local measurements). Because $\boldsymbol{M_1}, \ldots, \boldsymbol{M_5}$ are diagonal matrices, each sliding variable σ_i is defined by only local variables at node i.

By regarding the sliding function (6.6) as the output function of system (6.1), (6.5), it appears that the relative degree of the system is one. This implies that a first order sliding mode controller can be *naturally* applied [Utk92] in order to attain in a finite time, the sliding manifold defined by $\boldsymbol{\sigma} = \mathbf{0}$. However, the input $\boldsymbol{u}$ to the governor affects the first time derivative of the sliding function, i.e. $\boldsymbol{u}$ affects $\dot{\boldsymbol{\sigma}}$. Since sliding mode controllers generate a discontinuous signal, we additionally require $\dot{\boldsymbol{\sigma}} = \mathbf{0}$, to guarantee that the signal $\boldsymbol{u}$ is continuous. Therefore, we define the desired sliding manifold as

$$\{(\boldsymbol{\eta}, \boldsymbol{f}, \boldsymbol{P_t}, \boldsymbol{P_g}, \boldsymbol{\theta}) : \boldsymbol{\sigma} = \dot{\boldsymbol{\sigma}} = \mathbf{0}\}. \tag{6.7}$$

We continue by discussing a possible controller attaining the desired sliding manifold (6.7) while providing a continuous control input $\boldsymbol{u}$.

6.4.1 Suboptimal Second Order Sliding Mode Controller

To prevent chattering, it is important to provide a continuous control input $\boldsymbol{u}$ to the governor. Since sliding mode controllers generate a discontinuous control signal, we adopt the procedure suggested in [BFU98a] by artificially increasing the relative degree of the system. To do this, we introduce two auxiliary variables $\boldsymbol{\xi_1} = \boldsymbol{\sigma}$ and $\boldsymbol{\xi_2} = \dot{\boldsymbol{\sigma}}$, and define the so-called auxiliary system as follows

$$\begin{aligned} \dot{\boldsymbol{\xi}}_{\mathbf{1}} &= \boldsymbol{\xi_2} \\ \dot{\boldsymbol{\xi}}_{\mathbf{2}} &= \boldsymbol{\phi} + \boldsymbol{G w} \\ \dot{\boldsymbol{u}} &= \boldsymbol{w}, \end{aligned} \tag{6.8}$$

where $\boldsymbol{w}$ is the new (discontinuous) input generated by a sliding mode controller discussed below. Bearing in mind (6.6) and that $\dot{\boldsymbol{\xi}}_{\mathbf{2}} = \ddot{\boldsymbol{\sigma}} = \boldsymbol{\phi} + \boldsymbol{G w}$, the expressions for the mapping $\boldsymbol{\phi}$ and matrix $\boldsymbol{G}$ can be straightforwardly obtained from (6.6) by taking the second derivative of $\boldsymbol{\sigma}$ with respect to time, yielding for the latter[10] $\boldsymbol{G} = \boldsymbol{M_3} \boldsymbol{T_g}^{-1} \in \mathbb{R}^{n \times n}$. We assume that the entries of $\boldsymbol{\phi}$ and $\boldsymbol{G}$ have known bounds

$$\begin{aligned} &|\phi_i| \leq \Phi_i && \forall i \in \mathcal{V} \\ &0 < G_{\min_i} \leq G_{ii} \leq G_{\max_i} && \forall i \in \mathcal{V} \end{aligned} \tag{6.9}$$

with Φ_i, $G_{\min_i}$ and $G_{\max_i}$ being positive constants. Second, $\boldsymbol{w}$ is a discontinuous control input described by the SSOSM control algorithm [BFU98a], and consequently for each area $i \in \mathcal{V}$, the control law w_i is given by

$$w_i = -\alpha_i W_{\max_i} \operatorname{sign}\left(\xi_{1_i} - \frac{1}{2}\xi_{1,\max_i}\right), \tag{6.10}$$

with

$$W_{\max_i} > \max\left(\frac{\Phi_i}{\alpha_i^* G_{\min_i}}; \frac{4\Phi_i}{3G_{\min_i} - \alpha_i^* G_{\max_i}}\right), \tag{6.11}$$

$$\alpha_i^* \in (0, 1] \cap \left(0, \frac{3G_{\min_i}}{G_{\max_i}}\right), \tag{6.12}$$

α_i switching between α_i^* and 1, according to [BFU98a, Algorithm 1]. Note that indeed the input signal to the governor, $\boldsymbol{u}(t) = \int_0^t \boldsymbol{w}(\tau) d\tau$, is continuous, since the input $\boldsymbol{w}$ is piecewise constant. The extremal values $\xi_{1,\max_i}$ in (6.10) can be detected by implementing for instance a peak detection as in [BFU98b].

Remark 6.3 (Uncertainty of $\boldsymbol{\phi}$ and $\boldsymbol{G}$). The mapping $\boldsymbol{\phi}$ and matrix $\boldsymbol{G}$ are uncertain due to the presence of the unmeasurable power demand $\boldsymbol{P_d}$ and voltage angle $\boldsymbol{\theta}$, and possible uncertainties in the system parameters. In practical cases the bounds in (6.9) can be determined relying on data analysis and physical insights. However, if these bounds cannot be a-priori estimated, the adaptive version of the SSOSM algorithm proposed in [ICF16] can be used to dominate the effect of the uncertainties.

Remark 6.4 (Alternative SOSM controllers). In this work we rely on the SOSM control law proposed in [BFU98a]. However, to constrain system (6.1) augmented with dynamics (6.5) on the sliding manifold (6.7), where $\boldsymbol{\sigma} = \dot{\boldsymbol{\sigma}} = \boldsymbol{0}$, any other SOSM control law that does not need the measurement of $\dot{\boldsymbol{\sigma}}$ can be used (e.g. the super-twisting control [Lev93]). An interesting continuation of the presented results is to study the performance of various SOSM controllers within the setting of AGC.

6.5 Stability Analysis

In this section we study the stability of the proposed control scheme. In order to prove stability we formulate two (nonrestrictive) assumptions. In the first assumption the desired sliding manifold is defined.

[10] The expression for $\boldsymbol{\phi}$ is rather long and is omitted.

Assumption 6.3 (Desired sliding manifold). Let $\boldsymbol{M_1} \succ 0$, $\boldsymbol{M_2} \succeq 0$, $\boldsymbol{M_3} \succ 0$ diagonal matrices and let $\boldsymbol{M_4}$ and $\boldsymbol{M_5}$ be defined as

$$\begin{aligned} \boldsymbol{M_4} &= -(\boldsymbol{M_2} + \boldsymbol{M_3}) \\ \boldsymbol{M_5} &= \boldsymbol{M_1}\boldsymbol{X}, \end{aligned} \tag{6.13}$$

where $\boldsymbol{X}$ is a diagonal matrix satisfying[11]

$$\mathbf{0} < \boldsymbol{T_p}\boldsymbol{K_p}^{-1} - \boldsymbol{X}\boldsymbol{T_p}\boldsymbol{K_p}^{-1}\boldsymbol{\mathcal{B}}\boldsymbol{\Gamma}[\mathbf{cos}(\overline{\boldsymbol{\eta}})]\boldsymbol{\mathcal{B}}^T\boldsymbol{K_p}^{-1}\boldsymbol{T_p}\boldsymbol{X}, \tag{6.14}$$

and

$$\mathbf{0} < \boldsymbol{K_p}^{-1} - \frac{1}{4}\boldsymbol{K_p}^{-1}\boldsymbol{X}\boldsymbol{K_p}^{-1} - \frac{1}{2}(\boldsymbol{T_p}\boldsymbol{K_p}^{-1}\boldsymbol{X}\boldsymbol{\mathcal{B}}\boldsymbol{\Gamma}[\mathbf{cos}(\boldsymbol{\eta})]\boldsymbol{\mathcal{B}}^T + \boldsymbol{\mathcal{B}}\boldsymbol{\Gamma}[\mathbf{cos}(\boldsymbol{\eta})]\boldsymbol{\mathcal{B}}^T\boldsymbol{X}\boldsymbol{K_p}^{-1}\boldsymbol{T_p}). \tag{6.15}$$

Remark 6.5. (**Required information on the network topology**) The value of $\boldsymbol{X}$ needs to be calculated once for the whole network and can be determined offline. The obtained value of X_{ii} needs then to be transmitted to control area i. Since $\boldsymbol{M_1}, \ldots, \boldsymbol{M_5}$ are diagonal, the proposed control scheme is fully decentralized once the value of $\boldsymbol{X}$ is obtained. We note that (6.14) and (6.15) have the form of an algebraic Riccati inequality and a Lyapunov inequality respectively and efficient numerical methods exist to find a diagonal solution $\boldsymbol{X}$. To facilitate a distributed controller design that improves the scalability of the proposed solution, we provide a distributed algorithm to determine a value of $\boldsymbol{X}$ satisfying (6.14) and (6.15) in Subsection 6.5.1.

Second, the following assumption is made on the differences of voltage angles at steady state, which is generally satisfied under normal operating conditions of the power network.

Assumption 6.4 (Steady state voltage angles). The differences in voltage angles in (6.4) satisfy

$$\overline{\boldsymbol{\eta}} \in \left(-\frac{\pi}{2}, \frac{\pi}{2}\right)^m. \tag{6.16}$$

The restrictions on $\boldsymbol{M_1}, \ldots, \boldsymbol{M_5}$ and $\overline{\boldsymbol{\eta}}$ are required to apply LaSalle's invariance principle in Theorem 6.1, where stability of the proposed control scheme is proven. This shows how the sliding manifold can be designed relying on an energy (storage) function based stability analysis. Before discussing this main result, some useful intermediate results are derived. First, we show that the second order sliding mode controller (6.6)–(6.12) constrains the system in a finite time to the manifold characterized in the lemma below.

[11] Let $[\mathbf{cos}(\boldsymbol{\eta})]$ denote the $m \times m$ diagonal matrix $\mathrm{diag}\{\cos(\eta_1), \ldots, \cos(\eta_m)\}$.

Lemma 6.1 (Convergence to the sliding manifold). Let Assumption 6.1 hold. System (6.1) augmented with (6.5) converges in a finite time t_r to the sliding manifold where

$$\boldsymbol{P_g} = -\boldsymbol{M_3}^{-1}(\boldsymbol{M_1 f} + \boldsymbol{M_2 P_t} + \boldsymbol{M_4 \theta} + \boldsymbol{M_5 \mathcal{B}}(\boldsymbol{\Gamma}\mathbf{sin}(\boldsymbol{\eta}) - \overline{\boldsymbol{P}}_{\boldsymbol{f}})). \tag{6.17}$$

Proof. Following [BFU98a], the application of (6.10)–(6.12) to each control area guarantees that a second order sliding mode is enforced, i.e. $\exists\, t_r \geq t_0 \,:\, \boldsymbol{\sigma}(t) = \dot{\boldsymbol{\sigma}}(t) = \mathbf{0},\ \forall\, t \geq t_r$, where t_0 and t_r are the initial time instant and the reaching time, respectively. Then, from the definition of $\boldsymbol{\sigma}(t)$ in (6.6), one can easily obtain (6.17), where $\boldsymbol{M_3}$ is invertible since, according to Assumption 6.3, $\boldsymbol{M_3} \succ 0$. □

Exploiting relation (6.17), the equivalent system on the sliding manifold is as follows:

$$\begin{aligned}
\dot{\boldsymbol{\eta}} &= \boldsymbol{\mathcal{B}}^T \boldsymbol{f} \\
\boldsymbol{T_p K_p}^{-1} \dot{\boldsymbol{f}} &= -\boldsymbol{K_p}^{-1}\boldsymbol{f} + \boldsymbol{P_t} - \boldsymbol{P_d} - \boldsymbol{\mathcal{B}\Gamma}\mathbf{sin}(\boldsymbol{\eta}) \\
\boldsymbol{M_1}^{-1}\boldsymbol{M_3 T_t}\dot{\boldsymbol{P}}_{\boldsymbol{t}} &= -\boldsymbol{M_1}^{-1}(\boldsymbol{M_2}+\boldsymbol{M_3})\boldsymbol{P_t} - \boldsymbol{M_1}^{-1}\boldsymbol{M_4\theta} - \boldsymbol{f} - \boldsymbol{M_1}^{-1}\boldsymbol{M_5\mathcal{B}}(\boldsymbol{\Gamma}\mathbf{sin}(\boldsymbol{\eta}) - \overline{\boldsymbol{P}}_{\boldsymbol{f}}) \\
\boldsymbol{T_\theta}\dot{\boldsymbol{\theta}} &= -\boldsymbol{\theta} + \boldsymbol{P_t} \\
\boldsymbol{\sigma} &= \mathbf{0},
\end{aligned} \tag{6.18}$$

where we include the auxiliary system (6.5). As we now focus on the asymptotic convergence of the equivalent system we require the following assumption:

Assumption 6.5 (Constant power demand). The power demand (unmatched disturbance), $\boldsymbol{P_d}$ is constant.

As a consequence of Assumption 6.2 there exists a $(\overline{\boldsymbol{f}} = \mathbf{0}, \overline{\boldsymbol{\eta}}, \overline{\boldsymbol{P_t}}, \overline{\boldsymbol{\theta}})$ satisfying

$$\begin{aligned}
\mathbf{0} &= \boldsymbol{\mathcal{B}}^T\mathbf{0} \\
\mathbf{0} &= -\boldsymbol{K_p}^{-1}\mathbf{0} + \overline{\boldsymbol{P}}_{\boldsymbol{t}} - \boldsymbol{P_d} - \boldsymbol{\mathcal{B}\Gamma}\mathbf{sin}(\overline{\boldsymbol{\eta}}) \\
\mathbf{0} &= -\boldsymbol{M_1}^{-1}(\boldsymbol{M_2}+\boldsymbol{M_3})\overline{\boldsymbol{P}}_{\boldsymbol{t}} - \boldsymbol{M_1}^{-1}\boldsymbol{M_4}\overline{\boldsymbol{\theta}} - \mathbf{0} - \boldsymbol{M_1}^{-1}\boldsymbol{M_5\mathcal{B}}(\boldsymbol{\Gamma}\mathbf{sin}(\overline{\boldsymbol{\eta}}) - \overline{\boldsymbol{P}}_{\boldsymbol{f}}) \\
\mathbf{0} &= -\overline{\boldsymbol{\theta}} + \overline{\boldsymbol{P}}_{\boldsymbol{t}} \\
\boldsymbol{\sigma} &= \mathbf{0},
\end{aligned} \tag{6.19}$$

where in (6.4), $\overline{\boldsymbol{P}}_{\boldsymbol{g}} = \overline{\boldsymbol{\theta}} = \overline{\boldsymbol{u}}$.

To show the desired convergence properties of the equivalent system (6.18) we consider the function

$$\begin{aligned}
S(\boldsymbol{f}, \boldsymbol{\eta}, \boldsymbol{P_t}, \boldsymbol{\theta}) = {} & \frac{1}{2}\boldsymbol{f}^T\boldsymbol{T_p K_p}^{-1}\boldsymbol{f} - \mathbb{1}_m^T\boldsymbol{\Gamma}\mathbf{cos}(\boldsymbol{\eta}) + \boldsymbol{f}^T\boldsymbol{T_p K_p}^{-1}\boldsymbol{X\mathcal{B}\Gamma}\mathbf{sin}(\boldsymbol{\eta}) \\
& + \frac{1}{2}\boldsymbol{P_t}^T\boldsymbol{M_1}^{-1}\boldsymbol{M_3 T_t P_t} + \frac{1}{2}\boldsymbol{\theta}^T\boldsymbol{M_1}^{-1}(\boldsymbol{M_2}+\boldsymbol{M_3})\boldsymbol{T_\theta\theta},
\end{aligned} \tag{6.20}$$

that consists of an energy function of the power network [TBD16], a cross-term and common quadratic functions for the states of the turbine and the auxiliary dynamics. The stability of the system is then proven using an incremental storage function that is the Bregman distance [Bre67] associated to the function (6.20). The Bregman distance associated to S is defined as (notice the use of calligraphic $\mathcal{S}$):

$$\begin{aligned}
\mathcal{S} &= S(\boldsymbol{f},\boldsymbol{\eta},\boldsymbol{P_t},\boldsymbol{\theta}) - S(\boldsymbol{0},\overline{\boldsymbol{\eta}},\overline{\boldsymbol{P}}_{\boldsymbol{t}},\overline{\boldsymbol{\theta}}) \\
&\quad - \left.\frac{\partial S}{\partial \boldsymbol{f}}\right|_{\boldsymbol{f}=\boldsymbol{0}}^{T}(\boldsymbol{f}-\boldsymbol{0}) - \left.\frac{\partial S}{\partial \boldsymbol{\eta}}\right|_{\boldsymbol{\eta}=\overline{\boldsymbol{\eta}}}^{T}(\boldsymbol{\eta}-\overline{\boldsymbol{\eta}}) - \left.\frac{\partial S}{\partial \boldsymbol{P_t}}\right|_{\boldsymbol{P_t}=\overline{\boldsymbol{P}}_{\boldsymbol{t}}}^{T}(\boldsymbol{P_t}-\overline{\boldsymbol{P}}_{\boldsymbol{t}}) - \left.\frac{\partial S}{\partial \boldsymbol{\theta}}\right|_{\boldsymbol{\theta}=\overline{\boldsymbol{\theta}}}^{T}(\boldsymbol{\theta}-\overline{\boldsymbol{\theta}}) \\
&= \frac{1}{2}\boldsymbol{f}^T\boldsymbol{f} - \mathbb{1}_m^T\boldsymbol{\Gamma}\mathbf{cos}(\boldsymbol{\eta}) + \mathbb{1}_m^T\boldsymbol{\Gamma}\mathbf{cos}(\overline{\boldsymbol{\eta}}) - (\boldsymbol{\Gamma}\mathbf{sin}(\overline{\boldsymbol{\eta}}))^T(\boldsymbol{\eta}-\overline{\boldsymbol{\eta}}) \\
&\quad + \boldsymbol{f}^T\boldsymbol{T_p}\boldsymbol{K_p}^{-1}\boldsymbol{X}\boldsymbol{\mathcal{B}}(\boldsymbol{\Gamma}\mathbf{sin}(\boldsymbol{\eta}) - \boldsymbol{\Gamma}\mathbf{sin}(\overline{\boldsymbol{\eta}})) + \frac{1}{2}(\boldsymbol{P_t}-\overline{\boldsymbol{P}}_{\boldsymbol{t}})^T\boldsymbol{M_1}^{-1}\boldsymbol{M_3}\boldsymbol{T_t}(\boldsymbol{P_t}-\overline{\boldsymbol{P}}_{\boldsymbol{t}}) \\
&\quad + \frac{1}{2}(\boldsymbol{\theta}-\overline{\boldsymbol{\theta}})^T\boldsymbol{M_1}^{-1}(\boldsymbol{M_2}+\boldsymbol{M_3})(\boldsymbol{\theta}-\overline{\boldsymbol{\theta}}),
\end{aligned} \tag{6.21}$$

where $(\boldsymbol{0},\overline{\boldsymbol{\eta}},\overline{\boldsymbol{P}}_{\boldsymbol{t}},\overline{\boldsymbol{\theta}})$ satisfies (6.19). We remark that the Bregman distance $\mathcal{S}$ is equal to S minus the first order Taylor expansion of S around $(\boldsymbol{0},\overline{\boldsymbol{\eta}},\overline{\boldsymbol{P}}_{\boldsymbol{t}},\overline{\boldsymbol{\theta}})$. We now derive two useful properties of $\mathcal{S}$, namely that $\mathcal{S}$ has a local minimum at $(\boldsymbol{0},\overline{\boldsymbol{\eta}},\overline{\boldsymbol{P}}_{\boldsymbol{t}},\overline{\boldsymbol{\theta}})$ and that $\dot{\mathcal{S}} \le 0$. We start with the first claim.

Lemma 6.2 (Local minimum of $\mathcal{S}$). Let Assumptions 6.2–6.5 hold. Then $\mathcal{S}$ has a local minimum at $(\boldsymbol{0},\overline{\boldsymbol{\eta}},\overline{\boldsymbol{P}}_{\boldsymbol{t}},\overline{\boldsymbol{\theta}})$.

Proof. Since $\mathcal{S}$ is a Bregman distance associated to (6.20) it is sufficient to show that (6.20) is convex at the point $(\boldsymbol{0},\overline{\boldsymbol{\eta}},\overline{\boldsymbol{P}}_{\boldsymbol{t}},\overline{\boldsymbol{\theta}})$ in order to infer that $\mathcal{S}$ has a local minimum at that point. We consider therefore the Hessian matrix $\boldsymbol{H}(S(\boldsymbol{f},\boldsymbol{\eta},\boldsymbol{P_t},\boldsymbol{\theta}))$, evaluated at $(\boldsymbol{0},\overline{\boldsymbol{\eta}},\overline{\boldsymbol{P}}_{\boldsymbol{t}},\overline{\boldsymbol{\theta}})$, which we briefly denote $\overline{\boldsymbol{H}}(S)$. A straightforward calculation shows that

$$\overline{\boldsymbol{H}}(S) = \begin{bmatrix} \boldsymbol{Q} & \boldsymbol{0} \\ \boldsymbol{0} & \boldsymbol{M} \end{bmatrix}, \tag{6.22}$$

with

$$\boldsymbol{Q} = \begin{bmatrix} \boldsymbol{T_p}\boldsymbol{K_p}^{-1} & \boldsymbol{T_p}\boldsymbol{K_p}^{-1}\boldsymbol{X}\boldsymbol{\mathcal{B}}\boldsymbol{\Gamma}[\mathbf{cos}(\overline{\boldsymbol{\eta}})] \\ [\mathbf{cos}(\overline{\boldsymbol{\eta}})]\boldsymbol{\Gamma}\boldsymbol{\mathcal{B}}^T\boldsymbol{X}\boldsymbol{K_p}^{-1}\boldsymbol{T_p} & \boldsymbol{\Gamma}[\mathbf{cos}(\overline{\boldsymbol{\eta}})] \end{bmatrix}, \tag{6.23}$$

$$\boldsymbol{M} = \begin{bmatrix} \boldsymbol{M_1}^{-1}\boldsymbol{M_3}\boldsymbol{T_t} & \boldsymbol{0} \\ \boldsymbol{0} & \boldsymbol{M_1}^{-1}(\boldsymbol{M_2}+\boldsymbol{M_3})\boldsymbol{T_\theta} \end{bmatrix}. \tag{6.24}$$

It is immediate to see that $\boldsymbol{M} \succ \boldsymbol{0}$, such that $\overline{\boldsymbol{H}}(S) \succ \boldsymbol{0}$ if and only if $\boldsymbol{Q} \succ \boldsymbol{0}$. Since $\boldsymbol{\Gamma}[\mathbf{cos}(\overline{\boldsymbol{\eta}})] \succ \boldsymbol{0}$ as a result of Assumption 6.4, it is sufficient that the Schur complement of block $\boldsymbol{\Gamma}[\mathbf{cos}(\boldsymbol{\eta})]\big|_{\boldsymbol{\eta}=\overline{\boldsymbol{\eta}}}$ of matrix $\boldsymbol{Q}$ satisfies

$$\boldsymbol{0} < \boldsymbol{T_p}\boldsymbol{K_p}^{-1} - \boldsymbol{X}\boldsymbol{T_p}\boldsymbol{K_p}^{-1}\boldsymbol{\mathcal{B}}\boldsymbol{\Gamma}[\mathbf{cos}(\overline{\boldsymbol{\eta}})]\boldsymbol{\mathcal{B}}^T\boldsymbol{K_p}^{-1}\boldsymbol{T_p}\boldsymbol{X}. \tag{6.25}$$

The claim then follows from Assumption 6.3. □

We now show that $\mathcal{S}$ satisfies $\dot{\mathcal{S}} \leq 0$ along the solutions to (6.18).

Lemma 6.3 (Evolution of $\mathcal{S}$). Let Assumptions 6.2–6.5 hold. Then $\dot{\mathcal{S}} \leq 0$.

Proof. We have that

$$\begin{aligned}
\dot{\mathcal{S}} =\ & \boldsymbol{f}^T(-\boldsymbol{K_p}^{-1}\boldsymbol{f} + \boldsymbol{P_t} - \boldsymbol{P_d} - \boldsymbol{\mathcal{B}\Gamma}\mathbf{sin}(\boldsymbol{\eta})) + (\boldsymbol{\Gamma}\mathbf{sin}(\boldsymbol{\eta}) - \boldsymbol{\Gamma}\mathbf{sin}(\overline{\boldsymbol{\eta}}))^T\boldsymbol{\mathcal{B}}^T\boldsymbol{f} \\
& + \boldsymbol{f}^T\boldsymbol{T_p}\boldsymbol{K_p}^{-1}\boldsymbol{X}\boldsymbol{\mathcal{B}\Gamma}[\mathbf{cos}(\boldsymbol{\eta})]\boldsymbol{\mathcal{B}}^T\boldsymbol{f} \\
& + (\boldsymbol{\mathcal{B}\Gamma}(\mathbf{sin}(\boldsymbol{\eta}) - \mathbf{sin}(\overline{\boldsymbol{\eta}})))^T\boldsymbol{X}(-\boldsymbol{K_p}^{-1}f + \boldsymbol{P_t} - \overline{P}_l - \boldsymbol{\mathcal{B}\Gamma}\mathbf{sin}(\boldsymbol{\eta})) \\
& + (\boldsymbol{P_t} - \overline{\boldsymbol{P}}_{\boldsymbol{t}})^T(-\boldsymbol{M_1}^{-1}(\boldsymbol{M_2} + \boldsymbol{M_3})\boldsymbol{P_t} - \boldsymbol{M_1}^{-1}\boldsymbol{M_4}\boldsymbol{\theta} - \boldsymbol{f} \\
& - \boldsymbol{M_1}^{-1}\boldsymbol{M_5}\boldsymbol{\mathcal{B}}(\boldsymbol{\Gamma}\mathbf{sin}(\boldsymbol{\eta}) - \overline{\boldsymbol{P}}_{\boldsymbol{f}})) + (\boldsymbol{\theta} - \overline{\boldsymbol{\theta}})^T\boldsymbol{M_1}^{-1}(\boldsymbol{M_2} + \boldsymbol{M_3})(-\boldsymbol{\theta} + \boldsymbol{P_t}) \\
=& - \begin{pmatrix} \boldsymbol{f} \\ \boldsymbol{\mathcal{B}\Gamma}(\mathbf{sin}(\boldsymbol{\eta}) - \mathbf{sin}(\overline{\boldsymbol{\eta}})) \end{pmatrix}^T \boldsymbol{Z} \begin{pmatrix} \boldsymbol{f} \\ \boldsymbol{\mathcal{B}\Gamma}(\mathbf{sin}(\boldsymbol{\eta}) - \mathbf{sin}(\overline{\boldsymbol{\eta}})) \end{pmatrix} \\
& - (\boldsymbol{P_t} - \boldsymbol{\theta})^T\boldsymbol{M_1}^{-1}(\boldsymbol{M_2} + \boldsymbol{M_3})(\boldsymbol{P_t} - \boldsymbol{\theta}),
\end{aligned} \tag{6.26}$$

where we exploited (6.19) in the second equality above and define

$$\boldsymbol{Z} = \begin{bmatrix} \boldsymbol{K_p}^{-1} - \boldsymbol{T_p}\boldsymbol{K_p}^{-1}\boldsymbol{X}\boldsymbol{\mathcal{B}\Gamma}[\mathbf{cos}(\boldsymbol{\eta})]\boldsymbol{\mathcal{B}}^T & \frac{1}{2}\boldsymbol{K_p}^{-1}\boldsymbol{X} \\ \frac{1}{2}\boldsymbol{X}\boldsymbol{K_p}^{-1} & \boldsymbol{X} \end{bmatrix}. \tag{6.27}$$

Since $\boldsymbol{X} > \mathbf{0}$, it follows that $\dot{\mathcal{S}} \leq 0$ if the Schur complement of block $\boldsymbol{X}$ of matrix $\frac{1}{2}(\boldsymbol{Z} + \boldsymbol{Z}^T)$ satisfies

$$\mathbf{0} < \boldsymbol{K_p}^{-1} - \frac{1}{4}\boldsymbol{K_p}^{-1}\boldsymbol{X}\boldsymbol{K_p}^{-1} - \frac{1}{2}(\boldsymbol{T_p}\boldsymbol{K_p}^{-1}\boldsymbol{X}\boldsymbol{\mathcal{B}\Gamma}[\mathbf{cos}(\boldsymbol{\eta})]\boldsymbol{\mathcal{B}}^T + \boldsymbol{\mathcal{B}\Gamma}[\mathbf{cos}(\boldsymbol{\eta})]\boldsymbol{\mathcal{B}}^T\boldsymbol{X}\boldsymbol{K_p}^{-1}\boldsymbol{T_p}). \tag{6.28}$$

The claim then follows from Assumption 6.3. □

Now, we can prove the main result of this work concerning the evolution of the augmented system controlled via the proposed SSOSM control strategy.

Theorem 6.1 (Main result). *Let Assumptions 6.1–6.5 hold. Consider system (6.1), augmented with (6.5) and controlled via (6.6)–(6.12). Then, the solutions of the closed-loop system starting in a neighbourhood of the equilibrium ($\overline{\boldsymbol{f}} = \mathbf{0}, \overline{\boldsymbol{\eta}}, \overline{\boldsymbol{P}}_{\boldsymbol{t}}, \overline{\boldsymbol{P}}_{\boldsymbol{g}}$) approach the set where $\overline{\boldsymbol{f}} = \mathbf{0}$ and $\boldsymbol{\mathcal{B}\Gamma}\mathbf{sin}(\overline{\boldsymbol{\eta}}) = \boldsymbol{\mathcal{B}}\overline{\boldsymbol{P}}_{\boldsymbol{f}}$, where $\boldsymbol{\mathcal{B}}\overline{\boldsymbol{P}}_{\boldsymbol{f}}$ is the desired net power exchanged by the control areas.*

Proof. Following Lemma 6.1 we have that the SSOSM control enforces system (6.1), (6.5) to evolve $\forall\, t \geq t_r$ on the sliding manifold characterized by $\boldsymbol{\sigma} = \dot{\boldsymbol{\sigma}} = \mathbf{0}$, resulting in the reduced order system (6.18). Consider the incremental storage function $\mathcal{S}$, given by (6.21). In view of Lemma 6.2 and Lemma 6.3 we have that $\mathcal{S}$ has a local minimum at ($\overline{\boldsymbol{f}} = \mathbf{0}, \overline{\boldsymbol{\eta}}, \overline{\boldsymbol{P}}_{\boldsymbol{t}}, \overline{\boldsymbol{\theta}}$) and satisfies along the solutions to (6.18)

$$\begin{aligned}\dot{\mathcal{S}} = &-\begin{pmatrix} \boldsymbol{f} \\ \boldsymbol{\mathcal{B}\Gamma}(\mathbf{sin}(\boldsymbol{\eta}) - \mathbf{sin}(\overline{\boldsymbol{\eta}}))\end{pmatrix}^T \boldsymbol{Z} \begin{pmatrix} \boldsymbol{f} \\ \boldsymbol{\mathcal{B}\Gamma}(\mathbf{sin}(\boldsymbol{\eta}) - \mathbf{sin}(\overline{\boldsymbol{\eta}}))\end{pmatrix} \\ &- (\boldsymbol{P_t} - \boldsymbol{\theta})^T \boldsymbol{M_1}^{-1}(\boldsymbol{M_2} + \boldsymbol{M_3})(\boldsymbol{P_t} - \boldsymbol{\theta}) \\ \leq\ & \mathbf{0},\end{aligned} \tag{6.29}$$

where $\boldsymbol{Z} + \boldsymbol{Z}^T > \mathbf{0}$. Consequently, there exists a forward invariant set, Υ around $(\overline{\boldsymbol{f}} = \mathbf{0}, \overline{\boldsymbol{\eta}}, \overline{\boldsymbol{P}}_{\boldsymbol{t}}, \overline{\boldsymbol{\theta}})$ and by LaSalle's invariance principle the solutions that start in Υ approach the largest invariant set contained in

$$\Upsilon \cap \{\boldsymbol{f}, \boldsymbol{\eta}, \boldsymbol{P_t}, \boldsymbol{\theta}) : \boldsymbol{f} = \mathbf{0}, \boldsymbol{\mathcal{B}\Gamma}\mathbf{sin}(\boldsymbol{\eta}) = \boldsymbol{\mathcal{B}\Gamma}\mathbf{sin}(\overline{\boldsymbol{\eta}}), \boldsymbol{P_t} = \boldsymbol{\theta}\}. \tag{6.30}$$

Bearing in mind that $\boldsymbol{\mathcal{B}\Gamma}\mathbf{sin}(\overline{\boldsymbol{\eta}}) = \boldsymbol{\mathcal{B}}\overline{\boldsymbol{P}}_{\boldsymbol{f}}$, we can indeed observe hat system (6.1) approaches the set where the frequency deviation is zero, and where the net exchanged power is equal to the desired value, i.e., $\boldsymbol{\mathcal{B}\Gamma}\mathbf{sin}(\boldsymbol{\eta}) = \boldsymbol{\mathcal{B}}\overline{\boldsymbol{P}}_{\boldsymbol{f}}$. □

Remark 6.6 (Acyclic network topologies). In case the topology of the power network does not contain any cycles, we have that the corresponding incidence matrix $\boldsymbol{\mathcal{B}}$ has full column rank and therefore has a left-inverse satisfying $\boldsymbol{\mathcal{B}}^+\boldsymbol{\mathcal{B}} = \mathbb{I}_m$, such that we can conclude from Theorem 6.1 that the system approaches the set where

$$\begin{aligned}\boldsymbol{\mathcal{B}\Gamma}\mathbf{sin}(\overline{\boldsymbol{\eta}}) =& \boldsymbol{\mathcal{B}}\overline{\boldsymbol{P}}_{\boldsymbol{f}} \\ \boldsymbol{\mathcal{B}}^+\boldsymbol{\mathcal{B}\Gamma}\mathbf{sin}(\overline{\boldsymbol{\eta}}) =& \boldsymbol{\mathcal{B}}^+\boldsymbol{\mathcal{B}}\overline{\boldsymbol{P}}_{\boldsymbol{f}}. \\ \boldsymbol{\Gamma}\mathbf{sin}(\overline{\boldsymbol{\eta}}) =& \overline{\boldsymbol{P}}_{\boldsymbol{f}}.\end{aligned} \tag{6.31}$$

Remark 6.7 (Region of attraction). LaSalle's invariance principle can be applied to all bounded solutions. As follows from Lemma 6.2, we have that the considered incremental storage function has a local minimum at the desired steady state, whereas the time to converge to the sliding manifold can be made arbitrarily small by properly choosing the gains of the SSOSM control. This guarantees that solutions starting in the vicinity of the steady state of interest remain bounded. A thorough analysis of the region of attraction is outside the scope of this thesis and an interesting future direction is to incorporate recent results of [VT16, DLC15] where energy functions, similar to the one used in this chapter, are further characterized.

6.5.1 A distributed tuning algorithm

In this subsection we provide a distributed algorithm to determine a possible value of $\boldsymbol{X}$ that satisfies (6.14) and (6.15). We first derive two useful lemmas.

Lemma 6.4 (Satisfying (6.14)). If $\boldsymbol{X} = \epsilon_1 \boldsymbol{K_p}\boldsymbol{T_p}^{-1}$, with

$$\epsilon_1 < \min_{i \in \mathcal{V}} \left(\sqrt{\frac{T_{pi}}{2K_{pi}\sum_{k \in \mathcal{N}_i} \Gamma_k}} \right), \tag{6.32}$$

then (6.14) is satisfied.

Proof. Note that (6.14) becomes

$$\mathbf{0} < \boldsymbol{T_p}\boldsymbol{K_p}^{-1} - \epsilon_1^2 \boldsymbol{\mathcal{B}}\boldsymbol{\Gamma}[\mathbf{cos}(\overline{\boldsymbol{\eta}})]\boldsymbol{\mathcal{B}}^T, \tag{6.33}$$

which holds if the largest eigenvalue $\lambda_{\max}$ satisfies

$$\lambda_{\max}(\epsilon_1^2 \boldsymbol{T_p}^{-1}\boldsymbol{K_p}\boldsymbol{\mathcal{B}}\boldsymbol{\Gamma}[\mathbf{cos}(\overline{\boldsymbol{\eta}})]\boldsymbol{\mathcal{B}}^T) < 1. \tag{6.34}$$

By the Gershgorin circle theorem, every eigenvalue of $\epsilon_1^2 \boldsymbol{T_p}^{-1}\boldsymbol{K_p}\boldsymbol{\mathcal{B}}\boldsymbol{\Gamma}[\mathbf{cos}(\overline{\boldsymbol{\eta}})]\boldsymbol{\mathcal{B}}^T$ lies within at least one of the Gershgorin disk $D_i(c_i, r_i)$ centered at c_i, and with radius r_i, where

$$c_i = r_i = \epsilon_1^2 T_{pi}^{-1} K_{pi} \sum_{k\in\mathcal{N}_i} |\Gamma_k \cos(\overline{\eta}_k)|, \tag{6.35}$$

where $\mathcal{N}_i$ is the set of lines connecting control area i. We therefore have that

$$\lambda_{\max}(\epsilon_1^2 \boldsymbol{T_p}^{-1}\boldsymbol{K_p}\boldsymbol{\mathcal{B}}\boldsymbol{\Gamma}[\mathbf{cos}(\overline{\boldsymbol{\eta}})]\boldsymbol{\mathcal{B}}^T) < 1. \tag{6.36}$$

if

$$\epsilon_1 < \min_{i\in\mathcal{V}} \left(\sqrt{\frac{T_{pi}}{2K_{pi}\sum_{k\in\mathcal{N}_i}\Gamma_k}} \right). \tag{6.37}$$

□

Lemma 6.5 (Satisfying (6.15)). If $\boldsymbol{X} = \epsilon_2 \boldsymbol{K_p}\boldsymbol{T_p}^{-1}$, with

$$\epsilon_2 < \min_{i\in\mathcal{V}} \left(\frac{T_{pi}}{\frac{1}{2} + 2K_{pi}T_{pi}\sum_{k\in\mathcal{N}_i}\Gamma_k} \right). \tag{6.38}$$

then (6.15) is satisfied.

Proof. Note that (6.15) becomes

$$\mathbf{0} < \boldsymbol{K_p}^{-1}(\mathbb{I}_n - \frac{1}{4}\epsilon_2 \boldsymbol{T_p}^{-1}) - \epsilon_2 \boldsymbol{\mathcal{B}}\boldsymbol{\Gamma}[\mathbf{cos}(\boldsymbol{\eta})]\boldsymbol{\mathcal{B}}^T. \tag{6.39}$$

which holds, in analogy to Lemma 6.4, if

$$\lambda_{\max}(\epsilon_2 \boldsymbol{K_p}(\mathbb{I}_n - \frac{1}{4}\epsilon_2 \boldsymbol{T_p}^{-1})^{-1}\boldsymbol{\mathcal{B}}\boldsymbol{\Gamma}[\mathbf{cos}(\boldsymbol{\eta})]\boldsymbol{\mathcal{B}}^T) < 1. \tag{6.40}$$

Following the same argument as in Lemma 6.4, applying the Gershgorin circle theorem we have that (6.15) is satisfied when

$$\epsilon_2 < \min_{i\in\mathcal{V}} \left(\frac{T_{pi}}{\frac{1}{2} + 2K_{pi}T_{pi}\sum_{k\in\mathcal{N}_i}\Gamma_k} \right). \tag{6.41}$$

□

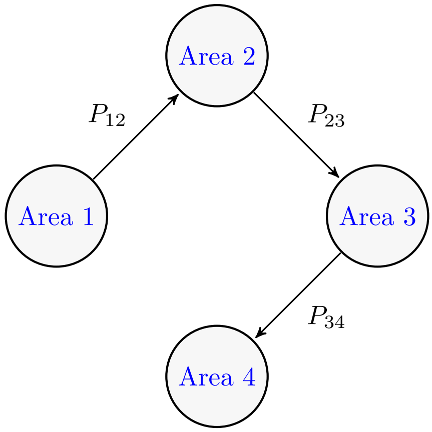

Fig. 6.1. Scheme of the considered power network partitioned into 4 control areas, where $P_{ij} = \frac{V_i^\star V_j^\star}{X_{ij}} \sin(\delta_i - \delta_j)$. The arrows indicate the positive direction of the power flows through the power network.

From Lemma 6.4 and Lemma 6.5 the following corollary is immediate.

Corollary 6.1 (Satisfying (6.14) and (6.15)). Let

$$\boldsymbol{X} = \epsilon \boldsymbol{K_p} \boldsymbol{T_p}^{-1}, \tag{6.42}$$

with $\epsilon = \min\{\epsilon_1, \epsilon_2\}$, then (6.14) and (6.15) are satisfied.

The result of this subsection can be used as follows. Every control area determines an upper bound for ϵ using (6.32) and (6.38), and broadcasts it to the rest of the network. Using the minimum of all estimated upper bounds of ϵ it is ensured that Assumption 6.3 holds.

6.6 Case Study

In this section, the proposed control solution is assessed in simulation by implementing a power network partitioned into four control areas (e.g. the IEEE New England 39-bus system [NC13]). The topology of the power network is represented in Fig. 6.1. The relevant network parameters of each area are provided in Table 6.1, where a base power of 1000 MW is assumed. The line parameters are $\Gamma_1 = 5.4$ p.u., $\Gamma_2 = 5.0$ p.u. and $\Gamma_3 = 5.2$ p.u., while the scheduled power flows are $\overline{P}_{f_1} = 0.015$ p.u., $\overline{P}_{f_2} = 0.0125$ p.u. and $\overline{P}_{f_3} = 0.01$ p.u. The matrices in (6.6) are chosen as $\boldsymbol{M_1} = 10\mathbb{I}_4$, $\boldsymbol{M_2} = \mathbb{I}_4$, $\boldsymbol{M_3} = 0.1\mathbb{I}_4$, $\boldsymbol{M_4} = -(\boldsymbol{M_2} + \boldsymbol{M_3})$ and $\boldsymbol{M_5} = 0.5\mathbb{I}_4$, $\mathbb{I}_4 \in \mathbb{R}^{4\times 4}$ being the identity matrix, while the control amplitude $W_{\max_i}$ and the parameter α_i^*, $i = 1, \ldots, 4$, in (6.10) are selected equal to 100 and 1, respectively.

In simulation, at the initial time instant $t_0 = 0$ s the system is at the steady state with

Table 6.1. Network parameters and power demand

		Area 1	Area 2	Area 3	Area 4
T_{p_i}	(s)	21.0	25.0	23.0	22.0
T_{t_i}	(s)	0.30	0.33	0.35	0.28
T_{g_i}	(s)	0.080	0.072	0.070	0.081
K_{p_i}	(Hz p.u.$^{-1}$)	120.0	112.5	115.0	118.5
R_i	(Hz p.u.$^{-1}$)	2.5	2.7	2.6	2.8
T_{θ_i}	(s)	0.1	0.1	0.1	0.1
$P_{d_i}(0)$	(p.u.)	0.010	0.014	0.012	0.013
$\overline{P}_{d_i}$	(p.u.)	0.020	0.028	0.024	0.026

power demand $P_{d_i}(0)$. Then, at the time instant $t = 2\,$s, the power demand in each area becomes $\overline{P}_{d_i}$ (see Table 6.1). From Fig. 6.2, one can observe that the frequency deviation converges asymptotically to zero after a transient during which the frequency drops because of the increasing load. Moreover, one can note that the proposed controllers increase the power generation in order to reach again a zero steady state frequency deviation, maintaining, at the steady state, the scheduled power flows $\overline{P}_{f_k}$ on each line.

6.7 Conclusions

A decentralized Suboptimal Second Order Sliding Mode control scheme has been proposed for Automatic Generation Control (AGC). We considered a power network partitioned into control areas, where each area is modelled by an equivalent generator including second-order turbine-governor dynamics, and where the areas are nonlinearly coupled through the power flows. Relying on stability considerations made on the basis of an incremental energy (storage) function, a suitable sliding manifold has been designed. Asymptotic convergence is proven to the state where the frequency deviation is zero and where the power flows are regulated towards their desired values. A case study shows the effectiveness of the proposed control scheme. In a future research we aim at including saturation [FR09] and measurement noise in the current setting.

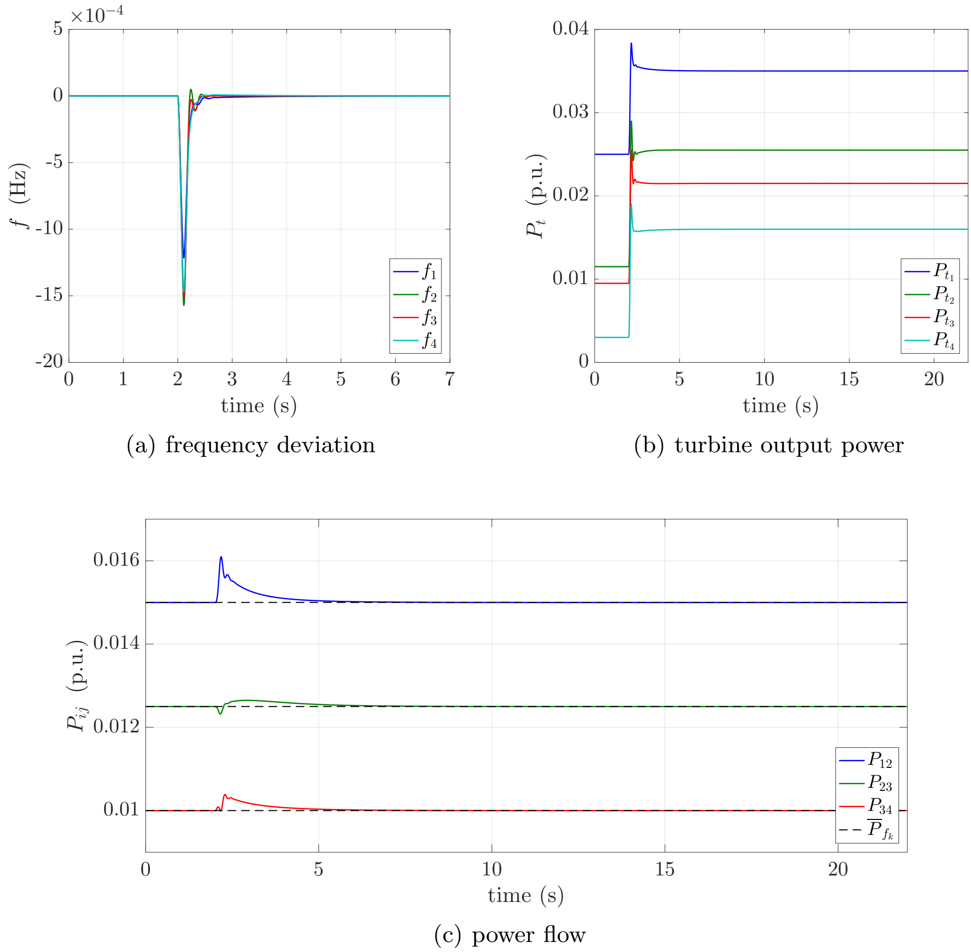

Fig. 6.2. Evolution of the controlled power system considering a power demand variation at the time instant $t = 2\,\mathrm{s}$. **(a)** Frequency deviation in each control area. **(b)** Generated power at the output of each steam turbine. **(c)** Power flows in each line (the scheduled power flows are given by the dashed lines).

7

Sliding Mode Observers for Power Systems

Abstract. This work deals with the design of a novel sliding mode observer-based scheme to estimate and reconstruct the unmeasured state variables in power networks including hydroelectric power plants and thermal power plants. The proposed approach is flexible to topological changes to power networks and can be easily updated only where changes occur.

7.1 Model Description

We consider a power network characterized by n_t thermal power plants and n_h hydroelectric power plants. For each kind of power plant, specific dynamic models are presented in this section. More precisely, each power plant is characterized by the turbine-governor dynamics, and the generator dynamics which is the same for the two considered types of plants. In addition, each power plant is linked to the neighboring plants via power transmission lines allowing exchange of electrical active power [KBL94]. Table 7.1 shows the physical meanings and the measurement units of the states variables and the model parameters adopted in this chapter.

A power network can be interpreted as an undirected graph $\mathcal{G}(\mathcal{V}, \mathcal{E})$. Specifically, $\mathcal{V}$ represents the set of nodes of the graph (which are the plants in this case), and it consists of two subsets, i.e., $\mathcal{V} = \mathcal{V}_t \cup \mathcal{V}_h$. The set $\mathcal{V}_t$ denotes all the n_t thermal power plants, whilst $\mathcal{V}_h$ denotes all the n_h hydroelectric power plants. The set of edges $\mathcal{E} = \{1, \ldots, k, \ldots, m\}$ comprises all the power transmission lines linking the plants. Each k-th edge is denoted as

$$k \triangleq [(i, j);\, X_{ij}]\,, \tag{7.1}$$

where (i, j) is the unordered pair of the distinct nodes linked by the k-th power transmission line, and X_{ij} is the reactance of the k-th power transmission line.

The topology of the graph can be encapsulated in the Laplacian Matrix $\mathcal{X} \in \mathbb{R}^{N \times N}$, where $N = n_t + n_h$, and its elements are defined as follows

$$\mathcal{X} = \begin{cases} \mathcal{X}_{ii} = \sum_{j \in \mathcal{N}_i} X_{ij} & \\ \mathcal{X}_{ij} = -X_{ij} & \text{if } \exists\ k = [(i, j);\, X_{ij}] \in \mathcal{E} \\ \mathcal{X}_{ij} = 0 & \text{otherwise,} \end{cases} \tag{7.2}$$

Table 7.1. State Variables and Model Parameters Adopted in the Paper

Symbols	Meanings	Units
$P_{m_{a_i}}$, $P_{m_{b_i}}$, $P_{m_{c_i}}$	a, b, c turbines powers	(p.u.)
P_{g_i}	governor power	(p.u.)
P_{m_i}	total mechanical power	(p.u.)
P_{d_i}	electrical power demand	(p.u.)
$T_{a_i} \in [0.1 - 0.4]$	a-turbine time constant	(s)
$T_{b_i} \in [4 - 11]$	b-turbine time constant	(s)
$T_{c_i} \in [0.3 - 0.5]$	c-turbine time constant	(s)
$T_{g_i} \in [0.2 - 0.3]$	governor time constant	(s)
$\alpha_i, \beta_i, \gamma_i$	power conversion constants	$(-)$
P_{c_i}	transient compensator power	(p.u.)
W_i	water speed	(p.u.)
$T_{c_{1_i}} \approx 5$	compensator time constant 1	(s)
$T_{c_{2_i}} \approx 50$	compensator time constant 2	(s)
$T_{h_i} \in [1 - 2]$	hydro turbine time constant	(s)
δ_i	generator angle	(rad)
ω_i	generator frequency deviation	(rad/s)
ω^*	network nominal frequency	(rad/s)
J_i	generator inertia	(kg m^2)
D_i	generator damping	$(\mathrm{N} \cdot \mathrm{m} \cdot \mathrm{s})$
X_{ij}	reactance of the line	(p.u.)
$\overline{V}_i$	constant voltage magnitude	(p.u.)

where $\mathcal{N}_i$ is the set of nodes directly connected to the i-th node via power transmission lines.

Remark 7.1 (Conservative topology). From the point of view of the power network operations, it is reasonable to suppose that the use of the power transmission lines changes with respect to time due to scheduled electricity trade among the plants. Therefore, the set of edges $\mathcal{E}$ represents all the possible interconnections among the plants in the most conservative situation, which means that all the available power transmission lines are used. Consequently, also the Laplacian Matrix in (7.2) encapsulates the power grid topology in the most conservative situation, as well as the set $\mathcal{N}_i$ for each node.

7.1.1 Steam Turbines and Governor Dynamics

The so-called single tandem reheat arrangement represents the most common configuration used for large thermal power plants [MBB08] and it is adopted in this chapter. In such arrangement, three steam turbines, denoted as a, b, and c, are attached to the same shaft. The steam coming from the boiler is expanded through three stages producing mechanical power and it is reheated only once in the boiler. The following differential equations describe the dynamics of the three steam turbines and the governor:

$$
\begin{aligned}
\dot{P}_{m_{a_i}} &= -\frac{1}{T_{a_i}} P_{m_{a_i}} + \frac{1}{T_{a_i}} P_{g_i} \\
\dot{P}_{m_{b_i}} &= -\frac{1}{T_{b_i}} P_{m_{b_i}} + \frac{1}{T_{b_i}} P_{m_{a_i}} \\
\dot{P}_{m_{c_i}} &= -\frac{1}{T_{c_i}} P_{m_{c_i}} + \frac{1}{T_{c_i}} P_{m_{b_i}} \\
\dot{P}_{g_i} &= -\frac{1}{T_{g_i}} P_{g_i} + \frac{1}{T_{g_i}} u_i - \frac{1}{R_i T_{g_i}} \omega_i \\
y_{t_{i_1}} &= \alpha_i P_{m_{a_i}} + \beta_i P_{m_{b_i}} + \gamma_i P_{m_{c_i}} = P_{m_i}.
\end{aligned}
\tag{7.3}
$$

We let the reader refers to Table 7.1 for the physical meaning and the measurement units of the introduced state variables and model parameters, and to Fig. 7.1 for a block-diagram representation of the adopted dynamics. Note that, according to (7.3), it is assumed to measure only the total mechanical power output P_{m_i}, which is given by the sum of the total power developed in each turbine stage (three contributions). Typical values for the constants are $\alpha_i = 0.3$, $\beta_i = 0.4$, $\gamma_i = 0.3$, and the basic relation $\alpha_i + \beta_i + \gamma_i = 1$ holds [MBB08].

It is possible to compactly rewritten equation (7.3) by introducing the following vectors and matrices:

$$
\boldsymbol{A_{t_i}} = \begin{bmatrix} -\frac{1}{T_{a_i}} & 0 & 0 & \frac{1}{T_{a_i}} \\ \frac{1}{T_{b_i}} & -\frac{1}{T_{b_i}} & 0 & 0 \\ 0 & \frac{1}{T_{c_i}} & -\frac{1}{T_{c_i}} & 0 \\ 0 & 0 & 0 & -\frac{1}{T_{g_i}} \end{bmatrix}, \boldsymbol{B_{t_i}} = \begin{bmatrix} 0 \\ 0 \\ 0 \\ \frac{1}{T_{g_i}} \end{bmatrix}, \tag{7.4}
$$

$$
\boldsymbol{C_{t_i}} = \begin{bmatrix} \alpha_i \ \beta_i \ \gamma_i \ 0 \end{bmatrix}, \boldsymbol{M_{t_i}} = \begin{bmatrix} 0, \\ 0 \\ 0 \\ -\frac{1}{R_i T_{g_i}} \end{bmatrix}, \tag{7.5}
$$

$$
\boldsymbol{x_{p_{t_i}}} = \begin{bmatrix} P_{m_{a_i}} \ P_{m_{b_i}} \ P_{m_{c_i}} \ P_{g_i} \end{bmatrix}^T. \tag{7.6}
$$

The following representation holds:

$$
\begin{aligned}
\dot{\boldsymbol{x}}_{\boldsymbol{p_{t_i}}} &= \boldsymbol{A_{t_i}} \boldsymbol{x_{p_{t_i}}} + \boldsymbol{B_{t_i}} u_i + \boldsymbol{M_{t_i}} \omega_i \\
y_{t_{i_1}} &= \boldsymbol{C_{t_i}} \boldsymbol{x_{p_{t_i}}}.
\end{aligned}
\tag{7.7}
$$

It is worth noting that the eigenvalues of the matrix $\boldsymbol{A_{t_i}}$ are $-1/T_{a_i}$, $-1/T_{b_i}$, $-1/T_{c_i}$, $-1/T_{g_i}$. System (7.7) will be used as a basis to design an observer to estimate all the three steam turbine powers.

7.1.2 Hydraulic Turbine and Governor Dynamics

The linearized hydraulic turbine and governor dynamics comprises a governor (similar to the one described for thermal power plants), a transient droop compensator and the hydraulic turbine. It is worth precising that the transient droop compensator is introduced between the governor and the hydraulic turbine to ensure and to enhance the stability of the system [KBL94, MBB08]. More precisely, according to [KBL94], the compensator is required considering the specific dynamics of the hydraulic turbines due to the particular response of water inertia. The hydraulic turbine can be considered as the transfer function block in Fig. 7.2, in which a zero with positive real part is introduced. The resulting differential equations describe the turbine-governor dynamics for the hydroelectric power plants:

$$
\begin{aligned}
\dot{P}_{g_i} &= -\frac{1}{T_{g_i}} P_{g_i} + \frac{1}{T_{g_i}} u_i - \frac{1}{R_i T_{g_i}} \omega_i \\
\dot{P}_{c_i} &= -\frac{1}{T_{c_{1_i}}} P_{c_i} + P_{g_i} \\
\dot{W}_i &= \frac{T_{c_{1_i}}}{T_{c_{2_i}}} P_{g_i} + \frac{T_{c_{2_i}} - T_{c_{1_i}}}{T_{c_{2_i}}^2} P_{c_i} - \frac{2}{T_{h_i}} W_i \\
y_{h_{i_1}} &= -2\frac{T_{c_{1_i}}}{T_{c_{2_i}}} P_{g_i} + 2\frac{T_{c_{1_i}} - T_{c_{2_i}}}{T_{c_{2_i}}^4} P_{c_i} + \frac{6}{T_{h_i}} W_i = P_{m_i}.
\end{aligned}
\tag{7.8}
$$

We let again the reader refers to Table 7.1 for the physical meanings and the measurement units of the introduced state variables and model parameters, and to Fig. 7.2 for a block-diagram representation of the adopted dynamics. Note that, according to (7.8), it is assumed to measure only the total mechanical output power P_{m_i}, which is a linear combination of the three state variables of the hydraulic turbine-governor. Also in this case, it is possible to compactly rewritten the system (7.8) by introducing the following vectors and matrices:

$$
\boldsymbol{A_{h_i}} = \begin{bmatrix} -\frac{1}{T_{g_i}} & 0 & 0 \\ 1 & -\frac{1}{T_{c_{2_i}}} & 0 \\ \frac{T_{c_{1_i}}}{T_{c_{2_i}}} & \frac{T_{c_{2_i}} - T_{c_{1_i}}}{T_{c_{2_i}}^2} & -\frac{2}{T_{h_i}} \end{bmatrix}, \ \boldsymbol{B_{h_i}} = \begin{bmatrix} \frac{1}{T_{g_i}} \\ 0 \\ 0 \end{bmatrix}, \tag{7.9}
$$

$$
\boldsymbol{C_{h_i}} = \begin{bmatrix} -2\frac{T_{c_{1_i}}}{T_{c_{2_i}}} & 2\frac{T_{c_{1_i}} - T_{c_{2_i}}}{T_{c_{2_i}}^4} & \frac{6}{T_{h_i}} \end{bmatrix}, \boldsymbol{M_{h_i}} = \begin{bmatrix} -\frac{1}{R_i T_{g_i}} \\ 0 \\ 0 \end{bmatrix}, \tag{7.10}
$$

$$
\boldsymbol{x_{p_{h_i}}} = \begin{bmatrix} P_{g_i} \ P_{c_i} \ W_i \end{bmatrix}^T. \tag{7.11}
$$

The following compact representation holds:

$$
\begin{aligned}
\dot{\boldsymbol{x}}_{\boldsymbol{p_{h_i}}} &= \boldsymbol{A_{h_i}} \boldsymbol{x_{p_{h_i}}} + \boldsymbol{B_{h_i}} u_i + \boldsymbol{M_{h_i}} \omega_i \\
y_{h_{i_1}} &= \boldsymbol{C_{h_i}} \boldsymbol{x_{p_{h_i}}}.
\end{aligned}
\tag{7.12}
$$

It is worth noting that the eigenvalues of the matrix $\boldsymbol{A_{h_i}}$ are $-1/T_{g_i}$, $-1/T_{c_{2_i}}$, $-2/T_{h_i}$. System (7.12) will be used as a basis to design an observer to estimate the governor power, the transient compensator power, and the water speed.

7.1.3 Generator Dynamics

Both the steam turbines and the hydroelectric turbines are coupled with a generator (typically a synchronous machine) which is capable of turning the mechanical input power delivered by the turbines into electrical active power to be injected into the power network. Several models have been adopted in the literature for the generator dynamics (see, e.g., the detailed description provided in [MBB08]). Moreover, a large number of works in the literature have adopted the so-called classical swing equations to model synchronous generators. However, in the last few years it has been shown that this model is not accurate and leads to erroneous behaviours, even under small oscillations [MDPMvdS16, CT15]. For the aforementioned reasons, in the present work, the generator of each thermal and hydroelectric power plant is modeled by using the so-called nonlinear improved swing equations proposed in [MDPMvdS16] given by:

$$\begin{aligned} \dot{\delta}_i &= \omega_i \\ \dot{\omega}_i &= -\frac{\sum_{j \in \mathcal{N}_i} \frac{\overline{V}_i \overline{V}_j}{X_{ij}} \sin(\delta_i - \delta_j)}{J_i(\omega_i + \omega^*)} + \frac{P_{m_i} - P_{d_i}}{J_i(\omega_i + \omega^*)} - \frac{D_i \omega_i}{J_i} \\ y_{\bullet_{i_2}} &= \delta_i . \end{aligned} \tag{7.13}$$

We let again the readers refer to Table 7.1 for the physical meaning and the measurements units of the introduced model parameters and state variables. It is worth noting from equation (7.13) that it is assumed to locally measure only the generator angle δ_i. This can be easily implemented in practice by equipping each generator with an encoder to measure the position of the rotor [CHD+15]. Moreover, the subscript $\bullet$ in $y_{\bullet_{i_2}}$ is equal to $\bullet = t$ in case of thermal power plant, and $\bullet = h$ in case of hydroelectric power plant.

Remark 7.2 (Mutual interactions). It is worth noting, by exploiting equation (7.13), that the only mutual interaction among the plants takes place at the level of electrical active power exchange, which can be modeled according to the power flow method [MBB08] as

$$P_{i_{\mathcal{N}_i}} \triangleq \sum_{j \in \mathcal{N}_i} \frac{\overline{V}_i \overline{V}_j}{X_{ij}} \sin(\delta_i - \delta_j), \tag{7.14}$$

where $P_{i_{\mathcal{N}_i}}$ is the total electrical active power transmitted by the i-th plant to its neighbors. This peculiar mutual interaction among the plants represents an interesting feature for the observer-design procedure as detailed in the rest of the present work.

Assumption 7.1 (Available informations). Each thermal power plant node is governed by (7.3) together with (7.13), whilst each hydroelectric power plant is governed by (7.8) together with (7.13). It is assumed to measure at the node level only the mechanical power delivered by the turbine P_{m_i} and the generator angle δ_i both in the thermal and hydroelectric power plants. Moreover, the matrices and vectors in (7.4)-(7.5) are assumed to be known at each thermal power plant node level, whilst the matrices and vectors in (7.9)-(7.10) are assumed to be known at each hydroelectric power plant node level.

In the next sections, the design procedures of the sliding mode observers to estimate the unmeasured state variables of each node of the power network is described in detail. Specifically, a first-order sliding mode observer is proposed to robustly estimate the powers

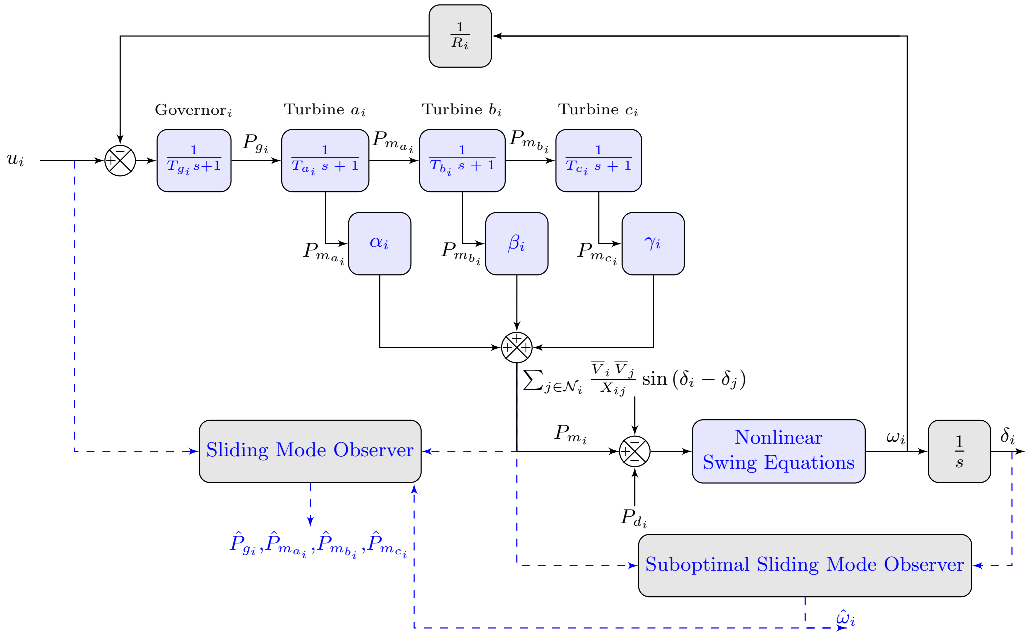

Fig. 7.1. The block diagram of the i-th thermal power plant node dynamics with the designed observers.

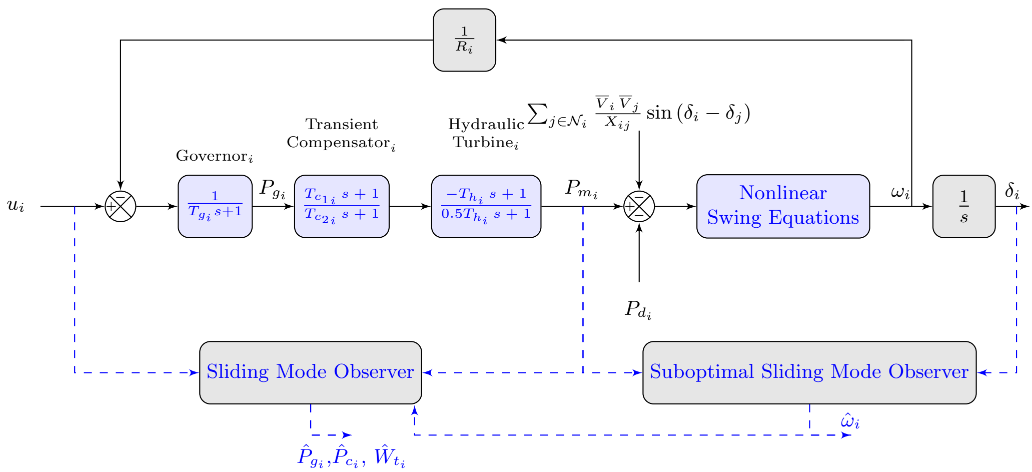

Fig. 7.2. The block diagram of the i-th hydroelectric power plant node dynamics with the designed observers.

associated with the three turbines and the governor of the thermal power plant node. By following the same idea, another similar first-order sliding mode observer is proposed to robustly estimate the governor power, the transient compensator power and the water speed of the hydraulic turbine. Moreover, we propose a sub-optimal sliding mode observer to robustly estimate the frequency deviation of each generator. This kind of observer is required to perform state estimation in nonlinear dynamic systems in the form of (7.13), as detailed in the sequel.

Specific rules to easily update the estimation scheme to topological changes affecting the power network will be discussed in Section 7.5, such as the addition or the removal of edges and nodes, making also reference to the physical meaning of these changes. From this analysis, one can derive that the proposed observer-based estimation scheme has interesting scalability and resilience properties.

7.2 Suboptimal Sliding Mode Observer for Generator

For the sake of clarity, it is better to start to design the sub-optimal sliding mode observer to robustly estimate the frequency deviation of each plant. The convergence results obtained in this section are instrumental to design the aforementioned sliding mode observers for the turbine-governor dynamics in Section 7.3.

Assumption 7.2 (Bounded disturbance). Introducing the signals

$$\phi_i \triangleq -\frac{\sum_{j\in\mathcal{N}_i}\frac{\overline{V}_i\overline{V}_j}{X_{ij}}\sin\left(\delta_i-\delta_j\right)}{J_i\left(\omega_i+\omega^*\right)}+\frac{P_{m_i}-P_{d_i}}{J_i\left(\omega_i+\omega^*\right)}+\frac{D_i\omega_i}{J_i}, \tag{7.15}$$

and

$$\varPhi_i \triangleq \left|\frac{\sum_{j\in\mathcal{N}_i}\frac{\overline{V}_i\overline{V}_j}{X_{ij}}}{J_i\left(\omega_i+\omega^*\right)}\right|+\left|\frac{P_{m_i}-P_{d_i}}{J_i\left(\omega_i+\omega^*\right)}\right|+\left|\frac{D_i\omega_i}{J_i}\right|, \tag{7.16}$$

it is assumed that ϕ_i is a bounded disturbance, i.e.,

$$|\phi_i| \leq \varPhi_i < \varLambda_i. \tag{7.17}$$

where $\varLambda_i$ is a known positive constant which can be determined from the understanding of the power network.

Assumption 7.2 is reasonable, considering the terms composing ϕ_i in equation (7.15). Note also that the term $\varPhi_i$ include all the neighboring plants in the most conservative situation specified by Remark 7.1. It follows that the condition (7.17) is fulfilled also in case the network is not operating in the most conservative situation. Moreover, in such approach, the interactions among the plants detailed in Remark 7.2 are threated as bounded disturbances. This gives to the sub-optimal sliding mode observers a completely decentralized feature.

Consider the following sub-optimal sliding mode observer

$$
\begin{aligned}
\dot{\hat{\delta}}_i &= \hat{\omega}_i \\
\dot{\hat{\omega}}_i &= u_{\mathrm{sub}_i},
\end{aligned}
\tag{7.18}
$$

where $\hat{\delta}_i$ is the estimate of δ_i, $\hat{\omega}_i$ is the estimate of ω_i, and u_{sub_i} is equal to (see [BFU98b])

$$
u_{\mathrm{sub}_i} \triangleq -\mu_i U_i^{\max} \mathrm{sgn}\left(e_{\delta_i} - \frac{1}{2} e_{\delta_i}^{\max}\right). \tag{7.19}
$$

Moreover, the following relations are considered

$$
\begin{aligned}
&\mu_i^* \in (0, 1] \\
&U_i^{\max} > \max\left(\frac{\Lambda_i}{\mu_i^*}, \frac{4\Lambda_i}{3 - \mu_i^*}\right).
\end{aligned}
\tag{7.20}
$$

The signal $e_{\delta_i}^{\max}$ can be detected by implementing for instance a peak detector as in [BFU98b]. Moreover, one defines

$$
\mu_i = \begin{cases} \mu_i^* & \text{if } \left(e_{\delta_i} - \frac{1}{2} e_{\delta_i}^{\max}\right)\left(e_{\delta_i}^{\max} - e_{\delta_i}\right) > 0 \\ 1 & \text{if } \left(e_{\delta_i} - \frac{1}{2} e_{\delta_i}^{\max}\right)\left(e_{\delta_i}^{\max} - e_{\delta_i}\right) \le 0. \end{cases} \tag{7.21}
$$

The following theorem can be proven.

Theorem 7.1 (Estimation of ω_i). *Given the generator dynamics (7.13), the Assumption 7.2, and the signal u_{sub_i} defined by (7.19), then, the suboptimal sliding mode observer in the form of (7.18) leads to a correct estimation of the frequency deviation ω_i of each generator in a finite time.*

Proof. The error dynamics is computed by subtracting the generator dynamics (7.13) to the sub-optimal observer dynamics (7.18) and is given by

$$
\begin{aligned}
\dot{e}_{\delta_i} &= e_{\omega_i} \\
\dot{e}_{\omega_i} &= \phi_i - \mu_i U_i^{\max} \mathrm{sgn}\left(e_{\delta_i} - \frac{1}{2} e_{\delta_i}^{\max}\right),
\end{aligned}
\tag{7.22}
$$

where $e_{\delta_i} \triangleq \hat{\delta}_i - \delta_i$, $e_{\omega_i} \triangleq \hat{\omega}_i - \omega_i$. Note that (7.22) is in the standard form for the sub-optimal sliding mode controlled system [BFU98b]. More precisely, if the signal u_{sub_i} is designed in such a way to fulfill the inequalities in (7.20), it follows that (7.22) converges to the origin in a finite time, guaranteeing a correct state estimation of the frequency deviation of each generator. □

It is worth noting that the proposed sub-optimal sliding mode observer differs from the one proposed in [CFdLF12]. In our approach the sliding surface to be reached is equal to $\sigma_i = e_{\delta_i}$, while in [CFdLF12], a linear combination of the two state errors has been measured in the form of $\sigma_i = e_{\delta_i} + \nu e_{\omega_i}$, where $\nu \in \mathbb{R}_+$.

7.3 Sliding Mode Observer for Steam Turbine and Governor

In order to design a sliding mode observer to estimate the unmeasured variables P_{g_i}, $P_{m_{a_i}}$, $P_{m_{b_i}}$, $P_{m_{c_i}}$ it is first necessary to verify the observability of the pair $(\boldsymbol{A_{t_i}}, \boldsymbol{C_{t_i}})$.

Theorem 7.2 (Observability of $(\boldsymbol{A_{t_i}}, \boldsymbol{C_{t_i}})$). *The pair $(\boldsymbol{A_{t_i}}, \boldsymbol{C_{t_i}})$ in (7.4)–(7.5) is observable.*

Proof. In order to ensure that the pair $(\boldsymbol{A_{t_i}}, \boldsymbol{C_{t_i}})$ in (7.4)–(7.5) is observable, one has to compute the Observability Matrix $\mathcal{O}_{t_i}$ and to verify that its determinant $\det(\mathcal{O}_{t_i})$ is different from zero [Kha96]. One has

$$\begin{aligned}\det(\mathcal{O}_{t_i}) = &-\frac{\gamma_i}{T_{a_i}^3 T_{b_i}^3 T_{c_i}^3 T_{g_i}^2}(T_{b_i} - T_{c_i} - \alpha_i T_{b_i} + \alpha_i T_{c_i} + \gamma_i T_{c_i}) \\ &\cdot (T_{g_i}^2 - T_{g_i} T_{c_i} + \alpha_i T_{b_i} T_{c_i} - \alpha_i T_{b_i} T_{g_i} + \gamma_i T_{g_i} T_{c_i}) \\ &\cdot (T_{a_i}^2 - T_{a_i} T_{c_i} + \alpha_i T_{b_i} T_{c_i} - \alpha_i T_{b_i} T_{a_i} + \gamma_i T_{a_i} T_{c_i}).\end{aligned} \tag{7.23}$$

The key-idea here is to show that the expression of the determinant in (7.23) is never equal to zero by analyzing the three terms constituting its expression, and by considering the possible values that all the time constants can assume according to Table 7.1. One has

$$-\frac{\gamma_i}{T_{a_i}^3 T_{b_i}^3 T_{c_i}^3 T_{g_i}^2} < 0. \tag{7.24}$$

and

$$\begin{aligned}T_{b_i} - T_{c_i} - \alpha_i T_{b_i} + \alpha_i T_{c_i} + \gamma_i T_{c_i} &= (1-\alpha_i) T_{b_i} + (\alpha_i + \gamma_i - 1) T_{c_i} \\ &= (\beta_i + \gamma_i) T_{b_i} + \beta_i T_{c_i} > 0.\end{aligned} \tag{7.25}$$

As for the term

$$\left(T_{g_i}^2 - T_{g_i} T_{c_i} + \alpha_i T_{b_i} T_{c_i} - \alpha_i T_{b_i} T_{g_i} + \gamma_i T_{g_i} T_{c_i}\right), \tag{7.26}$$

two possible situations can take place:

1. If $T_{g_i} = T_{c_i}$, then the term (7.26) can be simplified as:

$$T_{g_i}^2 - T_{g_i}^2 + \alpha_i T_{b_i} T_{g_i} - \alpha_i T_{b_i} T_{g_i} + \gamma_i T_{g_i}^2 = \gamma_i T_{g_i}^2 > 0,$$

   which is always greater than zero.
2. If $T_{g_i} < T_{c_i}$, then the term (7.26) can be simplified as:

$$(T_{g_i} - \alpha_i T_{b_i})(T_{g_i} - T_{c_i}) + \gamma_i T_{g_i} T_{c_i}. \tag{7.27}$$

   By exploiting (7.27), it is easy to show that $\gamma_i T_{g_i} T_{c_i} > 0$ and the product

$$(T_{g_i} - \alpha_i T_{b_i})(T_{g_i} - T_{c_i}) > 0,$$

   since $T_{g_i} - T_{c_i} < 0$ by assumption, and the inequality $T_{g_i} - \alpha_i T_{b_i} < 0$ is always fulfilled according to Table 7.1.

Therefore, the term in (7.26) is always strictly greater than zero. Consider now the term

$$\left(T_{a_i}^2 - T_{a_i}T_{c_i} + \alpha_i T_{b_i}T_{c_i} - \alpha_i T_{b_i}T_{a_i} + \gamma_i T_{a_i}T_{c_i}\right). \tag{7.28}$$

It is worth noting that equation (7.28) and (7.26) have the same structure. More precisely, equation (7.28) can be obtained by replacing in equation (7.26) the term T_{a_i} with T_{g_i}. Also in this case, two possible situations can take place

1. If $T_{a_i} = T_{c_i}$, then the term (7.28) becomes

$$\gamma_i T_{a_i}^2 > 0. \tag{7.29}$$

2. If $T_{a_i} < T_{c_i}$, then the term (7.28) can be simplified as:

$$\left(T_{a_i} - \alpha_i T_{b_i}\right)\left(T_{a_i} - T_{c_i}\right) + \gamma_i T_{a_i}T_{c_i}. \tag{7.30}$$

By exploiting (7.30), it is easy to show that $\gamma_i T_{a_i}T_{c_i} > 0$, and

$$\left(T_{a_i} - \alpha_i T_{b_i}\right)\left(T_{a_i} - T_{c_i}\right) > 0,$$

since, by assumption, $T_{a_i} - T_{c_i} < 0$, and according to Table 7.1, $T_{a_i} - \alpha_i T_{b_i} < 0$.

Therefore, also the term in (7.28) is always greater than zero. □

Consider now the linear change of coordinates $\overline{\boldsymbol{x}}_{\boldsymbol{p}_{\boldsymbol{t}_i}} = \boldsymbol{E}_{\boldsymbol{t}_i}\boldsymbol{x}_{\boldsymbol{p}_{\boldsymbol{t}_i}}$, in which

$$\boldsymbol{E}_{\boldsymbol{t}_i} = \begin{bmatrix} \boldsymbol{N}_{\boldsymbol{t}_i}^T \\ \boldsymbol{C}_{\boldsymbol{t}_i} \end{bmatrix} = \begin{bmatrix} 1 & 0 & -\alpha_i/\gamma_i & 1 \\ 0 & 1 & -\beta_i/\gamma_i & 1 \\ 1 & -\alpha_i/\beta_i & 0 & 1 \\ \alpha_i & \beta_i & \gamma_i & 0 \end{bmatrix}, \tag{7.31}$$

where the submatrix $\boldsymbol{N}_{\boldsymbol{t}_i}$ spans the null-space of the vector $\boldsymbol{C}_{\boldsymbol{t}_i}$ [SEFL14b]. By introducing the following vectors and matrices,

$$\overline{\boldsymbol{A}}_{\boldsymbol{t}_i} = \boldsymbol{E}_{\boldsymbol{t}_i}\boldsymbol{A}_{\boldsymbol{t}_i}\boldsymbol{E}_{\boldsymbol{t}_i}^{-1}, \tag{7.32}$$

$$\overline{\boldsymbol{C}}_{\boldsymbol{t}_i} = \boldsymbol{C}_{\boldsymbol{t}_i}\boldsymbol{E}_{\boldsymbol{t}_i}^{-1} = \left[0\ 0\ 0\ 1\right], \tag{7.33}$$

$$\overline{\boldsymbol{B}}_{\boldsymbol{t}_i} = \boldsymbol{E}_{\boldsymbol{t}_i}\boldsymbol{B}_{\boldsymbol{t}_i}, \qquad \overline{\boldsymbol{M}}_{\boldsymbol{t}_i} = \boldsymbol{E}_{\boldsymbol{t}_i}\boldsymbol{M}_{\boldsymbol{t}_i}, \tag{7.34}$$

then, the system (7.7) can be rewritten as

$$\begin{aligned} \dot{\overline{\boldsymbol{x}}}_{\boldsymbol{p}_{\boldsymbol{t}_i}} &= \overline{\boldsymbol{A}}_{\boldsymbol{t}_i}\overline{\boldsymbol{x}}_{\boldsymbol{p}_{\boldsymbol{t}_i}} + \overline{\boldsymbol{B}}_{\boldsymbol{t}_i}u_i + \overline{\boldsymbol{M}}_{\boldsymbol{t}_i}\omega_i \\ \overline{y}_{t_{i_1}} &= \overline{\boldsymbol{C}}_{\boldsymbol{t}_i}\overline{\boldsymbol{x}}_{\boldsymbol{p}_{\boldsymbol{t}_i}}. \end{aligned} \tag{7.35}$$

Note that according to equations (7.4) and (7.5), it yields $\boldsymbol{M}_{\boldsymbol{t}_i} = -\frac{1}{R_i}\boldsymbol{B}_{\boldsymbol{t}_i}$. Therefore, also the relation $\overline{\boldsymbol{M}}_{\boldsymbol{t}_i} = -\frac{1}{R_i}\overline{\boldsymbol{B}}_{\boldsymbol{t}_i}$ holds, and equations (7.35) can be rewritten as follows

$$\begin{aligned} \dot{\overline{\boldsymbol{x}}}_{\boldsymbol{p}_{\boldsymbol{t}_i}} &= \overline{\boldsymbol{A}}_{\boldsymbol{t}_i}\overline{\boldsymbol{x}}_{\boldsymbol{p}_{\boldsymbol{t}_i}} + \overline{\boldsymbol{B}}_{\boldsymbol{t}_i}\left(u_i - \frac{\omega_i}{R_i}\right) \\ \overline{y}_{t_{i_1}} &= \overline{\boldsymbol{C}}_{\boldsymbol{t}_i}\overline{\boldsymbol{x}}_{\boldsymbol{p}_{\boldsymbol{t}_i}}. \end{aligned} \tag{7.36}$$

Consider now the following sliding mode observer

$$\dot{\hat{\boldsymbol{x}}}_{\boldsymbol{p_{t_i}}} = \overline{\boldsymbol{A}}_{\boldsymbol{t_i}}\hat{\boldsymbol{x}}_{\boldsymbol{p_{t_i}}} + \overline{\boldsymbol{B}}_{\boldsymbol{t_i}}\left(u_i - \frac{\hat{\omega}_i}{R_i}\right) - \boldsymbol{G}_{\boldsymbol{t_i}}\overline{\boldsymbol{C}}_{\boldsymbol{t_i}}\boldsymbol{e}_{\boldsymbol{p_{t_i}}} - \overline{\boldsymbol{B}}_{\boldsymbol{t_i}}\rho_{t_i}\frac{F_i\overline{\boldsymbol{C}}_{\boldsymbol{t_i}}\boldsymbol{e}_{\boldsymbol{p_{t_i}}}}{\left|F_i\overline{\boldsymbol{C}}_{\boldsymbol{t_i}}\boldsymbol{e}_{\boldsymbol{p_{t_i}}}\right|}, \tag{7.37}$$

where $\boldsymbol{e}_{\boldsymbol{p_{t_i}}} \triangleq \hat{\boldsymbol{x}}_{\boldsymbol{p_{t_i}}} - \overline{\boldsymbol{x}}_{\boldsymbol{p_{t_i}}}$, $F_i \in \mathbb{R}$, $\rho_{t_i} \in \mathbb{R}_+$ is a positive design constant, $\boldsymbol{G}_{\boldsymbol{t_i}}$ is a design matrix, and $\hat{\omega}_i$ is the estimated value of the frequency deviation ω_i, communicated by the sub-optimal observer for the generator of the same plant. From the development in Section 7.2, it is reasonable to assume that

$$\psi_i \triangleq (\hat{\omega}_i - \omega_i)/R_i = e_{\omega_i}/R_i \tag{7.38}$$

is a bounded disturbance, which means that its modulus is upper-bounded. Moreover, ψ_i converges to zero by virtue of Theorem 7.1. The following Theorem holds.

Theorem 7.3 (Estimation of $\overline{\boldsymbol{x}}_{\boldsymbol{p_{t_i}}}$). *Given the thermal turbine-governor dynamics (7.36), suppose that for a positive definite symmetric matrix $\overline{\boldsymbol{P}}_{\boldsymbol{i}}$, one has*

$$\overline{\boldsymbol{P}}_{\boldsymbol{i}}\overline{\boldsymbol{A}}_{\boldsymbol{0_{t_i}}} + \overline{\boldsymbol{A}}_{\boldsymbol{0_{t_i}}}^T\overline{\boldsymbol{P}}_{\boldsymbol{i}} \prec \boldsymbol{0}, \tag{7.39}$$

where $\overline{\boldsymbol{A}}_{\boldsymbol{0_{t_i}}} \triangleq \overline{\boldsymbol{A}}_{\boldsymbol{t_i}} - \boldsymbol{G}_{\boldsymbol{t_i}}\overline{\boldsymbol{C}}_{\boldsymbol{t_i}}$ and the following structural constraint [ES94] is fulfilled

$$\overline{\boldsymbol{P}}_{\boldsymbol{i}}\overline{\boldsymbol{B}}_{\boldsymbol{t_i}} = \overline{\boldsymbol{C}}_{\boldsymbol{t_i}}^T F_i. \tag{7.40}$$

Then, the sliding mode observer in the form of (7.37) asymptotically leads to a correct state estimation of $\overline{\boldsymbol{x}}_{\boldsymbol{p_{t_i}}}$ provided that the positive design constant ρ_{t_i} is chosen such that

$$\rho_{t_i} > |\psi_i|\,. \tag{7.41}$$

Proof. By subtracting the first line of (7.36) to (7.37), the so-called error system dynamics can be obtained as follows

$$\dot{\boldsymbol{e}}_{\boldsymbol{p_{t_i}}} = \overline{\boldsymbol{A}}_{\boldsymbol{0_{t_i}}}\boldsymbol{e}_{\boldsymbol{p_{t_i}}} - \overline{\boldsymbol{B}}_{\boldsymbol{t_i}}\psi_i - \overline{\boldsymbol{B}}_{\boldsymbol{t_i}}\rho_{t_i}\frac{F_i\overline{\boldsymbol{C}}_{\boldsymbol{t_i}}\boldsymbol{e}_{\boldsymbol{p_{t_i}}}}{\left|F_i\overline{\boldsymbol{C}}_{\boldsymbol{t_i}}\boldsymbol{e}_{\boldsymbol{p_{t_i}}}\right|}, \tag{7.42}$$

Equation (7.42) is in the standard form of the perturbed sliding mode observer error dynamics [SEFL14b], with the associated sliding manifold $\sigma_i = F_i\overline{\boldsymbol{C}}_{\boldsymbol{t_i}}\boldsymbol{e}_{\boldsymbol{p_{t_i}}} = 0$ to be reached in a finite time. The aim here is to show, in analogy to [SEFL14b], that the function $V_{p_{t_i}}(\boldsymbol{e}_{\boldsymbol{p_{t_i}}}) \triangleq \boldsymbol{e}_{\boldsymbol{p_{t_i}}}^T\overline{\boldsymbol{P}}_{\boldsymbol{i}}\boldsymbol{e}_{\boldsymbol{p_{t_i}}}$ is a Lyapunov function for the system (7.42), ensuring that the point $\boldsymbol{e}_{\boldsymbol{p_{t_i}}} = \boldsymbol{0}$ is an asymptotically stable equilibrium point. It is immediate to show that $V_{p_{t_i}}(\boldsymbol{0}) = 0$. Moreover, by differentiating with respect to time $V_{p_{t_i}}$, it yields

$$\begin{aligned}
\dot{V}_{p_{t_i}} &= \dot{\boldsymbol{e}}_{\boldsymbol{p_{t_i}}}^T\overline{\boldsymbol{P}}_{\boldsymbol{i}}\boldsymbol{e}_{\boldsymbol{p_{t_i}}} + \boldsymbol{e}_{\boldsymbol{p_{t_i}}}^T\overline{\boldsymbol{P}}_{\boldsymbol{i}}\dot{\boldsymbol{e}}_{\boldsymbol{p_{t_i}}} \\
&= \boldsymbol{e}_{\boldsymbol{p_{t_i}}}^T\left(\overline{\boldsymbol{P}}_{\boldsymbol{i}}\overline{\boldsymbol{A}}_{\boldsymbol{0_{t_i}}} + \overline{\boldsymbol{A}}_{\boldsymbol{0_{t_i}}}^T\overline{\boldsymbol{P}}_{\boldsymbol{i}}\right)\boldsymbol{e}_{\boldsymbol{p_{t_i}}} - 2\boldsymbol{e}_{\boldsymbol{p_{t_i}}}^T\overline{\boldsymbol{P}}_{\boldsymbol{i}}\overline{\boldsymbol{B}}_{\boldsymbol{t_i}}\psi_i \\
&\quad - 2\boldsymbol{e}_{\boldsymbol{p_{t_i}}}^T\overline{\boldsymbol{P}}_{\boldsymbol{i}}\overline{\boldsymbol{P}}_{\boldsymbol{i}}^{-1}\overline{\boldsymbol{C}}_{\boldsymbol{t_i}}^T F_i\rho_{t_i}\frac{F_i\overline{\boldsymbol{C}}_{\boldsymbol{t_i}}\boldsymbol{e}_{\boldsymbol{p_{t_i}}}}{\left|F_i\overline{\boldsymbol{C}}_{\boldsymbol{t_i}}\boldsymbol{e}_{\boldsymbol{p_{t_i}}}\right|}.
\end{aligned} \tag{7.43}$$

By exploiting equation (7.43), one has that $\dot{V}_{p_{t_i}}(\mathbf{0}) = 0$. Consider now $\boldsymbol{e}_{\boldsymbol{p_{t_i}}} \neq \mathbf{0}$. By virtue of (7.39), it yields

$$\boldsymbol{e}_{\boldsymbol{p_{t_i}}}^T \left(\overline{\boldsymbol{P}}_{\boldsymbol{i}} \overline{\boldsymbol{A}}_{\mathbf{0}_{\boldsymbol{t_i}}} + \overline{\boldsymbol{A}}_{\mathbf{0}_{\boldsymbol{t_i}}}^T \overline{\boldsymbol{P}}_{\boldsymbol{i}} \right) \boldsymbol{e}_{\boldsymbol{p_{t_i}}} < 0, \quad \forall \boldsymbol{e}_{\boldsymbol{p_{t_i}}} \neq 0. \tag{7.44}$$

By using (7.40) and (7.44), after few algebraic simplifications in (7.43), the following inequality yields

$$\dot{V}_{p_{t_i}} \leq -2\boldsymbol{e}_{\boldsymbol{p_{t_i}}}^T \left(\overline{\boldsymbol{C}}_{\boldsymbol{t_i}}^T F_i \psi_i + \overline{\boldsymbol{C}}_{\boldsymbol{t_i}}^T F_i \rho_{t_i} \frac{F_i \overline{\boldsymbol{C}}_{\boldsymbol{t_i}} \boldsymbol{e}_{\boldsymbol{p_{t_i}}}}{\left| F_i \overline{\boldsymbol{C}}_{\boldsymbol{t_i}} \boldsymbol{e}_{\boldsymbol{p_{t_i}}} \right|} \right). \tag{7.45}$$

Multiplying and dividing the term $\overline{\boldsymbol{C}}_{\boldsymbol{t_i}}^T F_i \psi_i$ by $F_i \overline{\boldsymbol{C}}_{\boldsymbol{t_i}} \boldsymbol{e}_{\boldsymbol{p_{t_i}}}$, which is different from zero in our case, one can rewrite inequality (7.45) as follows

$$\dot{V}_{p_{t_i}} \leq -2\boldsymbol{e}_{\boldsymbol{p_{t_i}}}^T \overline{\boldsymbol{C}}_{\boldsymbol{t_i}}^T F_i \left(\frac{\psi_i}{F_i \overline{\boldsymbol{C}}_{\boldsymbol{t_i}} \boldsymbol{e}_{\boldsymbol{p_{t_i}}}} + \frac{\rho_{t_i}}{\left| F_i \overline{\boldsymbol{C}}_{\boldsymbol{t_i}} \boldsymbol{e}_{\boldsymbol{p_{t_i}}} \right|} \right) F_i \overline{\boldsymbol{C}}_{\boldsymbol{t_i}} \boldsymbol{e}_{\boldsymbol{p_{t_i}}}. \tag{7.46}$$

Considering the scalar nature of the terms ψ_i and ρ_{t_i}, the right hand side of inequality (7.46) is strictly negative if

$$\frac{\rho_{t_i}}{\left| F_i \overline{\boldsymbol{C}}_{\boldsymbol{t_i}} \boldsymbol{e}_{\boldsymbol{p_{t_i}}} \right|} > -\frac{\psi_i}{F_i \overline{\boldsymbol{C}}_{\boldsymbol{t_i}} \boldsymbol{e}_{\boldsymbol{p_{t_i}}}}, \tag{7.47}$$

which is surely fulfilled if

$$\frac{\rho_{t_i}}{\left| F_i \overline{\boldsymbol{C}}_{\boldsymbol{t_i}} \boldsymbol{e}_{\boldsymbol{p_{t_i}}} \right|} > \frac{|\psi_i|}{\left| F_i \overline{\boldsymbol{C}}_{\boldsymbol{t_i}} \boldsymbol{e}_{\boldsymbol{p_{t_i}}} \right|}, \tag{7.48}$$

or in other words

$$\rho_{t_i} > |\psi_i|\,. \tag{7.49}$$

By virtue of the Lyapunov Theorem [Kha96], $\boldsymbol{e}_{\boldsymbol{p_{t_i}}} = \mathbf{0}$ is an asymptotically stable equilibrium point, and therefore, a correct state estimation of the unmeasured state variables can be performed. It is worth noting that although $\boldsymbol{e}_{\boldsymbol{p_{t_i}}} = \mathbf{0}$ is asymptotically reached, according to [SEFL14b], $\overline{\boldsymbol{C}}_{\boldsymbol{t_i}} \boldsymbol{e}_{\boldsymbol{p_{t_i}}} = 0$ is reached in a finite time. □

It is worth underlining that a detailed algorithm to numerically solve the Linear Matrix Inequality in (7.39) combined with the linear constraint (7.40) has been provided in the literature (see for instance [ES94]), and is not reported here for the sake of simplicity.

Note that the estimate $\hat{\boldsymbol{x}}_{\boldsymbol{p_{t_i}}}$ has to be transformed according to the linear relation $\hat{\boldsymbol{x}}_{\boldsymbol{p_{t_i}}}^{\text{real}} = \boldsymbol{E}_{\boldsymbol{t_i}}^{-1} \hat{\boldsymbol{x}}_{\boldsymbol{p_{t_i}}}$ in order to obtain the estimates in the physical coordinates reference, which can be easily done in practice.

7.4 Sliding Mode Observer for Hydraulic Turbine and Governor

In this section, a sliding mode observer is designed to estimate the unmeasured state variables for the hydraulic turbine-governor dynamics. Since the design procedure is similar to the one discussed in Section 7.3, only the relevant key-ideas are here reported.

In order to design a sliding mode observer to estimate the governor power variation, the transient compensator power variation and the water speed, it is necessary to verify the observability of the pair $(\boldsymbol{A_{h_i}}, \boldsymbol{C_{h_i}})$.

Theorem 7.4 (Observability of $(\boldsymbol{A_{h_i}}, \boldsymbol{C_{h_i}})$). *The pair $(\boldsymbol{A_{h_i}}, \boldsymbol{C_{h_i}})$ in (7.9)-(7.10) is observable.*

Proof. In order to ensure that pair $(\boldsymbol{A_{h_i}}, \boldsymbol{C_{h_i}})$ in (7.9)- (7.10) is observable, one has to compute the Observability Matrix $\mathcal{O}_{h_i}$ and to ensure that its determinant $\det(\mathcal{O}_{h_i})$ is different from zero [Kha96]. One has

$$\det(\mathcal{O}_{h_i}) = 24\frac{(T_{g_i} + T_{t_i})\left(T_{c_{2_i}} + T_{h_i}\right)\left(T_{g_i} - T_{h_{1_i}}\right)\left(T_{c_{1_i}} - T_{c_{2_i}}\right)}{T_{g_i}^2 T_{c_{2_i}} T_{h_i}^3}. \tag{7.50}$$

The right side of (7.50) can be equal to zero only if $T_{g_i} = T_{h_{1_i}}$ or $T_{c_{1_i}} = T_{c_{2_i}}$. These two equalities are not acceptable according to the order of magnitude of the considered time constants. To this end, we let the reader refers to Table 7.1. □

Consider now the linear change of coordinates $\overline{\boldsymbol{x}}_{\boldsymbol{p_{h_i}}} = \boldsymbol{E_{h_i}} \boldsymbol{x_{p_{h_i}}}$, in which

$$\boldsymbol{E_{h_i}} = \begin{bmatrix} \boldsymbol{N_{h_i}^T} \\ \boldsymbol{C_{h_i}} \end{bmatrix} = \begin{bmatrix} \frac{T_{c_{2_i}}}{2T_{c_{1_i}}} & \frac{T_{c_{2_i}}^2}{2\left(T_{c_{1_i}} - T_{c_{2_i}}\right)} & 0 \\ \frac{T_{c_{2_i}}}{2T_{c_{1_i}}} & 0 & -\frac{T_{h_i}}{6} \\ -2\frac{T_{c_{1_i}}}{T_{c_{2_i}}} & 2\frac{T_{c_{1_i}} - T_{c_{2_i}}}{T_{c_{2_i}}^4} & \frac{6}{T_{h_i}} \end{bmatrix}, \tag{7.51}$$

where the submatrix $\boldsymbol{N_{h_i}}$ spans the null-space of the vector $\boldsymbol{C_{h_i}}$ [SEFL14b]. By introducing the following vectors and matrices,

$$\overline{\boldsymbol{A}}_{\boldsymbol{h_i}} = \boldsymbol{E_{h_i}} \boldsymbol{A_{h_i}} \boldsymbol{E_{h_i}^{-1}}, \tag{7.52}$$

$$\overline{\boldsymbol{C}}_{\boldsymbol{h_i}} = \boldsymbol{C_{h_i}} \boldsymbol{E_{h_i}^{-1}} = \begin{bmatrix} 0 \ 0 \ 1 \end{bmatrix}, \tag{7.53}$$

$$\overline{\boldsymbol{B}}_{\boldsymbol{h_i}} = \boldsymbol{E_{h_i}} \boldsymbol{B_{h_i}}, \quad \overline{\boldsymbol{M}}_{\boldsymbol{h_i}} = \boldsymbol{E_{h_i}} \boldsymbol{M_{h_i}} = -\frac{1}{R_i} \boldsymbol{E_{h_i}} \boldsymbol{B_{h_i}}, \tag{7.54}$$

then, the system (7.12) can be rewritten as

$$\begin{aligned} \dot{\overline{\boldsymbol{x}}}_{\boldsymbol{p_{h_i}}} &= \overline{\boldsymbol{A}}_{\boldsymbol{h_i}} \overline{\boldsymbol{x}}_{\boldsymbol{p_{t_i}}} + \overline{\boldsymbol{B}}_{\boldsymbol{h_i}} \left(u_i - \frac{\omega_i}{R_i} \right) \\ \overline{y}_{h_i} &= \overline{\boldsymbol{C}}_{\boldsymbol{h_i}} \overline{\boldsymbol{x}}_{\boldsymbol{h_i}}. \end{aligned} \tag{7.55}$$

In perfect analogy to Section 7.3, the following observer can be introduced

$$\dot{\hat{\boldsymbol{x}}}_{\boldsymbol{p_{h_i}}} = \overline{\boldsymbol{A}}_{\boldsymbol{h_i}} \hat{\boldsymbol{x}}_{\boldsymbol{p_{h_i}}} + \overline{\boldsymbol{B}}_{\boldsymbol{h_i}} \left(u_i - \frac{\hat{\omega}_i}{R_i} \right) - \boldsymbol{G}_{\boldsymbol{h_i}} \overline{\boldsymbol{C}}_{\boldsymbol{h_i}} \boldsymbol{e}_{\boldsymbol{p_{h_i}}} - \overline{\boldsymbol{B}}_{\boldsymbol{h_i}} \rho_{h_i} \frac{F_i \overline{\boldsymbol{C}}_{\boldsymbol{h_i}} \boldsymbol{e}_{\boldsymbol{p_{h_i}}}}{\left| F_i \overline{\boldsymbol{C}}_{\boldsymbol{h_i}} \boldsymbol{e}_{\boldsymbol{p_{h_i}}} \right|}, \tag{7.56}$$

where $\boldsymbol{e}_{\boldsymbol{p_{h_i}}} \triangleq \hat{\boldsymbol{x}}_{\boldsymbol{p_{h_i}}} - \overline{\boldsymbol{x}}_{p_{h_i}}$, $F_i \in \mathbb{R}$, $\rho_{h_i} \in \mathbb{R}_+$ is a positive design constant, $\boldsymbol{G}_{\boldsymbol{h_i}}$ is a design matrix, and $\hat{\omega}_i$ is the estimated value of the frequency deviation ω_i. The following Theorem holds.

Theorem 7.5 (Estimation of $\overline{\boldsymbol{x}}_{\boldsymbol{p_{h_i}}}$). *Given the hydraulic turbine-governor dynamics (7.55), suppose that for a positive definite symmetric matrix $\overline{\boldsymbol{P}}_{\boldsymbol{i}}$, one has*

$$\overline{\boldsymbol{P}}_{\boldsymbol{i}} \overline{\boldsymbol{A}}_{\boldsymbol{0}_{\boldsymbol{h_i}}} + \overline{\boldsymbol{A}}_{\boldsymbol{0}_{\boldsymbol{h_i}}}^T \overline{\boldsymbol{P}}_{\boldsymbol{i}} \prec 0, \tag{7.57}$$

where $\overline{\boldsymbol{A}}_{\boldsymbol{0}_{\boldsymbol{h_i}}} \triangleq \overline{\boldsymbol{A}}_{\boldsymbol{h_i}} - \boldsymbol{G}_{\boldsymbol{h_i}} \overline{\boldsymbol{C}}_{\boldsymbol{h_i}}$, and the following structural constraint is fulfilled

$$\overline{\boldsymbol{P}}_{\boldsymbol{i}} \overline{\boldsymbol{B}}_{\boldsymbol{h_i}} = \overline{\boldsymbol{C}}_{\boldsymbol{h_i}}^T F_i. \tag{7.58}$$

Then, the sliding mode observer in the form of (7.56) asymptotically leads to a correct state estimation of $\overline{\boldsymbol{x}}_{\boldsymbol{p_{h_i}}}$ provided that the positive design constant ρ_{h_i} is chosen such that

$$\rho_{h_i} > |\psi_i| \, . \tag{7.59}$$

Proof. Theorem 7.5 can be proven in perfect analogy to Theorem 7.3. □

7.5 Scalability and Resilience of Observers

The proposed estimation scheme can be easily adapted and modified in case topological changes affect the power network. For the convenience of the reader, we consider separately two possible kinds of changes. In case the changes take place simultaneously, one has to apply the following rules together.

Opening or Closing of a Power Transmission Line

As stated by Remark 7.1, the interconnection between the plants can change with respect to time. However, as detailed in Assumption 7.2, the sub-optimal sliding mode observer for the generators in each plant is designed taking into account the maximum source of uncertainty which is upper-bounded according to (7.17). This means that in case of a opening of the power transmission line linking the i-th and the j-th plant, the magnitude of uncertainty in the signals Φ_i and Φ_j decreases (see equation (7.16) to this end) and the sliding motion cannot be lost, guaranteeing a correct frequency estimation in each plant. For the same reason, if a power transmission line linking the i-th and the j-th plant is closed, all the estimation schemes do not need to be updated, as well. This is true because the gains are designed taking into account the maximum source of uncertainty.

Plugging-in of a Plant

Suppose now that a plant is plugged in a power network comprising a given number of thermal and hydroelectric power plants. This new j-th plant is linked to a given number of existing plants via power transmission lines. Let $\mathcal{N}_j$ be the set of the existing nodes directly connected to the new j-th node (considering also in this case the most conservative situation defined in Remark 7.1). Our proposed estimation scheme can be easily updated according to the following steps:

1. For the given j-th new plant, design a sliding mode observer to estimate the unmeasured state for the turbine-governor dynamics in the form of (7.37) in case of a new thermal power plant, or in the form of (7.56) in case of a new hydroelectric power plant.
2. Re-tune the gains of the preexisting sub-optimal observers for the generators of all the neighbours nodes $k \in \mathcal{N}_j$, by updating the terms Λ_k and fulfilling the tuning rules in (7.20). This is required considering that the source of uncertainty increases in the nodes directly connected to the new one (see equation (7.16)).
3. Design a new sub-optimal sliding mode observer to estimate the frequency deviation of the new k-th plant.

According to the highlighted considerations, it is clear that the proposed observer-based estimation scheme has to be updated only where topological changes occur: basically at the level of the new node and of its neighborhood. All the other observers do not need to be updated. Therefore, one can conclude that the estimation scheme is scalable in case of adding new plants and is resilient in case of changing in the operation of the power transmission lines.

7.6 Case Study

In this section, the observer-based scheme is assessed in simulation to verify its effectiveness. A power network comprising two thermal power plants and two hydroelectric power plants linked via power transmission lines is considered (see Fig. 7.3). For the sake of simplicity, in this simulation case it is assumed that each power plant is controlled only via primary frequency controller [KBL94]. This means that the control input u_i is set equal to zero in each plant during all the simulation.

The simulation time interval is of 200 seconds and the following three scenarios are considered:

1. **Scenario 6.1**, $0 \leq t < 20\,\mathrm{s}$, during which the power network is at steady state, which means that there is a perfect balance between electrical active power generation and consumption;
2. **Scenario 6.2**, $20 \leq t < 100\,\mathrm{s}$, during which, after a step variation of the active power demand in each node according to Table 7.2, the frequency decreases;
3. **Scenario 6.3**, $100 \leq t \leq 200\,\mathrm{s}$, during which the power transmission line X_{14} in Fig. 7.3 is removed.

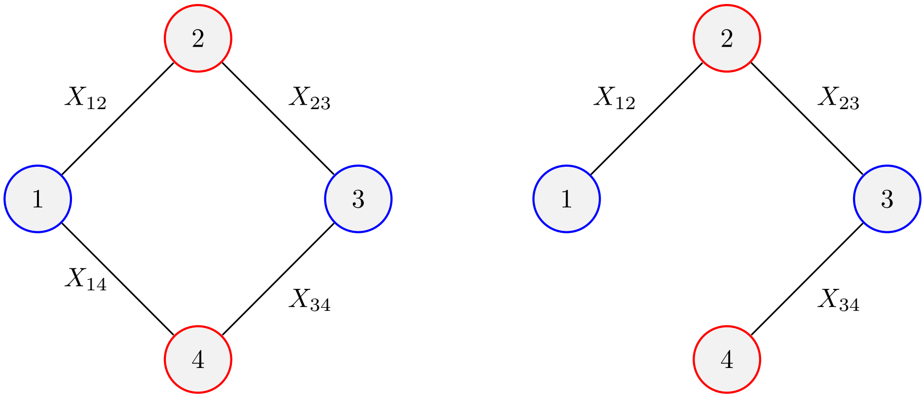

Fig. 7.3. Scheme of the considered power network comprising two thermal power plants and two hydroelectric power plants in the most conservative operation (left), and with the power transmission line X_{14} open (right). The blue circles indicate the hydroelectric power plants, whilst the red circles indicate the thermal power plants. The black arrows indicate the power transmission lines X_{ij}. The power transmission line X_{14} is open for any $t > 100$ s.

Table 7.2. Electrical Active Power Demand Variation in each plant

Plant	Demand Variation
Plant 1	0.1 (p.u.)
Plant 2	0.5 (p.u.)
Plant 3	0.2 (p.u.)
Plant 4	0.7 (p.u.)

Scenario 7.1 (Steady-state). During this scenario the power network is at steady-state. In such situation each sliding mode observer for turbine-governor dynamics and each sub-optimal sliding mode observer for the frequency deviation are capable of asymptotically estimating all the unmeasured states (see Figs. 7.4, 7.5, 7.6, 7.7). It is worth noting the presences of fast transients during the first seconds. These are due to the initial conditions of the observers which are set different from the actual states to be estimated (see again Figs. 7.4, 7.5, 7.6, 7.7).

Scenario 7.2 (Active power demand variation). During this scenario, the sudden variation of electrical active power demand P_{d_i} in each plant causes a transient during which the frequency of each generator decreases (see also equation (7.13) for a mathematical justification). All the plants, governed by the primary frequency controllers, response by increasing the electrical active power generation. All the observers are capable of tracking the time evolution of all the unmeasured state variables (see again Figs. 7.4, 7.5, 7.6, 7.7).

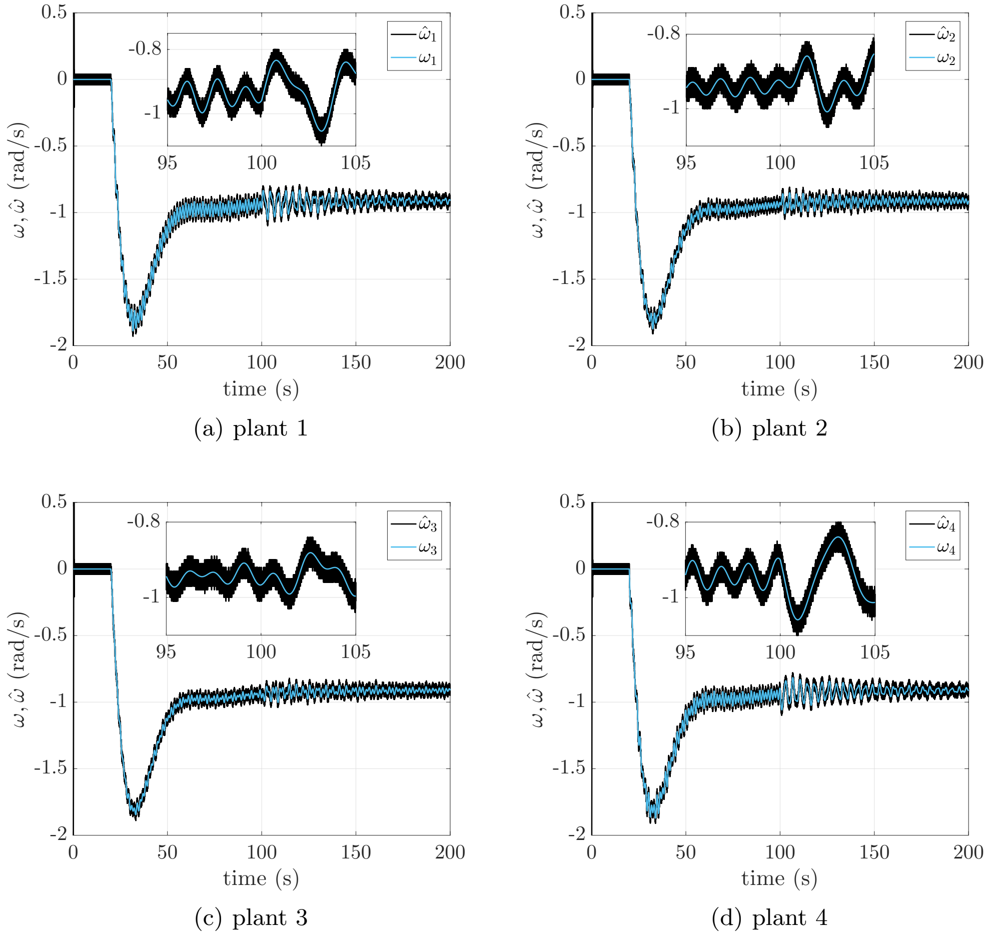

(a) plant 1 (b) plant 2

(c) plant 3 (d) plant 4

Fig. 7.4. Evolution of the of the frequency deviation ω_i in each plant and its estimated value $\hat{\omega}_i$. An enlarged view is provided for $95 \leq t \leq 105$ s.

Scenario 7.3 (Opening of the line $\{1, 4\}$). During this scenario, the power transmission line linking the 1-st plant and the 4-th plant is open. In such situation more relevant oscillations of the frequencies take place in these two plants (see the enlargements in Fig. 7.4). Also in such situation, all the observers track the unmeasured state without losing the induced sliding motion (see Figs. 7.4, 7.5, 7.6, 7.7).

7.7 Conclusions

In this chapter, a novel decentralized sliding mode observers scheme has been designed to estimate and track the unmeasured states of power networks comprising thermal and hydraulic power plants linked via power transmission lines. The flexibility of the proposed scheme to topological changes affecting the network has also been discussed. Moreover,

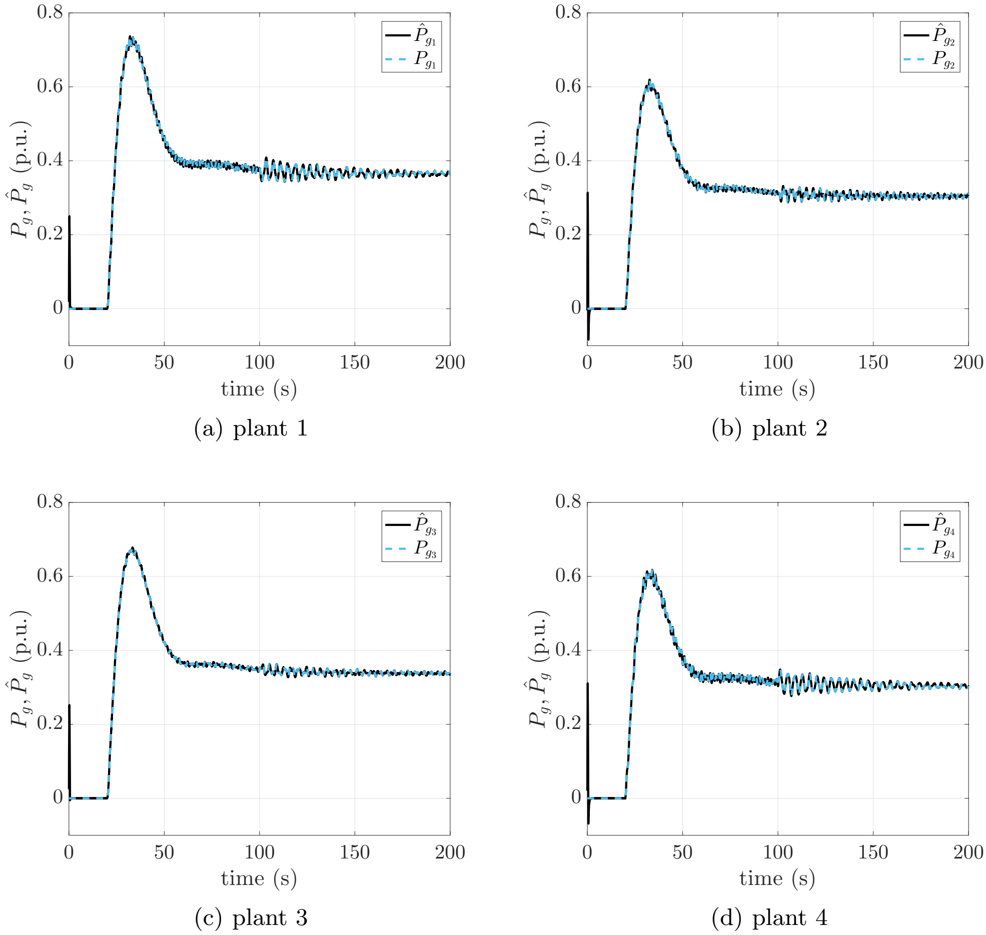

Fig. 7.5. Evolution of the of the governor power variation P_{g_i} in each plant and its estimated value $\hat{P}_{g_i}$.

the simulation performances in the discussed scenarios have validated the effectiveness of our proposal. Possible future works may involve the design of decentralized observers-based sliding mode control algorithms relying on the detailed mathematical models of the plants considered in this work.

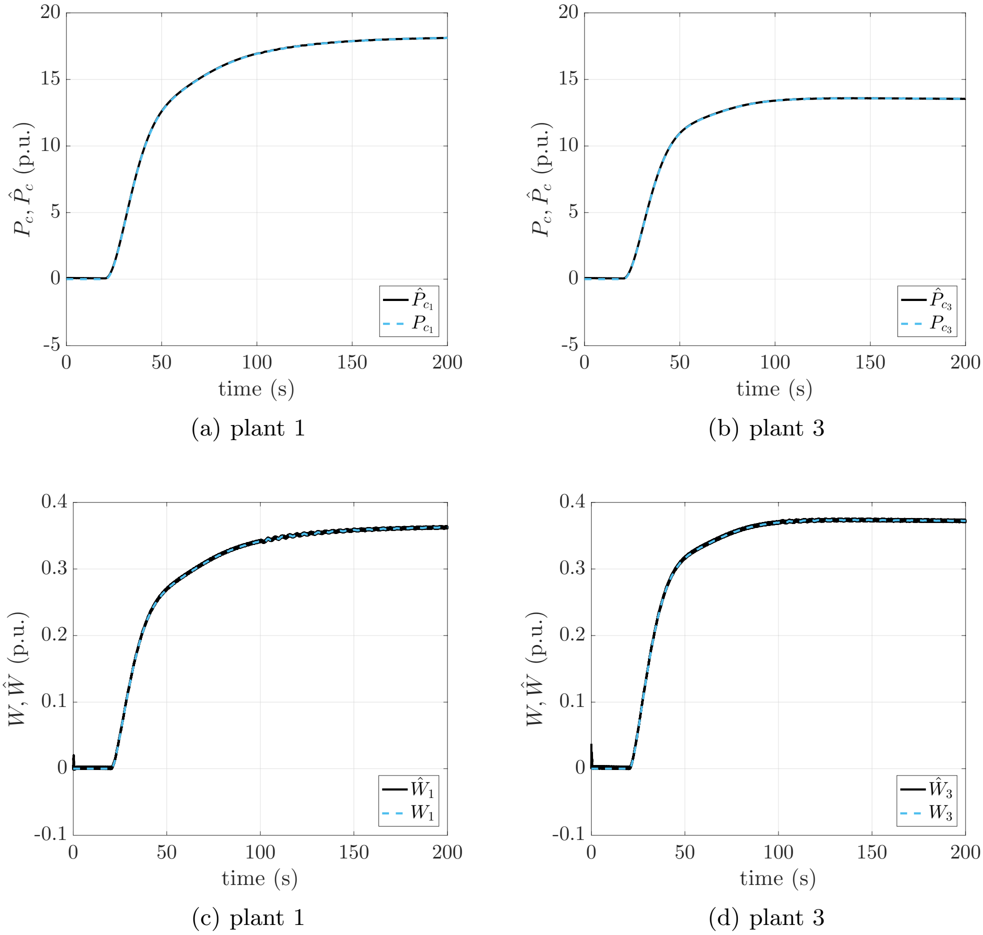

Fig. 7.6. Evolution of the transient compensator power variation P_{c_i}, and water speed variation W_i in each hydroelectric power plant and their estimated value $\hat{P}_{c_i}$ and $\hat{W}_i$.

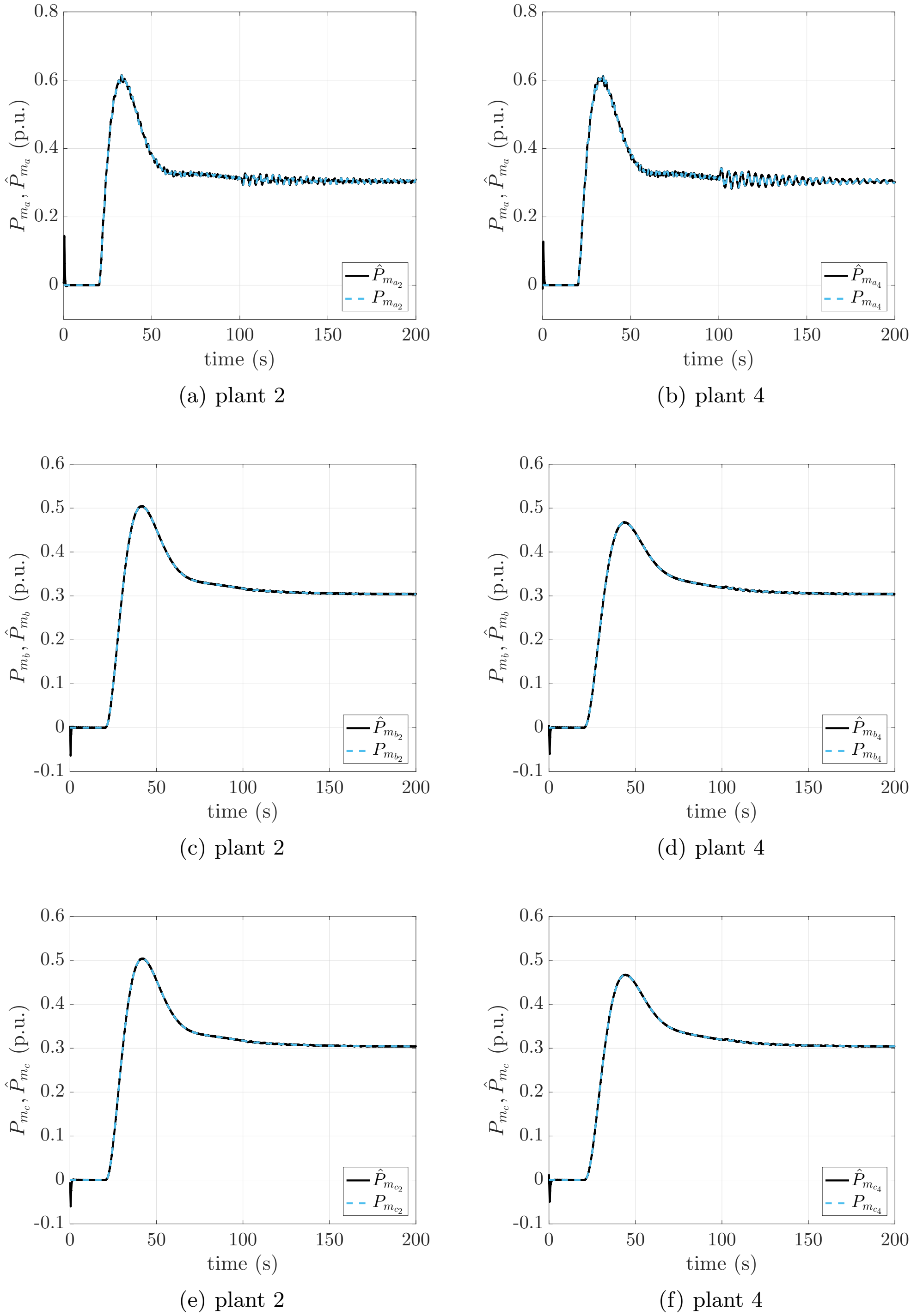

(a) plant 2 (b) plant 4

(c) plant 2 (d) plant 4

(e) plant 2 (f) plant 4

Fig. 7.7. Evolution of the turbine power variation $P_{m_{a_i}}$, $P_{m_{b_i}}$ and $P_{m_{c_i}}$ in each thermal power plant and their estimated value $\hat{P}_{m_{a_i}}$, $\hat{P}_{m_{b_i}}$ and $\hat{P}_{m_{c_i}}$.

Part III

APPLICATION TO MICROGRIDS

8

AC Microgrids

Abstract. The present chapter deals with modelling of complex microgrids and the design of advanced control strategies of sliding mode type to control them in a decentralized way. More specifically, the model of a microgrid including several distributed generation units (DGus) working in islanded operation mode (IOM), is proposed. Moreover, it takes into account the connection line parameters and it is affected by unknown load dynamics and unavoidable modelling uncertainties, which make sliding mode control algorithms suitable to solve the considered control problem. The overall control scheme is theoretically analyzed, proving the asymptotic stability of the whole microgrid system.

8.1 Preliminaries on AC Microgrids

In recent years, the increasing of energy sources of renewable type has given rise to a new paradigm in the power generation. There is a clear trend towards the realization of much smaller and geographically Distributed Generation units (DGus) [PML03], which enables to achieve technical, economical and environmental benefits, in terms of energy efficiency and reduced carbon emissions [LP04]. DGus also improve the service quality and continuity [GLLC13], by supplying at least a portion of the load, even after being disconnected from the main grid [KIL05].

In the literature, a set of multiple mutual connected DGus, which are usually strictly close to the energy consumers, is identified as a *microgrid* [Las02, PGdMA$^+$13, PKG14]. The latter, characterized by some intelligent computation and metering capability, can be considered as the basic unit of the so-called *smart grid* [AW05]. Each DGu, constituting the considered microgrid, can work in both grid-connected operation mode (GCOM) and islanded operation mode (IOM). Because of the intermittence, randomness and the uncertainty caused by meteorological factors, it is difficult to integrate renewable energy sources directly into the main grid. This is the reason why voltage control, fault detection, reliability enforcement, and power losses minimization are among the issues to solve in order to integrate DGus into the distribution network [PL06].

In past years, several control strategies have been proposed to deal with DGus. The majority of them uses traditional PI controllers in IOM [BK13]. In [KNI08], a structurally simple controller is proposed to stabilize a DGu in spite of the presence of some uncertainties. The stability properties of the algorithm proposed in [KNI08] are investigated in [KDI10], where the existence conditions, the design of the controllers and the robustness features are theoretically analyzed. Furthermore, master-slave configurations [BK13] and Plug-and-Play decentralized algorithms [RSFT15, SSK17] have been designed to manage the generation in a large scalable meshed microgrids, while an internal model approach and Bregman storage functions have been proposed in [TBD14, DM17].

The basic element V_{DC_i} of the i-th DGu is usually an energy source of renewable type, which can be represented by a direct current (DC) voltage source. The latter is interfaced with the main grid through two components: a voltage-sourced-converter (Vsc) and a filter. Usually, the first component is a Pulse Width Modulation (PWM) inverter, which converts DC to alternate current (AC), while the second component is a resistive-inductive-capacitive filter ($R_{t_i}L_{t_i}C_{t_i}$), able to extract the fundamental frequency of the Vsc output voltage. The electrical connection point of the DGu to the main grid (or to other DGus) is the so-called point of common coupling (PCC) where a local three-phase parallel resistive-inductive load (R_iL_i) is connected.

The single DGu can work in both GCOM and IOM.

8.1.1 Grid Connected Operation Mode

In this operation mode, the PCC voltage magnitude and frequency are dictated by the main grid. Thus, the system is forced to operate in stiff synchronization with the grid by using the so-called phase-locked-loop (PLL), which provides the reference angle θ for the Park's transformation [Par29]. According to the Park's transformation, the active and reactive power are expressed as

$$P_i = \frac{3}{2}(V_{d_i}I_{t_{d_i}} + V_{q_i}I_{t_{q_i}}), \quad Q_i = \frac{3}{2}(V_{q_i}I_{t_{d_i}} - V_{d_i}I_{t_{q_i}}) \tag{8.1}$$

with V_{d_i} and V_{q_i} being the direct and quadrature components of the load voltage v_i, $I_{t_{d_i}}$ and $I_{t_{q_i}}$ being the direct and quadrature components of the delivered current $\imath_{t_i}$. In order to achieve the lock with the main grid, a proportional-integral (PI) controller can be used to keep the PCC quadrature voltage component V_{q_i} equal to to zero. In such a case, the active and reactive power in (8.1) are equal to

$$P_i = \frac{3}{2}V_{d_i}I_{t_{d_i}}, \quad Q_i = -\frac{3}{2}V_{d_i}I_{t_{q_i}} \tag{8.2}$$

which depend only on the direct and quadrature current component, respectively. Hence, the DGu works in current control mode in order to supply the desired active and reactive power. According to the Park's transformation, the AC currents generated by the Vsc are referred to a synchronous rotating dq-frame and regulated like DC signals. The direct and quadrature components are compared with the corresponding current references to compute the errors, which are sent to the current controllers in order to generate the voltage references. The latter are transformed back into the stationary abc-frame according to the inverse Park's transformation, and used by the Vsc to generate the modulating signals through the comparison with a triangular carrier, according to the PWM technique.

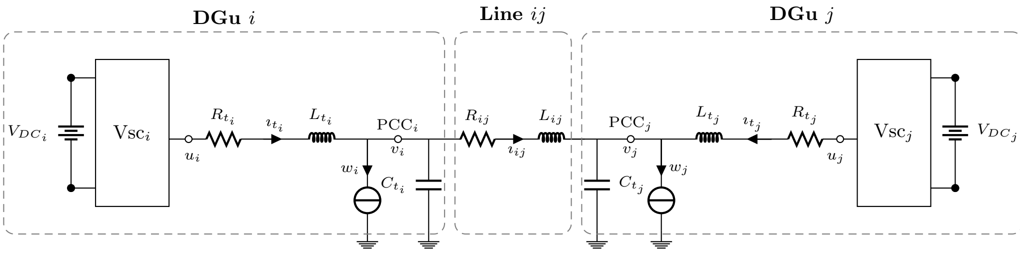

Fig. 8.1. The considered electrical single-line diagram of a typical AC microgrid composed of two DGus.

8.1.2 Islanded Operation Mode

When an islanding event occurs, the PCC voltage and frequency could deviate significantly from the rated values, due to the power mismatch between the DGu and the load. Therefore, in IOM the DGu has to provide the voltage and frequency control in order to keep the load voltage magnitude and frequency constant with respect to the reference values. According to the Park's transformation, the AC output voltages generated by the Vsc are referred to the synchronous rotating dq-frame. Then, the direct and quadrature voltage components are compared with the corresponding references to compute the errors, which are sent to the voltage controllers in order to generate the control variables. The latter are transformed back into the stationary abc-frame according to the inverse Park's transformation and used by the PWM to generate the modulating signals. In IOM the Park's transformation angle θ is provided by an internal oscillator set to the rated angular frequency, namely $\omega_0 = 2\pi f_0$. The transition from the GCOM to the IOM has to be smoothly performed to avoid system performance degradation. Thus, when the voltage control is activated, the instantaneous phase angle, provided by the PLL, in the current control mode, must be used as the initial condition for the internal oscillator. To avoid hard transients, also before the reconnection to the main grid, the PCC voltage must be resynchronized with the grid voltage, for instance as proposed in [VCR12, BLY+11]. Specifically, in this work we consider only the IOM case (we refer to [CIF15] for the GCOM case) and the frequency is controlled in open-loop by equipping each DGu in the microgrid with an internal oscillator which provides the Park's transformation angle $\theta(t) = \int_{t_0}^{t} \omega_0 d\tau$, with $\omega_0 = 2\pi f_0$, f_0 being the nominal frequency.

8.2 AC Microgrid Model

Consider a microgrid of n DGus (see Fig. 8.2 for the schematic electrical single-line diagram of a typical microgrid composed of two DGus). The network is represented by a connected and undirected graph $\mathcal{G} = (\mathcal{V}, \mathcal{E})$, where the nodes $\mathcal{V} = \{1, ..., n\}$, represent the DGus and the edges $\mathcal{E} \subset \mathcal{V} \times \mathcal{V} = \{1, ..., m\}$ represent the distribution lines interconnecting the DGus. The network structure can be represented by its corresponding incidence matrix $\boldsymbol{\mathcal{B}} \in \mathbb{R}^{n \times m}$. The ends of edge k are arbitrarily labeled with a '+' and a '-', i.e.,

$$\mathcal{B}_{ik} = \begin{cases} +1 & \text{if } i \text{ is the positive end of } k \\ -1 & \text{if } i \text{ is the negative end of } k \\ 0 & \text{otherwise .} \end{cases}$$

Consider the scheme reported in Fig. 8.2 and assume the system to be symmetric and balanced. For the sake of simplicity, the dependence of the variables on time t is omitted throughout this work. In the stationary abc-frame, by applying the Kirchhoff's current and voltage laws, the dynamics equations of the microgrid in IOM are expressed as follow,

$$\begin{aligned} [\boldsymbol{C_t}]\dot{\boldsymbol{v}} &= \boldsymbol{\imath_t} + [\boldsymbol{\mathcal{B}}]\boldsymbol{\imath} - \boldsymbol{w} \\ [\boldsymbol{L_t}]\dot{\boldsymbol{\imath}}_{\boldsymbol{t}} &= -[\boldsymbol{R_t}]\boldsymbol{\imath_t} - \boldsymbol{v} + \boldsymbol{u}, \\ [\boldsymbol{L}]\dot{\boldsymbol{\imath}} &= -[\boldsymbol{\mathcal{B}}^T]\boldsymbol{v} - [\boldsymbol{R}]\boldsymbol{\imath} \end{aligned} \tag{8.3}$$

where $\boldsymbol{s} = [\boldsymbol{s}_a^T, \boldsymbol{s}_b^T, \boldsymbol{s}_c^T]^T \in \mathbb{R}^{3n}$, $\boldsymbol{s}_\pi = [s_{\pi_1}, \dots, s_{\pi_n}]^T \in \mathbb{R}^n$, with $\pi = a, b, c$ and $\boldsymbol{s} \in \{\boldsymbol{v}, \boldsymbol{\imath_t}, \boldsymbol{w}, \boldsymbol{u}\}$, while $\boldsymbol{\imath} = [\boldsymbol{\imath}_a^T, \boldsymbol{\imath}_b^T, \boldsymbol{\imath}_c^T]^T \in \mathbb{R}^{3m}$, $\boldsymbol{\imath}_\pi = [\imath_{\pi_1}, \dots, \imath_{\pi_m}]^T \in \mathbb{R}^m$. In (8.3) $\boldsymbol{v}$, $\boldsymbol{\imath_t}$, $\boldsymbol{\imath}$, $\boldsymbol{w}$, and $\boldsymbol{u}$ represent the following three-phase signals: the loads voltages, the currents generated by the DGus, the currents along the interconnecting lines, the currents demanded by the loads, and the converters output voltages. Moreover, in system (8.3) we used $[\boldsymbol{M}]$ to denote the following block diagonal matrix

$$[\boldsymbol{M}] = \begin{bmatrix} \boldsymbol{M} & \boldsymbol{0} & \boldsymbol{0} \\ \boldsymbol{0} & \boldsymbol{M} & \boldsymbol{0} \\ \boldsymbol{0} & \boldsymbol{0} & \boldsymbol{M} \end{bmatrix},$$

where $\boldsymbol{M} \in \{\boldsymbol{C_t}, \boldsymbol{L_t}, \boldsymbol{R_t}, \boldsymbol{L}, \boldsymbol{R}\}$, with $\boldsymbol{C_t}$, $\boldsymbol{L_t}$, $\boldsymbol{R_t}$ being $n \times n$ diagonal matrices and $\boldsymbol{L}$, $\boldsymbol{R}$ being $m \times m$ diagonal matrices, e.g., $\boldsymbol{R_t} = \mathrm{diag}\{R_{t_1}, \dots, R_{t_n}\}$ and $\boldsymbol{R} = \mathrm{diag}\{R_1, \dots, R_m\}$, with $R_k = R_{ij}$.

Remark 8.1 (Kron reduction). Note that in (8.3), the load currents are located only at the PCC of each DGu (see also Fig. 8.2). However, in many cases the loads are not close to the DGus. Then, by using the well known Kron reduction method, it is possible to map arbitrary interconnections of DGus (boundary nodes) and loads (interior nodes), into a reduced network with only local loads [ZD15, DB13].

Each three-phase variable of (8.3) can be transferred to the rotating dq-frame by applying the Clarke's and Park's transformations. In the following we use $\boldsymbol{x}_{[S]}$ to denote the vector $[S_1, \dots, S_n]^T$ with $\boldsymbol{S} \in \{\boldsymbol{V}_d, \boldsymbol{V}_q, \boldsymbol{I}_{\boldsymbol{t}_d}, \boldsymbol{I}_{\boldsymbol{t}_q}\}$, and $\boldsymbol{x}_{[Z]}$ to denote the vector $[Z_1, \dots, Z_m]^T$, with $Z_k = Z_{ij}$ and $\boldsymbol{Z} \in \{\boldsymbol{I}_d, \boldsymbol{I}_q\}$. Then, the so-called state-space representation of the whole system (8.3) can be expressed as

$$
\begin{aligned}
\boldsymbol{C_t}\dot{\boldsymbol{x}}_{[V_d]} &= \omega_0 \boldsymbol{C_t}\boldsymbol{x}_{[V_q]} + \boldsymbol{x}_{[I_{t_d}]} + \boldsymbol{\mathcal{B}}\boldsymbol{x}_{[I_d]} - \boldsymbol{w}_d \\
\boldsymbol{C_t}\dot{\boldsymbol{x}}_{[V_q]} &= -\omega_0 \boldsymbol{C_t}\boldsymbol{x}_{[V_d]} + \boldsymbol{x}_{[I_{t_q}]} + \boldsymbol{\mathcal{B}}\boldsymbol{x}_{[I_q]} - \boldsymbol{w}_q \\
\boldsymbol{L_t}\dot{\boldsymbol{x}}_{[I_{t_d}]} &= -\boldsymbol{x}_{[V_d]} - \boldsymbol{R_t}\boldsymbol{x}_{[I_{t_d}]} + \omega_0 \boldsymbol{L_t}\boldsymbol{x}_{[I_{t_q}]} + \boldsymbol{u}_d \\
\boldsymbol{L_t}\dot{\boldsymbol{x}}_{[I_{t_q}]} &= -\boldsymbol{x}_{[V_q]} - \omega_0 \boldsymbol{L_t}\boldsymbol{x}_{[I_{t_d}]} - \boldsymbol{R_t}\boldsymbol{x}_{[I_{t_q}]} + \boldsymbol{u}_q \\
\boldsymbol{L}\dot{\boldsymbol{x}}_{[I_d]} &= -\boldsymbol{\mathcal{B}}^T \boldsymbol{x}_{[V_d]} - \boldsymbol{R}\boldsymbol{x}_{[I_d]} + \omega_0 \boldsymbol{L}\boldsymbol{x}_{[I_q]} \\
\boldsymbol{L}\dot{\boldsymbol{x}}_{[I_q]} &= -\boldsymbol{\mathcal{B}}^T \boldsymbol{x}_{[V_q]} - \omega_0 \boldsymbol{L}\boldsymbol{x}_{[I_d]} - \boldsymbol{R}\boldsymbol{x}_{[I_q]} \\
\boldsymbol{y}_d &= \boldsymbol{x}_{[V_d]} \\
\boldsymbol{y}_q &= \boldsymbol{x}_{[V_q]}
\end{aligned}, \tag{8.4}
$$

where $\boldsymbol{x} = \left[\boldsymbol{x}_{[V_d]}^T \, \boldsymbol{x}_{[V_q]}^T \, \boldsymbol{x}_{[I_{t_d}]}^T \, \boldsymbol{x}_{[I_{t_q}]}^T \, \boldsymbol{x}_{[I_d]}^T \, \boldsymbol{x}_{[I_q]}^T\right]^T \in \mathbb{R}^{4n+2m}$ is the state variables vector, $\boldsymbol{u} = [\boldsymbol{u}_d^T \, \boldsymbol{u}_q^T]^T \in \mathbb{R}^{2n}$ is the input vector, $\boldsymbol{w} = [\boldsymbol{w}_d^T \, \boldsymbol{w}_q^T]^T \in \mathbb{R}^{2n}$ is the disturbance vector, and $\boldsymbol{y} = [\boldsymbol{x}_{[V_d]}^T \, \boldsymbol{x}_{[V_q]}^T]^T \in \mathbb{R}^{2n}$ is the output vector. Then, the previous system can be written as

$$
\begin{aligned}
\dot{\boldsymbol{x}} &= \boldsymbol{A}\boldsymbol{x} + \boldsymbol{B}\boldsymbol{u} + \boldsymbol{B_w}\boldsymbol{w} \\
\boldsymbol{y} &= \boldsymbol{C}\boldsymbol{x}
\end{aligned}, \tag{8.5}
$$

where $\boldsymbol{A} \in \mathbb{R}^{(4n+2m)\times(4n+2m)}$ is the dynamics matrix of the microgrid, $\boldsymbol{B} \in \mathbb{R}^{(4n+2m)\times 2n}$, $\boldsymbol{B_w} \in \mathbb{R}^{(4n+2m)\times 2n}$, and $\boldsymbol{C} \in \mathbb{R}^{2n\times(4n+2m)}$, defined as

$$
\boldsymbol{A} = \begin{bmatrix}
\boldsymbol{0} & \omega_0 \mathbb{I}_n & \boldsymbol{C_t}^{-1} & \boldsymbol{0} & \boldsymbol{C_t}^{-1}\boldsymbol{\mathcal{B}} & \boldsymbol{0} \\
-\omega_0 \mathbb{I}_n & \boldsymbol{0} & \boldsymbol{0} & \boldsymbol{C_t}^{-1} & \boldsymbol{0} & \boldsymbol{C_t}^{-1}\boldsymbol{\mathcal{B}} \\
-\boldsymbol{L_t}^{-1} & \boldsymbol{0} & -\boldsymbol{L_t}^{-1}\boldsymbol{R_t} & \omega_0 \mathbb{I}_n & \boldsymbol{0} & \boldsymbol{0} \\
\boldsymbol{0} & -\boldsymbol{L_t}^{-1} & -\omega_0 \mathbb{I}_n & -\boldsymbol{L_t}^{-1}\boldsymbol{R_t} & \boldsymbol{0} & \boldsymbol{0} \\
-\boldsymbol{L}^{-1}\boldsymbol{\mathcal{B}}^T & \boldsymbol{0} & \boldsymbol{0} & \boldsymbol{0} & -\boldsymbol{L}^{-1}\boldsymbol{R} & \omega_0 \mathbb{I}_m \\
\boldsymbol{0} & -\boldsymbol{L}^{-1}\boldsymbol{\mathcal{B}}^T & \boldsymbol{0} & \boldsymbol{0} & -\omega_0 \mathbb{I}_m & -\boldsymbol{L}^{-1}\boldsymbol{R}
\end{bmatrix}, \qquad
\boldsymbol{B} = \begin{bmatrix}
\boldsymbol{0} & \boldsymbol{0} \\
\boldsymbol{0} & \boldsymbol{0} \\
\boldsymbol{L_t}^{-1} & \boldsymbol{0} \\
\boldsymbol{0} & \boldsymbol{L_t}^{-1} \\
\boldsymbol{0} & \boldsymbol{0} \\
\boldsymbol{0} & \boldsymbol{0}
\end{bmatrix},
$$

$$
\boldsymbol{B_w} = \begin{bmatrix}
-\boldsymbol{C_t}^{-1} & \boldsymbol{0} \\
\boldsymbol{0} & -\boldsymbol{C_t}^{-1} \\
\boldsymbol{0} & \boldsymbol{0} \\
\boldsymbol{0} & \boldsymbol{0} \\
\boldsymbol{0} & \boldsymbol{0} \\
\boldsymbol{0} & \boldsymbol{0}
\end{bmatrix}, \qquad
\boldsymbol{C} = \begin{bmatrix}
\mathbb{I}_n & \boldsymbol{0} & \boldsymbol{0} & \boldsymbol{0} & \boldsymbol{0} & \boldsymbol{0} \\
\boldsymbol{0} & \mathbb{I}_n & \boldsymbol{0} & \boldsymbol{0} & \boldsymbol{0} & \boldsymbol{0}
\end{bmatrix}.
$$

To permit the controller design in the next section, the following assumption is required on the state and the disturbance.

Assumption 8.1 (Available informations). The load voltages V_{d_i} and V_{q_i} are locally available at the i-th DGu, $i = 1, \dots, n$. The disturbances w_{d_i} and w_{q_i} are unknown but bounded, of class C and Lipschitz continuous.

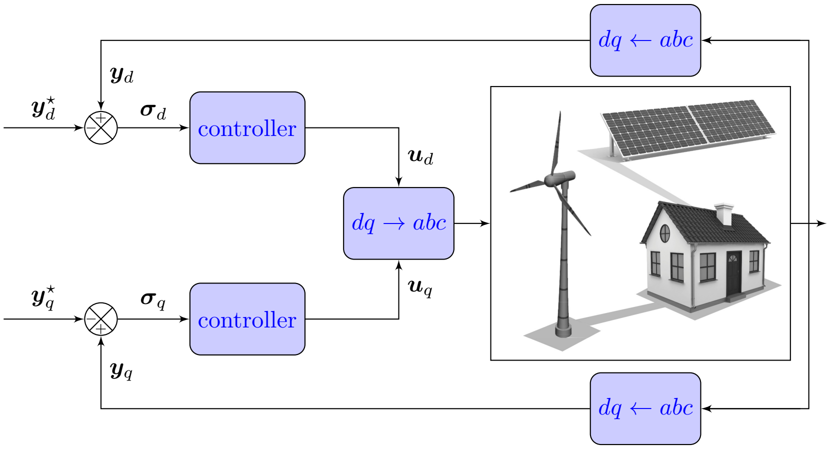

Fig. 8.2. The proposed SSOSM control scheme in IOM

Remark 8.2 (Decentralized control). Note that Assumption 8.1 requires only the local measurement of the load voltage that is used only by the controller of the i-th DGu.

Now we are in a position to formulate the control problem. *Let Assumption 8.1 hold. Given system* (8.3)-(8.5)*, design a decentralized control scheme capable of guaranteeing that the tracking error between any controlled variable and the corresponding reference is steered to zero in a finite time in spite of the uncertainties, such that the overall system is asymptotically stable.*

8.3 Decentralized Sliding Mode Voltage Control

In this section, the decentralized SSOSM control algorithm, used to solve the aforementioned control problem, is designed. Moreover, a Third Order Sliding Mode (3SM) control algorithm is proposed in order to obtain continuous control signals.

8.3.1 Suboptimal Second Order Sliding Mode (SSOSM) Control Algorithm

Consider the state-space model (8.5) and select the so-called sliding function as

$$\begin{aligned}\boldsymbol{\sigma} &= \boldsymbol{y} - \boldsymbol{y}^\star \\ &= \boldsymbol{C}\boldsymbol{x} - \boldsymbol{y}^\star,\end{aligned} \tag{8.6}$$

where $\boldsymbol{y}^\star = [\boldsymbol{x}^{\star^T}_{[V_d]}\ \boldsymbol{x}^{\star^T}_{[V_q]}]^T$ is the vector of reference values. To permit the controller design, the following assumption is required on the generation of reference values.

Assumption 8.2 (Desired voltages). The load voltage references $V^\star_{d_i}$ and $V^\star_{q_i}$ are of class C^2 and with first time derivatives Lipschitz continuous.

With reference to (8.6), it appears that the relative degree is equal to 2, so that a Second Order Sliding Mode (SOSM) control naturally applies [BFU97, BFU98a]. According to the SOSM control theory, the so-called auxiliary variables $\boldsymbol{\xi_{1}}_{\nu} = \boldsymbol{\sigma}_{\nu}$ and $\boldsymbol{\xi_{2}}_{\nu} = \dot{\boldsymbol{\sigma}}_{\nu}$, with the subscript $\nu = d, q$, have to be defined and the corresponding auxiliary systems can be expressed as

$$
\begin{aligned}
\dot{\boldsymbol{\xi}}_{\boldsymbol{1}_{\nu}} &= \boldsymbol{\xi}_{\boldsymbol{2}_{\nu}} \\
\dot{\boldsymbol{\xi}}_{\boldsymbol{2}_{\nu}} &= \boldsymbol{f}_{\nu}(\boldsymbol{x}, \boldsymbol{w}) + \boldsymbol{G}_{\nu}\boldsymbol{u}_{\nu}
\end{aligned}, \tag{8.7}
$$

where $\boldsymbol{u}_{\nu}$ are the control inputs previously defined, and $\boldsymbol{\xi}_{\boldsymbol{2}_{\nu}}$ is assumed to be unmeasurable. More specifically, one has that

$$
\begin{aligned}
\boldsymbol{f}_{d}(\boldsymbol{x}, \boldsymbol{w}) = &- \left(\omega_0^2 \mathbb{I}_n + \boldsymbol{C}_{\boldsymbol{t}}^{-1}\boldsymbol{L}_{\boldsymbol{t}}^{-1} + \boldsymbol{C}_{\boldsymbol{t}}^{-1}\boldsymbol{\mathcal{B}}\boldsymbol{L}^{-1}\boldsymbol{\mathcal{B}}^{T}\right)\boldsymbol{x}_{[V_d]} - \boldsymbol{C}_{\boldsymbol{t}}^{-1}\boldsymbol{L}_{\boldsymbol{t}}^{-1}\boldsymbol{R}_{\boldsymbol{t}}\boldsymbol{x}_{[I_{t_d}]} \\
&+ 2\omega_0 \boldsymbol{C}_{\boldsymbol{t}}^{-1}\boldsymbol{x}_{[I_{t_q}]} - \boldsymbol{C}_{\boldsymbol{t}}^{-1}\boldsymbol{\mathcal{B}}\boldsymbol{L}^{-1}\boldsymbol{R}\boldsymbol{x}_{[I_d]} + 2\omega_0 \boldsymbol{C}_{\boldsymbol{t}}^{-1}\boldsymbol{\mathcal{B}}\boldsymbol{x}_{[I_q]} \\
&- \boldsymbol{C}_{\boldsymbol{t}}^{-1}\dot{\boldsymbol{w}}_{d} - \omega_0 \boldsymbol{C}_{\boldsymbol{t}}^{-1}\boldsymbol{w}_{q} - \ddot{\boldsymbol{x}}^{\star}_{[V_d]}
\end{aligned}
$$

$$
\begin{aligned}
\boldsymbol{f}_{q}(\boldsymbol{x}, \boldsymbol{w}) = &- \left(\omega_0^2 \mathbb{I}_n + \boldsymbol{C}_{\boldsymbol{t}}^{-1}\boldsymbol{L}_{\boldsymbol{t}}^{-1} + \boldsymbol{C}_{\boldsymbol{t}}^{-1}\boldsymbol{\mathcal{B}}\boldsymbol{L}^{-1}\boldsymbol{\mathcal{B}}^{T}\right)\boldsymbol{x}_{[V_q]} - 2\omega_0 \boldsymbol{C}_{\boldsymbol{t}}^{-1}\boldsymbol{x}_{[I_{t_d}]} \\
&- \boldsymbol{C}_{\boldsymbol{t}}^{-1}\boldsymbol{L}_{\boldsymbol{t}}^{-1}\boldsymbol{R}_{\boldsymbol{t}}\boldsymbol{x}_{[I_{t_q}]} - 2\omega_0 \boldsymbol{C}_{\boldsymbol{t}}^{-1}\boldsymbol{\mathcal{B}}\boldsymbol{x}_{[I_d]} - \boldsymbol{C}_{\boldsymbol{t}}^{-1}\boldsymbol{\mathcal{B}}\boldsymbol{L}^{-1}\boldsymbol{R}\boldsymbol{x}_{[I_q]} \\
&+ \omega_0 \boldsymbol{C}_{\boldsymbol{t}}^{-1}\boldsymbol{w}_{d} - \boldsymbol{C}_{\boldsymbol{t}}^{-1}\dot{\boldsymbol{w}}_{q} - \ddot{\boldsymbol{x}}^{\star}_{[V_q]}
\end{aligned} \tag{8.8}
$$

$$
\boldsymbol{G}_{d} = \boldsymbol{G}_{q} = \boldsymbol{C}_{\boldsymbol{t}}^{-1}\boldsymbol{L}_{\boldsymbol{t}}^{-1},
$$

are allowed to be uncertain with known bounds for each entry, i.e.,

$$
|f_{\nu_i}(\cdot)| \leq F_{\nu_i}, \quad G_{\min_{\nu_i}} \leq G_{\nu_{ii}} \leq G_{\max_{\nu_i}}, \quad i = 1, \dots, n\,, \tag{8.9}
$$

with F_{ν_i}, $G_{\min_{\nu_i}}$ and $G_{\max_{\nu_i}}$, $\nu = d, q$, being positive constants. Note that, it is reasonable to assume that such bounds exist. In fact, the function $\boldsymbol{f}_{\nu}$ depends on electrical signals related to the finite power of the system, while $G_{\nu_{ii}}$ is an uncertain constant value. In practical cases, these bounds can be estimated relying on data analysis and engineering understanding.

The i-th control law, u_{ν_i} that we propose to steer $\xi_{1_{\nu_i}}$ and $\xi_{2_{\nu_i}}$, $i = 1, \dots, n$, to zero in a finite time in spite of the uncertainties, in analogy with [BFU98a], can be expressed as follows

$$
u_{\nu_i} = -\alpha_{\nu_i} U_{\max_{\nu_i}} \operatorname{sign}\left(\xi_{1_{\nu_i}} - \tfrac{1}{2}\xi_{1_{\max_{\nu_i}}}\right), \tag{8.10}
$$

with bounds

$$
U_{\max_{\nu_i}} > \max\left(\frac{F_{\nu_i}}{\alpha^{*}_{\nu_i} G_{\min_{\nu_i}}}; \frac{4F_{\nu_i}}{3G_{\min_{\nu_i}} - \alpha^{*}_{\nu_i} G_{\max_{\nu_i}}}\right) \tag{8.11}
$$

$$
\alpha^{*}_{\nu_i} \in (0, 1] \cap \left(0, \frac{3G_{\min_{\nu_i}}}{G_{\max_{\nu_i}}}\right). \tag{8.12}
$$

8.3.2 An Alternative Solution: Third Order Sliding Mode

Usually, to control inverters, the Pulse Width Modulation (PWM) technique is used. To do this, the Vsc requires continuous control signals u_{d_i} and u_{q_i}, that can be transferred back to the stationary *abc*-frame and used to generate the gating signals through the comparison with a triangular carrier. In order to obtain continuous control signals, as suggested in [BFU97], the system relative degree can be artificially increased. Then, a Third Order Sliding Mode (3SM) control law to solve the microgrid voltage control problem in question, can be introduced. Defining the auxiliary variables $\boldsymbol{\xi_1}_\nu = \boldsymbol{\sigma}_\nu$, $\boldsymbol{\xi_2}_\nu = \dot{\boldsymbol{\sigma}}_\nu$ and $\boldsymbol{\xi_3}_\nu = \ddot{\sigma}_\nu$, then the auxiliary system can be expressed as

$$\begin{aligned}\dot{\boldsymbol{\xi}}_{\boldsymbol{1}_\nu} &= \boldsymbol{\xi_2}_\nu \\ \dot{\boldsymbol{\xi}}_{\boldsymbol{2}_\nu} &= \boldsymbol{\xi_3}_\nu \\ \dot{\boldsymbol{\xi}}_{\boldsymbol{3}_\nu} &= \boldsymbol{\phi}_\nu(\boldsymbol{x}, \boldsymbol{w}, \boldsymbol{u}) + \boldsymbol{\Gamma}_\nu \boldsymbol{\mu}_\nu \\ \dot{\boldsymbol{u}}_\nu &= \boldsymbol{\mu}_\nu,\end{aligned} \tag{8.13}$$

where $\boldsymbol{\mu}_\nu$ is an auxiliary control variable, $\boldsymbol{\xi_2}_\nu$, $\boldsymbol{\xi_3}_\nu$ are assumed to be unmeasurable, while $\boldsymbol{\phi}_\nu = \dot{\boldsymbol{f}}_\nu$ and $\boldsymbol{\Gamma}_\nu = \boldsymbol{G}_\nu$ are uncertain smooth bounded functions, such that for each entry

$$|\phi_{\nu_i}(\cdot)| \leq \Phi_{\nu_i}, \quad \Gamma_{\min_{\nu_i}} \leq \Gamma_{\nu ii} \leq \Gamma_{\max_{\nu_i}}, \quad i = 1, \dots, n, \tag{8.14}$$

with Φ_{ν_i}, $\Gamma_{\min_{\nu_i}}$ and $\Gamma_{\max_{\nu_i}}$, $\nu = d, q$ being positive constants (in case of 3SM, Assumptions 8.1 and 8.2 are modified accordingly). The 3SM control algorithm requires that the discontinuous controls only affect $\boldsymbol{\sigma}_\nu^{(3)}$, but not $\ddot{\boldsymbol{\sigma}}_\nu$, so that the controls fed into the plant are continuous.

Let $\boldsymbol{s}_{\nu_i} = [\sigma_{\nu_i}, \dot{\sigma}_{\nu_i}, \ddot{\sigma}_{\nu_i}]^T$, then the i-th discontinuous control law μ_{ν_i} can be expressed as follows

$$\mu_{\nu_i} = -\alpha_{\nu_i} \begin{cases} \mu_{\nu_i,1} = \mathrm{sign}\,(\ddot{\sigma}_{\nu_i}), & \boldsymbol{s}_{\nu_i} \in \mathcal{M}_{\nu_i,1}/\mathcal{M}_{\nu_i,0} \\ \mu_{\nu_i,2} = \mathrm{sign}\,(\dot{\sigma}_{\nu_i} + \frac{\ddot{\sigma}^2_{\nu_i}\mu_{\nu_i,1}}{2\alpha_{\nu_i,r}}), & \boldsymbol{s}_{\nu_i} \in \mathcal{M}_{\nu_i,2}/\mathcal{M}_{\nu_i,1} \\ \mu_{\nu_i,3} = \mathrm{sign}\,(\psi_{\nu_i}), & \text{else} \end{cases} \tag{8.15}$$

where

$$\psi_{\nu_i} = \sigma_{\nu_i} + \frac{\ddot{\sigma}^3_{\nu_i}}{3\alpha^2_{\nu_i,r}} + \mu_{\nu_i,2}\Big[\frac{1}{\sqrt{\alpha_{\nu_i,r}}}(\mu_{\nu_i,2}\dot{\sigma}_{\nu_i} + \frac{\ddot{\sigma}^2_{\nu_i}}{2\alpha_{\nu_i,r}})^{\frac{3}{2}} + \frac{\dot{\sigma}_{\nu_i}\ddot{\sigma}_{\nu_i}}{\alpha_{\nu_i,r}}\Big], \tag{8.16}$$

with $\alpha_{\nu_i,r}$ being the reduced control amplitude, such that

$$\alpha_{\nu_i,r} = \alpha_{\nu_i}\Gamma_{\min_{\nu_i}} - \Phi_{\nu_i} > 0. \tag{8.17}$$

In (8.15) the manifolds $\mathcal{M}_{\nu_i,0}$, $\mathcal{M}_{\nu_i,1}$, $\mathcal{M}_{\nu_i,2}$ are defined as

$$\begin{aligned}\mathcal{M}_{\nu_i,0} &= \{\boldsymbol{s}_{\nu_i} \in \mathbb{R}^3 : \sigma_{\nu_i} = \dot{\sigma}_{\nu_i} = \ddot{\sigma}_{\nu_i} = 0\} \\ \mathcal{M}_{\nu_i,1} &= \{\boldsymbol{s}_{\nu_i} \in \mathbb{R}^3 : \sigma_{\nu_i} - \frac{\ddot{\sigma}^3_{\nu_i}}{6\alpha^2_{\nu_i,r}} = 0,\ \dot{\sigma}_{\nu_i} + \frac{\ddot{\sigma}_{\nu_i}|\ddot{\sigma}_{\nu_i}|}{2\alpha_{\nu_i,r}} = 0\} \\ \mathcal{M}_{\nu_i,2} &= \{\boldsymbol{s}_{\nu_i} \in \mathbb{R}^3 : \psi_{\nu_i} = 0\}.\end{aligned} \tag{8.18}$$

From (8.15), one can observe that the controller of the i-th DGu requires not only σ_{ν_i}, but also $\dot{\sigma}_{\nu_i}$ and $\ddot{\sigma}_{\nu_i}$. Yet, according to Assumption 8.1, only the load voltages V_{d_i} and V_{q_i} are measurable at the i-th DGu. Then, one can rely on Levant's second-order differentiator to retrieve $\dot{\sigma}_{\nu_i}$ and $\ddot{\sigma}_{\nu_i}$ in a finite time. With reference to system (8.13), for $\nu = d, q$, and $i = 1, \ldots, n$, one has

$$\begin{aligned}
\dot{\hat{\xi}}_{1_{\nu_i}} &= -\lambda_{0_{\nu_i}} \left| \hat{\xi}_{1_{\nu_i}} - \xi_{1_{\nu_i}} \right|^{\frac{2}{3}} \operatorname{sign}\left(\hat{\xi}_{1_{\nu_i}} - \xi_{1_{\nu_i}} \right) + \hat{\xi}_{2_{\nu_i}} \\
\dot{\hat{\xi}}_{2_{\nu_i}} &= -\lambda_{1_{\nu_i}} \left| \hat{\xi}_{2_{\nu_i}} - \dot{\hat{\xi}}_{1_{\nu_i}} \right|^{\frac{1}{2}} \operatorname{sign}\left(\hat{\xi}_{2_{\nu_i}} - \dot{\hat{\xi}}_{1_{\nu_i}} \right) + \hat{\xi}_{3_{\nu_i}} \\
\dot{\hat{\xi}}_{3_{\nu_i}} &= -\lambda_{2_{\nu_i}} \operatorname{sign}\left(\hat{\xi}_{3_{\nu_i}} - \dot{\hat{\xi}}_{2_{\nu_i}} \right),
\end{aligned} \tag{8.19}$$

where $\hat{\xi}_{1_{\nu_i}}, \hat{\xi}_{2_{\nu_i}}, \hat{\xi}_{3_{\nu_i}}$ are estimates of $\xi_{1_{\nu_i}}, \xi_{2_{\nu_i}}, \xi_{3_{\nu_i}}$, respectively, and $\lambda_{0_{\nu_i}} = 3\Lambda_{\nu_i}^{1/3}$, $\lambda_{1_{\nu_i}} = 1.5\Lambda_{\nu_i}^{1/2}$, $\lambda_{2_{\nu_i}} = 1.1\Lambda_{\nu_i}$, $\Lambda_{\nu_i} > 0$, is a possible choice of the differentiator parameters.

8.4 Stability Analysis

With reference to the proposed decentralized sliding mode control approach, the following results can be proved.

Lemma 8.1 (Convergence to the sliding manifold: SSOSM). Let Assumptions 8.1 and 8.2 hold. Given the auxiliary system (8.7) controlled via the SSOSM algorithm (8.10)-(8.12), then the sliding variables (8.6) and their first time derivatives are steered to zero in a finite time t_r, in spite of the uncertainties.

Proof. This result directly follows from [BFU98a, Theorem 1]. □

Let $\tilde{\boldsymbol{x}}$ be the error given by the difference between the state and the equilibrium point associated to the desired value of voltages $\boldsymbol{y}^\star$ when $\boldsymbol{w}$ is constant, and let $\tilde{\boldsymbol{u}}$ be the corresponding control input. Hence, the error system is defined as

$$\begin{aligned}
\dot{\tilde{\boldsymbol{x}}} &= \boldsymbol{A}\tilde{\boldsymbol{x}} + \boldsymbol{B}\tilde{\boldsymbol{u}} \\
\boldsymbol{\sigma} &= \boldsymbol{C}\tilde{\boldsymbol{x}}.
\end{aligned} \tag{8.20}$$

Theorem 8.1 (Main result). *Let Assumptions 8.1 and 8.2 hold. Consider system (8.3)-(8.5) controlled via the SSOSM control algorithm (8.10)-(8.12). Then, given constant reference $\boldsymbol{y}^\star$ and constant disturbance $\boldsymbol{w}$, $\forall\, t \geq t_r, \forall\, \boldsymbol{x}(t_r) \in \mathbb{R}^{4n+2m}$, the origin of the error system (8.20) is a robust exponentially stable equilibrium point.*

Proof. Consider the d component of the sliding variable $\boldsymbol{\sigma}_d = \tilde{\boldsymbol{x}}_{[V_d]}$. Compute now the first time derivative and the second time derivative of $\boldsymbol{\sigma}_d$, i.e.,

$$\dot{\boldsymbol{\sigma}}_d = \dot{\tilde{\boldsymbol{x}}}_{[V_d]} = \omega_0 \tilde{\boldsymbol{x}}_{[V_q]} + \boldsymbol{C_t}^{-1} \tilde{\boldsymbol{x}}_{[I_{t_d}]} + \boldsymbol{C_t}^{-1} \boldsymbol{\mathcal{B}} \tilde{\boldsymbol{x}}_{[I_d]}$$

$$\begin{aligned}\ddot{\boldsymbol{\sigma}}_d = \ddot{\tilde{\boldsymbol{x}}}_{[V_d]} = & - \left(\omega_0^2 \mathbb{I}_n + \boldsymbol{C_t}^{-1} \boldsymbol{L_t}^{-1} + \boldsymbol{C_t}^{-1} \boldsymbol{\mathcal{B}} \boldsymbol{L}^{-1} \boldsymbol{\mathcal{B}}^T\right) \tilde{\boldsymbol{x}}_{[V_d]} - \boldsymbol{C_t}^{-1} \boldsymbol{L_t}^{-1} \boldsymbol{R_t} \tilde{\boldsymbol{x}}_{[I_{t_d}]} \\ & + 2\omega_0 \boldsymbol{C_t}^{-1} \tilde{\boldsymbol{x}}_{[I_{t_q}]} - \boldsymbol{C_t}^{-1} \boldsymbol{\mathcal{B}} \boldsymbol{L}^{-1} \boldsymbol{R} \tilde{\boldsymbol{x}}_{[I_d]} + 2\omega_0 \boldsymbol{C_t}^{-1} \boldsymbol{\mathcal{B}} \tilde{\boldsymbol{x}}_{[I_q]} + \boldsymbol{C_t}^{-1} \boldsymbol{L_t}^{-1} \tilde{\boldsymbol{u}}_d.\end{aligned}$$

According to the equivalent control concept [Utk92], by posing $\ddot{\boldsymbol{\sigma}}_d = \mathbf{0}$, one obtains

$$\tilde{\boldsymbol{u}}_{d_{eq}} = \boldsymbol{R_t} \tilde{\boldsymbol{x}}_{[I_{t_d}]} - 2\omega_0 L_t \tilde{\boldsymbol{x}}_{[I_{t_q}]} + \boldsymbol{L_t} \boldsymbol{\mathcal{B}} \boldsymbol{L}^{-1} \boldsymbol{R} \tilde{\boldsymbol{x}}_{[I_d]} - 2\omega_0 \boldsymbol{L_t} \boldsymbol{\mathcal{B}} \tilde{\boldsymbol{x}}_{[I_q]}. \tag{8.21}$$

Analogously, the q component of the sliding variable $\boldsymbol{\sigma}_q = \tilde{\boldsymbol{x}}_{[V_q]}$ and its time derivatives can be computed as

$$\dot{\boldsymbol{\sigma}}_q = \dot{\tilde{\boldsymbol{x}}}_{[V_q]} = - \omega_0 \tilde{\boldsymbol{x}}_{[V_d]} + \boldsymbol{C_t}^{-1} \tilde{\boldsymbol{x}}_{[I_{t_q}]} + \boldsymbol{C_t}^{-1} \boldsymbol{\mathcal{B}} \tilde{\boldsymbol{x}}_{[I_q]}$$

$$\begin{aligned}\ddot{\boldsymbol{\sigma}}_q = \ddot{\tilde{\boldsymbol{x}}}_{[V_q]} = & - \left(\omega_0^2 \mathbb{I}_n + \boldsymbol{C_t}^{-1} \boldsymbol{L_t}^{-1} + \boldsymbol{C_t}^{-1} \boldsymbol{\mathcal{B}} \boldsymbol{L}^{-1} \boldsymbol{\mathcal{B}}^T\right) \tilde{\boldsymbol{x}}_{[V_q]} - 2\omega_0 \boldsymbol{C_t}^{-1} \tilde{\boldsymbol{x}}_{[I_{t_d}]} \\ & - \boldsymbol{C_t}^{-1} \boldsymbol{L_t}^{-1} \boldsymbol{R_t} \tilde{\boldsymbol{x}}_{[I_{t_q}]} - 2\omega_0 \boldsymbol{C_t}^{-1} \boldsymbol{\mathcal{B}} \tilde{\boldsymbol{x}}_{[I_d]} - \boldsymbol{C_t}^{-1} \boldsymbol{\mathcal{B}} \boldsymbol{L}^{-1} \boldsymbol{R} \tilde{\boldsymbol{x}}_{[I_q]} + \boldsymbol{C_t}^{-1} \boldsymbol{L_t}^{-1} \tilde{\boldsymbol{u}}_q \,.\end{aligned}$$

The corresponding equivalent control, obtained by posing $\ddot{\boldsymbol{\sigma}}_q = \mathbf{0}$ is

$$\tilde{\boldsymbol{u}}_{q_{eq}} = 2\omega_0 \boldsymbol{L_t} \tilde{\boldsymbol{x}}_{[I_{t_d}]} + \boldsymbol{R_t} \tilde{\boldsymbol{x}}_{[I_{t_q}]} + 2\omega_0 L_t \boldsymbol{\mathcal{B}} \tilde{\boldsymbol{x}}_{[I_d]} + \boldsymbol{L_t} \boldsymbol{\mathcal{B}} \boldsymbol{L}^{-1} \boldsymbol{R} \tilde{\boldsymbol{x}}_{[I_q]}. \tag{8.22}$$

Considering that, after t_r, $\boldsymbol{\sigma}_\nu = \dot{\boldsymbol{\sigma}}_\nu = \mathbf{0}$, that is $\tilde{\boldsymbol{x}}_{[V_d]} = \tilde{\boldsymbol{x}}_{[V_q]} = \dot{\tilde{\boldsymbol{x}}}_{[V_d]} = \dot{\tilde{\boldsymbol{x}}}_{[V_q]} = \mathbf{0}$, one obtains the following set of algebraic equations

$$\begin{aligned}\mathbf{0} &= \boldsymbol{C_t}^{-1} \tilde{\boldsymbol{x}}_{[I_{t_d}]} + \boldsymbol{C_t}^{-1} \boldsymbol{\mathcal{B}} \tilde{\boldsymbol{x}}_{[I_d]} \\ \mathbf{0} &= \boldsymbol{C_t}^{-1} \tilde{\boldsymbol{x}}_{[I_{t_q}]} + \boldsymbol{C_t}^{-1} \boldsymbol{\mathcal{B}} \tilde{\boldsymbol{x}}_{[I_q]}\end{aligned}. \tag{8.23}$$

Then, by using the relations in (8.23) and by substituting (8.21) and (8.22) into system (8.20), the residual dynamics results in being

$$\begin{aligned}\dot{\tilde{\boldsymbol{x}}}_{[I_{t_d}]} &= \boldsymbol{\mathcal{B}} \boldsymbol{L}^{-1} \boldsymbol{R} \tilde{\boldsymbol{x}}_{[I_d]} - \omega_0 \boldsymbol{\mathcal{B}} \tilde{\boldsymbol{x}}_{[I_q]} \\ \dot{\tilde{\boldsymbol{x}}}_{[I_{t_q}]} &= \omega_0 \boldsymbol{\mathcal{B}} \tilde{\boldsymbol{x}}_{[I_d]} + \boldsymbol{\mathcal{B}} \boldsymbol{L}^{-1} \boldsymbol{R} \tilde{\boldsymbol{x}}_{[I_q]} \\ \dot{\tilde{\boldsymbol{x}}}_{[I_d]} &= -\boldsymbol{L}^{-1} \boldsymbol{R} \tilde{\boldsymbol{x}}_{[I_d]} + \omega_0 \tilde{\boldsymbol{x}}_{[I_q]} \\ \dot{\tilde{\boldsymbol{x}}}_{[I_q]} &= -\omega_0 \tilde{\boldsymbol{x}}_{[I_d]} - \boldsymbol{L}^{-1} \boldsymbol{R} \tilde{\boldsymbol{x}}_{[I_q]}.\end{aligned} \tag{8.24}$$

Note that, since the relative degree of the system is $r = 2$, the original system with $4n+2m$ dynamic independent equations, $\forall\, t \geq t_r$, can be described by the $4n$ sliding constraints $\boldsymbol{\sigma}_d = \boldsymbol{\sigma}_q = \dot{\boldsymbol{\sigma}}_d = \dot{\boldsymbol{\sigma}}_q = \mathbf{0}$, and by $2m$ independent dynamic equations. More specifically, the resulting order reduction dynamics can be represented by the last two equations related to the distribution lines dynamics, i.e.,

$$\begin{bmatrix} \dot{\tilde{\boldsymbol{x}}}_{[I_d]} \\ \dot{\tilde{\boldsymbol{x}}}_{[I_q]} \end{bmatrix} = \tilde{\boldsymbol{A}} \begin{bmatrix} \tilde{\boldsymbol{x}}_{[I_d]} \\ \tilde{\boldsymbol{x}}_{[I_q]} \end{bmatrix} = \begin{bmatrix} -\boldsymbol{L}^{-1}\boldsymbol{R} & \omega_0 \mathbb{I}_m \\ -\omega_0 \mathbb{I}_m & -\boldsymbol{L}^{-1}\boldsymbol{R} \end{bmatrix} \begin{bmatrix} \tilde{\boldsymbol{x}}_{[I_d]} \\ \tilde{\boldsymbol{x}}_{[I_q]} \end{bmatrix}, \tag{8.25}$$

where the matrix $\tilde{\boldsymbol{A}}$ is Hurwitz so that $\tilde{\boldsymbol{x}}_{[I_d]}$ and $\tilde{\boldsymbol{x}}_{[I_q]}$ exponentially converge to zero. Then, from the algebraic equations (8.23), one can observe that also $\tilde{\boldsymbol{x}}_{[I_{td}]}$ and $\tilde{\boldsymbol{x}}_{[I_{tq}]}$ exponentially converge to zero, which concludes the proof. □

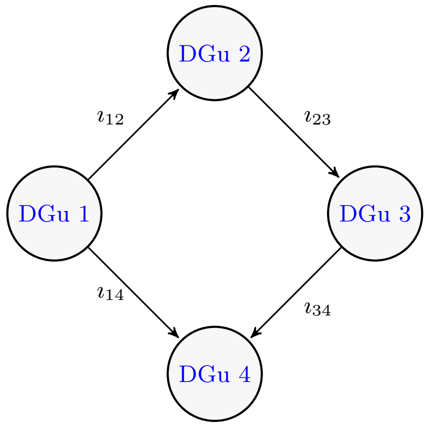

Fig. 8.3. Scheme of the considered microgrid composed of 4 DGus. The solid arrows indicate the positive direction of the currents flows through the distribution network.

Lemma 8.2 (Convergence to the sliding manifold: 3SM). Let Assumptions 8.1 and 8.2 hold. Let assume $t_0 \geq t_{Ld}$, t_0, t_{Ld} being the initial time instant and the finite time necessary for the convergence of the Levant's differentiator (8.19), respectively. Given the auxiliary system (8.13) controlled via the 3SM control law (8.15)-(8.18), then the sliding variables (8.6) and their first and second time derivatives are steered to zero in a finite time t_r, in spite of the uncertainties.

Proof. This result directly follows from [DF09, Theorem 2]. □

Theorem 8.2. *Let Assumptions 8.1 and 8.2 hold. Consider system* (8.3)-(8.5) *controlled via the 3-SM control law* (8.15)-(8.18)*. Then, given constant reference* $\boldsymbol{y}^\star$ *and constant disturbance* $\boldsymbol{w}$, $\forall\, t \geq t_r \geq t_0 \geq t_{Ld}$, $\forall\, \boldsymbol{x}(t_r) \in \mathbb{R}^{4n+2m}$*, the origin of the error system* (8.20) *is a robust exponentially stable equilibrium point.*

Proof. The proof is analogous to that of Theorem 8.1. □

8.5 Case Study

In this section, the proposed control solution is assessed in simulation by implementing the realistic model of an AC islanded microgrid with nominal frequency $f_0 = 60\,\mathrm{Hz}$, and composed of four DGus (n =4) for the sake of clarity, even if the proposed approach has a more general validity, even for more extended architectures. The DGus are in a ring topology (m =4), as depicted in Fig. 8.3. The incidence matrix $\boldsymbol{\mathcal{B}} \in \mathbb{R}^{4\times 4}$, which describes the network structure can be expressed as

$$\boldsymbol{\mathcal{B}} = \begin{bmatrix} -1 & 0 & 0 & -1 \\ 1 & -1 & 0 & 0 \\ 0 & 1 & -1 & 0 \\ 0 & 0 & 1 & 1 \end{bmatrix},$$

Table 8.1. Electrical parameters of the microgrid

DGus	Filter Parameters		Shunt capacitance	Load Currents		Reference Voltages	
	R_{t_i} [mΩ]	L_{t_i} [mH]	C_{t_i} [µF]	W_{d_i} [A]	W_{q_i} [A]	$V_{d_i}^{\star}$ [V]	$V_{q_i}^{\star}$ [V]
DGu_1	40.2	9.5	62.86	50	-20	$120.0\sqrt{2}$	0
DGu_2	38.7	9.2	62.86	100	-15	$120.0\sqrt{2}$	0
DGu_3	34.6	8.7	62.86	40	-10	$122.4\sqrt{2}$	0
DGu_4	31.8	8.3	62.86	80	-18	$117.6\sqrt{2}$	0

Table 8.2. Electrical parameters of the distribution lines

Line impedance Z_{ij}	R_{ij} [Ω]	L_{ij} [µH]
Z_{12}	0.25	1.2
Z_{23}	0.27	1.3
Z_{34}	0.24	1.8
Z_{14}	0.26	2.1

while the electrical parameters of the single DGus and of the interconnecting distribution lines are reported in Table 8.1 and in Table 8.2, respectively. The dynamic performances of the controlled microgrid system in Fig. 8.3 are validated considering unknown load dynamics and voltage reference changes. In particular, at $t = 0.04\,\mathrm{s}$, $V_{d_2}^{\star}$ becomes $114\sqrt{2}\mathrm{V}$, i.e., it is reduced by 5%, and at $t = 0.06\,\mathrm{s}$, the power demanded by the local load of the DGu_4 increases by 25%, i.e., W_{d_4} becomes 100 A.

In Fig. 8.4 the time evolution of the dq-components of the loads voltages is represented. One can observe the robustness of the proposed decentralized control approach with respect to both reference and load variations. In particular, the voltage dynamics of the nearby DGus are not affected neither by load nor by reference variations. The time evolution of the d-component of the generated and exchanged currents are also represented. In particular, one can observe that when the voltage reference $V_{d_2}^{\star}$ becomes lower than the d-component of the voltage at PCC_1 and PCC_3, respectively, then DGu_1 and DGu_3 (i.e., the neighbors of DGu_2) increase the generated current, and deliver, through the distribution lines, the extra power to the DGu_2, which, instead, decreases its own generation. On the other hand, when the local load of DGu_4 requires more power, only DGu_4 increases its own generation.

Fig. 8.5 shows the three-phase signals of the DGu_2, i.e., the load voltages (dashed lines) and the generated currents (solid lines). Moreover, one can observe that all the load voltages are synchronized, with frequency equal to the nominal one $f_0 = 60\,\mathrm{Hz}$.

8.6 Conclusions

In this chapter a decentralized SM control scheme has been designed for an AC microgrid with arbitrary topology, affected by load variations, operating in IOM. The system has been modelled by introducing an incidence matrix and the controller has been suitably

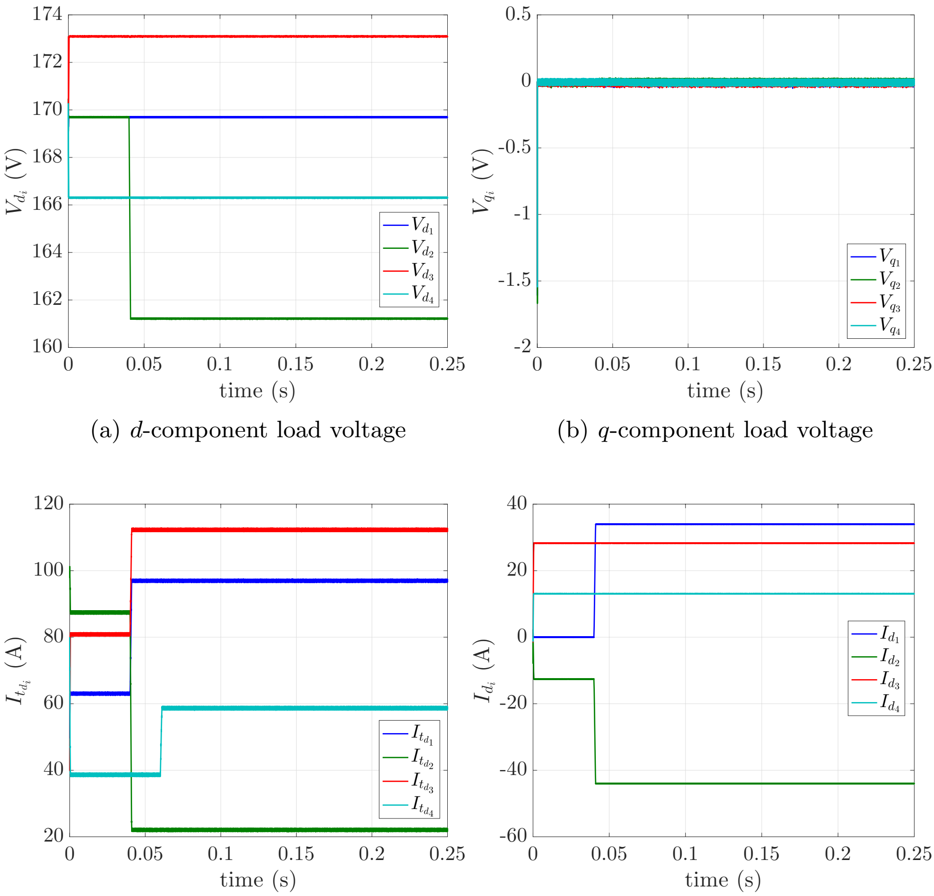

(a) d-component load voltage

(b) q-component load voltage

(c) d-component generated current

(d) d-component exchanged current

Fig. 8.4. **(a)** Time evolution of the d-component of the load voltages. **(b)** Time evolution of the q-component of the load voltages. **(c)** Time evolution of the d-component of the generated currents. **(d)** Time evolution of the d-component of the currents exchanged among the DGus through interconnecting power lines.

designed on the basis of the proposed model. The asymptotical stability of the whole microgrid has been proved and the performance of the proposed algorithm have been evaluated in simulation considering a microgrid with four DGus in a ring topology.

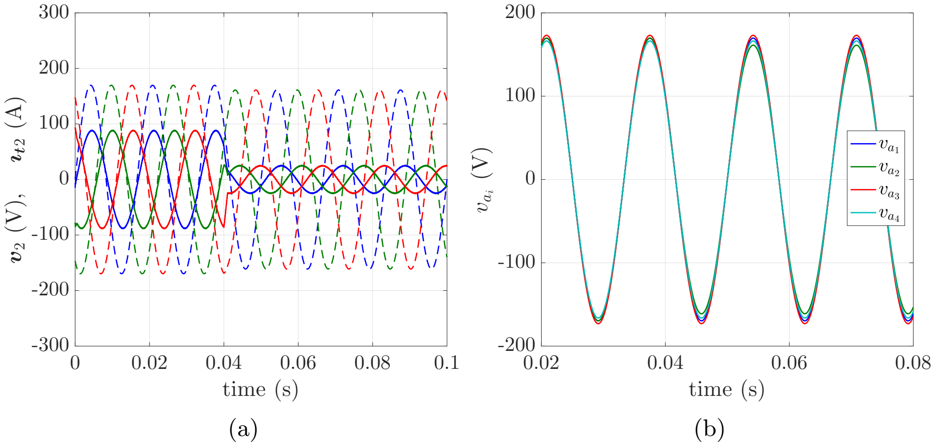

Fig. 8.5. (a) Time evolution of the three-phase signals (load voltage and generated current) of DGu_2. **(b)** Time evolution of the a-phase of the load voltages.

9

Buck-Based DC Microgrids

Abstract. In this paper a novel distributed control algorithm for current sharing and voltage regulation in Direct Current (DC) microgrids is proposed. The DC microgrid is composed of several Distributed Generation units (DGus), interfaced with Buck converters, and current loads. The considered model permits an arbitrary network topology and is affected by unknown load demand and modelling uncertainties. The proposed control strategy exploits a communication network to achieve proportional current sharing using a consensus-like algorithm. Voltage regulation is achieved by constraining the system to a suitable manifold. Two robust control strategies of Sliding Mode (SM) type are developed to reach the desired manifold in a finite time. The proposed control scheme is formally analyzed, proving the achievement of proportional current sharing, while guaranteeing that the weighted average voltage of the microgrid is identical to the weighted average of the voltage references. The latter objective is often desired in practical implementations, but difficult to obtain, even with advanced control methodologies, rendering the proposed solution relevant for the further deployment of DC microgrids.

9.1 Preliminaries on Buck-Based DC Microgrids

As discussed in Chapter 8, in the last decades, due to economic, technological and environmental aspects, the main trends in power systems focused on the modification of the traditional power generation and transmission systems towards incorporating smaller Distributed Generation units (DGus). Moreover, the ever-increasing energy demand and the concern about the climate change have encouraged the wide diffusion of Renewable Energy Sources (RES). The so-called microgrids have been proposed as conceptual solutions to integrate different types of RES and to electrify remote areas. Microgrids are low-voltage electrical distribution networks, composed of clusters of DGus, loads and storage systems interconnected through power lines [LP04].

Due to the widespread use of Alternate Current (AC) electricity in most industrial, commercial and residential applications, the recent literature on this topic mainly focused on AC microgrids [SSK17, TBD14, DM17, GLLC13]. However, several sources and loads (e.g. photovoltaic panels, batteries, electronic appliances and electric vehicles) can be directly connected to DC microgrids by using DC-DC converters. Indeed, several aspects make DC microgrids more efficient and reliable than AC microgrids [JMLJ13]: *i*) lossy DC-AC and AC-DC conversion stages are reduced, *ii*) there is not reactive power, *iii*) harmonics are not present, *iv*) frequency synchronization is overcame, *v*) skin effect is absent. Moreover, a DC microgrid can be connected to an islanded AC microgrid (even to the main grid) by a DC-AC bidirectional converter, forming a so-called hybrid microgrid [LWL11, GLLC13]. Moreover, the growing need of interconnecting distant power networks (e.g. off-shore wind farms) has encouraged the use of High Voltage Direct Current (HVDC) technology, which is advantageous not only for long distances, but also for underwater cables, asynchronous networks and grids running at different frequencies [FAD09]. Different control approaches have been investigated in the literature (see for instance [BdPFDC+16, AWD+17, ZOS17] and the references therein). Finally, DC microgrids are widely deployed in aircrafts and trains, and recently used in modern design for ships and large charging facilities for electric vehicles. For all these reasons, DC microgrids are attracting growing interest and receive much research attention.

Two main control objectives in DC microgrids are voltage regulation and current sharing (or, equivalently, load sharing). Regulating the voltages is required to ensure a proper functioning of connected loads, whereas current sharing prevents the overstressing of any source. Moreover, since a microgrid can include DGus with different generation capacity, it is often desired in practical cases that the DGus share the total current demand proportionally to their generation capacity. In order to achieve both objectives, hierarchical control schemes are conventionally adopted [GVM+11]. In these hierarchical control schemes, a primary (low level) control, typically based on a droop method, is designed to perform load sharing. However, since traditional droop controllers cannot guarantee to achieve both the aforementioned objectives simultaneously [LGSV14], the primary control is usually supplemented with a secondary (high level) control to maintain the voltages in a microgrid close to their desired reference values. Generally, the requirement of current sharing does not permit to regulate the voltage at each node towards the corresponding desired value. Then, a reasonable alternative is to satisfy the voltage requirement defined in [NMDL15], according to which the average voltage across the whole microgrid (not a specific node) should be regulated at the global voltage set point (e.g., the average of the voltage references). This kind of voltage regulation is called *global voltage regulation* or *voltage balancing* (see for instance [NDLG14, PAMD+16, SM17, PGA17, TMGFT16] and the references therein).

In the literature, these control problems in DC microgrids have been addressed by different approaches. To compensate steady state error due to primary droop controller, a distributed secondary controller based on averaging the total current supplied by the sources is proposed in [AFG13], while decentralized and distributed secondary integral control strategy are formally analyzed in [ZD15]. In [NMDL15] each power converter is equipped with current and voltage regulators. The latter uses the average voltage estimation made by an observer to perform global voltage regulation. In [TMGFT16] the authors propose a consensus-based secondary controller for current sharing and voltage balancing even in presence of plugging-in or -out of DGus. An oscillatory current sharing is designed in [HGMK15] for DC microgrids where single-phase inverter and/or three-phase unbalanced AC loads are introduced. A consensus algorithm that guarantees power sharing in presence of ‘ZIP’ (constant impedance, constant current, constant power) loads, as well as preservation of the weighted geometric average of the source voltages is designed and formally analyzed in [DWD16].

In this chapter we propose a novel robust control algorithm to obtain simultaneously proportional current sharing among the DGus and a form of voltage regulation in the DC power network, where the interconnecting lines of the microgrid are assumed to be resistive-inductive. In order to achieve current sharing, a communication network is exploited where each DGu communicates in real-time the value of its generated current to its neighbouring DGus. Adding this additional communication layer to achieve current sharing, leading to a distributed controller, has been widely adopted and studied thoroughly. In comparison to the existing results in the literature, we additionally propose the design of a manifold that couples the aforementioned objective of current sharing to the objective of voltage regulation. By doing this, the proposed control algorithm guarantees that the weighted average voltage of the microgrid is equal to the weighted average of the reference voltages, where the weights depend on the DGus generation capacities, performing the so called global voltage regulation or voltage balancing [TMGFT16]. This is achieved independently of the initial voltage conditions, facilitating plug-and-play capabilities.

To constrain the state of the system to the designed manifold in a finite time, we propose robust controllers of Sliding Mode (SM) type [Utk92, UGS99, YSE17]. SM control is appreciated for its robustness property against a wide class of modelling uncertainties and external disturbances, commonly present in DC microgrids. In this work, we first propose a Second Order Sliding Mode (SOSM) controller that determines the, possibly non-constant, switching frequency of the power converter, which might lead increased the power losses. Then, to overcome this issue, we additionally propose a third order sliding mode controller (3SM) to obtain a continuous control signal that can be used as the duty cycle of the power converter. Furthermore, the proposed control solution is robust with respect to failed communication. In fact, if the communication among the DGus is disabled, then the voltage of each node converges in a finite time to the corresponding reference value. For the considered microgrid model, convergence to the state of current sharing and voltage regulation is theoretically analyzed, and we show that convergence is achieved globally, for any initialization of the microgrid.

The remainder of this chapter is organized as follows. In Section 9.2 the microgrid model is presented, while in Section 9.3 the control problem is formulated. In Section 9.4 the proposed manifold-based consensus algorithm is designed, and in Section 9.5 sliding mode control strategies are proposed to reach the desired manifold. In Section 9.6 the stability properties of the controlled system are analyzed, while in Section 9.7 the simulation results are illustrated and discussed. Some conclusions are gathered in Section 9.8.

9.2 Buck-Based DC Microgrid Model

In this work we consider a typical buck converter-based DC microgrid of which a schematic electrical diagram is provided in Fig. 9.1 for a two DGus network. The energy source of a DGu is represented by a DC voltage source V_{DC_i}, and it is interfaced with the electric DC network through a DC-DC Buck converter. The local DC load is connected to the so-called Point of Common Coupling (PCC) and it can be treated as a current disturbance

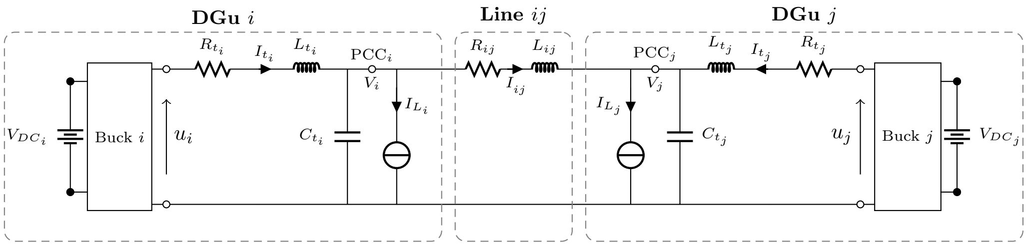

Fig. 9.1. The considered electrical diagram of a (Kron reduced) DC microgrid composed of two DGus.

I_{L_i} (see also Remark 9.2). At the output of the Buck converter a low-pass filter $R_{t_i}L_{t_i}C_{t_i}$ is considered, where R_{t_i} represents the filter parasitic resistance. Moreover, the DGu$_i$ can exchange power with the DGu$_j$ through a line with resistance R_{ij} and inductance L_{ij}.

By applying the Kirchhoff's current and voltage laws, the governing dynamic equations[12] of the i-th node (DGu) are the following:

$$\begin{aligned} L_{t_i}\dot{I}_{t_i} &= -R_{t_i}I_{t_i} - V_i + u_i \\ C_{t_i}\dot{V}_i &= I_{t_i} - I_{L_i} - \sum_{j\in\mathcal{N}_i} I_{ij}, \end{aligned} \tag{9.1}$$

where $\mathcal{N}_i$ is the set of nodes (i.e., the DGus) connected to the i-th DGu by distribution lines, while the control input u_i represents the buck converter output voltage[13]. The current from DGu i to DGu j is denoted by I_{ij} and its dynamic is given by

$$L_{ij}\dot{I}_{ij} = (V_i - V_j) - R_{ij}I_{ij}. \tag{9.2}$$

The symbols used in (9.1) and (9.2) are described in Table 9.1.

The overall network is represented by a connected and undirected graph $\mathcal{G} = (\mathcal{V}, \mathcal{E})$, where the nodes, $\mathcal{V} = \{1, ..., n\}$, represent the DGus and the edges, $\mathcal{E} = \{1, ..., m\}$, represent the distribution lines interconnecting the DGus. The network topology is represented by its corresponding incidence matrix $\boldsymbol{\mathcal{B}} \in \mathbb{R}^{n\times m}$. The ends of edge k are arbitrarily labeled with a + and a −, and the entries of $\boldsymbol{\mathcal{B}}$ are given by

$$\mathcal{B}_{ik} = \begin{cases} +1 & \text{if } i \text{ is the positive end of } k \\ -1 & \text{if } i \text{ is the negative end of } k \\ 0 & \text{otherwise.} \end{cases}$$

By substituting (9.2) in (9.1), the overall microgrid system can be written compactly for all nodes $i \in \mathcal{V}$ as

[12]For notational simplicity, the dependence of the variables on time t is omitted throughout most of the chapter.

[13]Note that u_i in (9.1) can be expressed as $\delta_i V_{DC_i}$, where δ_i is the duty cycle of the Buck i and V_{DC_i} is the DC voltage source provided by a generic renewable energy source or a battery at node i.

Table 9.1. Description of the used symbols

	State variables
I_{t_i}	Generated current
V_i	Load voltage
I_{ij}	Exchanged current
	Parameters
R_{t_i}	Filter resistance
L_{t_i}	Filter inductance
C_{t_i}	Shunt capacitor
R_{ij}	Line resistance
L_{ij}	Line inductance
	Inputs
u_i	Control input
I_{L_i}	Unknown current demand

$$\begin{aligned} \boldsymbol{L_t}\dot{\boldsymbol{I}}_{\boldsymbol{t}} &= -\boldsymbol{R_t}\boldsymbol{I_t} - \boldsymbol{V} + \boldsymbol{u} \\ \boldsymbol{C_t}\dot{\boldsymbol{V}} &= \boldsymbol{I_t} + \boldsymbol{\mathcal{B}}\boldsymbol{I} - \boldsymbol{I_L} \\ \boldsymbol{L}\dot{\boldsymbol{I}} &= -\boldsymbol{\mathcal{B}}^T\boldsymbol{V} - \boldsymbol{R}\boldsymbol{I}, \end{aligned} \tag{9.3}$$

where $\boldsymbol{V}, \boldsymbol{I_t}, \boldsymbol{I_L}, \boldsymbol{u} \in \mathbb{R}^n$, and $\boldsymbol{I} \in \mathbb{R}^m$. Moreover, $\boldsymbol{C_t}, \boldsymbol{L_t}, \boldsymbol{R_t} \in \mathbb{R}^{n\times n}$ and $\boldsymbol{R}, \boldsymbol{L} \in \mathbb{R}^{m\times m}$ are positive definite, diagonal matrices, e.g. $\boldsymbol{R_t} = \mathrm{diag}(R_{t_1}, \ldots, R_{t_n})$. To permit the controller design in the next sections, the following assumption is introduced on the available information of the system:

Assumption 9.1 (Available information). The state variables I_{t_i} and V_i are locally available at the i-th DGu. The network parameters $\boldsymbol{R_t}, \boldsymbol{L_t}, \boldsymbol{C_t}, \boldsymbol{R}, \boldsymbol{L}$, and the current demand $\boldsymbol{I_L}$ are constant and unknown, but with known bounds.

Remark 9.1 (Varying parameters and current demand). We assume that the parameters and the current demand are constant, to allow for a steady state solution and to theoretically analyze the stability of the microgrid. Yet, the control strategy that we propose in the next sections is applicable even if this assumption is removed.

Remark 9.2 (Kron reduction). Note that in (9.1), the load currents are located at the PCC of each DGu (see also Fig. 9.1). This situation is generally obtained by a Kron reduction of the original network, yielding an equivalent representation of the network [ZMD15, DB13]. It is important to realize that the network (topology) of the Kron reduced network is generally unknown and differs from the original network. It is therefore desirable that a control structure is independent of the underlying distribution network.

9.3 Current Sharing and Voltage Balancing

In this section we make the considered control objectives explicit. First, we note that for a given constant control input $\overline{\boldsymbol{u}}$, a steady state solution $(\overline{\boldsymbol{I}}_{\boldsymbol{t}}, \overline{\boldsymbol{V}}, \overline{\boldsymbol{I}})$ to system (9.3) satisfies

$$\begin{aligned} \overline{\boldsymbol{V}} &= -\boldsymbol{R_t}\overline{\boldsymbol{I}}_{\boldsymbol{t}} + \overline{\boldsymbol{u}} \\ -\boldsymbol{\mathcal{B}}\overline{\boldsymbol{I}} &= \overline{\boldsymbol{I}}_{\boldsymbol{t}} - \boldsymbol{I_L} \\ \overline{\boldsymbol{I}} &= -\boldsymbol{R}^{-1}\boldsymbol{\mathcal{B}}^T\overline{\boldsymbol{V}}, \end{aligned} \tag{9.4}$$

The second line of (9.4) implies[14] that, at steady state, the total generated current $\mathbb{1}_n^T\overline{\boldsymbol{I}}_{\boldsymbol{t}}$ is equal to the total current demand $\mathbb{1}_n^T\boldsymbol{I_L}$. To improve the generation efficiency, it is generally desired that the total current demand is shared among the various DGus proportionally to the generation capacity of their corresponding energy sources (proportional current sharing). This desire can be expressed as $w_iI_{ti} = w_jI_{tj}$ for all $i, j \in \mathcal{V}$, where w_i relates to the generation capacity of converter i, and leads to the first objective concerning the desired steady state value of the generated currents $\overline{\boldsymbol{I}}_{\boldsymbol{t}}$.

Objective 9.1 (Proportional current sharing).

$$\lim_{t\to\infty} \boldsymbol{I_t}(t) = \overline{\boldsymbol{I}}_{\boldsymbol{t}} = \boldsymbol{W}^{-1}\mathbb{1}_n i_t^*, \tag{9.5}$$

with $i_t^* = \mathbb{1}_n^T\boldsymbol{I_L}/(\mathbb{1}_n^T\boldsymbol{W}^{-1}\mathbb{1}_n) \in \mathbb{R}$, $\boldsymbol{W} = \operatorname{diag}\{w_1, \dots, w_n\}$, $w_i > 0$, for all $i \in \mathcal{V}$.

Note that (9.5) indeed satisfies $\mathbb{1}_n^T\overline{\boldsymbol{I}}_{\boldsymbol{t}} = \mathbb{1}^T\boldsymbol{W}^{-1}\mathbb{1}_n i_t^* = \mathbb{1}_n^T\boldsymbol{I_L}$. From the second and third lines of (9.4) it follows that the corresponding steady state voltages $\overline{\boldsymbol{V}}$ satisfy

$$\boldsymbol{\mathcal{B}}\boldsymbol{R}^{-1}\boldsymbol{\mathcal{B}}^T\overline{\boldsymbol{V}} = \boldsymbol{W}^{-1}\mathbb{1}_n i_t^* - \boldsymbol{I_L}, \tag{9.6}$$

that prescribes the value of the required differences in voltages, $\boldsymbol{\mathcal{B}}^T\overline{\boldsymbol{V}}$, achieving proportional current sharing. This admits the freedom to shift all steady state voltages with the same constant value, since $\boldsymbol{\mathcal{B}}^T\overline{\boldsymbol{V}} = \boldsymbol{\mathcal{B}}^T\left(\overline{\boldsymbol{V}} + a\mathbb{1}_n\right)$, with $a \in \mathbb{R}$ any scalar. To define the optimal steady state voltages, we assume that for every DGu i, there exists a desired reference voltage $V_i^\star$.

Assumption 9.2 (Desired voltages). There exists a constant reference voltage $V_i^\star$ at the PCC, for all $i \in \mathcal{V}$.

Often the values for $V_i^\star$ are chosen identical for all $i \in \mathcal{V}$, and are set to the desired voltage level of the overall network. Generally, the requirement of current sharing does not permit for $\overline{\boldsymbol{V}} = \boldsymbol{V}^\star$, and might cause voltages deviations from the corresponding reference values. Then, a reasonable alternative is to keep the average value of the PCC voltages at the steady state identical to the weighted average value of the desired reference voltages of $\boldsymbol{V}^\star$ (voltage balancing) [TMGFT16]. Particularly, we choose the weights to be $1/w_i$, for

[14] The incidence matrix $\boldsymbol{\mathcal{B}}$, satisfies $\mathbb{1}_n^T\boldsymbol{\mathcal{B}} = \boldsymbol{0}$, where $\mathbb{1}_n \in \mathbb{R}^n$ is the vector consisting of all ones.

all $i \in \mathcal{V}$, such that at the converters with a relatively large current generation, there is a relatively large voltage deviation. Therefore, given a $\boldsymbol{V}^\star$, we aim at designing a controller that, in addition to Objective 9.1, also guarantees voltage balancing, i.e.,

Objective 9.2 (Voltage balancing).

$$\lim_{t\to\infty} \mathbb{1}_n^T \boldsymbol{W}^{-1}\boldsymbol{V}(t) = \mathbb{1}_n^T \boldsymbol{W}^{-1}\overline{\boldsymbol{V}} = \mathbb{1}_n^T \boldsymbol{W}^{-1}\boldsymbol{V}^\star. \tag{9.7}$$

Remark 9.3. (**Equal current sharing**) Note that by setting in (9.5) and (9.7) the weights w_i, for all $i \in \mathcal{V}$, identical, the total current demand is equally shared among the DGus and the arithmetic average of the microgrid voltage is equal to the arithmetic average of the voltage references.

By substituting (9.5) and (9.7), in (9.4), one can easily verify that the achievement of Objective 9.1 and Objective 9.2 prescribes the (optimal) steady state output voltages of the buck converters, $\boldsymbol{u} = \overline{\boldsymbol{u}}^{opt}$.

Lemma 9.1 (Optimal feedforward input). If system (9.3), at steady state, achieves Objective 9.1 and Objective 9.2, then the control input $\boldsymbol{u}$ to system (9.3) is given by

$$\overline{\boldsymbol{u}}^{opt} = -\Big(\boldsymbol{\mathcal{B}}\boldsymbol{R}^{-1}\boldsymbol{\mathcal{B}}^T - \boldsymbol{\varPsi}\Big)^{-1}\Big(\boldsymbol{\varPsi}\boldsymbol{V}^\star + \boldsymbol{I_L}\Big), \tag{9.8}$$

with

$$\boldsymbol{\varPsi} = \frac{(\mathbb{I}_n + \boldsymbol{\mathcal{B}}\boldsymbol{R}^{-1}\boldsymbol{\mathcal{B}}^T\boldsymbol{R_t})\boldsymbol{W}^{-1}\mathbb{1}_n\mathbb{1}_n^T\boldsymbol{W}^{-1}}{\mathbb{1}_n^T\boldsymbol{W}^{-1}\boldsymbol{R_t}\boldsymbol{W}^{-1}\mathbb{1}_n}, \tag{9.9}$$

and $\mathbb{I}_n \in \mathbb{R}^{n\times n}$ the identity matrix.

Proof. When Objective 9.1 and Objective 9.2 hold, the steady state of (9.3) necessarily satisfies

$$\begin{aligned}
\boldsymbol{0} &= -\boldsymbol{R_t}\boldsymbol{W}^{-1}\mathbb{1}_n i_t^* - \overline{\boldsymbol{V}} + \overline{\boldsymbol{u}}^{opt}\\
\boldsymbol{0} &= \boldsymbol{W}^{-1}\mathbb{1}_n i_t^* - \boldsymbol{\mathcal{B}}\boldsymbol{R}^{-1}\boldsymbol{\mathcal{B}}^T\overline{\boldsymbol{V}} - \boldsymbol{I_L}\\
\boldsymbol{0} &= \mathbb{1}_n^T\boldsymbol{W}^{-1}\overline{\boldsymbol{V}} - \mathbb{1}_n^T\boldsymbol{W}^{-1}\boldsymbol{V}^\star,
\end{aligned} \tag{9.10}$$

with $i_t^* = \mathbb{1}_n^T\boldsymbol{I_L}/(\mathbb{1}_n^T\boldsymbol{W}^{-1}\mathbb{1}_n) \in \mathbb{R}$ A tedious, but straightforward, calculation permits to solve (9.10) for $\overline{\boldsymbol{u}}^{opt}$, yielding (9.8). □

In order to determine (9.8), exact knowledge of almost all network parameters, as well as the current demand $\boldsymbol{I_L}$, is required. Since this information is not available (see also Assumption 9.1), we propose in the next sections distributed controllers that, provably, achieve voltage balancing using only local measurements of V_i, and that achieve proportional current sharing by exchanging information on I_{t_i} among neighbours over a communication network. In the remainder of this section we further elaborate on the steady state voltages imposed by the control objectives.

9.3.1 Steady state voltages

First, we notice that it follows from (9.5) and (9.10) that the steady state voltages $\overline{\boldsymbol{V}}$ satisfy

$$\overline{\boldsymbol{V}} = -\frac{\boldsymbol{R_t}\boldsymbol{W}^{-1}\mathbb{1}_n\mathbb{1}_n^T\boldsymbol{I_L}}{\mathbb{1}_n^T\boldsymbol{W}^{-1}\mathbb{1}_n} + \overline{\boldsymbol{u}}^{opt}. \tag{9.11}$$

From (9.8) and (9.11) it is evident that the steady state values of the voltages at each node depend on the loads $\boldsymbol{I_L}$ and the voltage references $\boldsymbol{V}^\star$. Since $\boldsymbol{V}^\star$ is free to design, it can be potentially chosen in such a way that too low or too high voltages are avoided. To help the design of $\boldsymbol{V}^\star$, we show that the the steady state voltages $\overline{V}_i$, for all $i \in \mathcal{V}$, are shifted by the same quantity, when $\boldsymbol{V}^\star$ is altered.

Lemma 9.2. (**Voltage shifting property**) Let Objective 9.1 and Objective 9.2 hold, and let $\overline{\boldsymbol{V}}_{(1)} \in \mathbb{R}^n$ denote the steady state voltage value associated to the voltage reference $\boldsymbol{V}^\star_{(1)} \in \mathbb{R}^n$. Consider the new voltage reference $\boldsymbol{V}^\star_{(2)} \in \mathbb{R}^n$ and the corresponding steady state voltage value $\overline{\boldsymbol{V}}_{(2)} \in \mathbb{R}^n$. Then, $\varDelta\overline{\boldsymbol{V}} = \overline{\boldsymbol{V}}_{(2)} - \overline{\boldsymbol{V}}_{(1)}$ satisfies

$$\varDelta\overline{\boldsymbol{V}} = \mathbb{1}_n\frac{\mathbb{1}_n^T\boldsymbol{W}^{-1}\varDelta\boldsymbol{V}^\star}{\mathbb{1}_n^T\boldsymbol{W}^{-1}\mathbb{1}_n}, \tag{9.12}$$

with $\varDelta\boldsymbol{V}^\star = \boldsymbol{V}^\star_{(2)} - \boldsymbol{V}^\star_{(1)}$.

Proof. When Objective 9.2 holds, we have

$$\mathbb{1}_n^T\boldsymbol{W}^{-1}(\overline{\boldsymbol{V}}_{(1)} + \varDelta\overline{\boldsymbol{V}}) = \mathbb{1}_n^T\boldsymbol{W}^{-1}(\boldsymbol{V}^\star_{(1)} + \varDelta\boldsymbol{V}^\star), \tag{9.13}$$

which implies

$$\mathbb{1}_n^T\boldsymbol{W}^{-1}\varDelta\overline{\boldsymbol{V}} = \mathbb{1}_n^T\boldsymbol{W}^{-1}\varDelta\boldsymbol{V}^\star. \tag{9.14}$$

Bearing in mind that the voltage differences between any node of the microgrid are prescribed by the achievement of current sharing (see the paragraph below Objective 9.1), we have $\boldsymbol{\mathcal{B}}^T\overline{\boldsymbol{V}}_{(1)} = \boldsymbol{\mathcal{B}}^T\overline{\boldsymbol{V}}_{(2)}$, implying $\varDelta\overline{\boldsymbol{V}} = \mathbb{1}_n\nu$, with $\nu \in \mathbb{R}$. Then, from (9.14), $\nu = \mathbb{1}_n^T\boldsymbol{W}^{-1}\varDelta\boldsymbol{V}^\star/\mathbb{1}_n^T\boldsymbol{W}^{-1}\mathbb{1}_n$, i.e., all the voltages are shifted by the same quantity. □

Consequently, any node i in the network can lower or increase its steady state voltage $\overline{V}_i$, by adjusting its own reference $V_i^\star$. Although, the design and the analysis of a voltage reference generator is postponed to a future research, the property proven in Lemma 9.2 could be exploited to avoid that the voltages at some nodes could be lower or higher than some given thresholds.

9.4 Distributed Sliding Mode Control

In this section we introduce the key aspects of the proposed solution to achieve Objective 9.1 and Objective 9.2, consisting of a consensus algorithm and the design of a manifold to where the solutions to the system should converge. First, we augment system (9.3) with additional state variables (distributed integrators) θ_i, $i \in \mathcal{V}$, with dynamics given by

$$\dot{\theta}_i = -\sum_{j\in\mathcal{N}_i^c} \gamma_{ij}(w_i I_{t_i} - w_j I_{t_j}), \tag{9.15}$$

where $\mathcal{N}_i^c$ is the set of the DGus that communicate with the i-th DGu, and $\gamma_{ij} = \gamma_{ji} \in \mathbb{R}_{>0}$ are additional gain constants, and $w_i, w_j \in \mathbb{R}_{>0}$ are constant weights depending on the DGus generation capacity. Let $\boldsymbol{\mathcal{L}_c}$ denote the (weighted) Laplacian matrix associated with the communication graph, which can be different from the topology of the (reduced) microgrid. Then, the dynamics in (9.15) can be expressed compactly for all nodes $i \in \mathcal{V}$ as

$$\dot{\boldsymbol{\theta}} = -\boldsymbol{\mathcal{L}_c} \boldsymbol{W} \boldsymbol{I_t}, \tag{9.16}$$

that indeed has the form of a consensus protocol, permitting a steady state where $\boldsymbol{W}\overline{\boldsymbol{I}}_{\boldsymbol{t}} \in \operatorname{im}(\mathbb{1}_n)$ (see also Objective 9.1). We impose the following restrictions on (9.16):

Assumption 9.3 (Controller structure). For all $i \in \mathcal{V}$, the integrators states θ_i are initialized such that $\mathbb{1}_n^T \boldsymbol{\theta}(0) = 0$. Furthermore, the graph corresponding to the topology of the communication network is undirected and connected.

The most straightforward choice of initialization of the state $\theta_i(0)$, that satisfies Assumption 9.3, is to initialize all θ_i to zero, i.e. $\boldsymbol{\theta}(0) = \boldsymbol{0}$. Whereas connectedness of the communication graph is needed to ensure power sharing among *all* DGus, the consequence of the required initialization of $\boldsymbol{\theta}(0)$ is that the average value of the entries of $\boldsymbol{\theta}$ is preserved and identical to zero for all $t \geq 0$, as proved in the following lemma.

Lemma 9.3 (Preservation of $\mathbb{1}_n^T \boldsymbol{\theta}$). Let Assumption 9.3 hold. Given system (9.16), the average value $\frac{1}{n}\sum_{i\in\mathcal{V}} \theta_i$ is preserved, i.e.,

$$\frac{1}{n}\mathbb{1}_n^T \boldsymbol{\theta}(t) = \frac{1}{n}\mathbb{1}_n^T \boldsymbol{\theta}(0) \quad \forall t \geq 0. \tag{9.17}$$

Proof. Pre-multiplying both sides of (9.16) by $\mathbb{1}_n^T$ yields

$$\mathbb{1}_n^T \dot{\boldsymbol{\theta}} = -\mathbb{1}_n^T \boldsymbol{\mathcal{L}_c} \boldsymbol{W} \boldsymbol{I_t} = 0, \tag{9.18}$$

where $\mathbb{1}_n^T \boldsymbol{\mathcal{L}_c} = \boldsymbol{0}$, follows from $\boldsymbol{\mathcal{L}_c}$ being the Laplacian matrix associated with an undirected graph. $\square$

The fact that $\mathbb{1}_n^T \boldsymbol{\theta}(t) = 0$, is essential to the second aspect of the proposed solution, the design of a manifold. Bearing in mind Objective 9.2, we propose the following desired manifold:

$$\{(\boldsymbol{I_t}, \boldsymbol{V}, \boldsymbol{I}, \boldsymbol{\theta}) : \boldsymbol{W}^{-1}(\boldsymbol{V} - \boldsymbol{V}^\star) - \boldsymbol{\theta} = \boldsymbol{0}\}. \tag{9.19}$$

Indeed, exploiting the preservation of $\mathbb{1}_n^T \boldsymbol{\theta}$, we have on the desired manifold (9.19), $\mathbb{1}_n^T \boldsymbol{W}^{-1}\boldsymbol{V} = \mathbb{1}_n^T(\boldsymbol{\theta} + \boldsymbol{W}^{-1}\boldsymbol{V}^\star) = \mathbb{1}_n^T \boldsymbol{W}^{-1}\boldsymbol{V}^\star$. Constraining the solutions to a system to a specific manifold is typical for sliding mode based controllers, and we will discuss some suitable controller designs in the next section.

Remark 9.4. (**Plug-and-Play**) The main results in this work assume a constant network topology. Nevertheless, an interesting extension is to consider the plugging in or out of various converters. The analysis of the corresponding switched/hybrid system is outside the scope of this work. Here, we merely describe how the required initialization θ_i should be extended towards the setting of changing topologies, in order to preserve the crucial property $\mathbb{1}_n^T \boldsymbol{\theta} = 0$. First, if a new DGu (say DGu$_{n+1}$) wants to join the network, its integrator state is initialized to zero, i.e., $\theta_{n+1}(t_{new}) = 0$, t_{new} being the time instant when DGu$_{n+1}$ is plugged-in. Second, if a DGu (say DGu i) is unplugged at the time instant t_{out}, we let $\theta_i(t) = \theta_i(t_{out})$ for all $t > t_{out}$, without re-setting any integrator. If DGu i wants to join again the network at the time instant $t_{in} > t_{out}$, the dynamic of θ_i is described again by (9.15) for all $t > t_{in}$. Since $\theta_i(t_{in}) = \theta_i(t_{out})$, also the plug-in operation occurs without re-setting any integrator state.

9.5 Sliding mode controllers

We now propose a Distributed Second Order Sliding Mode (D-SOSM) control law, and a Distributed Third Order Sliding Mode (D-3SM) control law, to steer, in a finite time, the state of system (9.3), augmented with (9.16), to the desired manifold (9.19). As will be discussed in the coming subsections, the choice of the particular control law, D-SOSM or D-3SM, depends on the desired implementation.

Bearing in mind the desired manifold (9.19), we consider the following sliding function $\boldsymbol{\sigma} \in \mathbb{R}^n$:

$$\boldsymbol{\sigma}(\boldsymbol{V}, \boldsymbol{\theta}) = \boldsymbol{W}^{-1} (\boldsymbol{V} - \boldsymbol{V}^\star) - \boldsymbol{\theta}. \tag{9.20}$$

9.5.1 Second order SM control: variable switching frequency

Regarding the sliding function (9.20) as the output function of system (9.3), (9.16), it appears that the relative degree[15] is two. This implies that a second order sliding mode (SOSM) controller can be *naturally* applied in order to make the state of the controlled system reach, in a finite time, the sliding manifold $\{(\boldsymbol{I_t}, \boldsymbol{V}, \boldsymbol{I}, \boldsymbol{\theta}) : \boldsymbol{\sigma} = \dot{\boldsymbol{\sigma}} = \boldsymbol{0}\}$. According to the SOSM control theory, the auxiliary variables $\boldsymbol{\xi_1} = \boldsymbol{\sigma}$ and $\boldsymbol{\xi_2} = \dot{\boldsymbol{\sigma}}$ have to be defined, resulting in the so-called auxiliary system

$$\begin{aligned} \dot{\boldsymbol{\xi}}_{\boldsymbol{1}} &= \boldsymbol{\xi_2} \\ \dot{\boldsymbol{\xi}}_{\boldsymbol{2}} &= \boldsymbol{b}(\boldsymbol{I_t}, \boldsymbol{V}, \boldsymbol{I}, \boldsymbol{u}) + \boldsymbol{G_d u}. \end{aligned} \tag{9.21}$$

Taking into account the expressions for $\boldsymbol{\sigma}$ and $\dot{\boldsymbol{\sigma}}$, a straightforward calculation shows that, in the auxiliary system (9.21), the expression for $\boldsymbol{b} \in \mathbb{R}^n$ is given by

$$\begin{aligned} \boldsymbol{b} = &- \left(\boldsymbol{W}^{-1}\boldsymbol{C_t}^{-1} + \boldsymbol{\mathcal{L}_c W}\right) \boldsymbol{L_t}^{-1} \boldsymbol{R_t I_t} \\ &- \left(\left(\boldsymbol{W}^{-1}\boldsymbol{C_t}^{-1} + \boldsymbol{\mathcal{L}_c W}\right) \boldsymbol{L_t}^{-1} + \boldsymbol{W}^{-1}\boldsymbol{C_t}^{-1}\boldsymbol{\mathcal{B}L}^{-1}\boldsymbol{\mathcal{B}}^T\right) \boldsymbol{V} \\ &- \boldsymbol{W}^{-1}\boldsymbol{C_t}^{-1}\boldsymbol{\mathcal{B}L}^{-1}\boldsymbol{RI} - \boldsymbol{G_a u}, \end{aligned} \tag{9.22}$$

[15] The relative degree is the minimum order ρ of the time derivative $\sigma_i^{(\rho)}, i \in \mathcal{V}$, of the sliding variable associated with the i-th node in which the control $u_i, i \in \mathcal{V}$ explicitly appears.

and $\boldsymbol{G_d}, \boldsymbol{G_a} \in \mathbb{R}^{n\times n}$ are

$$\begin{aligned}\boldsymbol{G_d} &= (\boldsymbol{W}^{-1}\boldsymbol{C_t}^{-1} + \boldsymbol{\mathcal{D}_c}\boldsymbol{W})\boldsymbol{L_t}^{-1},\\ \boldsymbol{G_a} &= \boldsymbol{\mathcal{A}_c}\boldsymbol{W}\boldsymbol{L_t}^{-1}.\end{aligned} \tag{9.23}$$

Here, $\boldsymbol{\mathcal{D}_c}$ and $\boldsymbol{\mathcal{A}_c}$ are the degree matrix and the adjacency matrix of the communication graph, respectively, i.e. $\boldsymbol{\mathcal{L}_c} = \boldsymbol{\mathcal{D}_c} - \boldsymbol{\mathcal{A}_c}$. We assume that the entries of $\boldsymbol{b}$ and $\boldsymbol{G_d}$ have known bounds for all $i \in \mathcal{V}$:

$$\begin{aligned}|b_i| &\leq b_{\max_i}\\ G_{\min_i} \leq G_{d_{ii}} &\leq G_{\max_i},\end{aligned} \tag{9.24}$$

with $b_{\max_i}$, $G_{\min_i}$ and $G_{\max_i}$ being positive constants. According to the theory underlying the so-called Suboptimal SOSM (SSOSM) control algorithm [BFU98a], the i-th SOSM control law, that can be used to steer ξ_{1_i} and ξ_{2_i}, to zero in a finite time, even in presence of uncertainties, is given by

$$u_i = -\mu_i U_{\max_i} \operatorname{sign}\left(\xi_{1_i} - \tfrac{1}{2}\xi_{1_i}^{\max}\right), \tag{9.25}$$

with

$$U_{\max_i} > \max\left(\frac{b_{\max_i}}{\mu_i^* G_{\min_i}}; \frac{4b_{\max_i}}{3G_{\min_i} - \mu_i^* G_{\max_i}}\right), \tag{9.26}$$

$$\mu_i^* \in (0,1] \cap \left(0, \frac{3G_{\min_i}}{G_{\max_i}}\right), \tag{9.27}$$

μ_i switching between μ_i^* and 1, according to [BFU98a, Algorithm 1]. The extremal value $\xi_{1_i}^{\max}$ in (9.25) can be detected by implementing for instance a peak detector as in [BFU98b]. Note that only the value of ξ_{1_i}, i.e., $V_i - V_i^\star - \theta_i$, is required to generate the control signal u_i.

Remark 9.5 (Switching frequency). The discontinuous control signal (9.25) can be directly used in practice to open and close the switch of the Buck converter. As a result, the Insulated Gate Bipolar Transistors (IGBTs) switching frequency cannot be a-priori fixed and the power losses could be high. Usually, in order to achieve a constant IGBTs switching frequency, Buck converters are controlled by implementing the so-called Pulse Width Modulation (PWM) technique. To do this, a continuous control signal, that represents the so-called duty cycle of the Buck converter, is required. In the next subsection we will clarify how a continuous control input can be obtained.

9.5.2 Third Order SM control: duty cycle

To ensure a continuous control input (duty cycle), we adopt the procedure suggested in [BFU98a] and first integrate the (discontinuous) control signal generated by a sliding mode controller, yielding for system (9.3) augmented with (9.16)

$$\begin{aligned}\boldsymbol{L_t}\dot{\boldsymbol{I}}_{\boldsymbol{t}} &= -\boldsymbol{R_t}\boldsymbol{I_t} - \boldsymbol{V} + \boldsymbol{u}\\ \boldsymbol{C_t}\dot{\boldsymbol{V}} &= \boldsymbol{I_t} + \boldsymbol{\mathcal{B}}\boldsymbol{I} - \boldsymbol{I_L}\\ \boldsymbol{L}\dot{\boldsymbol{I}} &= -\boldsymbol{\mathcal{B}}^T\boldsymbol{V} - \boldsymbol{R}\boldsymbol{I}\\ \dot{\boldsymbol{\theta}} &= -\boldsymbol{\mathcal{L}_c}\boldsymbol{W}\boldsymbol{I_t}\\ \dot{\boldsymbol{u}} &= \boldsymbol{v},\end{aligned} \tag{9.28}$$

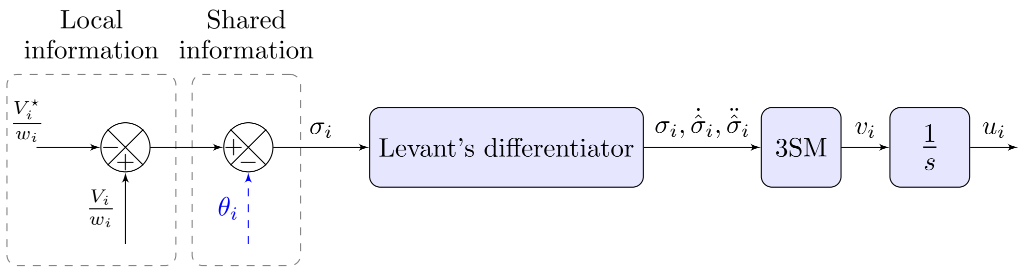

Fig. 9.2. Block diagram of the proposed Distributed Third Order Sliding Mode (D–3SM) control strategy.

where $\boldsymbol{v}$ is the new (discontinuous) control input. Note that the input signal to the converter, $\boldsymbol{u}(t) = \int_0^t \boldsymbol{v}(\tau)d\tau$, is continuous, so that u_i can be used as duty cycle for the switch of the i-th Buck converter. A consequence is that the system relative degree (with respect to the new control input $\boldsymbol{v}$) is now equal to three, so that we need to rely on a third order sliding mode (3SM) control strategy to reach the sliding manifold $\{(\boldsymbol{I_t}, \boldsymbol{V}, \boldsymbol{I}, \boldsymbol{\theta}) : \boldsymbol{\sigma} = \dot{\boldsymbol{\sigma}} = \ddot{\boldsymbol{\sigma}} = \boldsymbol{0}\}$ in a finite time. To do so, we define the auxiliary variables $\boldsymbol{\xi_1} = \boldsymbol{\sigma}$, $\boldsymbol{\xi_2} = \dot{\boldsymbol{\sigma}}$ and $\boldsymbol{\xi_3} = \ddot{\boldsymbol{\sigma}}$, and build the auxiliary system as follows

$$\begin{aligned} \dot{\boldsymbol{\xi}}_{\boldsymbol{1}} &= \boldsymbol{\xi_2} \\ \dot{\boldsymbol{\xi}}_{\boldsymbol{2}} &= \boldsymbol{\xi_3} \\ \dot{\boldsymbol{\xi}}_{\boldsymbol{3}} &= \dot{\boldsymbol{b}}(\boldsymbol{I_t}, \boldsymbol{V}, \boldsymbol{I}, \boldsymbol{u}) + \boldsymbol{G_d}\boldsymbol{v} \\ \dot{\boldsymbol{u}} &= \boldsymbol{v}, \end{aligned} \tag{9.29}$$

with $\boldsymbol{b}$ as in (9.22), $\boldsymbol{G_d}$ and $\boldsymbol{G_a}$ as in (9.23). Then, we assume that the entries of $\dot{\boldsymbol{b}}$ can be bounded as

$$|\dot{b}_i(\cdot)| \leq \beta_{\max_i} \; \forall i \in \mathcal{V}, \tag{9.30}$$

where $\beta_{\max_i}$ is a known positive constant.

Remark 9.6 (Uncertainty of $\boldsymbol{b}, \dot{\boldsymbol{b}}$ and $\boldsymbol{G_d}$). The mappings $\boldsymbol{b}, \dot{\boldsymbol{b}}$ and matrix $\boldsymbol{G_d}$ are uncertain due to the presence of the unmeasurable current demand $\boldsymbol{I_L}$ and possible network parameter uncertainties. However, relying on Assumption 9.1 and observing that $\boldsymbol{b}$ and $\dot{\boldsymbol{b}}$ depend on the electric signals related to the finite power of the microgrid, $\boldsymbol{b}, \dot{\boldsymbol{b}}$ and $\boldsymbol{G_d}$ are in practice bounded. Generally, the bounds of the unknown quantities can be determined by data analysis and engineering understanding.

Now, the 3SM control law proposed in [DF09] can be used to steer ξ_{1_i}, ξ_{2_i} and ξ_{3_i}, $i \in \mathcal{V}$, to zero in a finite time. It is given by

$$v_i = -\alpha_i \begin{cases} v_{1_i} = \operatorname{sign}(\ddot{\sigma}_i) & \boldsymbol{s}_i \in \mathcal{M}_{1_i}/\mathcal{M}_{0_i} \\ v_{2_i} = \operatorname{sign}\left(\dot{\sigma}_i + \frac{\ddot{\sigma}_i^2 v_{1_i}}{2\alpha_{r_i}}\right) & \boldsymbol{s}_i \in \mathcal{M}_{2_i}/\mathcal{M}_{1_i} \\ v_{3_i} = \operatorname{sign}(\phi_i(\boldsymbol{s}_i)) & \text{otherwise,} \end{cases} \tag{9.31}$$

where $\boldsymbol{s}_i = [\sigma_i, \dot{\sigma}_i, \ddot{\sigma}_i]^T$ and

$$\phi_i(\boldsymbol{s}_i) = \sigma_i + \frac{\ddot{\sigma}_i^3}{3\alpha_{r_i}^2} + \upsilon_{2_i}\left[\frac{1}{\sqrt{\alpha_{r_i}}}\left(\upsilon_{2_i}\dot{\sigma}_i + \frac{\ddot{\sigma}_i^2}{2\alpha_{r_i}}\right)^{\frac{3}{2}} + \frac{\dot{\sigma}_i\ddot{\sigma}_i}{\alpha_{r_i}}\right],$$

with

$$\alpha_{r_i} = \alpha_i G_{\min_i} - \beta_{\max_i} > 0. \tag{9.32}$$

Then, given the bounds $G_{\min_i}$ and $\beta_{\max_i}$, the control amplitude α_i is chosen such that α_{r_i} is positive. The manifolds $\mathcal{M}_{1_i}$, $\mathcal{M}_{2_i}$, $\mathcal{M}_{3_i}$ in (9.31) are defined as

$$\begin{aligned}
\mathcal{M}_{0_i} &= \left\{\boldsymbol{s}_i \in \mathbb{R}^3 : \sigma_i = \dot{\sigma}_i = \ddot{\sigma}_i = 0\right\} \\
\mathcal{M}_{1_i} &= \left\{\boldsymbol{s}_i \in \mathbb{R}^3 : \sigma_i - \frac{\ddot{\sigma}_i^3}{6\alpha_{r_i}^2} = 0, \dot{\sigma}_i + \frac{\ddot{\sigma}_i|\ddot{\sigma}_i|}{2\alpha_{r_i}} = 0\right\} \\
\mathcal{M}_{2_i} &= \left\{\boldsymbol{s}_i \in \mathbb{R}^3 : \phi_i(\boldsymbol{s}_i) = 0\right\}.
\end{aligned}$$

From (9.31), one can observe that the controller of DGu$_i$ requires not only σ_i, but also $\dot{\sigma}_i$ and $\ddot{\sigma}_i$. Yet, according to Assumption 9.1, only I_{t_i} and V_i are measurable at the i-th DGu. Then, one can rely on Levant's second-order differentiator [Lev03] to retrieve $\dot{\sigma}_i$ and $\ddot{\sigma}_i$ in a finite time. Consequently, for system (9.29), the estimators are given by

$$\begin{aligned}
\dot{\hat{\xi}}_{1_i} &= -\lambda_{0_i}\left|\hat{\xi}_{1_i} - \xi_{1_i}\right|^{\frac{2}{3}} \operatorname{sign}\left(\hat{\xi}_{1_i} - \xi_{1_i}\right) + \hat{\xi}_{2_i} \\
\dot{\hat{\xi}}_{2_i} &= -\lambda_{1_i}\left|\hat{\xi}_{2_i} - \dot{\hat{\xi}}_{1_i}\right|^{\frac{1}{2}} \operatorname{sign}\left(\hat{\xi}_{2_i} - \dot{\hat{\xi}}_{1_i}\right) + \hat{\xi}_{3_i} \\
\dot{\hat{\xi}}_{3_i} &= -\lambda_{2_i} \operatorname{sign}\left(\hat{\xi}_{3_i} - \dot{\hat{\xi}}_{2_i}\right),
\end{aligned} \tag{9.33}$$

where $\hat{\xi}_{1_i} = \hat{\sigma}_i$, $\hat{\xi}_{2_i} = \dot{\hat{\sigma}}_i$ and $\hat{\xi}_{3_i} = \ddot{\hat{\sigma}}_i$ are the estimated values of $\xi_{1_i} = \sigma_i, \xi_{2_i} = \dot{\sigma}_i$ and $\xi_{3_i} = \ddot{\sigma}_i$, respectively. The estimates obtained via (9.33) can be used in (9.31), replacing the original variables. The other parameters are $\lambda_{0_i} = 3\Lambda_i^{1/3}$, $\lambda_{1_i} = 1.5\Lambda_i^{1/2}$, $\lambda_{2_i} = 1.1\Lambda_i$, $\Lambda_i > 0$, as suggested in [Lev03]. The block diagram of the proposed control strategy is depicted in Fig. 9.2.

Remark 9.7 (Scalability and distributed control). Since the selected sliding function (9.20) is designed by using the additional state $\boldsymbol{\theta}$ in (9.16), the overall control scheme is indeed distributed, and only information on generated currents $\boldsymbol{I_t}$ needs to be shared. More precisely, the controller of the i-th DGu needs information only from the DGus that communicate with it. Note that the design of the local controller for each DGu is not based on the knowledge of the whole microgrid, so that the complexity of the control synthesis does not depend on the microgrid size. Specifically, the synthesis of the i-th local controller requires the knowledge of the bounds of $G_{\min_i}$, $G_{\max_i}$, $b_{\max_i}$ (SSOSM), $\beta_{\max_i}$ (3SM), which depend on the parameters of the i-th DGu and of the DGus and lines connected to it. Note that only the estimate of the bounds of these parameters is required, not their exact knowledge.

Remark 9.8 (Alternative SM controllers). In this work we rely on the SOSM control algorithm proposed in [BFU98a] and on the 3SM control law proposed in [DF09]. However, the results in this work are obtained independent of the particular choice of sliding mode controller. In case of the SOSM controller, any other SOSM control algorithm that does not need the measurement of $\dot{\boldsymbol{\sigma}}$ can be used to constrain system (9.3) augmented with dynamics (9.16) on the sliding manifold $\boldsymbol{\sigma} = \dot{\boldsymbol{\sigma}} = \mathbf{0}$, with $\boldsymbol{\sigma}$ as in (9.20). Similarly, any other 3SM control law can be used (e.g. the one proposed in [Lev03]), to constrain system (9.3) augmented with dynamics (9.29) on the sliding manifold $\boldsymbol{\sigma} = \dot{\boldsymbol{\sigma}} = \ddot{\boldsymbol{\sigma}} = \mathbf{0}$, with $\boldsymbol{\sigma}$ as in (9.20). An interesting continuation of the presented results is to study the performance of various SM controllers within the setting of current sharing and voltage regulation in DC microgrids.

9.6 Stability Analysis

In this section we first show that the states of the controlled microgrid are constrained, after a finite time, to the manifold $\boldsymbol{\sigma} = \mathbf{0}$, where Objective 9.2 is achieved. Thereafter, we prove that the solutions to the system, once the sliding manifold is attained, converge exponentially to a constant point, achieving additionally Objective 9.1.

9.6.1 Equivalent reduced order system

As a first step, we study the convergence to the sliding manifold when the SSOSM or the 3SM control law is applied to the system.

Lemma 9.4 (Convergence to the sliding manifold: SSOSM). Let Assumption 9.1 hold. The solutions to system (9.3) augmented with (9.16), controlled via the SSOSM control law (9.25), converge in a finite time T_r, to the sliding manifold $\{(\boldsymbol{I_t}, \boldsymbol{V}, \boldsymbol{I}, \boldsymbol{\theta}) : \boldsymbol{\sigma} = \dot{\boldsymbol{\sigma}} = \mathbf{0}\}$, with $\boldsymbol{\sigma}$ given by (9.20).

Proof. Following [BFU98a], the application of (9.25) to each converter guarantees that $\boldsymbol{\sigma} = \dot{\boldsymbol{\sigma}} = \mathbf{0}$, for all $t \geq T_r$. The details are omitted, since they are an immediate consequence of the used SSOSM control algorithm [BFU98a]. □

Lemma 9.5 (Convergence to the sliding manifold: 3SM). Let Assumption 9.1 hold. The solutions to system (9.3) augmented with (9.16), controlled via 3SM control algorithm (9.29)-(9.33), converge in a finite time T_r, to the sliding manifold $\{(\boldsymbol{I_t}, \boldsymbol{V}, \boldsymbol{I}, \boldsymbol{\theta}) : \boldsymbol{\sigma} = \dot{\boldsymbol{\sigma}} = \ddot{\boldsymbol{\sigma}} = \mathbf{0}\}$, with $\boldsymbol{\sigma}$ given by (9.20).

Proof. By implementing the Levant's differentiator (9.33) in each node, the values of $\boldsymbol{\xi_1}, \boldsymbol{\xi_2}$ and $\boldsymbol{\xi_3}$ are estimated in a finite time $T_{Ld} \geq 0$. Then, the application of (9.31) to each converter guarantees that $\boldsymbol{\sigma} = \dot{\boldsymbol{\sigma}} = \ddot{\boldsymbol{\sigma}} = \mathbf{0}$, for all $t \geq T_r \geq T_{Ld}$. The details are omitted, since they are an immediate consequence of the used Levant's second order differentiator [Lev03], and the 3SM control algorithm [DF09]. □

As we will show in the proof of Theorem 9.2 in the next subsection, converging to the sliding manifold where $\boldsymbol{\sigma} = \mathbf{0}$, is sufficient to conclude that Objective 9.2 (voltage balancing) is achieved. We postpone the analysis, in order show additionally convergence to a *constant* voltage.

For the analysis of the system, when the solutions are constrained to the sliding manifold, it is convenient to exploit the so-called system order reduction property, typical of sliding mode control methodology (see Subsection 2.2.8). Indeed, when the state of system (9.3) augmented with (9.16) is constrained to the sliding manifold $\{(\boldsymbol{I_t}, \boldsymbol{V}, \boldsymbol{I}, \boldsymbol{\theta}) : \boldsymbol{\sigma} = \dot{\boldsymbol{\sigma}} = \boldsymbol{0}\}$, with $\boldsymbol{\sigma}$ given by (9.20), the controlled system is described by $3n+m$ differential equations and $2n$ algebraic equations. Then, it is possible to obtain $2n$ state variables depending on the other $n+m$ ones. The resulting system of order $n+m$ represents the reduced order system equivalent to the system controlled with a discontinuous law, with the initial condition $(\boldsymbol{I_t}(T_r), \boldsymbol{V}(T_r), \boldsymbol{I}(T_r), \boldsymbol{\theta}(T_r))$, when $\boldsymbol{\sigma} = \dot{\boldsymbol{\sigma}} = \boldsymbol{0}$.

Lemma 9.6. (**Equivalent reduced order system**) For all $t \geq T_r$, the dynamics of the controlled system (9.3) augmented with (9.16) are given by the following equivalent system of reduced order

$$\begin{aligned} \boldsymbol{C_t}\dot{\boldsymbol{V}} = & \left(\mathbb{I}_n - (\mathbb{I}_n + \boldsymbol{C_t}\boldsymbol{W}\boldsymbol{\mathcal{L}_c}\boldsymbol{W})^{-1}\right)\boldsymbol{\mathcal{B}}\boldsymbol{I} \\ & - \left(\mathbb{I}_n - (\mathbb{I}_n + \boldsymbol{C_t}\boldsymbol{W}\boldsymbol{\mathcal{L}_c}\boldsymbol{W})^{-1}\right)\boldsymbol{I_L} \\ \boldsymbol{L}\dot{\boldsymbol{I}} = & -\boldsymbol{\mathcal{B}}^T\boldsymbol{V} - \boldsymbol{R}\boldsymbol{I}, \end{aligned} \tag{9.34}$$

together with the following algebraic relations

$$\boldsymbol{\theta} = \boldsymbol{W}^{-1}(\boldsymbol{V} - \boldsymbol{V}^\star) \tag{9.35}$$

$$\boldsymbol{I_t} = (\mathbb{I}_n + \boldsymbol{C_t}\boldsymbol{W}\boldsymbol{\mathcal{L}_c}\boldsymbol{W})^{-1}(-\boldsymbol{\mathcal{B}}\boldsymbol{I} + \boldsymbol{I_L}). \tag{9.36}$$

Proof. Given the sliding function (9.20), by virtue of Lemma 9.4 and Lemma 9.5, the state of system (9.3) augmented with (9.16) is constrained to the manifold $\{(\boldsymbol{I_t}, \boldsymbol{V}, \boldsymbol{I}, \boldsymbol{\theta}) : \boldsymbol{\sigma} = \dot{\boldsymbol{\sigma}} = \boldsymbol{0}\}$, where $\boldsymbol{\theta} = \boldsymbol{W}^{-1}(\boldsymbol{V} - \boldsymbol{V}^\star)$ and $\dot{\boldsymbol{V}} = \boldsymbol{W}\dot{\boldsymbol{\theta}}$. From the latter, one can straightforwardly obtain (9.36). After substituting expression (9.36) for $\boldsymbol{I_t}$ in (9.3), the dynamics of the voltage $\boldsymbol{V}$ become as in (9.34). □

9.6.2 Exponential convergence and objectives attainment

In the pervious subsection, we established that after a finite time T_r, the dynamics of the controlled microgrid are described by the equivalent system (9.34). In this subsection we study the convergence properties of this equivalent system. To do so, we rely on the concept of semistability [BB95], of which we recall the definition for convenience.

Definition 9.1 (Semistability). Consider the autonomous system

$$\dot{\boldsymbol{x}}(t) = \boldsymbol{A}\boldsymbol{x}(t), \tag{9.37}$$

where $t \geq 0$, $\boldsymbol{x} \in \mathbb{R}^n$ and $\boldsymbol{A} \in \mathbb{R}^{n \times n}$. System (9.37) is semistable if $\lim_{t\to\infty} \boldsymbol{x}(t)$ exists for all initial conditions $\boldsymbol{x}(0)$.

Furthermore, the following lemma turns out to be useful in the upcoming analysis:

Lemma 9.7 ($\boldsymbol{P} - \left(\boldsymbol{P}^{-1} + \boldsymbol{Q}\right)^{-1} \succeq \mathbf{0}$). Given a positive definite matrix $\boldsymbol{P} \in \mathbb{R}^{n\times n}$ and a positive semidefinite matrix $\boldsymbol{Q} \in \mathbb{R}^{n\times n}$, then

$$\boldsymbol{P} - \left(\boldsymbol{P}^{-1} + \boldsymbol{Q}\right)^{-1} \succeq \mathbf{0}. \tag{9.38}$$

Proof. Let $\tilde{\boldsymbol{Q}} = \boldsymbol{P}^{\frac{1}{2}}\boldsymbol{Q}\boldsymbol{P}^{\frac{1}{2}}$. Clearly, $\tilde{\boldsymbol{Q}} \succeq \mathbf{0}$, and $\mathbb{I}_{n\times n} + \tilde{\boldsymbol{Q}} \succ \mathbf{0}$. Then,

$$\boldsymbol{P} - \left(\boldsymbol{P}^{-1} + \boldsymbol{Q}\right)^{-1} = \boldsymbol{P}^{\frac{1}{2}}\left[\mathbb{I}_{n\times n} - \left(\mathbb{I}_{n\times n} + \tilde{\boldsymbol{Q}}\right)^{-1}\right]\boldsymbol{P}^{\frac{1}{2}} \tag{9.39}$$

is a positive semidefinite matrix if and only if $\mathbb{I}_{n\times n} - (\mathbb{I}_{n\times n}+\tilde{\boldsymbol{Q}})^{-1} = \tilde{\boldsymbol{Q}}(\mathbb{I}_{n\times n}+\tilde{\boldsymbol{Q}})^{-1} \succeq \mathbf{0}$. Observing that $(\mathbb{I}_{n\times n} + \tilde{\boldsymbol{Q}})^{-1} \succ \mathbf{0}$, it yields

$$\tilde{\boldsymbol{Q}}(\mathbb{I}_{n\times n} + \tilde{\boldsymbol{Q}})^{-1} \backsim (\mathbb{I}_{n\times n} + \tilde{\boldsymbol{Q}})^{-\frac{1}{2}}\tilde{\boldsymbol{Q}}(\mathbb{I}_{n\times n} + \tilde{\boldsymbol{Q}})^{-\frac{1}{2}} \succeq \mathbf{0}, \tag{9.40}$$

which completes the proof. □

Next, we show that the line currents $\boldsymbol{I}$ converge to a constant value.

Lemma 9.8 (Convergence of $\boldsymbol{I}$). Let Assumptions 9.1 and 9.2 hold. Given the equivalent reduced order system (9.34), $\lim_{t\to\infty} I(t)$ exists for all initial conditions $I(T_r)$.

Proof. Let $\tilde{\boldsymbol{V}} = \boldsymbol{V} - \overline{\boldsymbol{V}}$ and $\tilde{\boldsymbol{I}} = \boldsymbol{I} - \overline{\boldsymbol{I}}$ be the error given by the difference between the state of system (9.34) and the steady state value. Then, the dynamics of the corresponding error system are given by

$$\begin{aligned} \boldsymbol{C_t}\dot{\tilde{\boldsymbol{V}}} &= \left(\mathbb{I}_n - (\mathbb{I}_n + \boldsymbol{C_t}\boldsymbol{W}\boldsymbol{\mathcal{L}_c}\boldsymbol{W})^{-1}\right)\boldsymbol{\mathcal{B}}\tilde{\boldsymbol{I}} \\ \boldsymbol{L}\dot{\tilde{\boldsymbol{I}}} &= -\boldsymbol{\mathcal{B}}^T\tilde{\boldsymbol{V}} - \boldsymbol{R}\tilde{\boldsymbol{I}}, \end{aligned} \tag{9.41}$$

From (9.41), we obtain

$$\begin{aligned} \dot{\tilde{\boldsymbol{V}}} &= \boldsymbol{C_t}^{-1}\left(\mathbb{I}_n - (\mathbb{I}_n + \boldsymbol{C_t}\boldsymbol{W}\boldsymbol{\mathcal{L}_c}\boldsymbol{W})^{-1}\right)\boldsymbol{\mathcal{B}}\tilde{\boldsymbol{I}} \\ &= \left(\boldsymbol{C_t}^{-1} - (\boldsymbol{C_t} + \boldsymbol{C_t}\boldsymbol{W}\boldsymbol{\mathcal{L}_c}\boldsymbol{W}\boldsymbol{C_t})^{-1}\right)\boldsymbol{\mathcal{B}}\tilde{\boldsymbol{I}}, \end{aligned} \tag{9.42}$$

and

$$\boldsymbol{L}\ddot{\tilde{\boldsymbol{I}}} + \boldsymbol{R}\dot{\tilde{\boldsymbol{I}}} + \boldsymbol{\mathcal{B}}^T\dot{\tilde{\boldsymbol{V}}} = \mathbf{0}. \tag{9.43}$$

Substituting expression (9.42) for $\dot{\tilde{V}}$ in (9.43) leads to

$$\boldsymbol{L}\ddot{\tilde{\boldsymbol{I}}} + \boldsymbol{R}\dot{\tilde{\boldsymbol{I}}} + \underbrace{\boldsymbol{\mathcal{B}}^T\left(\boldsymbol{C_t}^{-1} - (\boldsymbol{C_t} + \boldsymbol{C_t}\boldsymbol{W}\boldsymbol{\mathcal{L}_c}\boldsymbol{W}\boldsymbol{C_t})^{-1}\right)\boldsymbol{\mathcal{B}}}_{\boldsymbol{K}}\,\tilde{\boldsymbol{I}} = \mathbf{0}. \tag{9.44}$$

Since, by virtue of Lemma 9.7 (with $\boldsymbol{P} = \boldsymbol{C}_t^{-1}, \boldsymbol{Q} = \boldsymbol{C}_t \boldsymbol{W} \boldsymbol{\mathcal{L}}_c \boldsymbol{W} \boldsymbol{C}_t$), $\boldsymbol{C}_t^{-1} - (\boldsymbol{C}_t + \boldsymbol{C}_t \boldsymbol{W} \boldsymbol{\mathcal{L}}_c \boldsymbol{W} \boldsymbol{C}_t)^{-1} \succeq \boldsymbol{0}$, then we also have

$$\boldsymbol{K} = \boldsymbol{\mathcal{B}}^T \left(\boldsymbol{C}_t^{-1} - (\boldsymbol{C}_t + \boldsymbol{C}_t \boldsymbol{W} \boldsymbol{\mathcal{L}}_c \boldsymbol{W} \boldsymbol{C}_t)^{-1} \right) \boldsymbol{\mathcal{B}} \succeq \boldsymbol{0}. \tag{9.45}$$

According to [BB95, Corollary 2], system (9.44) is semistable (see Definition 9.1) if and only if

$$\operatorname{rank} \begin{bmatrix} \boldsymbol{R} \\ \boldsymbol{R}(\boldsymbol{L}^{-1}\boldsymbol{K}) \\ \boldsymbol{R}(\boldsymbol{L}^{-1}\boldsymbol{K})^2 \\ \vdots \\ \boldsymbol{R}(\boldsymbol{L}^{-1}\boldsymbol{K})^{m-1} \end{bmatrix} = m. \tag{9.46}$$

Since $\boldsymbol{R}$ is a positive definite $m \times m$ diagonal matrix it can be readily confirmed that condition (9.46) holds, such that system (9.44) is indeed semistable. Since $\overline{\boldsymbol{I}}$ is a constant vector, it immediately follows that $\lim_{t\to\infty} \boldsymbol{I}(t)$ exists. □

Lemma 9.8 established that $\lim_{t\to\infty} \boldsymbol{I}(t)$ exists for all initial conditions $\boldsymbol{I}(T_r)$. This result can now be exploited to show that also the voltages converge to constant values.

Lemma 9.9 (Convergence of $\boldsymbol{V}$). Let Assumptions 9.1–9.3 hold. Given the equivalent reduced order system (9.34), $\lim_{t\to\infty} \boldsymbol{V}(t)$ exists for all initial conditions $\boldsymbol{V}(T_r)$.

Proof. Exploiting the convergence of $\boldsymbol{I}$ to a constant vector (see Lemma 9.8), from (9.43) we have

$$\lim_{t\to\infty} \boldsymbol{\mathcal{B}}^T \dot{\boldsymbol{V}}(t) = \boldsymbol{0}, \tag{9.47}$$

implying that

$$\lim_{t\to\infty} \dot{\boldsymbol{V}}(t) = \mathbb{1}_n \kappa, \tag{9.48}$$

with $\kappa \in \mathbb{R}$. By virtue of Lemma 9.3 and Lemma 9.4 or Lemma 9.5, for all $t \geq T_r$, we also have

$$\mathbb{1}_n^T \boldsymbol{W}^{-1} \boldsymbol{V} = \mathbb{1}_n^T (\boldsymbol{\theta} + \boldsymbol{W}^{-1} \boldsymbol{V}^\star) = \mathbb{1}_n^T \boldsymbol{\theta}(0) + \mathbb{1}_n^T \boldsymbol{W}^{-1} \boldsymbol{V}^\star. \tag{9.49}$$

Taking the derivative with respect to time on both sides of (9.49), it follows that $\mathbb{1}_n^T \boldsymbol{W}^{-1} \dot{\boldsymbol{V}}(t) = 0$ for all $t \geq T_r$. Exploiting (9.48), we obtain

$$\begin{aligned} \lim_{t\to\infty} \mathbb{1}_n^T \boldsymbol{W}^{-1} \dot{\boldsymbol{V}}(t) &= \mathbb{1}_n^T \boldsymbol{W}^{-1} \lim_{t\to\infty} \dot{\boldsymbol{V}}(t) \\ &= \mathbb{1}_n^T \boldsymbol{W}^{-1} \mathbb{1}_n \kappa \\ &= 0, \end{aligned} \tag{9.50}$$

which implies $\kappa = 0$ and consequently that $\lim_{t\to\infty} \boldsymbol{V}(t)$ exists for all initial conditions $\boldsymbol{V}(T_r)$. □

We are now ready to establish the first main result of this paper.

Theorem 9.1 (Achieving current sharing). *Let Assumptions 9.1–9.3 hold. Consider system (9.3), (9.16), controlled with the proposed distributed SSOSM (Subsection 9.5.1) or 3SM (Subsection 9.5.2) control scheme. Then, the generated currents* $\boldsymbol{I_t}(t)$ *converge, after a finite time, exponentially to* $\boldsymbol{W}^{-1}\mathbb{1}_n\mathbb{1}_n^T\boldsymbol{I_L}/(\mathbb{1}_n^T\boldsymbol{W}^{-1}\mathbb{1}_n)$*, achieving proportional current sharing.*

Proof. According to Lemma 9.6, for all $t \geq T_r$, the dynamics of the controlled system (9.3), (9.16) are given by the autonomous system (9.34) together with the algebraic equations (9.35) and (9.36). Bearing in mind the results proved in Lemma 9.8 and Lemma 9.9, the dynamics of the line current $\boldsymbol{I}$ and the voltage $\boldsymbol{V}$ are semistable. From the algebraic equations (9.35) and (9.36), it follows that $\lim_{t\to\infty}\boldsymbol{\theta}(t)$ and $\lim_{t\to\infty}\boldsymbol{I_t}(t)$ exist as well. Since (9.34) is linear and $\ker(\boldsymbol{\mathcal{L}_c}) = \operatorname{im}(\mathbb{1}_n)$, (9.16) implies that the vector $\boldsymbol{I_t}(t)$, with initial condition $\boldsymbol{I_t}(T_r)$, converges exponentially to a constant vector, achieving proportional current sharing.

We now proceed with establishing the second main result of this paper.

Theorem 9.2 (Achieving voltage balancing). *Let Assumptions 9.1–9.3 hold. Consider system (9.3), (9.16), controlled with the proposed distributed SSOSM (Subsection 9.5.1) or 3SM (Subsection 9.5.2) control scheme. Then, given a desired references vector* $\boldsymbol{V}^\star$*, the voltages* $\boldsymbol{V}(t)$ *satisfy* $\mathbb{1}_n^T\boldsymbol{W}^{-1}\boldsymbol{V}(t) = \mathbb{1}_n^T\boldsymbol{W}^{-1}\boldsymbol{V}^\star$ *for all* $t \geq T_r$*, with* T_r *a finite time.*

Proof. Following Lemma 9.4 or Lemma 9.5, for all $t \geq T_r$, the equality $\boldsymbol{W}^{-1}\boldsymbol{V}(t) = \boldsymbol{W}^{-1}\boldsymbol{V}^\star + \boldsymbol{\theta}(t)$ holds. Pre-multiplying both sides by $\mathbb{1}_n^T$ yields $\mathbb{1}_n^T\boldsymbol{W}^{-1}\boldsymbol{V}(t) = \mathbb{1}_n^T\boldsymbol{W}^{-1}\boldsymbol{V}^\star + \mathbb{1}_n^T\boldsymbol{\theta}(t)$. Due to Assumption 9.3 and by virtue of Lemma 9.3, one has that $\mathbb{1}_n^T\boldsymbol{\theta}(t) = \mathbb{1}_n^T\boldsymbol{\theta}(0) = 0$. Then, one can conclude that voltage balancing is achieved for all $t \geq T_r$.

Remark 9.9 (Robustness to failed communication). The proposed control scheme is distributed and as such requires a communication network to share information on the generated currents. However, note that the integrators $\boldsymbol{\theta}$ in (9.16) are not needed to regulate the voltages in the microgrid to their desired values, but are only required to achieve current sharing and voltage balancing. In fact, by omitting the variable $\boldsymbol{\theta}$ in the analysis, the controlled microgrid converges, in a finite time, to the manifold $\boldsymbol{\sigma} = \boldsymbol{0}$, where $\boldsymbol{V} = \boldsymbol{V}^\star$. Moreover, considering constant value of θ_i (e.g. after the plug-out of the DGu i, or the failing of the communication link between DGu i and DGu j), the controlled DGu i converges, in a finite time, to the manifold $\sigma_i = 0$, where $V_i = V_i^\star + w_i\overline{\theta}_i$.

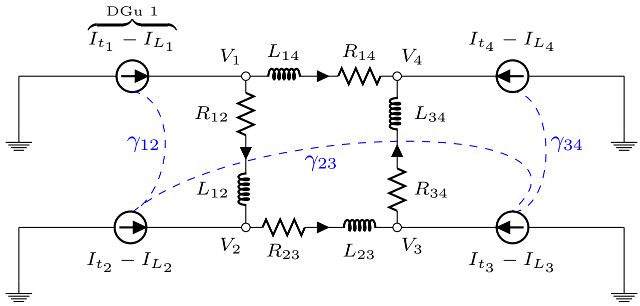

Fig. 9.3. Scheme of the considered microgrid with 4 power converters. The dashed lines represent the communication network.

Table 9.2. Microgrid Parameters and Current Demand

DGu		1	2	3	4
R_{t_i}	(Ω)	0.2	0.3	0.5	0.1
L_{t_i}	(mH)	1.8	2.0	3.0	2.2
C_{t_i}	(mF)	2.2	1.9	2.5	1.7
$V_i^\star$	(V)	380.0	380.0	380.0	380.0
$V_i(0)$	(V)	380.2	380.05	379.95	379.8
$I_{L_i}(0)$	(A)	25.0	15.0	10.0	30.0
ΔI_{L_i}	(A)	5.0	7.5	12.5	−5.0

Remark 9.10 (Perturbations in the controller states). In case Assumption 9.3 is violated, we have $\mathbb{1}_n^T\boldsymbol{\theta}(t) = \mathbb{1}_n^T\boldsymbol{\theta}(0)$, and consequently $\mathbb{1}_n^T\boldsymbol{W}^{-1}\boldsymbol{V}(t) = \mathbb{1}_n^T\boldsymbol{W}^{-1}\boldsymbol{V}^\star + \mathbb{1}_n^T\boldsymbol{\theta}(0)$ on the sliding manifold, implying that the weighted average voltage of the microgrid is shifted by $\mathbb{1}_n^T\boldsymbol{\theta}(0)$. However, the presented stability analysis is still valid such that the stability of the whole microgrid and the achievement of proportional current sharing is still guaranteed.

9.7 Case Study

In this section, the proposed manifold-based consensus algorithm is assessed in simulation by implementing the third order sliding mode control strategy discussed in Subsection 9.5.2. We consider a microgrid composed of 4 DGus interconnected as shown in Fig. 9.3, where also the communication network is depicted. The parameters of each DGu, including the current demand, and the line parameters are reported in Tables 9.2 and 9.3, respectively. The weights associated with the edges of the communication graph are $\gamma_{12} = \gamma_{23} = \gamma_{34} = 1 \times 10^3$. For all the DGus the controller parameter α_i in (9.31) is set to 2.5×10^3, while the gain Λ_i of Levant's differentiator (9.33) is set to 5.0×10^5. In order to investigate the performance of the proposed control approach within a low voltage DC microgrid, four different scenarios are implemented (see Fig. 9.4).

Table 9.3. Line Parameters

Line	{1,2}	{2,3}	{3,4}	{1,4}
R_{ij} (mΩ)	70	50	80	60
L_{ij} (µH)	2.1	2.3	2.0	1.8

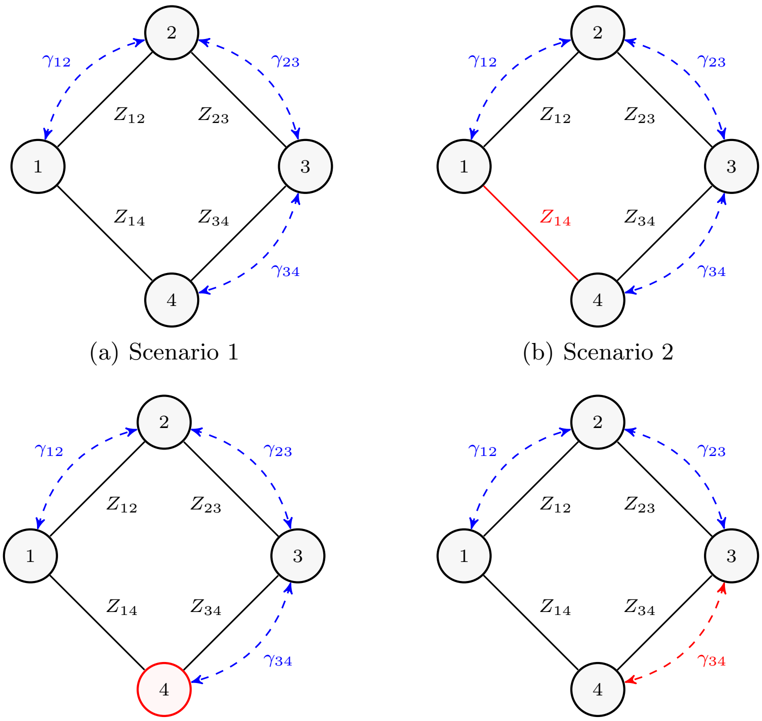

Fig. 9.4. Configurations of the considered microgrid implemented in simulations. Z_{ij} denotes the resistive-inductive impedance of the distribution line interconnecting DGu i with DGu j.

9.7.1 Scenario 1: proportional current sharing

The system is initially at the steady state. Then, consider a current demand variation ΔI_{L_i} at the time instant $t = 1\,\mathrm{s}$ (see Table 9.2). The PCC voltages and the generated currents are illustrated at the top of Fig. 9.5. One can appreciate that the weighted average of the PCC voltages (denoted by V_{av}) is always equal to the weighted average of the corresponding references (see Objective 9.2), and the current generated by each DGu converges to the desired value, achieving proportional current sharing (see Objective 9.1). Note that, even during the transient phase, current sharing is practically maintained. Moreover, at the bottom of Fig. 9.5 the currents shared among the DGus are reported together with the control signals generated by the 3SM control algorithm (9.31). Note that the 3SM controllers, which require only local measurements of V_i and information on I_t from neighbours over the communication network, generate control signals that are

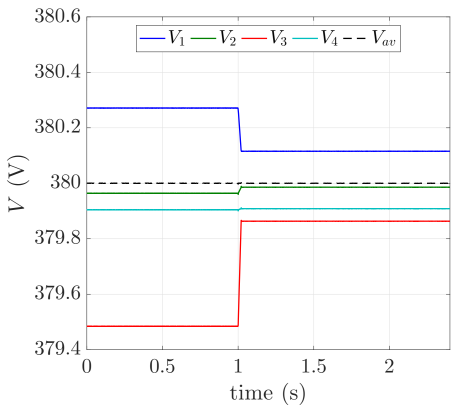

(a) voltage

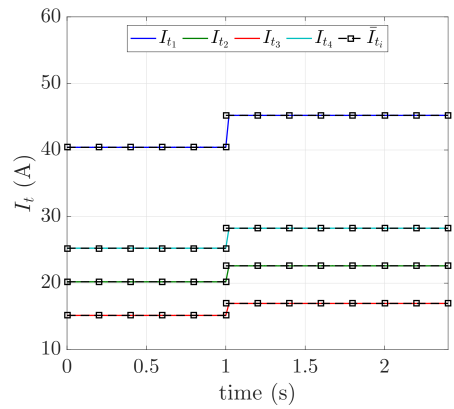

(b) generated current

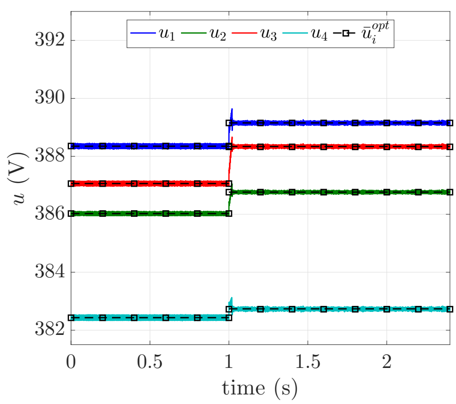

(c) control input

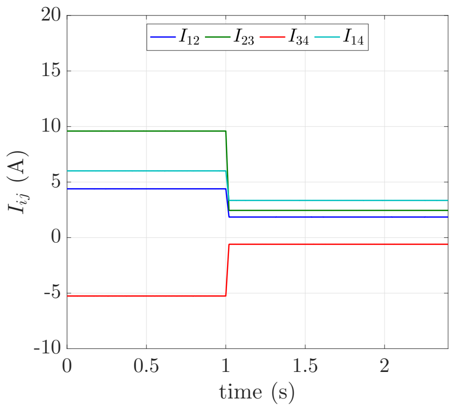

(d) exchanged current

Fig. 9.5. Scenario 1: **(a)** Voltage at the PCC of each DGu together with its weighted average value (dashed line). **(b)** Generated currents together with the corresponding values (dashed line) that allow the achievement of proportional current sharing. **(c)** control inputs $u_i(t) = \int_0^t v_i(\tau)d\tau$, v_i as in (9.31), together with the optimal feedforward inputs (9.8) indicated by the dashed lines. **(d)** Currents shared among the DGus through the lines.

equal to the optimal feedforward input (9.8), without exact knowledge on the network parameters and the current demand I_L.

9.7.2 Scenario 2: opening of a distribution line

In the second scenario, we investigate the performance of the proposed controllers when a distribution line is opened (e.g. due to an electric fault). The system is initially at the steady state, and at the time instant $t = 0.4\,$s, the distribution line interconnecting the DGus 1 and 4 is opened. Then, consider a current demand variation as in Scenario 1. The PCC voltages and the generated currents are illustrated at the top of Fig. 9.6. One

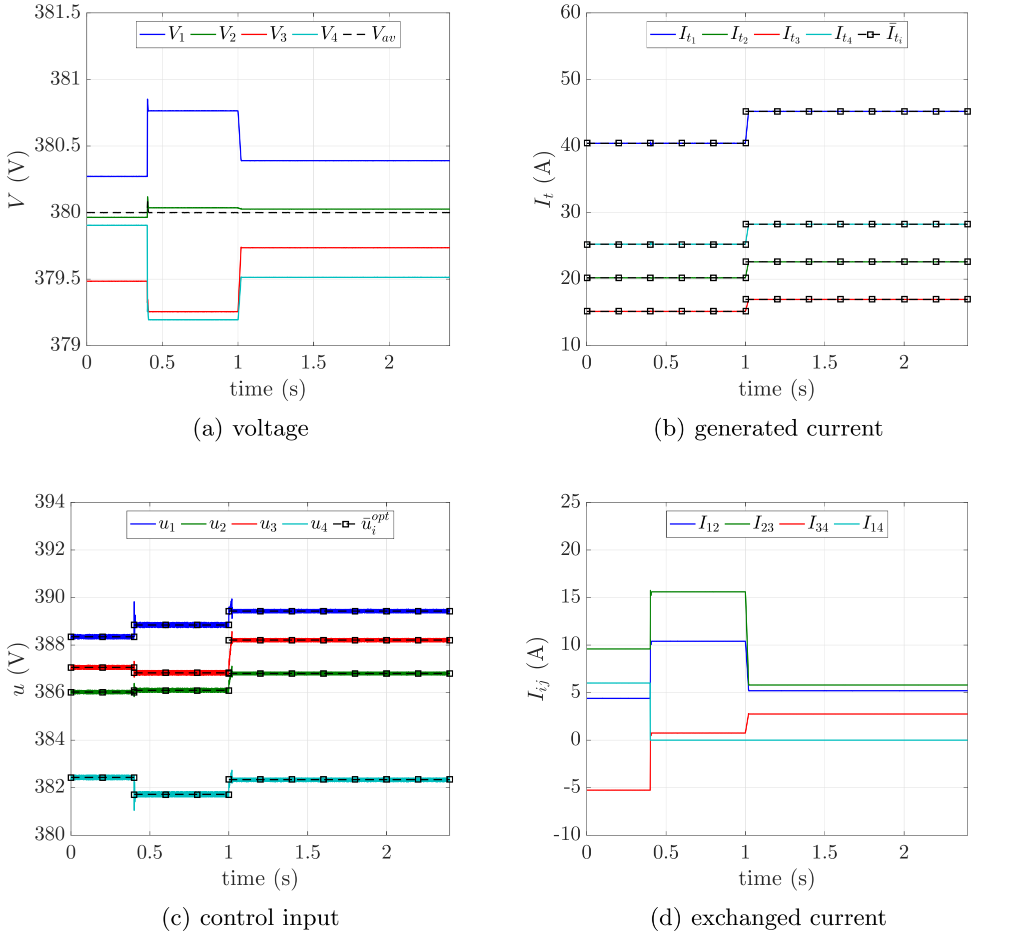

(a) voltage (b) generated current

(c) control input (d) exchanged current

Fig. 9.6. Scenario 2: **(a)** Voltage at the PCC of each DGu together with its weighted average value (dashed line). **(b)** Generated currents together with the corresponding values (dashed line) that allow the achievement of proportional current sharing. **(c)** control inputs $u_i(t) = \int_0^t v_i(\tau)d\tau$, v_i as in (9.31), together with the optimal feedforward inputs (9.8) indicated by the dashed lines. **(d)** Currents shared among the DGus through the lines.

can appreciate that the weighted average of the PCC voltages (denoted by V_{av}) is always equal to the weighted average of the corresponding references (see Objective 9.2), and the current generated by each DGu converges to the desired value, achieving proportional current sharing (see Objective 9.1). Note that, even during the transient phases, current sharing is practically maintained. Moreover, at the bottom of Fig. 9.6 the currents shared among the DGus are reported together with the control signals generated by the 3SM control algorithm (9.31).

9.7.3 Scenario 3: plug-out and plug-in of a DGu

In the third scenario, we investigate the Plug-and-Play (PnP) capabilities of the proposed controllers. For the sake of clarity, in this scenario and the next one we consider equal current sharing among the DGus. The system is initially at the steady state, and at the time instant $t = 0.4\,\mathrm{s}$, the DGu 4 is disconnected from the considered DC network (in this configuration the impedance of the line interconnecting DGu 1 and DGu 3 is equal to the sum of the line impedances Z_{14} and Z_{34}). After a current demand variation as in Scenario 1, at the time instant $t = 1.4\,\mathrm{s}$, the DGu 4 is reconnected to the DC network. The PCC voltages and the generated currents are illustrated at the top of Fig. 9.7. One can appreciate that the arithmetic average of the PCC voltages (denoted by V_{av}) is equal to the arithmetic average of the corresponding references (see Remark 9.3), even after disconnecting the DGu 4. Moreover, when the DGu 4 operates isolated from the considered DC network, equal current sharing is achieved only among the DGus 1, 2 and 3, while the DGu 4 supplies its local load. However, when the DGu 4 is reconnected to the DC network, current sharing among all the DGus is again reestablished. Moreover, at the bottom of Fig. 9.7 the currents shared among the DGus are reported together with the control signals generated by the 3SM control algorithm (9.31). Note that, when the DGu 4 is isolated from the network, the comparison between u_4 and the corresponding optimal feedforward input loses its meaning.

9.7.4 Scenario 4: failing of a communication link

In the last scenario, we investigate the robustness of the proposed controllers to failed communication. The system is initially at the steady state, and at the time instant $t = 0.4\,\mathrm{s}$, the communication between DGu 3 and DGu 4 is interrupted. We observe that as long as the demand does not change, current sharing among all the DGus in mainteined. The PCC voltages and the generated currents are illustrated at the top of Fig. 9.8. One can note that after a current demand variation (see Table 9.2), equal current sharing is achieved only among the DGus 1, 2 and 3, while the DGu 4 generates a current such that the voltage at node 4 is kept constant. One can appreciate that the arithmetic average of the PCC voltages (denoted by V_{av}) is equal to the arithmetic average of the corresponding references (see Remark 9.3), even after interrupting the communication between DGu 3 and DGu 4. Moreover, at the bottom of Fig. 9.8 the currents shared among the DGus are reported together with the control signals generated by the 3SM control algorithm (9.31). Note that, when the communication with DGu 4 fails, the comparison between u_4 and the corresponding optimal feedforward input loses its meaning.

Even if IEEE Standards or guidlines for DC power distribution networks do not exist yet (to the best of our knowledge), it is usually required in practical cases that the voltage deviations are within the 5 % of the desired value (see for instance [TMGFT16, SASS17, Sch07]). In all the previous scenarios, the voltage at the PCC of each DGu is within the range 380 ± 1 V, implying that the voltage deviations are less than the 0.3 % of the nominal value $V^{\star} = 380\,\mathrm{V}$, even during transients and critical conditions.

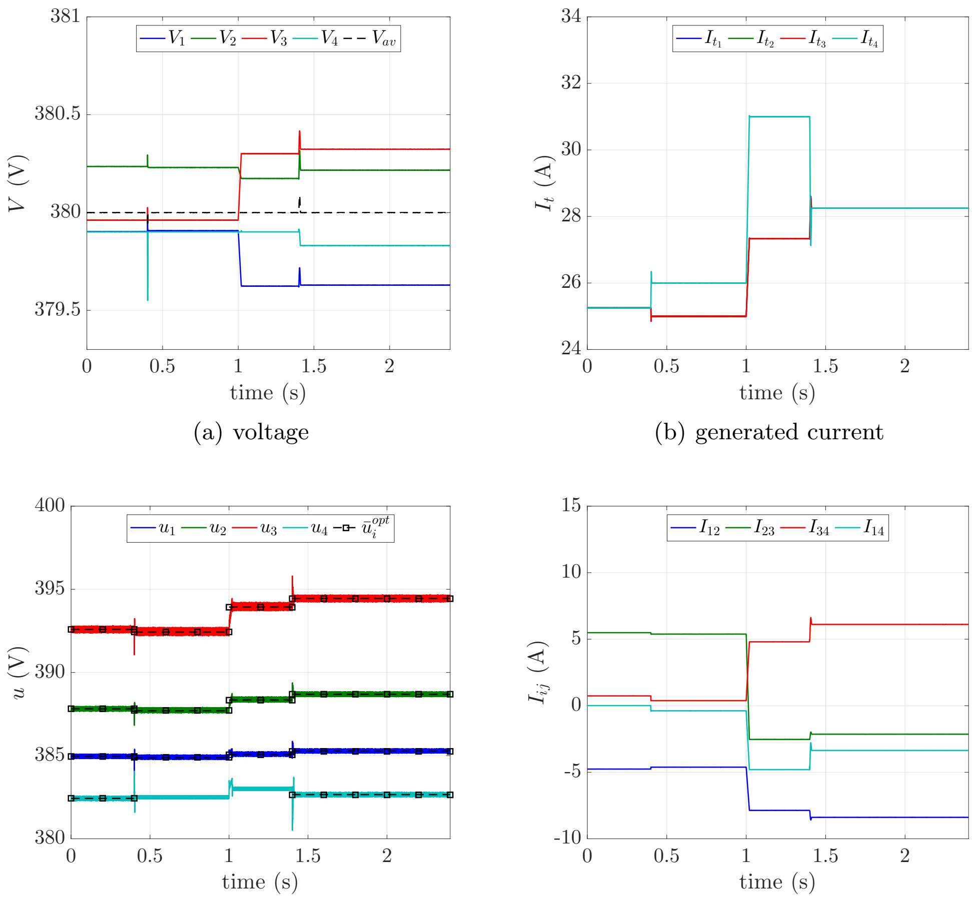

(a) voltage

(b) generated current

(c) control input

(d) exchanged current

Fig. 9.7. Scenario 3: **(a)** Voltage at the PCC of each DGu together with its arithmetic average value (dashed line). **(b)** Generated currents in case of equal current sharing, which is achieved by DGus 1, 2, 3 for all the simulation time interval, and by DGu 4 only when it is connected to the microgrid. **(c)** control inputs $u_i(t) = \int_0^t v_i(\tau)d\tau$, v_i as in (9.31), together with the optimal feedforward inputs (9.8) indicated by the dashed lines. **(d)** Currents shared among the DGus through the lines.

9.8 Conclusions

In this chapter we have developed a distributed control algorithm, obtaining current sharing and voltage regulation in DC microgrids. Its convergence properties have been analytically investigated, and a case study shows the effectiveness of the proposed solution. The proposed control scheme exploits a communication network to achieve current sharing using a consensus-like algorithm. Another useful feature of the proposed control scheme is that the average voltage of the microgrid converges to the average of the voltage references, independently of the initial voltage conditions. The latter is achieved by constraining the

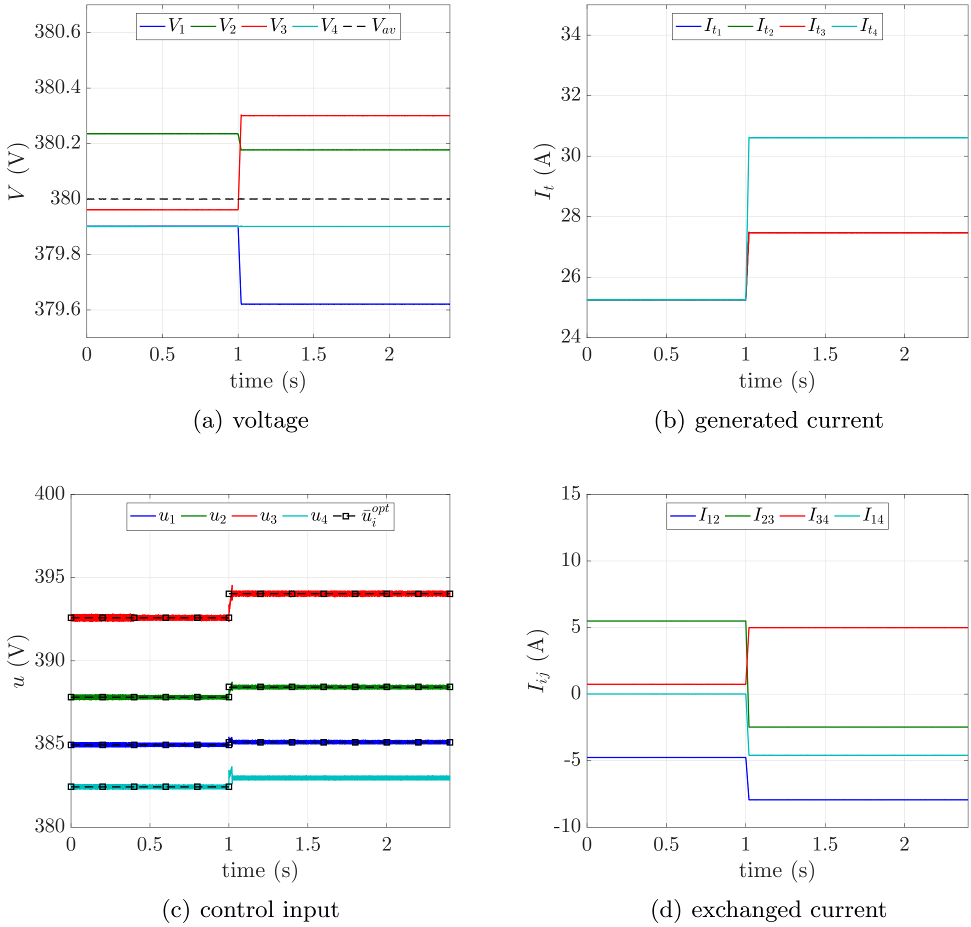

(a) voltage

(b) generated current

(c) control input

(d) exchanged current

Fig. 9.8. Scenario 4: **(a)** Voltage at the PCC of each DGu together with its arithmetic average value (dashed line). **(b)** Generated currents in case of equal current sharing, which is achieved by DGus 1, 2, 3 for all the simulation time interval, and by DGu 4 only before the failing of the communication link. **(c)** control inputs $u_i(t) = \int_0^t v_i(\tau)d\tau$, v_i as in (9.31), together with the optimal feedforward inputs (9.8) indicated by the dashed lines. **(d)** Currents shared among the DGus through the lines.

system to a suitable manifold. To ensure that the desired manifold is reached in a finite time, even in presence of modelling uncertainties, two sliding mode control strategies have been proposed, that provide the switching frequencies or the duty cycle of the power converters.

10

Boost-Based DC Microgrids

Abstract. This chapter deals with the design of a robust decentralized control scheme for voltage regulation in boost-based DC microgrids. The proposed solution consists of the design of a suitable manifold on which voltage regulation is achieved even in presence of unknown load demand and modelling uncertainties. A second order sliding mode control is used to constrain the state of the microgrid to this manifold by generating continuous control inputs that can be used as duty cycles of the power converters. The proposed control scheme has been theoretically analyzed and validated through experiments on a real DC microgrid.

10.1 Preliminaries on Boost-Based DC Microgrids

As described in the previous chapter (see Section 9.1), voltage regulation and current (or power) sharing are the two main control objectives in DC microgrids. Typically, both objectives are simultaneously achieved by designing hierarchical control schemes, and they have been addressed by different approaches in the literature (see for instance [AFG13, ZD15, NMDL15, TMGFT16, HGMK15, DWD16] and the references there in). However, all these works deal with DC-DC buck converters only (or do not take into account the model of the power converter), while, in many battery-powered applications such as hybrid electric vehicles and lighting systems, DC-DC boost converters are used in order to achieve higher voltage and reduce the number of cells[16]. Since the dynamics of the boost converter are nonlinear, regulating the output voltage in presence of unknown load demand and uncertain network parameters is not an easy task. For all these reasons, the solution in this chapter relies on a Sliding Mode (SM) control methodology to solve the voltage control problem in boost-based DC microgrids affected by nonlinearities and uncertainties [Utk92, ES98, UGS99]. Indeed, sliding modes are well known for their robustness properties and, belonging to the class of Variable Structure Control Systems, have been extensively applied in power electronics, since they are perfectly adequate to control the inherently variable structure nature of DC-DC converters. SM controllers require to operate at very high (ideally infinite) and variable switching frequency. This condition increases the power losses and the issues related to the electromagnetic interference noise, making the design of the input and output filters more complicated. SM

[16] Battery-powered applications often stack cells in series to increase the voltage level.

controllers based on the hysteresis-modulation (also known as delta-modulation) have been proposed in order to restrict the switching frequency (see for instance [CMMC92]). To do this, additional tools such as constant timer circuits or adaptive hysteresis band are required, making the solution more elaborated and then unattractive. Moreover, this approach (called quasi-SM) reduces the robustness of the control system [Bar98]. Alternatively, the so-called equivalent control approach has been proposed together with the Pulse Width Modulation (PWM) technique (otherwise known as duty cycle control) to achieve constant switching frequency. However, computing the equivalent control often requires the perfect knowledge of the model parameters as well as the load and the input voltage [FGO06], or alternatively the implementation of observers to estimate them [OG13]. In this work, in order to control the output voltage of a boost converter, a fully decentralized Second Order SM (SOSM) control solution is proposed, capable of dealing with unknown load and input voltage dynamics, as well as uncertain model parameters, without requiring the use of observers. Making reference to the hierarchical control levels of a microgrid adopted in [GVM+11], the proposed control scheme lies in "Level 0", which is also known as "inner voltage control loop". Due to its decentralized and robust nature, the design of each local controller does not depend on the knowledge of the whole microgrid, making the control synthesis simple and the control scheme scalable and suitable for be coupled with higher-level control schemes aimed at generating voltage references that guarantee load sharing. Since a higher order sliding modes methodology is used, the proposed controllers generate continuous inputs that can be used as duty cycles, in order to achieve constant switching frequency. Besides, being of higher order, a distinguishing feature of the proposed control scheme is that an additional auxiliary integral controller is coupled to the controlled converter, via suitable designed sliding function. Moreover, with respect to the existing literature (to the best of our knowledge) in this work the local stability of a boost-based microgrid is analyzed, instead of the single boost converter, theoretically proving that on the obtained sliding manifold, the desired operating point is locally exponentially stable. Additionally, the analysis is useful to choose suitable controller parameters ensuring the stability, and facilitates the tuning of the controllers. The proposed control scheme has been validated through experimental tests on a real DC microgrid test facility at Ricerca sul Sistema Energetico (RSE), in Milan, Italy [RL16], showing satisfactory closed-loop performances.

10.2 Boost-Based DC Microgrid Model

Before introducing the model of the considered boost-based DC microgrid, for the readers' convenience, some basic notions on DC microgrids are presented.

Fig. 10.1 shows the electrical scheme of a typical boost-based DC microgrid, where two DGus, with local loads, exchange power through the distribution line represented by the resistance R_{ij}. The energy source of a DGu, which can be of renewable type, is represented, for simplicity, by a DC voltage source V_{DC_i}. The boost converter feeds a local DC load with a voltage level V_i higher than V_{DC_i}. Note that, the boost converter allows to obtain an output voltage level higher than or equal to the voltage input. This is done due to the quick succession of two different operation stages during which the inductance L_{t_i} accumulates or supplies energy. The resistance R_{t_i}, instead, represents all

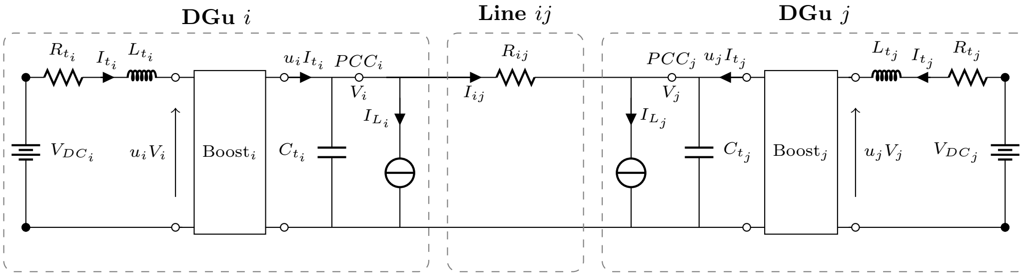

Fig. 10.1. The considered electrical scheme of a typical boost-based DC microgrid composed of two DGus.

the unavoidable energy losses. Finally the capacitor C_{t_i} is used in order to maintain a constant voltage at the output. The local DC load is connected to the so-called Point of Common Coupling (PCC) and it can be treated as a current disturbance I_{L_i}.

The network is represented by a connected and undirected graph $\mathcal{G} = (\mathcal{V}, \mathcal{E})$, where the nodes $\mathcal{V} = \{1, ..., n\}$, represent the DGus and the edges $\mathcal{E} = \{1, ..., m\}$, represent the distribution lines interconnecting the DGus. First, consider the scheme reported in Fig. 10.1. By applying the Kirchhoff's current and voltage laws, and by using an average switching method, the governing dynamic equations[17] of the i-th node are the following

$$\begin{aligned} L_{t_i}\dot{I}_{t_i} &= -R_{t_i}I_{t_i} - u_iV_i + V_{DC_i} \\ C_{t_i}\dot{V}_i &= u_iI_{t_i} - I_{L_i} - \sum_{j\in\mathcal{N}_i} I_{ij}, \end{aligned} \tag{10.1}$$

where $\mathcal{N}_i$ is the set of nodes (i.e., DGus) connected to the i-th DGu by distribution lines, while $u_i = 1 - d_i$ is the control input and d_i is the duty cycle ($0 \le d_i \le 1$). Exploiting the Quasi Stationary Line (QSL) approximation of power lines [VSZ95, AWA07], for each $j \in \mathcal{N}_i$, one has

$$I_{ij} = \frac{1}{R_{ij}}(V_i - V_j). \tag{10.2}$$

The symbols used in (10.1) and (10.2) are described in Table 10.1.

Remark 10.1 (Kron reduction). Note that in (10.1), the load currents are located only at the PCC of each DGu (see also Fig. 10.1). However, in many cases the loads are not close to the DGus. Then, by using the well known Kron reduction method, it is possible to map arbitrary interconnections of DGus (boundary nodes) and loads (interior nodes), into a reduced network with only local loads [ZD15, DB13].

The network topology can be represented by its corresponding incidence matrix $\boldsymbol{\mathcal{B}} \in \mathbb{R}^{n\times m}$. The ends of edge k are arbitrarily labeled with a $+$ and a $-$. More precisely, one has that

[17] For the sake of simplicity, the dependence of all the variables on time t is omitted throughout the chapter.

Table 10.1. Description of the used symbols

	State variables
I_{t_i}	Inductor current
V_i	Boost output voltage
I_{ij}	Exchanged current
	Parameters
R_{t_i}	Filter resistance
L_{t_i}	Filter inductance
C_{t_i}	Shunt capacitor
R_{ij}	Line resistance
	Inputs
u_i	Control input
V_{DC_i}	Voltage source
I_{L_i}	Unknown current demand

$$\mathcal{B}_{ik} = \begin{cases} +1 & \text{if } i \text{ is the positive end of } k \\ -1 & \text{if } i \text{ is the negative end of } k \\ 0 & \text{otherwise.} \end{cases}$$

Let '$\circ$' denote the so-called Hadamard product (also known as Schur product). Given the vectors $\boldsymbol{p} \in \mathbb{R}^n, \boldsymbol{q} \in \mathbb{R}^n$, then $(\boldsymbol{p} \circ \boldsymbol{q}) \in \mathbb{R}^n$ with $(\boldsymbol{p} \circ \boldsymbol{q})_i = p_i q_i$ for all $i \in \mathcal{V}$. After substituting (10.2) in (10.1), the overall microgrid system can be written compactly for all nodes $i \in \mathcal{V}$ as

$$\begin{aligned} \boldsymbol{L_t} \dot{\boldsymbol{I}}_{\boldsymbol{t}} &= -\boldsymbol{R_t} \boldsymbol{I_t} - \boldsymbol{u} \circ \boldsymbol{V} + \boldsymbol{V_{DC}} \\ \boldsymbol{C_t} \dot{\boldsymbol{V}} &= \boldsymbol{u} \circ \boldsymbol{I_t} - \boldsymbol{\mathcal{B}} \boldsymbol{R}^{-1} \boldsymbol{\mathcal{B}}^T \boldsymbol{V} - \boldsymbol{I_L}, \end{aligned} \tag{10.3}$$

where $\boldsymbol{I_t} = [I_{t_1}, \ldots, I_{t_n}]^T$, $\boldsymbol{V} = [V_1, \ldots, V_n]^T$, $\boldsymbol{V_{DC}} = [V_{DC_1}, \ldots, V_{DC_n}]^T$, $\boldsymbol{I_L} = [I_{L_1}, \ldots, I_{L_n}]^T$, and $\boldsymbol{u} = [u_1, \ldots, u_n]^T$. Moreover $\boldsymbol{C_t}, \boldsymbol{L_t}$ and $\boldsymbol{R_t}$ are $n \times n$ positive definite diagonal matrices, while $\boldsymbol{R}$ is a $m \times m$ positive definite diagonal matrix, e.g. $\boldsymbol{R_t} = \text{diag}\{R_{t_1}, \ldots, R_{t_n}\}$ and $\boldsymbol{R} = \text{diag}\{R_1, \ldots, R_m\}$, with $R_k = R_{ij}$ for all $k \in \mathcal{E}$, where line k connects nodes i and j.

10.3 Problem Formulation

Before introducing the control problem and in order to permit the controller design in the next sections, the following assumption is introduced:

Assumption 10.1 (Available information). The state variables I_{t_i} and V_i are locally available only at the i-th DGu. The network parameters $R_{t_i}, R_i, L_{t_i}, C_{t_i}$, the current disturbance I_{L_i}, and the voltage source V_{DC_i} are constant, unknown but bounded, with bounds a-priori known.

Remark 10.2 (Decentralized control). Since, according to Assumption 10.1, I_{t_i} and V_i are available only at the i-th DGu, the control scheme needs to be designed in a decentralized manner.

Remark 10.3 (Varying parameters and current demand). Note that the parameter uncertainty, the current disturbance and the voltage source are required to be constant (Assumption 10.1) only to allow for a steady state solution and to theoretically analyze its stability. In fact, since a robust control strategy is adopted, Assumption 10.1 is not needed to reach and remain on the desired sliding manifold that is designed in Section 10.4.

Note that given a constant current disturbance $\boldsymbol{I_L}$, and a constant voltage source $\boldsymbol{V_{DC}}$, there exist a constant control input $\overline{\boldsymbol{u}}$ and a steady state solution $(\overline{\boldsymbol{I}}_{\boldsymbol{t}}, \overline{\boldsymbol{V}})$ to system (10.3) that satisfy

$$\begin{aligned} \overline{\boldsymbol{I}}_{\boldsymbol{t}} &= \boldsymbol{R_t}^{-1}\left(-\overline{\boldsymbol{u}} \circ \overline{\boldsymbol{V}} + \boldsymbol{V_{DC}}\right) \\ \boldsymbol{\mathcal{B}}\boldsymbol{R}^{-1}\boldsymbol{\mathcal{B}}^T\overline{\boldsymbol{V}} &= \overline{\boldsymbol{u}} \circ \overline{\boldsymbol{I}}_{\boldsymbol{t}} - \boldsymbol{I_L}. \end{aligned} \tag{10.4}$$

The second line of (10.4) implies[18] that at the steady state the total generated current $\mathbb{1}_n^T(\overline{\boldsymbol{u}} \circ \overline{\boldsymbol{I}}_{\boldsymbol{t}})$ is equal to the total current demand $\mathbb{1}_n^T \boldsymbol{I_L}$. To formulate the control objective, aiming at voltage regulation, it is assumed that for every DGu, there exists a desired reference voltage $V_i^\star$.

Assumption 10.2 (Desired voltages). There exists a constant reference voltage $V_i^\star$ at the PCC, for all $i \in \mathcal{V}$.

The objective is then formulated as follows: Given system (10.3), and given a $\boldsymbol{V}^\star = [V_1^\star, \ldots, V_n^\star]^T$, we aim at designing a fully decentralized control scheme capable of guaranteeing voltage regulation, i.e.

Objective 10.1 (Voltage regulation).

$$\lim_{t\to\infty} \boldsymbol{V}(t) = \overline{\boldsymbol{V}} = \boldsymbol{V}^\star. \tag{10.5}$$

10.4 Decentralized Sliding Mode Voltage Control

In this section a fully decentralized Suboptimal Second Order Sliding Mode (SSOSM) control scheme is proposed in order to achieve Objective 10.1, providing a continuous control input. As a first step, system (10.3) is augmented with additional state variables θ_i for all $i \in \mathcal{V}$, resulting in:

[18] The incidence matrix $\boldsymbol{\mathcal{B}}$ satisfies $\mathbb{1}_n^T\boldsymbol{\mathcal{B}} = \boldsymbol{0}$, where $\mathbb{1}_n \in \mathbb{R}^n$ is the vector consisting of all ones.

$$
\begin{aligned}
\boldsymbol{L_t}\dot{\boldsymbol{I}}_{\boldsymbol{t}} &= -\boldsymbol{R_t}\boldsymbol{I_t} - \boldsymbol{u}\circ\boldsymbol{V} + \boldsymbol{V_{DC}} \\
\boldsymbol{C_t}\dot{\boldsymbol{V}} &= \boldsymbol{u}\circ\boldsymbol{I_t} - \boldsymbol{\mathcal{B}}\boldsymbol{R}^{-1}\boldsymbol{\mathcal{B}}^T\boldsymbol{V} - \boldsymbol{I_L} \\
\dot{\boldsymbol{\theta}} &= -(\boldsymbol{V} - \boldsymbol{V}^{\star})\,.
\end{aligned}
\tag{10.6}
$$

The additional state $\boldsymbol{\theta}$ will be coupled to the control input $\boldsymbol{u}$ via the proposed control scheme, and its dynamics provide a form of integral action that is helpful to obtain the desired voltage regulation.

Now, a suitable sliding function $\boldsymbol{\sigma}(\boldsymbol{I_t},\boldsymbol{V},\boldsymbol{\theta})$ for system (10.6) will be introduced, that permits to prove the achievement of Objective 10.1. The choice is indeed motivated by the stability analysis in the Section 10.5, but is stated here for the sake of exposition. First, the sliding function $\boldsymbol{\sigma}:\mathbb{R}^{3n}\to\mathbb{R}^n$ is given by

$$
\boldsymbol{\sigma}(\boldsymbol{I_t},\boldsymbol{V},\boldsymbol{\theta}) = \boldsymbol{M_1}\boldsymbol{I_t} + \boldsymbol{M_2}(\boldsymbol{V}-\boldsymbol{V}^{\star}) - \boldsymbol{M_3}\boldsymbol{\theta}, \tag{10.7}
$$

where $\boldsymbol{M_1} = \mathrm{diag}\{m_{1_1},\ldots,m_{1_n}\}$, $\boldsymbol{M_2} = \mathrm{diag}\{m_{2_1},\ldots,m_{2_n}\}$, $\boldsymbol{M_3} = \mathrm{diag}\{m_{3_1},\ldots,m_{3_n}\}$ are positive definite diagonal matrices suitable selected in order to assign the dynamics of system (10.3) when it is constrained on the manifold $\boldsymbol{\sigma} = \mathbf{0}$. Since $\boldsymbol{M_1}$, $\boldsymbol{M_2}$, $\boldsymbol{M_3}$ are diagonal matrices, $\sigma_i, i\in\mathcal{V}$, depends, according to Assumption 10.1, only on the state variables locally available at the i-th node, facilitating the design of a decentralized control scheme (see Remark 10.2).

By regarding the sliding function (10.7) as the output function of system (10.3), it appears that the relative degree[19] of the system is one. This implies that a first order sliding mode controller can be *naturally* applied [Utk92] in order to attain in a finite time the sliding manifold $\boldsymbol{\sigma} = \mathbf{0}$. In this case, the discontinuous control signal generated by a first order sliding mode controller can be directly used to open and close the switch of the boost converter.

Remark 10.4 (Switching frequency). By using a (discontinuous) first order sliding mode control law to open and close the switch of the boost converter, the Insulated Gate Bipolar Transistors (IGBTs) switching frequency cannot be a-priori fixed and the corresponding power losses could be very high. Usually, in order to achieve a constant IGBTs switching frequency, boost converters are controlled by implementing the so-called Pulse Width Modulation (PWM) technique. To do this, a continuous control signal that represents the so-called duty cycle of the boost converter is required.

10.4.1 Suboptimal Second Order Sliding Mode Controller

Since sliding mode controllers generate a discontinuous control signal, in order to obtain a continuous control signal, the procedure suggested in [BFU98a] is adopted where the discontinuous signal is integrated, yielding for system (10.6)

[19] The relative degree is the minimum order ρ of the time derivative $\sigma_i^{(\rho)}, i\in\mathcal{V}$, of the sliding function associated to the i-th node in which the control $u_i, i\in\mathcal{V}$, explicitly appears.

$$
\begin{aligned}
\boldsymbol{L_t} \dot{\boldsymbol{I}}_{\boldsymbol{t}} &= -\boldsymbol{R_t} \boldsymbol{I_t} - \boldsymbol{u} \circ \boldsymbol{V} + \boldsymbol{V_{DC}} \\
\boldsymbol{C_t} \dot{\boldsymbol{V}} &= \boldsymbol{u} \circ \boldsymbol{I_t} - \boldsymbol{\mathcal{B}} \boldsymbol{R}^{-1} \boldsymbol{\mathcal{B}}^T \boldsymbol{V} - \boldsymbol{I_L} \\
\dot{\boldsymbol{\theta}} &= -(\boldsymbol{V} - \boldsymbol{V}^\star) \\
\dot{\boldsymbol{u}} &= \boldsymbol{h},
\end{aligned}
\tag{10.8}
$$

where $\boldsymbol{h} \in \mathbb{R}^n$ is the new (discontinuous) sliding mode control input. From (10.8) one can observe that the system relative degree (with respect to the new control input $\boldsymbol{h}$) is now two. Then, it is possible to rely on second order sliding mode control strategy in order to steer the state of system (10.8) to the sliding manifold $\boldsymbol{\sigma} = \dot{\boldsymbol{\sigma}} = \boldsymbol{0}$ for all $t \geq T_r$. To make the controller design explicit, a specific second order sliding mode controller is discussed, namely, the well known 'Suboptimal Second Order Sliding Mode' (SSOSM) controller proposed in [BFU98a].

Define d_i equal to $\sum_{j\in\mathcal{N}_i} I_{ij}$, with I_{ij} given by (10.2). For each node two auxiliary variables are defined, $\xi_{1_i} = \sigma_i$ and $\xi_{2_i} = \dot{\sigma}_i, i \in \mathcal{V}$, and the so-called auxiliary system is build as follows:

$$
\begin{aligned}
\dot{\xi}_{1_i} &= \xi_{2_i} \\
\dot{\xi}_{2_i} &= \phi_i(\dot{I}_{t_i}, \dot{V}_i, \dot{d}_i, u_i) - \gamma_i(I_{t_i}, V_i) h_i \\
\dot{u}_i &= h_i,
\end{aligned}
\tag{10.9}
$$

where ξ_{2_i} is not measurable. Indeed, according to Assumption 10.1, I_{L_i} is unknown and the parameters of the model are uncertain. Bearing in mind that $\dot{\xi}_{2_i} = \ddot{\sigma}_i = \phi_i + \gamma_i h_i$, the expressions for the mapping ϕ_i and matrix γ_i are straightforwardly obtained from (10.7) by taking the second derivative of σ_i with respect to time, yielding

$$
\begin{aligned}
\phi_i(\cdot) &= -m_{1_i} L_{t_i}^{-1} R_{t_i} \dot{I}_{t_i} + m_{3_i} \dot{V}_i - m_{1_i} L_{t_i}^{-1} \dot{V}_i u_i + m_{2_i} C_{t_i}^{-1} \dot{I}_{t_i} u_i - m_{2_i} C_{t_i}^{-1} \dot{d}_i \\
\gamma_i(\cdot) &= m_{1_i} L_{t_i}^{-1} V_i - m_{2_i} C_{t_i}^{-1} I_{t_i}.
\end{aligned}
\tag{10.10}
$$

The following assumption is made on the uncertain functions ϕ_i and $\gamma_i, i \in \mathcal{V}$.

Assumption 10.3 (Bounded uncertainty). Functions ϕ_i and γ_i in (10.9) have known bounds, i.e.,

$$
|\phi_i(\cdot)| \leq \varPhi_i \qquad \forall i \in \mathcal{V}, \tag{10.11}
$$

$$
0 < \varGamma_{\min_i} \leq \gamma_i(\cdot) \leq \varGamma_{\max_i} \qquad \forall i \in \mathcal{V}, \tag{10.12}
$$

$\varPhi_i$, $\varGamma_{\min_i}$ and $\varGamma_{\max_i}$ being positive constants.

Remark 10.5 (Unknown bounds). Note that in practical cases the bounds in (10.11) and (10.12) can be determined relying on data analysis and physical insights. However, if these bounds cannot be a-priori estimated, the adaptive version of the SSOSM algorithm proposed in [ICF16] can be used to dominate the effect of the uncertainties.

With reference to [BFU98a], for each DGu $i \in \mathcal{V}$, the control law that is proposed to steer ξ_{1_i} and ξ_{2_i}, to zero in a finite time can be expressed as

$$h_i = \alpha_i H_{\max_i} \operatorname{sign}\left(\xi_{1_i} - \frac{1}{2}\xi_{1,\max_i}\right), \tag{10.13}$$

with

$$H_{\max_i} > \max\left(\frac{\Phi_i}{\alpha_i^* \Gamma_{\min_i}}; \frac{4\Phi_i}{3\Gamma_{\min_i} - \alpha_i^* \Gamma_{\max_i}}\right), \tag{10.14}$$

$$\alpha_i^* \in (0,1] \cap \left(0, \frac{3\Gamma_{\min_i}}{\Gamma_{\max_i}}\right), \tag{10.15}$$

α_i switching between α_i^* and 1, according to [BFU98a, Algorithm 1]. Note that the control input $u_i(t) = \int_0^t h_i(\tau)d\tau$, is continuous, since w_i is piecewise constant. Then, $d_i = 1 - u_i$ can be used as duty cycle of the i-th boost converter. The extremal values $\xi_{1,\max_i}$ in (10.13) can be detected by implementing for instance a peak detector as in [BFU98b]. Note also that the design of the local controller for each DGu is not based on the knowledge of the whole microgrid, making the control synthesis simpler and the proposed control scheme scalable.

Remark 10.6 (Alternative SOSM controllers). In this work the control scheme relies on the SSOSM control law proposed in [BFU98a]. However, to constrain system (10.8) on the sliding manifold $\boldsymbol{\sigma} = \dot{\boldsymbol{\sigma}} = \mathbf{0}$, any other SOSM control law that does not need the measurement of $\dot{\boldsymbol{\sigma}}$ can be used (e.g. the super-twisting control algorithm [Lev93]).

10.5 Stability Analysis

In this section the (local) stability of the desired steady state $(\overline{\boldsymbol{I}}_{\boldsymbol{t}}, \boldsymbol{V}^\star, \overline{\boldsymbol{\theta}})$ is studied, that satisfies under an appropriate control input $\overline{\boldsymbol{u}}$ the steady state equations

$$\begin{aligned}
\mathbf{0} &= -\boldsymbol{R_t}\overline{\boldsymbol{I}}_{\boldsymbol{t}} - \overline{\boldsymbol{u}} \circ \boldsymbol{V}^\star + \boldsymbol{V_{DC}} \\
\mathbf{0} &= \overline{\boldsymbol{u}} \circ \overline{\boldsymbol{I}}_{\boldsymbol{t}} - \boldsymbol{\mathcal{B}}\boldsymbol{R}^{-1}\boldsymbol{\mathcal{B}}^T\boldsymbol{V}^\star - \boldsymbol{I_L} \\
\mathbf{0} &= -\left(\boldsymbol{V}^\star - \boldsymbol{V}^\star\right).
\end{aligned} \tag{10.16}$$

As a first step, system (10.6) is linearized around the point $(\overline{\boldsymbol{I}}_{\boldsymbol{t}}, \boldsymbol{V}^\star, \overline{\boldsymbol{\theta}})$, resulting in the linearized system

$$\begin{aligned}
\boldsymbol{L_t}\dot{\boldsymbol{I}}_{\boldsymbol{t}} &= -\boldsymbol{R_t}(\boldsymbol{I_t} - \overline{\boldsymbol{I}}_{\boldsymbol{t}}) - \overline{\boldsymbol{u}} \circ (\boldsymbol{V} - \boldsymbol{V}^\star) - \boldsymbol{V}^\star \circ (\boldsymbol{u} - \overline{\boldsymbol{u}}) \\
\boldsymbol{C_t}\dot{\boldsymbol{V}} &= \overline{\boldsymbol{u}} \circ (\boldsymbol{I_t} - \overline{\boldsymbol{I}}_{\boldsymbol{t}}) + \overline{\boldsymbol{I}}_{\boldsymbol{t}} \circ (\boldsymbol{u} - \overline{\boldsymbol{u}}) - \boldsymbol{\mathcal{B}}\boldsymbol{R}^{-1}\boldsymbol{\mathcal{B}}^T(\boldsymbol{V} - \boldsymbol{V}^\star) \\
\dot{\boldsymbol{\theta}} &= -(\boldsymbol{V} - \boldsymbol{V}^\star).
\end{aligned} \tag{10.17}$$

Next, it is investigated how the linearized system behaves on the sliding manifold under the proposed sliding mode control scheme. For this, one notices that the proposed SSOSM control scheme ensures that, after a finite time, the system (10.6) is constrained to the manifold characterized by $\boldsymbol{\sigma} = \dot{\boldsymbol{\sigma}} = \mathbf{0}$. This is made explicit in the lemma below.

Lemma 10.1 (Convergence to the sliding manifold). Let Assumptions 10.1-10.3 hold. The solutions to system (10.6), controlled via the SSOSM control law (10.9)–(10.15), converge in a finite time T_r, to the sliding manifold $\{(\boldsymbol{I_t}, \boldsymbol{V}, \boldsymbol{\theta}) : \boldsymbol{\sigma} = \dot{\boldsymbol{\sigma}} = \boldsymbol{0}\}$, with $\boldsymbol{\sigma}$ given by (10.7).

Proof. Following [BFU98a], the application of (10.9)–(10.15) to each converter guarantees that $\boldsymbol{\sigma} = \dot{\boldsymbol{\sigma}} = \boldsymbol{0}$, for all $t \geq T_r$. The details are omitted, since they are an immediate consequence of the used SSOSM control algorithm [BFU98a]. □

The so-called equivalent system for (10.17) is obtained by substituting the equivalent control $\boldsymbol{u_{eq}}$ for $\boldsymbol{u}$, and is determined explicitly in the following lemma.

Lemma 10.2 (Equivalent system). Let Assumptions 10.1-10.3 hold. For all $t \geq T_r$, the linearized dynamics of the controlled microgrid are given by the equivalent version of system (10.17) and are as follows:

$$\begin{bmatrix} \dot{\tilde{\boldsymbol{V}}} \\ \dot{\tilde{\boldsymbol{\theta}}} \end{bmatrix} = \underbrace{\begin{bmatrix} \boldsymbol{F} & \boldsymbol{G} \\ -\mathbb{I}_n & \boldsymbol{0} \end{bmatrix}}_{\boldsymbol{\mathcal{A}}} \begin{bmatrix} \tilde{\boldsymbol{V}} \\ \tilde{\boldsymbol{\theta}} \end{bmatrix}, \tag{10.18}$$

where $\tilde{\boldsymbol{V}} = \boldsymbol{V} - \boldsymbol{V}^\star$ and $\tilde{\boldsymbol{\theta}} = \boldsymbol{\theta} - \overline{\boldsymbol{\theta}}$. Furthermore, the matrices $\boldsymbol{F}$ and $\boldsymbol{G}$ are given by

$$\begin{aligned} \boldsymbol{F} =& -\boldsymbol{M_1}^{-1}\boldsymbol{M_2}\mathrm{diag}(\overline{\boldsymbol{u}}) - \boldsymbol{\mathcal{B}}\boldsymbol{R}^{-1}\boldsymbol{\mathcal{B}}^T + \boldsymbol{W}\boldsymbol{M_1}\boldsymbol{L_t}^{-1}\mathrm{diag}(\overline{\boldsymbol{I}}_{\boldsymbol{t}}) \left(\boldsymbol{M_1}^{-1}\boldsymbol{M_2}\boldsymbol{R_t} - \mathrm{diag}(\overline{\boldsymbol{u}})\right) \\ & - \boldsymbol{W}\boldsymbol{M_2}\boldsymbol{C_t}^{-1}\mathrm{diag}(\overline{\boldsymbol{I}}_{\boldsymbol{t}}) \left(\mathrm{diag}(\overline{\boldsymbol{u}})\boldsymbol{M_1}^{-1}\boldsymbol{M_2} + \boldsymbol{\mathcal{B}}\boldsymbol{R}^{-1}\boldsymbol{\mathcal{B}}^T\right) + \boldsymbol{W}\boldsymbol{M_3}\mathrm{diag}(\overline{\boldsymbol{I}}_{\boldsymbol{t}}), \end{aligned} \tag{10.19}$$

and

$$\begin{aligned} \boldsymbol{G} =& \boldsymbol{M_3}\boldsymbol{M_1}^{-1}\mathrm{diag}(\overline{\boldsymbol{u}}) - \boldsymbol{M_3}\boldsymbol{W}\boldsymbol{L_t}^{-1}\boldsymbol{R_t}\mathrm{diag}(\overline{\boldsymbol{I}}_{\boldsymbol{t}}) \\ & + \boldsymbol{M_3}\boldsymbol{W}\boldsymbol{M_2}\boldsymbol{M_1}^{-1}\boldsymbol{C_t}^{-1}\mathrm{diag}(\overline{\boldsymbol{I}}_{\boldsymbol{t}})\mathrm{diag}(\overline{\boldsymbol{u}}), \end{aligned} \tag{10.20}$$

where

$$\boldsymbol{W} = \left(\boldsymbol{L_t}^{-1}\boldsymbol{M_1}\mathrm{diag}(\boldsymbol{V}^\star) - \boldsymbol{C_t}^{-1}\boldsymbol{M_2}\mathrm{diag}(\overline{\boldsymbol{I}}_{\boldsymbol{t}})\right)^{-1}. \tag{10.21}$$

Proof. The relation $\dot{\boldsymbol{\sigma}} = \boldsymbol{0}$ is equivalent to

$$\boldsymbol{M_1}\dot{\boldsymbol{I}}_{\boldsymbol{t}} + \boldsymbol{M_2}\dot{\boldsymbol{V}} - \boldsymbol{M_3}\dot{\boldsymbol{\theta}} = \boldsymbol{0}. \tag{10.22}$$

Bearing in mind the dynamics (10.17), equation (10.22) can be solved for $\boldsymbol{u}$, where it is additionally exploited that on the manifold $\boldsymbol{\sigma} = \boldsymbol{0}$ one has $\boldsymbol{M_1}\boldsymbol{I_t} = \boldsymbol{M_3}\boldsymbol{\theta} - \boldsymbol{M_2}(\boldsymbol{V} - \boldsymbol{V}^\star)$ and that at the point $(\overline{\boldsymbol{I}}_{\boldsymbol{t}}, \boldsymbol{V}^\star, \overline{\boldsymbol{\theta}})$ it holds that $\boldsymbol{M_1}\overline{\boldsymbol{I}}_{\boldsymbol{t}} = \boldsymbol{M_3}\overline{\boldsymbol{\theta}}$. This yields the following equivalent control $\boldsymbol{u_{eq}}$:

$$\boldsymbol{u_{eq}} = \overline{\boldsymbol{u}} + \boldsymbol{W}\left(\boldsymbol{M_1}\boldsymbol{L_t}^{-1}(-\boldsymbol{R_t}\tilde{\boldsymbol{I}}_{\boldsymbol{t}} - \overline{\boldsymbol{u}} \circ \tilde{\boldsymbol{V}}) + \boldsymbol{M_2}\boldsymbol{C_t}^{-1}(\overline{\boldsymbol{u}} \circ \tilde{\boldsymbol{I}}_{\boldsymbol{t}} - \boldsymbol{\mathcal{B}}\boldsymbol{R}^{-1}\boldsymbol{\mathcal{B}}^T\tilde{\boldsymbol{V}}) + \boldsymbol{M_3}\tilde{\boldsymbol{V}}\right), \tag{10.23}$$

where $\tilde{\boldsymbol{I}}_{\boldsymbol{t}} = \boldsymbol{I_t} - \overline{\boldsymbol{I}}_{\boldsymbol{t}}$ and $\boldsymbol{W}$ is given by (10.21). Substituting $\boldsymbol{u_{eq}}$ for $\boldsymbol{u}$ in (10.17), and using again the relations $\boldsymbol{M_1}\boldsymbol{I_t} = \boldsymbol{M_3}\boldsymbol{\theta} - \boldsymbol{M_2}(\boldsymbol{V} - \boldsymbol{V}^\star)$ and $\boldsymbol{M_1}\overline{\boldsymbol{I}}_{\boldsymbol{t}} = \boldsymbol{M_3}\overline{\boldsymbol{\theta}}$, it can be readily confirmed that the last two equations of (10.17) reduce to (10.18). □

Lemma 10.3 (Positive definiteness of (10.20)). Let Assumption 10.3 hold. The matrix $\boldsymbol{G}$ in (10.20) is positive definite.

Proof. The matrix $\boldsymbol{M_3}$ in (10.7) is positive definite, and as a consequence of Assumption 10.3 also the matrix $\boldsymbol{W} = \text{diag}\{w_1, \ldots, w_n\}$ is positive definite, since w_i is the steady state value of $\gamma_i(\cdot) > 0$. From (10.20), we have

$$(\boldsymbol{M_3 W L_t^{-1}})^{-1}\boldsymbol{G} = \text{diag}(\overline{\boldsymbol{u}})\text{diag}(\boldsymbol{V}^\star) - \boldsymbol{R_t}\text{diag}(\overline{\boldsymbol{I}}_{\boldsymbol{t}}). \tag{10.24}$$

Since in practical cases $\boldsymbol{R_t} \approx \boldsymbol{0}$, then $\boldsymbol{G} > \boldsymbol{0}$. □

As a consequence of the lemmas above, in order to prove that system (10.17) is exponentially stable on the attained sliding manifold, matrix $\boldsymbol{\mathcal{A}}$ in (10.18) needs to be Hurwitz. However, explicitly characterizing all the eigenvalues of $\boldsymbol{\mathcal{A}}$ is difficult, mainly due to the coupling term $\boldsymbol{BR}^{-1}\boldsymbol{B}^T$. Generally, the eigenvalues depend indeed on the particular microgrid, its parameters and its operation point. In the following proposition, it is shown that, by LaSalle's invariance principle, the desired operating point of the controlled microgrid can always be made locally exponentially stable by choosing appropriate values for $\boldsymbol{M_1}, \boldsymbol{M_2}$ and $\boldsymbol{M_3}$ in the controller and consequently causing matrix $\boldsymbol{\mathcal{A}}$ to be Hurwitz.

Theorem 10.1 (Local exponential stability). *Let Assumptions 10.1-10.3 hold. The desired operating point* $(\overline{\boldsymbol{I}}_{\boldsymbol{t}}, \boldsymbol{V}^\star, \overline{\boldsymbol{\theta}})$*, satisfying* (10.16) *can be made locally exponentially stable on the sliding manifold characterized by* $\boldsymbol{\sigma} = \dot{\boldsymbol{\sigma}} = \boldsymbol{0}$*, by choosing the entries of* $\boldsymbol{M_2}$ *sufficiently big.*

Proof. Consider the Lyapunov function

$$S(\tilde{\boldsymbol{V}}, \tilde{\boldsymbol{\theta}}) = \tilde{\boldsymbol{V}}^T\tilde{\boldsymbol{V}} + \tilde{\boldsymbol{\theta}}^T\boldsymbol{G}\tilde{\boldsymbol{\theta}}, \tag{10.25}$$

where $\boldsymbol{G} > \boldsymbol{0}$ follows from Lemma 10.3. A straightforward calculation shows that $S(\tilde{\boldsymbol{V}}, \tilde{\boldsymbol{\theta}})$ satisfies along the solutions to (10.18)

$$\dot{S}(\tilde{\boldsymbol{V}}, \tilde{\boldsymbol{\theta}}) = \tilde{\boldsymbol{V}}^T(\boldsymbol{F} + \boldsymbol{F}^T)\tilde{\boldsymbol{V}} \leq 0. \tag{10.26}$$

From (10.19) we have

$$\begin{aligned} \boldsymbol{W}^{-1}\boldsymbol{F} = &- \boldsymbol{M_2 L_t^{-1}}\left(\text{diag}(\overline{\boldsymbol{u}})\text{diag}(\boldsymbol{V}^\star) - \boldsymbol{R_t}\text{diag}(\overline{\boldsymbol{I}}_{\boldsymbol{t}})\right) \\ &- \boldsymbol{M_1 L_t^{-1}}\text{diag}(\overline{\boldsymbol{u}})\text{diag}(\overline{\boldsymbol{I}}_{\boldsymbol{t}}) + \boldsymbol{M_3}\text{diag}(\overline{\boldsymbol{I}}_{\boldsymbol{t}}) \\ &- \boldsymbol{M_1 BR}^{-1}\boldsymbol{B}^T\boldsymbol{L_t^{-1}}\text{diag}(\boldsymbol{V}^\star). \end{aligned} \tag{10.27}$$

Since in practical cases $\boldsymbol{R_t} \approx \boldsymbol{0}$, then by choosing the entries of $\boldsymbol{M_2}$ sufficiently big, the diagonal of $\boldsymbol{F}$ can be made sufficiently negative such that $\boldsymbol{F} + \boldsymbol{F}^T < \boldsymbol{0}$. By LaSalle's invariance principle, the solutions to (10.18) converge to the largest invariant set where $\tilde{\boldsymbol{V}} = \boldsymbol{0}$. Moreover, on this invariant set it holds, due to the invertibility of $\boldsymbol{G}$, that $\tilde{\boldsymbol{\theta}} = \boldsymbol{0}$. This in turn implies that all the eigenvalues of $\boldsymbol{\mathcal{A}}$ are negative when the entries of $\boldsymbol{M_2}$ are chosen sufficiently big, and consequently (10.18) is exponentially stable. Furthermore, on the set where $\boldsymbol{\sigma} = \boldsymbol{0}$, $\boldsymbol{V} = \boldsymbol{V}^\star$ and $\boldsymbol{\theta} = \overline{\boldsymbol{\theta}}$, it holds that $\boldsymbol{I_t} = \boldsymbol{M_1^{-1} M_3}\overline{\boldsymbol{\theta}}$. □

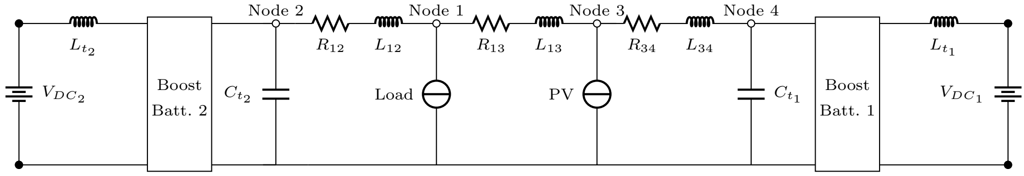

Fig. 10.2. The considered electrical scheme of the RSE's DC microgrid adopted during the test.

Remark 10.7 (Tuning rules). First, we notice that for any $i \in \mathcal{V}$, the requirement of $\gamma_i > 0$ in Assumption 10.3 provides the following tuning rule

$$m_{1_i} > \frac{L_{t_i}\overline{I}_{t_i}}{C_{t_i}V_i^\star} m_{2_i} \qquad \text{if } \overline{I}_{t_i} > 0. \tag{10.28}$$

If instead $\overline{I}_{t_i} \leq 0$, then γ_i is positive for any m_{1_i}, m_{2_i}. Secondly, one can notice that under the assumption of constant current exchanged with the neighbouring nodes, $\boldsymbol{F}$ becomes a diagonal matrix. Then, a tedious, but straightforward, calculation provides explicit bounds on the permitted values of $\boldsymbol{M_1}, \boldsymbol{M_2}$ and $\boldsymbol{M_3}$ such that the dynamics matrix

$$\boldsymbol{\mathcal{A}}_i = \begin{bmatrix} F_i & G_i \\ -1 & 0 \end{bmatrix} \in \mathbb{R}^{2\times 2} \tag{10.29}$$

of the i-th boost converter is Hurwitz for any $i \in \mathcal{V}$, i.e.,

$$\begin{aligned} m_{1_i} &> \frac{L_{t_i}}{\overline{u}_i} m_{3_i} + \frac{R_{t_i}}{\overline{u}_i} m_{2_i} - \frac{V_i^\star}{\overline{I}_{t_i}} m_{2_i} \qquad \text{if } \overline{I}_{t_i} > 0 \\ m_{1_i} &< \frac{L_{t_i}}{\overline{u}_i} m_{3_i} + \frac{R_{t_i}}{\overline{u}_i} m_{2_i} - \frac{V_i^\star}{\overline{I}_{t_i}} m_{2_i} \qquad \text{if } \overline{I}_{t_i} \leq 0. \end{aligned} \tag{10.30}$$

Finally, combining (10.28) and (10.30), we have that

$$\underline{\mu}_i < m_{1_i} < \overline{\mu}_i, \tag{10.31}$$

with

$$\begin{aligned} \underline{\mu}_i &= \max\left(\frac{L_{t_i}}{\overline{u}_i} m_{3_i} + \frac{R_{t_i}}{\overline{u}_i} m_{2_i} - \frac{V_i^\star}{|\overline{I}_{t_i}|} m_{2_i}; \frac{L_{t_i}|\overline{I}_{t_i}|}{C_{t_i}V_i^\star} m_{2_i} \right) \\ \overline{\mu}_i &= \frac{L_{t_i}}{\overline{u}_i} m_{3_i} + \frac{R_{t_i}}{\overline{u}_i} m_{2_i} + \frac{V_i^\star}{|\overline{I}_{t_i}|} m_{2_i}. \end{aligned} \tag{10.32}$$

10.6 Experimental Results

In order to verify the proposed control strategy, experimental tests are carried out using the DC microgrid test facility at RSE, shown in Figs. 10.2 and 10.3. The RSE's DC grid is unipolar with a nominal voltage of 380 V and, during the test, includes one resistive load, with a maximum power of 30 kW at 400 V, one DC generator with a maximum power of 30 kW, that can be used as a PV emulator, and two Energy Storage Systems,

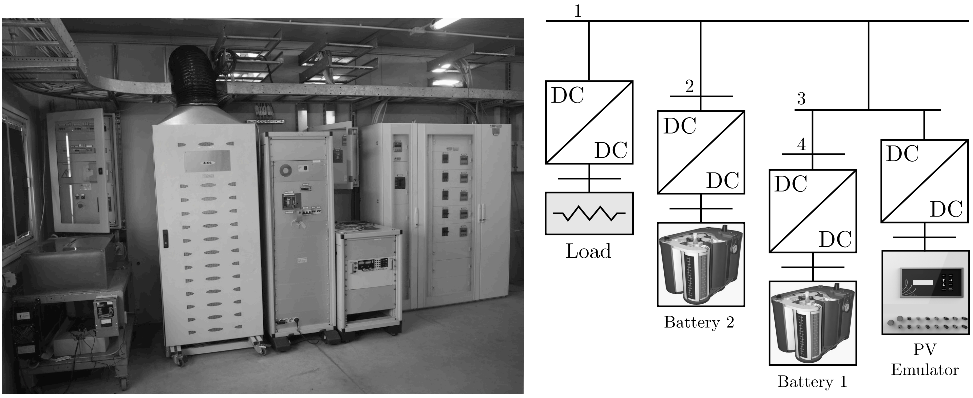

(a) photo (b) layout

Fig. 10.3. RSE's DC microgrid adopted during the tests.

based on high temperature NaNiCl batteries, each of them with an energy of 18 kWh and a maximum power of 30 kW for 10 s. These components are connected to a common DC link through four 35 kW DC-DC boost synchronous converters. The DC-DC converters are distributed and connected to the DC link with power distribution lines characterized by different parameters, as reported in Table 10.2.

The control of each converter is realized through two dSpace controllers that measure the inductor current and the boost output voltage and drive the power electronic converters. The DC-DC converters of the load and of the generator have input voltages equal to 266 V and 320 V, respectively. They are controlled in constant power mode and are treated, during the test, as current disturbances (see Fig. 10.2). The bidirectional converters of the batteries are controlled through the SSOSM control strategy described in Section 10.4, in order to regulate the voltage at Node 2 and Node 4 (see Fig. 10.2). The voltage reference $V^\star$ for these nodes is set equal to 380 V, while the input voltages V_{DC_1} and V_{DC_2} are both equal to 278 V. According to the stability results in Section 10.5, the SSOSM control parameters for the battery converters are reported in Table 10.3. In order to investigate the performance of the proposed control approach within a low voltage DC microgrid, four different scenarios are implemented. Note that in the following figures it is arbitrarily assumed that the current entering any node is positive (passive sign convention).

Scenario 10.1 (Disturbance with a limited ramp rate power variation). In the first scenario it is assumed that the system is in a steady state condition with zero power absorbed by the load or provided by the generator. Each battery converter regulates its output voltage at a fixed value equal to 380 V and there is no exchange of power between these two components. At the time instant $t = 5$ s the power reference for the load converter or for the generator converter (see Fig. 10.4) is set to 20 kW and at the time instant $t = 35$ s, is reset to 0 kW with the ramp rate limited to 1 kW/s. As shown in the pictures, when the disturbance has a limited ramp rate, the proposed control strategy is able to keep the output voltage of both the batteries DC-DC converter to their reference without any voltage variation. When the system reaches the steady state condition, the

Table 10.2. RSE DC Microgrid parameters

Symbol	Value	Unit	Description
V_{DC_1}, V_{DC_2}	278	V	Batteries nominal voltage
$V^\star$	380	V	DC nominal voltage
R_{12}	250	mΩ	Tie-Line resistance 1-2
R_{13}	39	mΩ	Tie-Line resistance 1-3
R_{34}	250	mΩ	Tie-Line resistance 3-4
L_{12}	140	µH	Tie-Line inductance 1-2
L_{13}	86	µH	Tie-Line inductance 1-3
L_{34}	140	µH	Tie-Line inductance 3-4
C_{t_1}, C_{t_2}	6.8	mF	Output capacitance
L_{t_1}, L_{t_2}	1.12	mH	Input inductance
f_{sw}	4	kHz	Switching frequency

Table 10.3. SSOSM control parameters

Parameter	Value
m_{1_i}	0.01
m_{2_i}	0.1
m_{3_i}	1
$H_{\max_i}$	4
α_i^*	0.05

two battery converters exchange power with the DC network in order to maintain the voltage equal to the desired value. In this situation there is not a perfect current sharing between the two battery converters because the load and the generator are not connected to the same node of the grid and different line impedances connect the components.

Scenario 10.2 (Disturbance with a step power variation). In the second scenario the same tests explained in Scenario 10.1 are replicated, but in this case without the ramp rate limitation. In this situation it is possible to see, as shown in Fig. 10.5, a transient in the DC network voltage due to the step power variation of the load (subfigures (a) and (b)), and the generator (subfigures (c) and (d)). The transient is different in these two cases because the dynamics of the load and the generator are different. In any case the system exhibits a stable performance thanks to the robustness of the proposed decentralized SSOSM control approach with respect to the disturbances.

Scenario 10.3 (Step variation of the voltage reference). In this third scenario it is assumed that the system is in a steady state condition with a constant power equal to 20 kW absorbed by the load or provided by the generator. Each battery converter regulates its output voltage at a fixed value equal to 380 V, and the power exchanged by the two batteries is different due to the different line impedances. At the time instant $t =$

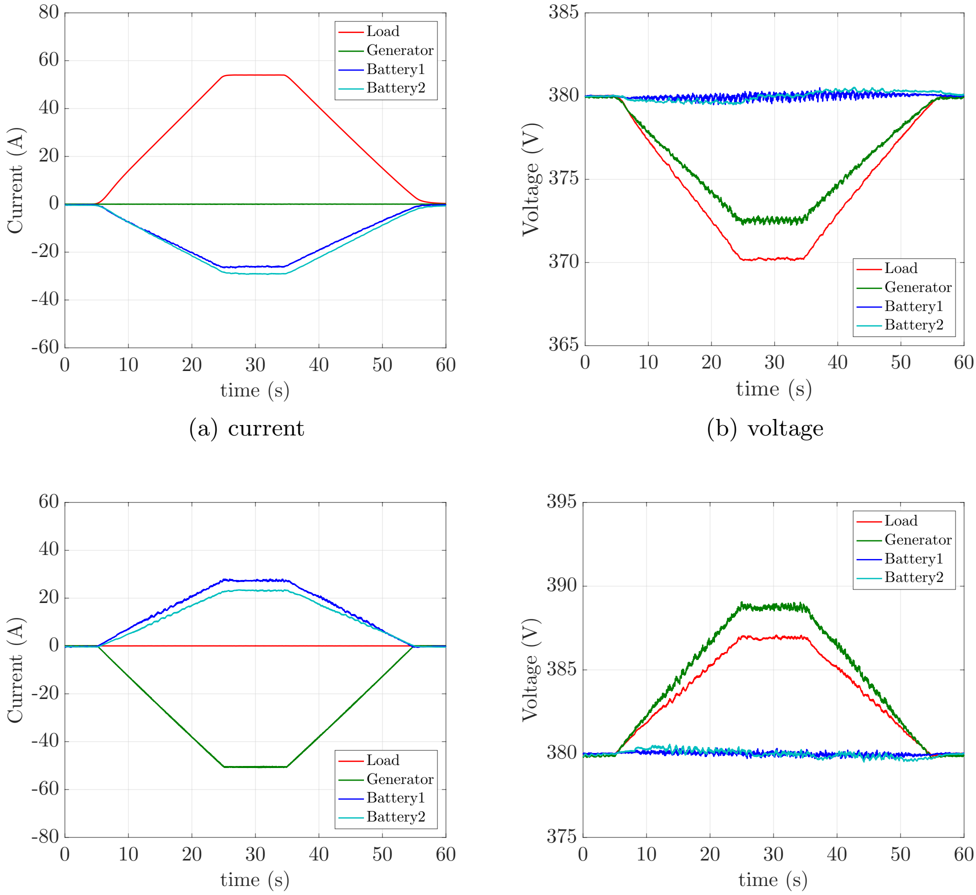

(a) current (b) voltage

(c) current (d) voltage

Fig. 10.4. Scenario 1. **(a)**, **(b)** Currents and voltages in presence of a load variation of about 20 kW with a ramp rate equal to 1 kW/s. **(c)**, **(d)** Currents and voltages in presence of a generator variation of about 20 kW with a ramp rate equal to 1 kW/s.

5 s the DC voltage reference for one of the two battery converters is modified. Fig. 10.6 (subfigures (a) and (b)) shows the system performances when the constant load is set to 20 kW and the reference voltage of the first battery converter is increased by 5 V, while Fig. 10.6 (subfigures (c) and (d)) shows the opposite situation with the constant generation set to 20 kW and the reference voltage of the second battery converter decreased by 5 V. In these situations it is possible to observe that the DC voltage variation in one battery converter has no effect on the voltage at the other battery converter. The system exhibits a stable performance thanks to the robustness of the proposed decentralized SSOSM control approach with respect to voltage reference variations. By modifying the voltage reference of the two battery converters it is possible to obtain a different current sharing among the batteries of the microgrid. Acting on the voltage references, it is also possible,

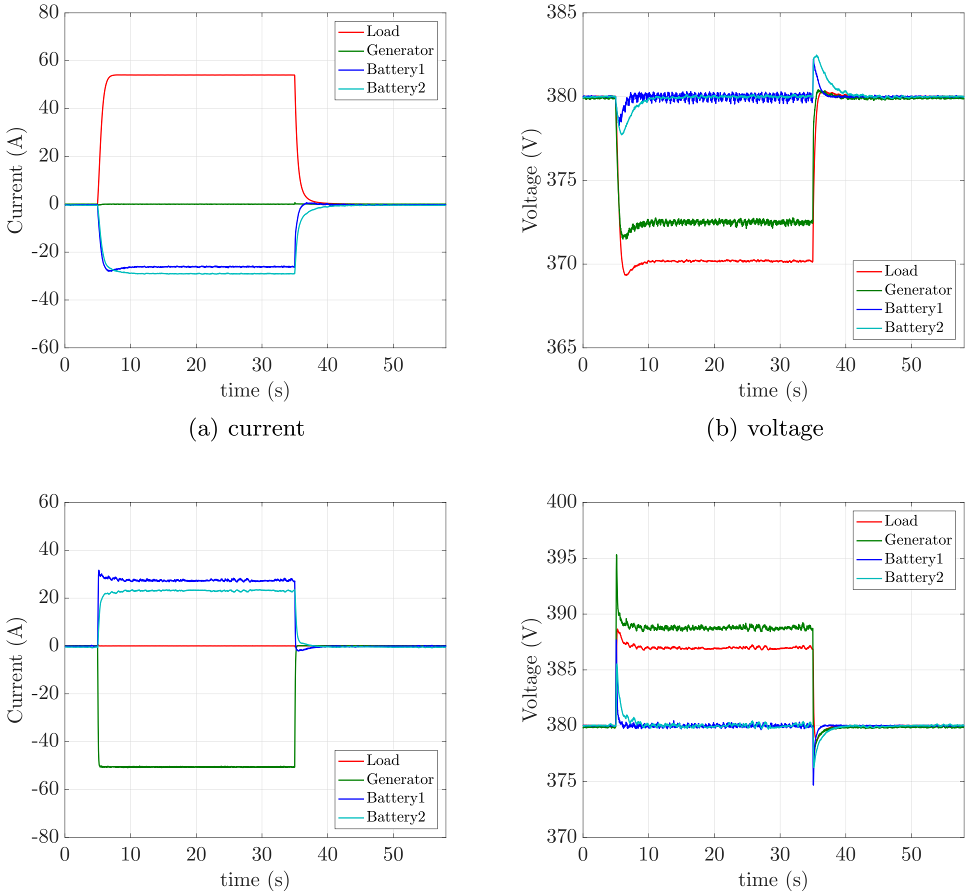

(a) current (b) voltage

(c) current (d) voltage

Fig. 10.5. Scenario 2. **(a)**, **(b)** Currents and voltages in presence of a step load variation of about 20 kW. **(c)**, **(d)** Currents and voltages in presence of a step generator variation of about 20 kW.

as illustrated in the Scenario 10.4, to cover the control objectives related to the current sharing.

Scenario 10.4 (Current sharing). In this scenario the proposed primary controllers have been coupled with a secondary control scheme that calculates the voltage references for the battery converters in order to achieve current sharing among the batteries (see Fig. 10.7). Although the analysis of a secondary control level is not discussed in this paper, Scenario 4 is aimed at showing that the proposed primary controllers, due to their robustness property in tracking the voltage references, can be coupled with a secondary control scheme that guarantees current or power sharing.

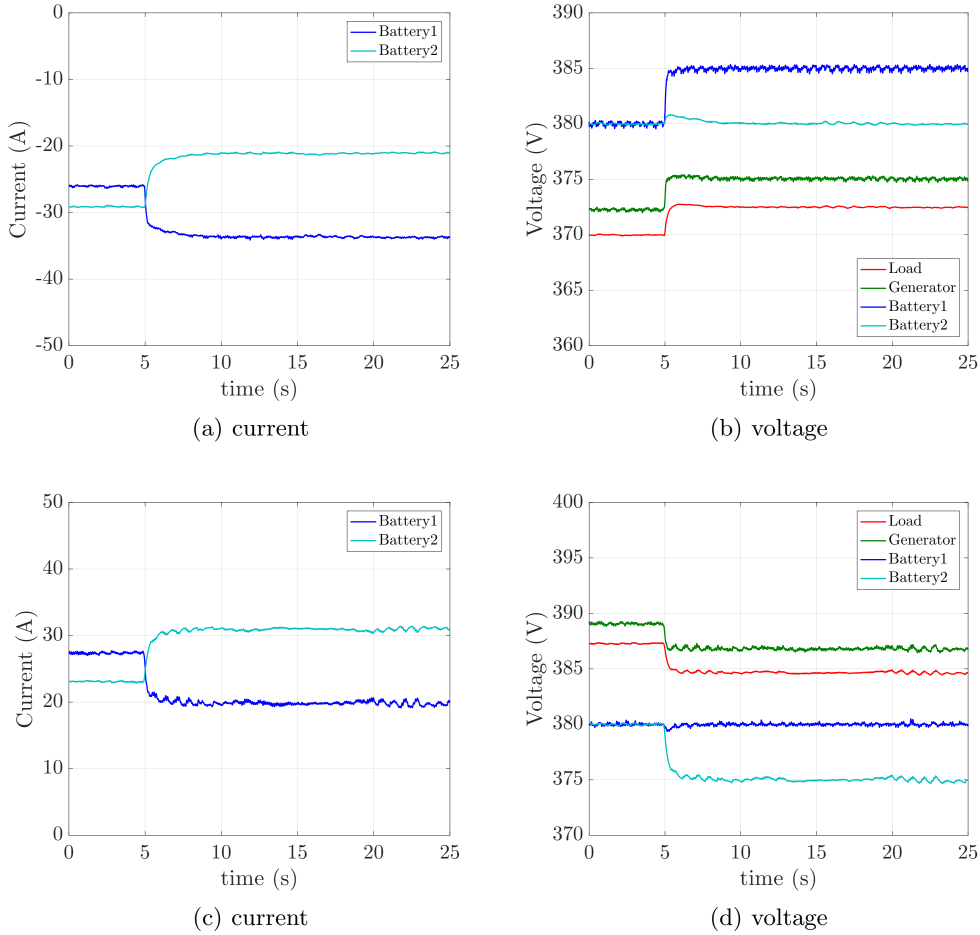

Fig. 10.6. Scenario 3. **(a)**, **(b)** Currents and voltages in presence of a step DC voltage reference variation of battery converter number 1. **(c)**, **(d)** Currents and voltages in presence of a step DC voltage reference variation of battery converter number 2.

Finally, note that in the discussed scenarios, only the voltage at Node 2 and Node 4 have been controlled with the proposed strategy. Nevertheless, the voltage deviations from the nominal value in the other two nodes (i.e., Node 1 and Node 3), depending on the line impedances, are always less than the 5% of the desired voltage value.

10.7 Conclusions

In this chapter a robust control strategy has been designed to regulate the voltage in boost-based DC microgrids. The proposed control scheme is fully decentralized and is based on higher order sliding mode control methodology, which allows to obtain continuous control

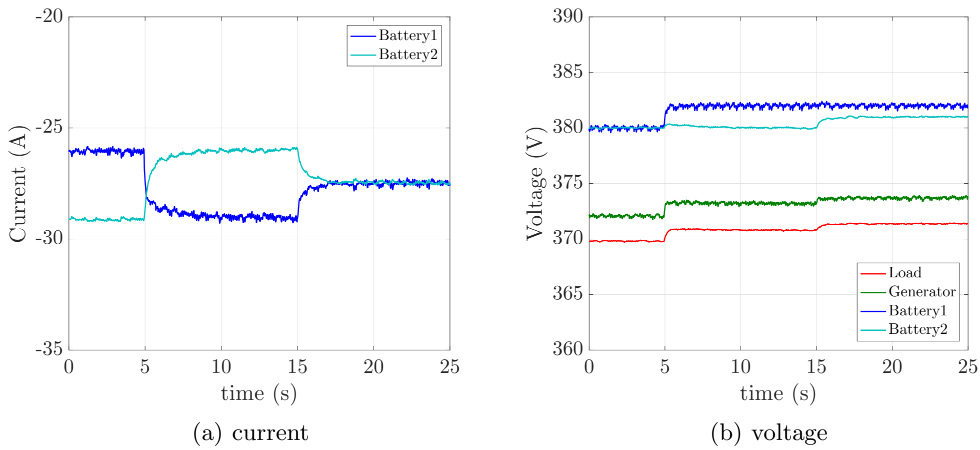

Fig. 10.7. Scenario 4. Currents and voltages in presence of constant load (20 kW) and voltage reference variation for the DC-DC battery converters in order to obtain current sharing.

inputs. The latter can be used as duty cycles of the boost converters, achieving constant switching frequency and facilitating a PWM-based implementation. The stability of a boost-based microgrid has been theoretically analyzed proving that, on the proposed sliding manifold, the desired operating point is locally exponentially stable. The proposed control scheme has been validated through experimental tests on a real DC microgrid, showing satisfactory closed-loop performances. Interesting future research includes the stability analysis of the obtained nonlinear equivalent system, as well as studying the performance of the proposed control scheme in more heterogeneous networks, possibly including different converter types and the presence of local control strategies that differ from the one proposed here.

11

Conclusions and Future Research

11.1 Conclusions

In this thesis, we have first focused on the design of novel robust control strategies of sliding mode type for a class of nonlinear uncertain systems. In particular, we have proposed an adaptive suboptimal second order sliding mode control algorithm in order to relax the assumption on the knowledge of the bounds of the uncertainty, required in the design of conventional sliding mode controllers. Then, we have proposed a second order sliding mode control algorithm aimed at reducing the control effort, which is beneficial in many mechanical and electromechanical applications. We have designed a nonsmooth switching line, based on the quantization of the uncertainties affecting the system. The quantized uncertainty levels allow one to define nested box sets in the auxiliary state space, where different control amplitudes are suitably selected for each set. Moreover, event-triggered sliding mode control schemes have been designed for networked control systems. The control objective is indeed to reduce the number of data transmissions over the communication network, in order to avoid problems typically due to the network congestion such as jitter and packet loss. The proposed control strategy is capable of robustly enforcing practical sliding modes even in presence of delayed transmission, while guaranteeing the avoidance of the notorious Zeno behaviour.

In the second part of this work, we have proposed robust sliding mode control (and observer) schemes for power systems. In particular, a distributed sliding mode control scheme has been proposed to solve an optimal load frequency control problem in power systems, including voltage dynamics and second order turbine-governor dynamics. Based on a suitable chosen sliding manifold, the controlled turbine-governor system, constrained to this manifold, possesses an incremental passivity property that is exploited to prove that the frequency deviation asymptotically approaches zero and an economic dispatch is achieved. Furthermore, relying on stability considerations made on the basis of an incremental energy (storage) function, a suitable sliding manifold has been designed, where the frequency deviation is zero and the power flows are regulated towards their desired values. Finally, novel decentralized sliding mode observers scheme has been designed to estimate the unmeasured states of power networks including thermal and hydraulic power plants.

In the third and last part of this work, we have proposed robust sliding mode control schemes for microgrids. In particular, we have addressed the voltage control problem in islanded AC microgrids by designing a decentralized sliding mode control scheme, where the controller of each node requires that voltage is available only locally. Moreover, we have developed a distributed sliding mode control algorithm for buck-based DC microgrids. The proposed control scheme exploits a communication network to achieve proportional current sharing using a consensus-like algorithm. Another useful feature of the proposed control scheme is that the weighted average voltage of the microgrid converges to the weighted average of the voltage references, independently of the initial system conditions. Finally, a robust fully decentralized control strategy has been designed to regulate the voltage in boost-based DC microgrids. The local stability of the whole microgrid has been theoretically analyzed and validated through experimental tests on a real DC microgrid, showing satisfactory closed-loop performances.

To conclude, all the proposed solutions have been theoretically analyzed. The experimental and simulation tests presented in this work validate the theoretical results and provide some rules to practitioners who would like to use the proposed algorithms in industrial field applications.

11.2 Future Research

Future research will address the following challenges:

- extend and improve the design of distributed robust control strategies for general flow networks, exploiting a communication network to achieve consensus;
- the design of robust control strategies aimed at achieving power (not current) sharing among the agents of both AC and DC microgrids;
- the design of robust control strategies for hybrid microgrids;
- the development of control algorithms capable to optimize matching of demand and supply that are acceptable to the end-users, considering, in the control loop, their needs and the market price.

References

[ABK$^+$93] J. Ackermann, A. Bartlett, D. Kaesbauer, W. Sienel, and R. Steinhauser. *Robust Control: Systems with Uncertain Physical Parameters*. Springer-Verlag, London, 1993.

[AC84] J. P. Aubin and A. Cellina. *Differential Inclusions*. Springer-Verlag, 1984.

[ADGS16] D. Apostolopoulou, A. D. Domínguez-García, and P. W. Sauer. An assessment of the impact of uncertainty on automatic generation control systems. *IEEE Transactions on Power Systems*, 31(4):2657–2665, July 2016.

[ADJS13] M. Andreasson, D. V. Dimarogonas, K. H. Johansson, and H. Sandberg. Distributed vs. centralized power systems frequency control. In *Proc. European Control Conference*, pages 3524–3529, Zurich, Switzerland, July 2013.

[AF66] M. Athans and P. L. Falb. *Optimal Control*. New York: McGraw Hill, 1966.

[AFG13] S. Anand, B. G. Fernandes, and J. Guerrero. Distributed control to ensure proportional load sharing and improve voltage regulation in low-voltage DC microgrids. *IEEE Transactions on Power Electronics*, 28(4):1900–1913, Apr. 2013.

[ASDG15] D. Apostolopoulou, P. W. Sauer, and A. D. Domínguez-García. Distributed optimal load frequency control and balancing authority area coordination. In *North American Power Symposium*, pages 1–5, Oct. 2015.

[Ast08] K. J. Aström. Event based control. In A. Astolfi and L. Marconi, editors, *Analysis and Design of Nonlinear Control Systems*, pages 127–147. Springer Berlin Heidelberg, 2008.

[ATS06] Aaron D. Ames, Paulo Tabuada, and Shankar Sastry. *On the Stability of Zeno Equilibria*, pages 34–48. Springer Berlin Heidelberg, Berlin, Heidelberg, 2006.

[AW05] S. M. Amin and B. F. Wollenberg. Toward a smart grid: power delivery for the 21st century. *IEEE Power and Energy Magazine*, 3(5):34–41, Sep. 2005.

[AWA07] Hirofumi Akagi, Edson Hirokazu Watanabe, and Mauricio Aredes. *Instantaneous power theory and applications to power conditioning*, volume 31. John Wiley & Sons, 2007.

[AWD+17] Martin Andreasson, Roger Wiget, Dimos V Dimarogonas, Karl H Johansson, and Göran Andersson. Distributed frequency control through mtdc transmission systems. *IEEE Transactions on Power Systems*, 32(1):250–260, Jan. 2017.

[Bar98] A. Bartoszewicz. Discrete-time quasi-sliding-mode control strategies. *IEEE Transactions on Industrial Electronics*, 45(4):633–637, Aug 1998.

[BB95] DS Bernstein and SP Bhat. Lyapunov stability, semistability, and asymptotic stability of matrix second-order systems. *Journal of Vibration and Acoustics*, 117(B):145–153, June 1995.

[BB16] Abhisek K. Behera and Bijnan Bandyopadhyay. Event-triggered sliding mode control for a class of nonlinear systems. *International Journal of Control*, 89(9):1916–1931, Mar. 2016.

[BDL+14] G. Binetti, A. Davoudi, F. L. Lewis, D. Naso, and B. Turchiano. Distributed consensus-based economic dispatch with transmission losses. *IEEE Transactions on Power Systems*, 29(4):1711–1720, July 2014.

[BdPFDC+16] E. Benedito, D. del Puerto-Flores, A. Dòria-Cerezo, O. van der Feltz, and J. M. A. Scherpen. Strictly convex loss functions for port-hamiltonian based optimization algorithm for mtdc networks. In *Proc. 55th IEEE Conference on Decision and Control*, pages 7483–7488, Las Vegas, NV, USA, Dec. 2016.

[BDT14] M. Bürger, C. De Persis, and S. Trip. An internal model approach to (optimal) frequency regulation in power grids. In *Proc. of the 21th International Symposium on Mathematical Theory of Networks and Systems (MTNS)*, pages 577–583, Groningen, the Netherlands, 2014.

[BFLU99] G. Bartolini, A. Ferrara, A. Levant, and E. Usai. On second order sliding mode controllers. In K. D. Young and Ü. Özgüner, editors, *Variable Structure Systems, Sliding Mode and Nonlinear Control*, Lecture Notes in Control and Information, pages 329–350. Springer-Verlag, London, UK, 1999.

[BFPU98] G. Bartolini, A. Ferrara, A. Pisano, and E. Usai. Adaptive reduction of the control effort in chattering-free sliding-mode control of uncertain nonlinear systems. *Int. J. Applied Mathematics and Computer Science*, 8:51–57, Jan. 1998.

[BFPU07] I. Boiko, L. Fridman, A. Pisano, and E. Usai. Analysis of chattering in systems with second-order sliding modes. *IEEE Transactions on Automatic Control*, 52(11):2085–2102, Nov. 2007.

[BFU97] G. Bartolini, A. Ferrara, and E. Usai. Output tracking control of uncertain nonlinear second-order systems. *Automatica*, 33(12):2203–2212, Dec. 1997.

[BFU98a] G. Bartolini, A. Ferrara, and E. Usai. Chattering avoidance by second-order sliding mode control. *IEEE Transactions on Automatic Control*, 43(2):241–246, Feb. 1998.

[BFU98b] G. Bartolini, A. Ferrara, and E. Usai. On boundary layer dimension reduction in sliding mode control of siso uncertain nonlinear systems. In *Proc. IEEE Interantional Conference on Control Applications*, volume 1, pages 242–247, Trieste, Italy, Sep. 1998.

[BFUU00] G. Bartolini, A. Ferrara, E. Usai, and V. I. Utkin. On multi-input chattering-free second-order sliding mode control. *IEEE Transactions on Automatic Control*, 45(9):1711–1717, Sep. 2000.

[BFUZ97] G. Bartolini, A. Ferrara, V. I. Utkin, and T. Zolezzi. A control vector approach to variable structure control of nonlinear systems. *International Journal of Robust and Nonlinear Control*, 7(4):321–335, Apr. 1997.

[BK13] M. Babazadeh and H. Karimi. A robust two-degree-of-freedom control strategy for an islanded microgrid. *IEEE Transactions on Power Delivery*, 28(3):1339–1347, Jul. 2013.

[BLY+11] I. J. Balaguer, Q. Lei, S. Yang, U. Supatti, and F. Z. Peng. Control for grid-connected and intentional islanding operations of distributed power generation. *IEEE Transactions on Industrial Electronics*, 58(1):147–157, Jan. 2011.

[Boi11] I. Boiko. Analysis of chattering in sliding mode control systems with continuous boundary layer approximation of discontinuous control. In *Proc. American Control Conference*, pages 757–762, San Francisco, CA, USA, Jul. 2011.

[BPPU03] G. Bartolini, A. Pisano, E. Punta, and E. Usai. A survey of applications of second-order sliding mode control to mechanical systems. *International Journal of Control*, 76(9–10):875–892, Jan. 2003.

[BPZ07] G. Bartolini, E. Punta, and T. Zolezzi. Approximability properties for second-order sliding mode control systems. *IEEE Transactions on Automatic Control*, 52:1813–1825, Oct. 2007.

[Bre67] L.M. Bregman. The relaxation method of finding the common point of convex sets and its application to the solution of problems in convex programming. *USSR Computational Mathematics and Mathematical Physics*, 7(3):200–217, 1967.

[CF97] C.S. Chang and Weihui Fu. Area load frequency control using fuzzy gain scheduling of pi controllers. *Electric Power Systems Research*, 42(2):145–152, Aug. 1997.

[CF12] L. M. Capisani and A. Ferrara. Trajectory planning and second-order sliding mode motion/interaction control for robot manipulators in unknown environments. *IEEE Transactions on Industrial Electronics*, 59(8):3189–3198, Aug. 2012.

[CFdLF12] Luca M. Capisani, Antonella Ferrara, Alejandra Ferreira de Loza, and Leonid Fridman. Manipulator fault diagnosis via higher order sliding-mode observers. *IEEE Transactions on Industrial Electronics*, 59(10):3979–3986, Oct. 2012.

[CFF10] L. M. Capisani, T. Facchinetti, and A. Ferrara. Real-time networked control of an industrial robot manipulator via discrete-time second-order sliding modes. *International Journal of Control*, 83(8):1595–1611, Jul. 2010.

[CFM09] L. M. Capisani, A. Ferrara, and L. Magnani. Design and experimental validation of a second-order sliding-mode motion controller for robot manipulators. *International Journal of Control*, 82(2):365–377, Jan. 2009.

[CHD+15] Mujaddid Morshed Chowdhury, Md Enamul Haque, Debasish Das, Ameen Gargoom, and Michael Negnevitsky. Modeling, parameter measurement and sensorless speed estimation of ipm synchronous generator for direct drive variable speed wind turbine application. *International Transactions on Electrical Energy Systems*, 25(9):1814–1830, Sept. 2015.

[CIF15] M. Cucuzzella, G. P. Incremona, and A. Ferrara. Design of robust higher order sliding mode control for microgrids. *IEEE Journal on Emerging and Selected Topics in Circuits and Systems*, 5(3):393–401, Sep. 2015.

[CKF+16] Asif Chalanga, Shyam Kamal, Leonid M Fridman, Bijnan Bandyopadhyay, and Jaime A Moreno. Implementation of super-twisting control: Super-twisting and higher order sliding-mode observer-based approaches. *IEEE Transactions on Industrial Electronics*, 63(6):3677–3685, June 2016.

[CMMC92] B. J. Cardoso, A. F. Moreira, B. R. Menezes, and P. C. Cortizo. Analysis of switching frequency reduction methods applied to sliding mode controlled dc-dc converters. In *Applied Power Electronics Conference and Exposition*, pages 403–410, Feb. 1992.

[CMW15] D. Cai, E. Mallada, and A. Wierman. Distributed optimization decomposition for joint economic dispatch and frequency regulation. In *in Proc. 54th IEEE Conf. on Decision and Control*, pages 15–22, Dec. 2015.

[CT15] Sina Y Caliskan and Paulo Tabuada. Uses and abuses of the swing equation model. In *Proc. 54th IEEE Conference on Decision and Control*, pages 6662–6667, Osaka, Japan, 2015.

[DB13] F. Dörfler and F. Bullo. Kron reduction of graphs with applications to electrical networks. *IEEE Transactions on Circuits and Systems I: Regular Papers*, 60(1):150–163, Jan. 2013.

[DF09] F. Dinuzzo and A. Ferrara. Higher order sliding mode controllers with optimal reaching. *IEEE Transactions on Automatic Control*, 54(9):2126–2136, Sep. 2009.

[DG17] Florian Dörfler and Sergio Grammatico. Gather-and-broadcast frequency control in power systems. *Automatica*, 79:296–305, May 2017.

[DGJ13] B. Demirel, V. Gupta, and M. Johansson. On the trade-off between control performance and communication cost for event-triggered control over lossy networks. In *European Control Conference*, pages 1168–1174, Zürich, Switzerland, July 2013.

[DLC15] Krishnamurthy Dvijotham, Steven Low, and Michael Chertkov. Convexity of energy-like functions: theoretical results and applications to power system operations. *arXiv preprint*, 2015.

[DM17] C. De Persis and N. Monshizadeh. Bregman storage functions for microgrid control. *IEEE Transactions on Automatic Control*, 2017.

[Don16] L. Dong. Decentralized load frequency control for an interconnected power system with nonlinearities. In *Proc. American Control Conference*, pages 5915–5920, Boston, MA, USA, 2016.

[DPM17] Claudio De Persis and Nima Monshizadeh. Bregman storage functions for microgrid control. *IEEE Transactions on Automatic Control*, 2017.

[DTPH17] V. S. Dolk, P. Tesi, C. De Persis, and W. P. M. H. Heemels. Event-triggered control systems under denial-of-service attacks. *IEEE Transactions on Control of Network Systems*, 4(1):93–105, Mar. 2017.

[DWD16] C. De Persis, E. Weitenberg, and F. Dörfler. A power consensus algorithm for DC microgrids. *arXiv preprint*, 2016.

[DZM88] R. A. De Carlo, S. H. Zak, and G. P. Matthews. Variable structure control of nonlinear multivariable systems: a tutorial. *Proceedings of the IEEE*, 76(3):212–232, Mar. 1988.

[EIU16] A. M. Ersdal, L. Imsland, and K. Uhlen. Model predictive load-frequency control. *IEEE Transactions on Power Systems*, 31(1):777–785, Jan. 2016.

[ES94] Christopher Edwards and Sarah K. Spurgeon. On the development of discontinuous observers. *International Journal of control*, 59(5):1211–1229, Jan. 1994.

[ES98] C. Edwards and S. Spurgeon. *Sliding Mode Control: Theory and Applications*. Systems and Control. Taylor & Francis, 1998.

[FAD09] N. Flourentzou, V. G. Agelidis, and G. D. Demetriades. Vsc-based hvdc power transmission systems: An overview. *IEEE Transactions on Power Electronics*, 24(3):592–602, Mar. 2009.

[FBP03] T. Floquet, J.-P. Barbot, and W. Perruquetti. Higher-order sliding mode stabilization for a class of nonholonomic perturbed systems. *Automatica*, 39(6):1077–1083, Jun. 2003.

[FGO06] H. El Fadil, F. Giri, and H. Ouadi. Adaptive sliding mode control of pwm boost dc-dc converters. In *IEEE Conference on Computer Aided Control System Design, IEEE International Conference on Control Applications, IEEE International Symposium on Intelligent Control*, pages 3151–3156, Oct. 2006.

[Fil88] A. F. Filippov. *Differential Equations with Discontinuous Right-Hand Sides*, volume 18 of *Mathematics and its Applications*. Springer Netherlands, 1988.

[FIM14] A. Ferrara, G. P. Incremona, and L. Magni. Model-based event-triggered robust MPC/ISM. In *Proc. European Control Conference*, pages 2931–2936, Strasbourg, France, Jun. 2014.

[FR09] A. Ferrara and M. Rubagotti. A sub-optimal second order sliding mode controller for systems with saturating actuators. *IEEE Transactions on Automatic Control*, 54(5):1082–1087, May 2009.

[Fri02] L. Fridman. Singularly perturbed analysis of chattering in relay control systems. *IEEE Transactions on Automatic Control*, 47(12):2079–2084, Dec. 2002.

[FSS14] A. Ferrara, S. Sacone, and S. Siri. Event-triggered strategies for the networked control of freeway traffic systems. In *Proc. European Control Conference*, pages 2594–2599, Strasbourg, France, Jun. 2014.

[FSS15] A. Ferrara, S. Sacone, and S. Siri. Model-based event-triggered control for freeway traffic systems. In *Proc. 1st IEEE International Conference on Event-Based Control, Communication, and Signal Processing*, Krakow, Poland, Jun. 2015.

[GA13] E. Garcia and P. J. Antsaklis. Model-based event-triggered control for systems with quantization and time-varying network delays. *IEEE Transactions on Automatic Control*, 58(2):422–434, Feb. 2013.

[GBZ+10] J. M. Guerrero, F. Blaabjerg, T. Zhelev, K. Hemmes, E. Monmasson, S. Jemei, M. P. Comech, R. Granadino, and J. I. Frau. Distributed generation: Toward a new energy paradigm. *IEEE Industrial Electronics Magazine*, 4(1):52–64, Mar. 2010.

[GC10] R. A. Gupta and M.-Y. Chow. Networked control system: overview and research trends. *IEEE Transactions on Industrial Electronics*, 57(7):2527–2535, Jul. 2010.

[GLLC13] J. M. Guerrero, P. C. Loh, T-L Lee, and M. Chandorkar. Advanced control architectures for intelligent microgrids - part ii: power quality, energy storage, and AC/DC microgrids. *IEEE Transactions on Industrial Electronics*, 60(4):1263–1270, Apr. 2013.

[GVM+11] J. M. Guerrero, J. C. Vasquez, J. Matas, L. G. de Vicuna, and M. Castilla. Hierarchical control of droop-controlled AC and DC microgrids – a general approach toward standardization. *IEEE Transactions on Industrial Electronics*, 58(1):158–172, Jan. 2011.

[HC08] Wassim M Haddad and VijaySekhar Chellaboina. *Nonlinear dynamical systems and control: a Lyapunov-based approach.* Princeton University Press, 2008.

[HGMK15] M. Hamzeh, A. Ghazanfari, Y. A. R. I. Mohamed, and Y. Karimi. Modeling and design of an oscillatory current-sharing control strategy in DC microgrids. *IEEE Transactions on Industrial Electronics*, 62(11):6647–6657, Nov. 2015.

[HIU+12] Abdul Motin Howlader, Yuya Izumi, Akie Uehara, Naomitsu Urasaki, Tomonobu Senjyu, Atsushi Yona, and Ahmed Yousuf Saber. A minimal order observer based frequency control strategy for an integrated wind-battery-diesel power system. *Energy*, 46(1):168–178, Oct. 2012.

[HJT12] W.P.M.H. Heemels, K. Johansson, and P. Tabuada. An introduction to event-triggered and self-triggered control. In *Proc. 51st IEEE Conference on Decision and Control*, pages 3270–3285, Maui, HI, USA, Dec. 2012.

[HNX07] J. P. Hespanha, P. Naghshtabrizi, and Y. Xu. A survey of recent results in networked control systems. *Proc. of the IEEE*, 95(1):138–162, Jul. 2007.

[HSVDB08] W. P. M. H. Heemels, J. H. Sandee, and P. P. J. Van Den Bosch. Analysis of event-driven controllers for linear systems. *International Journal of Control*, 81(4):571–590, Apr. 2008.

[ICF16] Gian Paolo Incremona, Michele Cucuzzella, and Antonella Ferrara. Adaptive suboptimal second-order sliding mode control for microgrids. *International Journal of Control*, 89(9):1849–1867, Jan. 2016.

[IF16] Gian Paolo Incremona and Antonella Ferrara. Adaptive model-based event-triggered sliding mode control. *Int. J. Adaptive Control Signal Process.*, 30:1298–1316, Jan. 2016.

[IRF16] G. P. Incremona, M. Rubagotti, and A. Ferrara. Sliding mode control of constrained nonlinear systems. *IEEE Transactions on Automatic Control*, 62(6):2965–2972, June 2016.

[JLSE99] Karl H Johansson, John Lygeros, Shankar Sastry, and Magnus Egerstedt. Simulation of zeno hybrid automata. In *Proc. 38th IEEE Conference on Decision and Control*, volume 4, pages 3538–3543, Phoenix, AZ, USA, Dec. 1999.

[JLvdB09] A. Jokic, M. Lazar, and P.P.J. van den Bosch. Real-time control of power systems using nodal prices. *International Journal of Electrical Power & Energy Systems*, 31(9):522–530, Oct. 2009.

[JMLJ13] Jackson John Justo, Francis Mwasilu, Ju Lee, and Jin-Woo Jung. AC-microgrids versus DC-microgrids with distributed energy resources: A review. *Renewable Sustain. Energy Rev.*, 24:387–405, Aug. 2013.

[JWW+01] L Jiang, QH Wu, J Wang, C Zhang, and XX Zhou. Robust observer-based nonlinear control of multimachine power systems. In *IEE Proc. Generation Transmission Distribution*, pages 623–631. IET, Nov. 2001.

[KBL94] Prabha Kundur, Neal J Balu, and Mark G Lauby. *Power system stability and control.* McGraw-hill New York, 1994.

[KDI10] H. Karimi, E.J. Davison, and R. Iravani. Multivariable servomechanism controller for autonomous operation of a distributed generation unit: design and performance evaluation. *IEEE Transactions on Power Systems*, 25(2):853–865, May 2010.

[KDSL16] A. Kasis, E. Devane, C. Spanias, and I. Lestas. Primary frequency regulation with load-side participation part I: stability and optimality. *IEEE Transactions on Power Systems*, 32(5):3505–3518, Sept. 2016.

[KH12] S. Kar and G. Hug. Distributed robust economic dispatch in power systems: A consensus + innovations approach. In *IEEE Power and Energy Society General Meeting*, pages 1–8, San Diego, CA, USA, July 2012.

[Kha96] H. K. Khalil. *Nonlinear Systems.* Prentice Hall, 1996.

[KIL05] F. Katiraei, M. R. Iravani, and P. W. Lehn. Micro-grid autonomous operation during and subsequent to islanding process. *IEEE Transactions on Power Delivery*, 20(1):248–257, Jan. 2005.

[KMDL17] Andreas Kasis, Nima Monshizadeh, Eoin Devane, and Ioannis Lestas. Stability and optimality of distributed secondary frequency control schemes in power networks. *arXiv preprint*, 2017.

[KNI08] H. Karimi, H. Nikkhajoei, and R. Iravani. Control of an electronically-coupled distributed resource unit subsequent to an islanding event. *IEEE Transactions on Power Delivery*, 23(1):493–501, Jan. 2008.

[KPA+04] P. Kundur, J. Paserba, V. Ajjarapu, G. Andersson, A. Bose, C. Canizares, N. Hatziargyriou, D. Hill, A. Stankovic, C. Taylor, T. Van Cutsem, and V. Vittal. Definition and classification of power system stability IEEE/CIGRE joint task force on stability terms and definitions. *IEEE Transactions on Power Systems*, 19(3):1387–1401, Aug. 2004.

[Lai01] Loi Lei Lai. *Power system restructuring and deregulation: trading, performance and information technology.* John Wiley & Sons, 2001.

[Las02] R. H. Lasseter. Microgrids. In *Proc. IEEE Power Engineering Society Winter Meeting*, volume 1, pages 305–308, New York, NY, USA, 2002.

[Lev93] A. Levant. Sliding order and sliding accuracy in sliding mode control. *International Journal of Control*, 58(6):1247–1263, Dec. 1993.

[Lev03] A. Levant. Higher-order sliding modes, differentiation and output-feedback control. *International Journal of Control*, 76(9–10):924–941, Jan. 2003.

[Lev05] A. Levant. Quasi-continuous high-order sliding-mode controllers. *IEEE Transactions on Automatic Control*, 50(11):1812–1816, Nov. 2005.

[Lev10] A. Levant. Chattering analysis. *IEEE Transactions on Automatic Control*, 55(6):1380–1389, Jun. 2010.

[LGSV14] X. Lu, J. M. Guerrero, K. Sun, and J. C. Vasquez. An improved droop control method for dc microgrids based on low bandwidth communication with dc bus voltage restoration and enhanced current sharing accuracy. *IEEE Transactions on Power Electronics*, 29(4):1800–1812, Apr. 2014.

[LP04] R. H. Lasseter and P. Paigi. Microgrid: a conceptual solution. In *Proc. 35th IEEE Power Electronics Specialists Conference*, volume 6, pages 4285–4290, Aachen, Germany, June 2004.

[LR90] Rogelio Luck and Asok Ray. An observer-based compensator for distributed delays. *Automatica*, 26(5):903–908, Sept. 1990.

[LSH10] M. Liserre, T. Sauter, and J. Y. Hung. Future energy systems: Integrating renewable energy sources into the smart power grid through industrial electronics. *IEEE Industrial Electronics Magazine*, 4(1):18–37, Mar. 2010.

[LSL12] Joseph La Salle and Solomon Lefschetz. *Stability by Lyapunov's Direct Method with Applications*, volume 4. Elsevier, 2012.

[LWL11] X. Liu, P. Wang, and P. C. Loh. A hybrid AC/DC microgrid and its coordination control. *IEEE Transactions on Smart Grid*, 2(2):278–286, June 2011.

[LXC+07] G.-P. Liu, Y. Xia, J. Chen, D. Rees, and W. Hu. Networked predictive control of systems with random network delays in both forward and feedback channels. *IEEE Transactions on Industrial Electronics*, 54(3):1282–1297, Jun. 2007.

[LZC16] N. Li, C. Zhao, and L. Chen. Connecting automatic generation control and economic dispatch from an optimization view. *IEEE Transactions on Control of Network Systems*, 3(3):254–264, Sept. 2016.

[MA04] L. A. Montestruque and P. Antsaklis. Stability of model-based networked control systems with time-varying transmission times. *IEEE Transactions on Automatic Control*, 49:1562–1572, Sep. 2004.

[MBB08] Jan Machowski, Janusz Bialek, and Dr Jim Bumby. *Power System Dynamics: Stability and Control*. Wiley, 2 edition edition, 2008.

[MDC12] R. Mudumbai, S. Dasgupta, and B. B. Cho. Distributed control for optimal economic dispatch of a network of heterogeneous power generators. *IEEE Transactions on Power Systems*, 27(4):1750–1760, Nov. 2012.

[MDPMvdS16] Pooya Monshizadeh, Claudio De Persis, Nima Monshizadeh, and Arjan J van der Schaft. Nonlinear analysis of an improved swing equation. In *Proc. 55th IEEE Conference on Decision and Control*, pages 4116–4121, Las Vegas, NV, USA, 2016.

[MDPvdSS17] Nima Monshizadeh, Claudio De Persis, Arjan J van der Schaft, and Jacquelien M A Scherpen. A novel reduced model for electrical networks with constant power loads. *IEEE Trans. Automat. Control*, 2017.

[MDS+17] D. K. Molzahn, F. Dörfler, H. Sandberg, S. H. Low, S. Chakrabarti, R. Baldick, and J. Lavaei. A survey of distributed optimization and control algorithms for electric power systems. *IEEE Transactions on Smart Grid*, 2017.

[MF16] Z. Miao and L. Fan. Achieving economic operation and secondary frequency regulation simultaneously through local feedback control. *IEEE Transactions on Power Systems*, 32(1):85–93, Jan. 2016.

[MFL+16] Yang Mi, Yang Fu, Dongdong Li, Chengshan Wang, Poh Chiang Loh, and Peng Wang. The sliding mode load frequency control for hybrid power system based on disturbance observer. *International Journal of Electrical Power and Energy Systems*, 74:446–452, Jan. 2016.

[MFWW13] Y. Mi, Y. Fu, C. Wang, and P. Wang. Decentralized sliding mode load frequency control for multi-area power systems. *IEEE Transactions on Power Systems*, 28(4):4301–4309, Nov. 2013.

[MMEF15] Chiara Mellucci, Prathyush P Menon, Christopher Edwards, and Antonella Ferrara. Load alteration fault detection and reconstruction in power networks modelled in semi-explicit differential algebraic equation form. In *Proc. American Control Conf.*, pages 5836–5841, Chicago, IL, USA, July 2015. IEEE.

[MT08] M. Mazo and P. Tabuada. On event-triggered and self-triggered control over sensor/actuator networks. In *Proc. 47th IEEE Conference on Decision and Control*, pages 435–440, Cancun, Mexico, Dec. 2008.

[NB96] J. Nilsson and B. Bernhardsson. Analysis of real-time control systems with time delays. In *Proc. 35th IEEE Conference on Decision and Control*, volume 3, pages 3173–3178, Kobe, Japan, Dec. 1996.

[NC13] S. Nabavi and A. Chakrabortty. Topology identification for dynamic equivalent models of large power system networks. In *Proc. American Control Conference*, pages 1138–1143, Washington, DC, USA, June 2013. IEEE.

[NDLG14] V. Nasirian, A. Davoudi, F. L. Lewis, and J. M. Guerrero. Distributed adaptive droop control for dc distribution systems. *IEEE Transactions on Energy Conversion*, 29(4):944–956, Dec. 2014.

[NMDL15] V. Nasirian, S. Moayedi, A. Davoudi, and F. L. Lewis. Distributed cooperative control of DC microgrids. *IEEE Transactions on Power Electronics*, 30(4):2288–2303, Apr. 2015.

[OG13] S. Oucheriah and L. Guo. Pwm-based adaptive sliding-mode control for boost dc–dc converters. *IEEE Transactions on Industrial Electronics*, 60(8):3291–3294, Aug. 2013.

[ORM+15] Fernando A Ortiz-Ricardez, Jaime A Moreno, et al. Smooth Lyapunov function and gain design for a second order differentiator. In *Proc. 54th IEEE Conf. Decision Control*, pages 5402–5407, Osaka, Japan, Dec. 2015.

[PAMD+16] S. Peyghami-Akhuleh, H. Mokhtari, P. Davari, P. C. Loh, and F. Blaabjerg. A new secondary control approach for voltage regulation in dc microgrids. In *2016 IEEE Energy Conversion Congress and Exposition (ECCE)*, pages 1–6, Sept. 2016.

[Par29] R. H. Park. Two-reaction theory of synchronous machines-generalized method of analysis-part i. *Transactions of the American Institute of Electrical Engineers*, 48(3):716–727, Jul. 1929.

[PDH+05] G. Pepermans, J. Driesen, D. Haeseldonckx, R. Belmans, and W. D'haeseleer. Distributed generation: definition, benefits and issues. *Energy Policy*, 33(6):787 – 798, 2005.

[PGA17] P. Prajof, Y. Goyal, and V. Agarwal. A novel communication based average voltage regulation scheme for a droop controlled dc microgrid. *IEEE Transactions on Smart Grid*, PP(99):1–1, Oct. 2017.

[PGdMA+13] E. Planas, A. Gil-de Muro, J. Andreu, I. Kortabarria, and I. M. de Alegría. General aspects, hierarchical controls and droop methods in microgrids: A review. *Renewable and Sustainable Energy Reviews*, 17(0):147–159, Jan. 2013.

[PKG14] O. Palizban, K. Kauhaniemi, and J. M. Guerrero. Microgrids in active network management—part i: hierarchical control, energy storage, virtual power plants, and market participation. *Renewable and Sustainable Energy Reviews*, 36(0):428–439, 2014.

[PKK11] N. L. Panwar, S. C. Kaushik, and Surendra Kothari. Role of renewable energy sources in environmental protection: A review. *Renewable and Sustainable Energy Reviews*, 15(3):1513 – 1524, 2011.

[PL06] P. Piagi and R. H. Lasseter. Autonomous control of microgrids. In *Proc. Power Engineering Society General Meeting*, page 8, Montréal, Canada, 2006.

[PML03] H. B. Puttgen, P. R. MacGregor, and F. C. Lambert. Distributed generation: semantic hype or the dawn of a new era? *IEEE Power and Energy Magazine*, 1(1):22–29, Jan. 2003.

[PPK15] S. Prasad, S. Purwar, and N. Kishor. On design of a non-linear sliding mode load frequency control of interconnected power system with communication time delay. In *Proc. of the IEEE Conference on Control Applications*, pages 1546–1551, Sept. 2015.

[PSW13] C. De Persis, R. Sailer, and F. Wirth. Parsimonious event-triggered distributed control: A zeno free approach. *Automatica*, 49(7):2116–2124, July 2013.

[RAOZC14] N. Rahbari-Asr, U. Ojha, Z. Zhang, and M. Y. Chow. Incremental welfare consensus algorithm for cooperative distributed generation/demand response in smart grid. *IEEE Transactions on Smart Grid*, 5(6):2836–2845, Nov. 2014.

[RF10] M. Rubagotti and A. Ferrara. Second order sliding mode control of a perturbed double integrator with state constraints. In *Proc. American Control Conference*, pages 985–990, Baltimore, MD, Jun. 2010.

[RKTR07] Y. G. Rebours, D. S. Kirschen, M. Trotignon, and S. Rossignol. A survey of frequency and voltage control ancillary services – part i: Technical features. *IEEE Transactions on Power Systems*, 22(1):350–357, Feb. 2007.

[RL16] D. Ronchegalli and R. Lazzari. Development of the control strategy for a direct current microgrid: A case study. In *AEIT International Annual Conference*, pages 1–6, Oct. 2016.

[RSFT15] S. Riverso, F. Sarzo, and G. Ferrari-Trecate. Plug-and-play voltage and frequency control of islanded microgrids with meshed topology. *IEEE Transactions on Smart Grid*, 6(3):1176–1184, May 2015.

[SASS17] M. A. Setiawan, A. Abu-Siada, and F. Shahnia. A new technique for simultaneous load current sharing and voltage regulation in dc microgrids. *IEEE Transactions on Industrial Informatics*, PP(99):1–1, Oct. 2017.

[Sch07] W. Schulz. Etsi standards and guides for efficient powering of telecommunication and datacom. In *INTELEC 07 - 29th International Telecommunications Energy Conference*, pages 168–173, Sept. 2007.

[SD16] Johannes Schiffer and Florian Dörfler. On stability of a distributed averaging pi frequency and active power controlled differential-algebraic power system model. In *Proc. European Control Conference*, pages 1487–1492, Aalborg, Denmark, June 2016.

[SDPvdS17] Tjerk Stegink, Claudio De Persis, and Arjan van der Schaft. A unifying energy-based approach to stability of power grids with market dynamics. *IEEE Transactions on Automatic Control*, 62(6):2612–2622, June 2017.

[SEFL14a] Y. Shtessel, C. Edwards, L. Fridman, and A. Levant. Higher-order sliding mode controllers and differentiators. In *Sliding Mode Control and Observation*, Control Engineering, pages 213–249. Springer New York, 2014.

[SEFL14b] Yuri Shtessel, Christopher Edwards, Leonid Fridman, and Arie Levant. *Sliding mode control and observation*, volume 10. Springer, 2014.

[SJK12] Rodolphe Sepulchre, Mrdjan Jankovic, and Petar V Kokotovic. *Constructive nonlinear control*. Springer, 2012.

[SL91] J. J. E. Slotine and W. Li. *Applied Nonlinear Control*. Prentice Hall, 1991.

[SM17] S. Sahoo and S. Mishra. A distributed finite-time secondary average voltage regulation and current sharing controller for dc microgrids. *IEEE Transactions on Smart Grid*, PP(99):1–1, Aug. 2017.

[SSK17] M. S. Sadabadi, Q. Shafiee, and A. Karimi. Plug-and-play voltage stabilization in inverter-interfaced microgrids via a robust control strategy. *IEEE Transactions on Control Systems Technology*, 25(3):781–791, May 2017.

[Tab07] P. Tabuada. Event-triggered real-time scheduling of stabilizing control tasks. *IEEE Transactions on Automatic Control*, 52(9):1680–1685, Sep. 2007.

[TBD14] S. Trip, M. Bürger, and C. De Persis. An internal model approach to frequency regulation in inverter-based microgrids with time-varying voltages. In *Proc. 53rd IEEE Conference on Decision and Control*, pages 223–228, Los Angeles, CA, USA, Dec. 2014.

[TBD16] Sebastian Trip, Mathias Bürger, and Claudio De Persis. An internal model approach to (optimal) frequency regulation in power grids with time-varying voltages. *Automatica*, 64:240–253, Feb. 2016.

[TD17a] Sebastian Trip and Claudio De Persis. Communication requirements in a master-slave control structure for optimal load frequency control. In *Proc. of the 2017 IFAC World Congress*, Toulouse, France, 2017.

[TD17b] Sebastian Trip and Claudio De Persis. Optimal load frequency control with non-passive dynamics. *IEEE Transactions on Control of Network Systems*, PP(99):1–1, 2017.

[TMGFT16] Michele Tucci, Lexuan Meng, Josep M Guerrero, and Giancarlo Ferrari Trecate. Consensus algorithms and plug-and-play control for current sharing in DC microgrids. *arXiv preprint*, 2016.

[UGS99] V. I. Utkin, J. Guldner, and J. Shi. *Sliding Model Control in Electromechanical Systems*. Taylor and Francis, 1999.

[Utk92] V.I. Utkin. *Sliding Modes in Control and Optimization*. Communication and control engineering. Springer-Verlag, 1992.

[Utk93] V. I. Utkin. Sliding modes control in discrete-time and difference systems. In *Variable Structure and Lyapunov Control*, volume 193 of *Lecture Notes in Control and Information Sciences*, pages 87–107. Springer Berlin Heidelberg, 1993.

[VCR12] R. J. Vijayan, S. Ch, and R. Roy. Dynamic modeling of microgrid for grid connected and intentional islanding operation. In *Proc. International Conference on Advances in Power Conversion and Energy Technologies*, pages 1–6, Mylavaram, Andhra Pradesh, Aug. 2012.

[vdS00] Arjan J van der Schaft. *L_2-gain and passivity techniques in nonlinear control*. Springer, 2000.

[vdSS16] Arjan van der Schaft and Tjerk Stegink. Perspectives in modeling for control of power networks. *Annual Reviews in Control*, 41:119–132, 2016.

[VPP10] K. Vrdoljak, N. Perić, and I. Petrović. Sliding mode based load-frequency control in power systems. *Electrical Power Systems Research*, 80(5):514–527, May 2010.

[VSZ95] V. Venkatasubramanian, H. Schattler, and J. Zaborszky. Fast time-varying phasor analysis in the balanced three-phase large electric power system. *IEEE Transactions on Automatic Control*, 40(11):1975–1982, Nov. 1995.

[VT16] T. L. Vu and K. Turitsyn. Lyapunov functions family approach to transient stability assessment. *IEEE Transactions on Power Systems*, 31(2):1269–1277, Mar. 2016.

[Wil07] Jan C. Willems. Dissipative dynamical systems. *European Journal of Control*, 13(2–3):134–151, 2007.

[WL08] F. Y. Wang and D. Liu. *Networked Control Systems: Theory and Applications*. Springer-Verlag London, 2008.

[WW08] Chengshan Wang and Shouxiang Wang. Study on some key problems related to distributed generation systems. *Automation of Electric Power Systems*, 20(32):1–4, 2008.

[XDLvS17] Kaihua Xi, Johan LA Dubbeldam, Hai Xiang Lin, and Jan H van Schuppen. Power-imbalance allocation control of power systems-secondary frequency control. *arXiv preprint*, 2017.

[XLSvS17] Kaihua Xi, Hai Xiang Lin, Chen Shen, and Jan H van Schuppen. Multi-level power-imbalance allocation control for secondary frequency control in power systems. *arXiv preprint*, 2017.

[YA11] H. Yu and P. J. Antsaklis. Event-triggered real-time scheduling for stabilization of passive and output feedback passive systems. In *Proc. American Control Conference*, pages 1674–1679, San Francisco, CA, USA, Jul. 2011.

[YC14] S. You and L. Chen. Reverse and forward engineering of frequency control in power networks. In *in Proc. 53rd IEEE Conf. on Decision and Control*, pages 191–198, Los Angeles, CA, USA, Dec. 2014.

[YHL15] Peng Yi, Yiguang Hong, and Feng Liu. Distributed gradient algorithm for constrained optimization with application to load sharing in power systems. *Systems & Control Letters*, 83:45–52, Sept. 2015.

[YHL16] Peng Yi, Yiguang Hong, and Feng Liu. Initialization-free distributed algorithms for optimal resource allocation with feasibility constraints and application to economic dispatch of power systems. *Automatica*, 74:259–269, Dec. 2016.

[YSE17] Xing-Gang Yan, Sarah K. Spurgeon, and Christopher Edwards. Application of decentralised sliding mode control to multimachine power systems. In *Variable Structure Control of Complex Systems*, pages 297–313. Springer, 2017.

[YTX13] S. Yang, S. Tan, and J. X. Xu. Consensus based approach for economic dispatch problem in a smart grid. *IEEE Transactions on Power Systems*, 28(4):4416–4426, Nov. 2013.

[YWSL16] T. Yang, D. Wu, Y. Sun, and J. Lian. Minimum-time consensus-based approach for power system applications. *IEEE Transactions on Industrial Electronics*, 63(2):1318–1328, Feb. 2016.

[YX13] Ke-You You and Li-Hua Xie. Survey of recent progress in networked control systems. *Acta Automatica Sinica*, 39(2):101–117, Feb. 2013.

[ZARA05] M. Zribi, M. Al-Rashed, and M. Alrifai. Adaptive decentralized load frequency control of multi-area power systems. *International Jorunal on Electrical Power and Energy Systems*, 27(8):575–583, Oct. 2005.

[ZBP01] Wei Zhang, M.S. Branicky, and S.M. Phillips. Stability of networked control systems. *IEEE Control Systems*, 21(1):84–99, Feb. 2001.

[ZC12] Z. Zhang and M. Y. Chow. Convergence analysis of the incremental cost consensus algorithm under different communication network topologies in a smart grid. *IEEE Transactions on Power Systems*, 27(4):1761–1768, Nov. 2012.

[ZD15] Jinxin Zhao and Florian Dörfler. Distributed control and optimization in DC microgrids. *Automatica*, 61:18–26, Nov. 2015.

[ZMD15] C. Zhao, E. Mallada, and F. Dörfler. Distributed frequency control for stability and economic dispatch in power networks. In *Proc. American Control Conference*, pages 2359–2364, Chicago, IL, USA, July 2015.

[ZOS17] D. Zonetti, R. Ortega, and J. Schiffer. A tool for stability and power sharing analysis of a generalized class of droop controllers for high-voltage direct-current transmission systems. *IEEE Transactions on Control of Network Systems*, 2017.

[ZP15] Xuan Zhang and Antonis Papachristodoulou. A real-time control framework for smart power networks: Design methodology and stability. *Automatica*, 58:43–50, Aug. 2015.

About the Author

Michele Cucuzzella
University of Pavia,
Via Ferrata 1
Pavia - Italy, 27100
michele.cucuzzella@gmail.com

Michele Cucuzzella was born in Ragusa, Italy, in 1990. He received the Bachelor Degree (with highest honor) in Industrial Engineering and the Master Degree (with highest honor) in Electrical Engineering from the University of Pavia, Italy in 2012 and 2014, respectively. The title of his master project was 'Sliding mode control of microgrids'. From November 2017 he is a postdoc for the ENgineering and TEchnology institute Groningen (ENTEG), Faculty of Science and Engineering, University of Groningen, the Netherlands, under the supervision of Professor Jacquelien Scherpen. From November 2014 to October 2017 he attended the PhD course in Electronics, Computer Since and Electrical Engineering at the Identification and Control of Dynamic Systems Laboratory of the University of Pavia, under the supervision of Professor Antonella Ferrara. From April 2016 to June 2016, and from February 2017 to March 2017 he was with the Johann Bernoulli Institute for Mathematics and Computer Science at the University of Groningen, the Netherlands, under the supervision of Professor Arjan van der Schaft. His research activities are mainly in the area of nonlinear control, sliding mode control and event-triggered control with application to power systems and microgrids. He has authored or co-authored more than 15 papers, including also international journal papers.

Alphabetical Index